VILNIUS UNIVERSITY

Rokas Borusevičius

Accuracy of Dental Implant Navigation Techniques and Biocompatibility of Materials used for Immediate Prostheses

DOCTORAL DISSERTATION

Medicine and Health Science,
Odontology (M 002)

VILNIUS, 2023

The dissertation was prepared between 2017 and 2022 at Vilnius Universtity, Faculty of Medicine, Institute of Odontology. The research was supported by Research Council of Lithuania.

Academic supervisor – Prof. Dr. Vygandas Rutkūnas (Vilnius University, Medicine and Health Science, Odontology, M 002).

This doctoral dissertation will be defended in a public meeting of the Dissertation Defence Panel:

Chairman – **Prof. Dr. Vytautė Pečiulienė** (Vilnius University, Medicine and Health Science, Odontology, M 002).

Members:
Dr. Daiva Baltriukienė (Vilnius University, Natural Sciences, Biochemistry, N 004),
Prof. Dr. Dainius Razukevičius (Lithuanian University of Health Sciences, Medicine and Health Science, Odontology, M 002),
Prof. Dr. Murali Srinivasan (University of Zürich, Medicine and Health Science, Odontology, M 002),
Assoc. Prof. Dr. Linas Zaleckas (Vilnius University, Medicine and Health Science, Medicine, M 001).

The dissertation shall be defended at a public meeting of the Dissertation Defence Panel at 14:00 on September 28, 2023 in Main meeting room of the Vilnius University Hospital Žalgiris Clinic.
Address: Žalgirio str. 117, LT-08215 Vilnius, Lithuania.
Phone No.: +370 5 2727589; email: mf@mf.vu.lt

The text of this dissertation can be accessed at the Vilnius University library, as well as on the website of Vilnius University:
www.vu.lt/lt/naujienos/ivykiu-kalendorius

VILNIAUS UNIVERSITETAS

Rokas Borusevičius

Dantų implantacijos navigacijos metodų tikslumas ir neatidėliotiniems protezams naudojamų medžiagų biologinis suderinamumas

DAKTARO DISERTACIJA

Medicinos ir sveikatos mokslai,
Odontologija (M 002)

VILNIUS, 2023

Acknowledgements

THE LIST OF ABBREVIATIONS

AI –   artificial intelligence
AFI   – accordion fringe interferometry
ANOVA   – analysis of variance
AWS   – active wavefront sampling
BL   – buccolingual
CAD/CAM   – computer-assisted design and manufacturing
CBCT   – cone-beam computed tomography
CCP   – conventional cleaning protocol
CLIP   – continuous liquid interface printing
CMOS   – complementary metal-oxide semiconductor
CT   – computed tomography
DICOM   – digital imaging and communications in medicine
DLP   – digital light processing
DMSO   – dimethyl sulfoxide
EMAX   – lithium disilicate glass-ceramics "e.max"
FCS   – fetal calf serum
FDI   – World Dental Federation (French: Fédération Dentaire
             Internationale)
FDM   – fused deposition modelling
FOV   – field of view
HD   – high-definition
HGF   – human gingival fibroblasts
IMDM   – Iscove's Modified Dulbecco's Medium
ICP   – iterative closest point
IOS   – intraoral scanning (scanner; scan)
K1   – Kennedy class I defect
K2   – Kennedy class II defect
K3   – Kennedy class III defect
MD   – mesiodistal
MRI   – magnetic resonance imaging
MTT   – 3-(4,5-dimetiltiazol-2-il)-2,5-diphenyltetrazolium bromide
MVT   – Monte-Carlo corrected p-value based on multivariate normal
             t-test distribution
NICE   – lithium disilicate glass-ceramics "n!ce"

OCT   – optical coherent tomography
OD   – optical density
PEEK   – polyetheretherketone
PEKK   – polyetherketoneketone
PL   – porgressive-line
PMMA   – polymethylmethacrylate
PMMA-Bre – milled "Bredent" polymethylmethacrylate
PMMA-Ker – milled "Kerox" polymethylmethacrylate
PMMA-3D – three-dimensionally printed polymethylmethacrylate
POI   – point of interest
RCP   – research cleaning protocol
Sa   – mean surface area roughness
SD   – standard deviation
SL   – screw-line
SLA   – stereolithography
SLS   – selective laser sintering
STL   – standard tessellation language
Ti   – titanium
UV   – ultraviolet
UV-C   – ultraviolet C (ultraviolet radiation with wavelengths between
            200 and 290 nm)
WCA   – water contact angle
ZrO   – zirconium oxide (ZrO2, also known as zirconia) ceramics
ZrO-HT   – high translucent zirconium oxide ceramics
ZrO-UTML – ultra translucent multilayered zirconium oxide ceramics
ZrO-V   – feldspar veneered zirconium oxide ceramics
3D   – three-dimensional

CONTENTS

INTRODUCTION

RELEVANCE OF THE STUDY

We live in a particularly exciting time due to the rapid advancement of technology. Modern dentistry and medicine do not only address the eradication of the disease, but simultaneously seek to restore the quality of the patient's life, including both function and aesthetics. This tendency is observed in various interrelated fields of head and neck medicine, including but not limited to oral and maxillofacial surgery, orthognathic surgery, dentistry, orthopedics, and oncology. A common goal encourages reducing the interdisciplinary barrier, sharing knowledge, improving treatment protocols and workflow. Therefore, there is a growing recognition of the importance of treatment planning and the accurate execution of those plans. Furthermore, implementing these plans often requires the seamless connection of different stages of treatment that were historically separated by technical terms. In light of modern scientific advancements, the significance of considering the entire treatment process (from surgery to functionality and aesthetics) is becoming more apparent, rather than solely relying on individual evidence-based elements.

Digital three-dimensional technologies open new possibilities in dentistry and medicine for this purpose [1–5]. These innovations evolve rapidly and make their way into everyday practice, benefiting both the practitioner and the patient [6–8]. Moreover, several advancements in technology, such as Cone Beam Computed Tomography (CBCT), Intraoral Scanning (IOS), and Computer-Aided Design/Computer-Aided Manufacturing (CAD/CAM), have now become widely adopted in dental and medical practices. These innovations have significantly improved efficiency, patient safety, and the ability to meet high aesthetic expectations [1,9–12]. In addition, dental implants are a highly widespread and predictable treatment method for rehabilitating partially or completely edentulous patients with cumulative survival rates reported up to 99 % [13–15]. Digital technologies can be applied at various patient's treatment stages: from treatment planning and implant surgery to prosthesis manufacturing and accuracy assessment [1,3]. Moreover, there is a growing interest in the innovative development of biomaterials, with the ultimate goal of providing the highest quality patient-centred healthcare services [16]. Technological advancement enables the application of individual instruments and fundamentally increases the synergy between surgery and prosthetics.

Conceptually and practically, by reducing the division between implant placement and prosthesis delivery, it also changes the treatment standards. This growing synergism is based on scientific research tendencies and methods applied in dental practice: from immediate implant placement and prosthetics, continuing with guided implant surgery and ending with individualized healing abutments as well as one-time abutment concepts [17–23]. This enables precise digital implantology and prosthodontics protocols with absolute respect for biology, function, and aesthetics. However, although technology is evolving rapidly, research is necessary to establish these protocols as an evidence-based [12]. Moreover, published research often evaluates only a single aspect or small portion of the workflow questions [24]. It has been recognized that each individual step, either independently or in conjunction with other steps within this digital workflow, has the potential to lead to inaccuracies [25]. Therefore, these findings underscore the need for further research to investigate the accuracy and explore the factors that influence these inaccuracies. This research aims to evaluate two main stages of such a workflow: the three-dimensional (3D) accuracy of the implant positioning and the response of soft tissue cells to the materials of the transmucosal prosthetic element.

One of the essential criteria for the success of placing dental implants is the correct positioning of the implant in the bone, according to the biological and anatomical conditions [26]. This is most important for adjacent anatomical structures (nerves, adjacent teeth, sinuses, blood vessels, etc.) [27]. However, an incorrect three-dimensional position of the dental implant is an occasional error in implant dentistry that might lead to severe and challenging complications, including esthetic failures [28–30]. Therefore, during the last decades, a significant focus has also been placed on the prosthetically correct position of dental implants [31]. Guidance in implant dentistry has increasingly become a common tool for patient safety providing accurate implant positioning [32,33]. Guided implant placement has been proven to be more accurate compared to a free-hand surgery [34–37]. There are two main guidance methods: static and dynamic navigation [24]. The first method is based on a 3D-printed surgical template and is used more commonly [38]. The second method uses real-time tracking of the drill (typically on a screen) using the patients' CBCT [39]. Both options are available for fully guided and flapless implant surgery [6]. Dynamic guidance is a relatively new technique in clinical practice compared to static guides [24]. It has the unique advantage of continuous real-time tracking and the possibility to adjust the initial plan depending on a clinical situation [40].

Although an emerging number of studies investigate the accuracy of guided implantation, few studies evaluate the influencing factors [40,41].

Most studies that assess the accuracy of dynamic implant placement use post-operative CBCT scans [39,42,43]. This approach overlaps a pre-operative CBCT scan containing planned implant position information with a post-operative CBCT scan showing the actual implant position [42]. Although this method can be informative, it is not without limitations. One of the primary disadvantages is the requirement for additional patient exposure to ionizing radiation (X-rays), which has little clinical reasoning and applicability [42,44]. In addition, using this method the accuracy of the implant position measurement might be negatively affected by the peri-implant image artifacts due to its metallic nature [44]. This observation has also been highlighted in recent literature reviews, suggesting the search for the alternative evaluation methods that avoid the use of X-rays [39,42,45]. Non-maleficence is an essential part of bioethics: first, do no harm (Latin: *primum non nocere*).

The correct position of implants enables immediate prosthetics, which significantly improves the quality of a patient's life and has already become an important aim of the whole treatment plan [46–49]. Recent scientific studies prove such protocols to be successful [17,47–49]. Response of bone tissue to dental implant and the process of osseointegration is a comprehensively studied concept and at present increasing number of studies focus on the soft tissue surrounding dental implants supported prostheses as an essential component for achieving desired esthetical and functional results [50–54]. It has been proven that soft tissue quantity and quality are important factors for bone stability around dental implants [55]. The topic of peri-implant soft tissue health is currently experiencing a paradigm shift – more and more attention is paid to the whole supracrestal complex, consisting of soft tissue and the transmucosal element of the implant [23,56]. Clinical research evidence validates the significance of immediate implant restoration in achieving the most favourable aesthetic outcome [57]. Soft tissue (primarily gingiva) forms a barrier that at health protects the implant-surrounding osseous tissue from hazardous agents and allows a patient to maintain proper oral hygiene [58]. If this barrier fails – it might eventually lead to bone loss, compromised aesthetics, and even implant failure [54,59]. Different materials and their surface modifications have been shown to bear different biocompatibility properties for the soft tissue [60]. There is a growing number of prosthetic materials on the market including new-generation polymers and 3D-printed materials

[20,61]. Furthermore, the surfaces of these materials are modified in various ways: different surface polishing protocols, washing methods, photofunctionalization using ultraviolet, plasma activation, and laser treatment [62]. There are still few studies that evaluate the surfaces of various immediate prosthetic materials, their properties and at the same time biocompatibility with soft tissue cells using a uniform protocol. Due to the lack of comparable findings from fundamental studies, it is challenging to interpret and discuss the clinical applicability of these materials comprehensively. Consequently, the data concerning soft tissue response are equally crucial to the treatment process as the accurate positioning of the implant within the bone. This is essential for promoting favourable healing and achieving optimal treatment outcomes.

AIMS OF THE STUDY

I. To investigate and evaluate the accuracy of digitally planned implantation procedures.

II. To evaluate human gingival fibroblast response to prosthetic materials for immediate implant loading

OBJECTIVES OF THE RESEARCH

1. To assess the 3D accuracy of digitally planned dental implantation using dynamic navigation technology, evaluating the influence of dental implant design, dental arch defect modification, and implant position.

2. To compare the 3D accuracy of digitally planned dental implant placement using static and dynamic guidance.

3. To evaluate the 3D accuracy of digitally planned dental implantation comparing teeth and reference objects as the dynamic guidance reference.

4. To assess the response of human gingival fibroblasts to polymeric materials for immediate prosthetics, evaluating surface roughness, hydrophilicity, and washing protocols.

5. To evaluate the response of human gingival fibroblasts to ceramic materials used for immediate prosthetics, evaluating surface roughness, and hydrophilicity.

6. To evaluate the influence of UV photofunctionalization of the zirconia ceramic surface on the response of human gingival fibroblasts.

NOVELTY AND SIGNIFICANCE OF THE STUDY

This study investigates and emphasizes the synergy of surgery and prosthetics in the field of dental implantology. It combines two crucial areas that hold significant relevance for the contemporary treatment workflow: the accurate 3D placement of implants within the bone and the biocompatibility of materials used for the subsequent prosthetic transmucosal component. These aspects play a crucial role not only in the initial stages of implantation, such as wound healing, but also in ensuring the long-term stability and health of both hard and soft tissues. By focusing on this integrated theme, the study highlights the importance of considering biological and anatomical factors while also striving for advanced treatment approaches that facilitate the timely restoration of patient function and aesthetics.

Current research involves integrating and assessing state-of-the-art digitally advanced 3D technologies with practical clinical applications. Recent studies and clinical practice demonstrate a high interest in the accuracy and practicality of these digital tools, reflecting significant interest in their implementation. This topic's data significantly complements the evidence for novel technologies in implant dentistry and prosthodontics. Importantly, this study assesses various factors influencing the accuracy of guided implantation: guidance method (static and dynamic), edentulous defect (Kenney classes I, II and III), implant design (less and more conical/aggressive), implant position (mesial and distal). The evaluation of these factors contributes significantly to the research's innovative character. So far, data in this niche have been scarce and nonhomogeneous, thus not providing opportunities for enhancing fundamental clinical knowledge. This approach enables to address the issue of accuracy more comprehensively and consistently, allowing for continuous evaluation and comparison of results using standardized criteria. Ultimately, these advancements can greatly enhance the selection of the most favourable treatment modalities, benefiting patients and clinicians

Most conducted reviews emphasize the necessity for methods that ensure patient safety when assessing the accuracy of implant placement. This study represents one of the initial attempts to evaluate the accuracy of fully-guided implantation using a non-invasive, X-ray-free method of post-operative evaluation. This approach offers a more rational and safer way of assessing accuracy than previous research methods. It represents a crucial component of future advancements in dentistry.

In addition, this study also evaluates immediate prosthetics and human gingival fibroblast response to prosthetic materials as well as other surface-related factors. This reflects the prevailing trend in dental practice to choose immediate prosthetics or a transmucosal element that forms gingiva, thus avoiding the need for a second-stage surgery in a favourable situation with accurate implant positioning. One of the key features contributing to the novelty of this study is the comprehensive inclusion of a wide array of materials for investigation, from polymeric materials (including innovative ones) to titanium and various ceramics. In addition to the existence of previous publications that assess materials individually or selectively based on specific criteria, the current study simultaneously evaluates the influence of surface preparation techniques on multiple factors including roughness, water contact angle, and the vitality and proliferation of human gingival fibroblasts. This comprehensive approach allows for a more thorough understanding of the impact of surface preparation on various aspects of material performance. At the same time, this knowledge allows for creating a complete picture of immediate prosthetic material selection in clinical practice with respect to less studied soft tissue response.

Additionally, the study evaluates the importance of surface cleaning, which has not been extensively addressed elsewhere, and the UV surface activation by photofunctionalization. Both of these aspects make substantial contributions to the research's novelty.

In conclusion, the main focus of the whole study is to make a substantial contribution to the understanding of the accuracy of emerging digital 3D technologies in the field of implantation, while also recognizing the significance of biological factors in immediate prosthetics. This research significantly advances the concept of evidence-based, accurate digital implantology and prosthodontics total fit workflows (TFW) while establishing their clinical applicability.

STATEMENTS TO DEFEND

1. Static and dynamic guided implant placement has a high accuracy of the procedures.
2. Dynamic navigation registration based on reference objects is a favourable alternative to achieve accurate implant positioning.

3. The material of the transmucosal element of the immediate prosthesis and its surface influences the response of human gingival fibroblasts.

4. Cleaning method of the prosthetic materials affects surface roughness, contact angle, and human gingival fibroblast viability.

5. Surface modification of zirconia oxide ceramics by photofunctionalization using UV radiation is a potential method to alter the response of human gingival fibroblasts.

APPROBATION OF THE RESEARCH

Original publications (Clarivate Analytics Web of Science):

1. Rutkunas V, Borusevicius R, Liaudanskaite D, Jasinskyte U, Drukteinis S, Bukelskiene V, Mijiritsky E. The Effect of Different Cleaning Protocols of Polymer-Based Prosthetic Materials on the Behavior of Human Gingival Fibroblasts. IJERPH 2020; 17: 7753. DOI: 10.3390/ijerph17217753.

2. Rutkunas V, Borusevicius R, Balciunas E, Jasinskyte U, Alksne M, Simoliunas E, Zlatev S, Ivanova V, Bukelskiene V, Mijiritsky E. The Effect of UV Treatment on Surface Contact Angle, Fibroblast Cytotoxicity, and Proliferation with Two Types of Zirconia-Based Ceramics. IJERPH 2022; 19: 11113. DOI: 10.3390/ijerph191711113.

Conference abstracts published (Clarivate Analytics Web of Science):

1. Borusevicius R, Bukelskiene V, Alksne M, Balciunas E, Simonaitis T, Jurgaityte R, Liaudanskaite D, Rutkunas V. Implant abutment material and surface modifications effect on human gingival fibroblast behavior. Clin Oral Impl Res 2019; 30: 332–332. DOI: 10.1111/clr.288_13509

2. Borusevicius R, Rutkunas V, Simonaitis T, Gendviliene I, Pletkus J. Accuracy of dynamic implant navigation in partially- and fully-edentulous models: a novel NO-invasive x-ray free method. Clin Oral Impl Res 2020; 31: 20–1. DOI: 10.1111/clr.16_13643

3. Liaudanskaite D, Borusevicius R, Rutkunas V, Bukelskiene V, Alksne M, Simoliunas E, Gendviliene I, Jurgaityte R. The impact of implant abutment preparation on proliferation of human gingival fibroblasts. Clin Oral Impl Res 2020; 31: 167–167. DOI: 10.1111/clr.109_13644

Other science journals, and science publications:

1. Rutkunas V, <u>Borusevicius R</u>. Skaitmeniniu būdu paruoštų dantų implantacijos gidų tikslumas ir gydymo rezultatai. Stomatologija : VšĮ "Odontologijos studija". ISSN 1392-8589. 2016, T. 19, nr. 1, p. 11-17.

Monographs, textbooks:

1. Rutkunas V, <u>Borusevicius R</u>, Geciauskaitė A, Pletkus J. Digital Technologies in Clinical Restorative Dentistry. Practical Advanced Periodontal Surgery 2020; 213–32.

Oral presentations:

1. <u>Borusevicius R</u>. Digital technologies in guided implantation and tissue regeneration. Conference „4x2 PLUS". Vilnius, Lithuania, 2019.
2. <u>Borusevicius R</u>. Effect of implant abutment material on peri-implant tissues. Odontologijos kompasas 2019, Lithuania, 2019.
3. <u>Borusevicius R</u>. Guided dynamic navigation in dental implantology and its accuracy. Odontologijos naujoves. Vanagupe 2020, Lithuania, 2020.
4. <u>Borusevicius R</u>. Accuracy of dynamic implant navigation in partially- and fully-edentulous models: a novel non-invasive x-ray free method. EAO Digital days, 2020.

1. LITERATURE REVIEW

1.1. MODERN DENTAL IMPLANTOLOGY

The response of bone tissue and osseointegration of implants, which have been studied for several decades since the introduction, are described in great detail today [50,63,64]. Furthermore, based on the published research data, the 20-year cumulative survival rates of dental implants have been reported to range between 89.5 % and 98.9 % [13,14]. These are the primary factors contributing to the widespread adoption of dental implantation as a standard procedure in treating edentulism. The art and science of contemporary dental implantology encompass a comprehensive approach beyond mere osseointegration and implant survival [65]. A paradigm shift has occurred, emphasizing the significant influence and importance of soft tissues and the associated transmucosal complex in relation to the stability of the underlying bone, aesthetics and long-term functional longevity [56,66]. Furthermore, recognizing the importance of a prosthetically driven implant position is paramount [67]. All these scientific advances are combined to achieve the best treatment result by responding to the patient's complaints and expectations (Fig. 1).
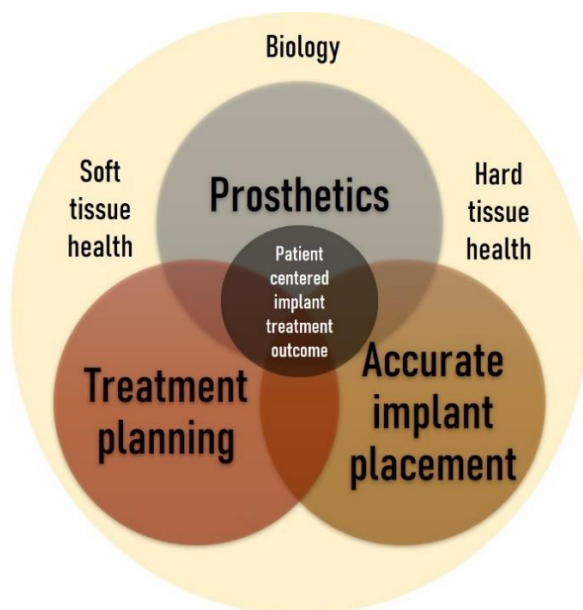
Fig. 1. Modern patient-centred implant treatment outcome concept based on current scientific evidence.

The literature emphasizes that objective measurements of surgical procedures and patient perception are important in evaluating the treatment [68,69]. Correspondingly, most operative techniques have recently focused on minimal invasiveness, decreasing surgical trauma and reducing the number of separate surgical stages [6,70,71]. In the appropriate clinical situation, one-stage implant surgery (non-submerged healing) has become common dental practice, reducing the number of surgical interventions while at the same time ensuring non-inferior results [72,73]. It is also one of the key reasons for immediate implant placement after tooth extraction and immediate implant-supported full-arch fixed restoration in the oral rehabilitation of fully edentulous patients [48,74–76]. Immediate implantation with immediate restoration in the maxillary aesthetic zone has the same long-term marginal bone stability as the delayed prosthetic protocol [77]. Although the data are heterogeneous, the evidence suggests that this approach is favourably evaluated by patients [78]. In addition, immediate dental implant placement and provisionalization are characterized by excellent gingival aesthetic outcomes and better chair-time efficiency [77,79,80]. Long-term survival and success rate is close to the delayed approach. Still, to achieve the most successful result for immediacy, it is particularly important to manage various criteria: surgical technique, implant positioning, soft and hard tissues, and prosthetic component [81,82]. Meanwhile, when immediate prosthetics are not feasible or necessary, customized healing abutments have been substantiated as the optimal treatment approach, ensuring consistent and reliable outcomes [20,83,84]. Various contemporary protocols for dental implant treatment focus primarily on patient expectations and comfort, but also aim to provide equally favourable results with minimal surgical intervention and timely provision of prosthetics.

The significance of treatment implementation is indisputable; however, the contemporary focus is predominantly directed toward treatment planning, which facilitates identifying and selecting the optimal strategy. Innovative technologies enable digital simulation of the case and treatment plan, benefiting the doctor and the patient [85]. Digital smile design and wax-up techniques offer patient-centred benefits such as improved final result estimation, enhanced communication, and the ability to visualize and modify the intended outcome of dental procedures [86]. Various technologies are used to create a "digital patient", including but not limited to: photography, facial and intraoral scanning, cone beam computed tomography, jaw tracking, and occlusal

analysis devices [87,88]. Patients favourably evaluate intraoral scanning (optical/digital impression taking) compared to the conventional putty-based impression-taking technique [89,90]. In addition, these contemporary tools enable the evaluation of the pre-operative situation in terms of anatomical and prosthetic constraints, thereby facilitating the selection of the most effective treatment solution [24]. Various guidance methods can be utilized to transfer the treatment plan from the computer to the patient's mouth [91], with the primary goals being to enhance patient safety and minimize errors resulting from human intervention [28,30]. The combined surgical and prosthetic efforts aided by modern technologies, result in functional and aesthetic outcomes that enhance the patient's oral health and overall satisfaction in implant dentistry.

Technological advances are beneficial in treatment planning and guidance and in the production of transmucosal prosthetic components (e.g.: CAD/CAM, 3D printing) and surface modifications of materials [92]. Moreover, these technologies are applied to even more complex areas, such as scaffold 3D printing for bone regeneration and tissue engineering [93,94]. Furthermore, the advent of novel high-performance and 3D-printable polymers has opened up a new direction of active research, focusing on their comparative analysis with materials that have long been present in the market [95]. In materials science, research focused on surface properties plays a crucial role as it aims to achieve optimal tissue response and compatibility [96]. Although bone tissue and cellular response have already been studied to some extent, soft tissue research is still trending [97]. Specifically, the concept of tissue response and compatibility is closely linked to the transmucosal component of dental implants, such as the abutment in a two-piece bone-level implant, and its impact on the overall health of the surrounding soft tissues [23,98]. When examining the tissue response and compatibility of dental implant components, the commonly assessed criteria include the material composition, surface roughness, topography, and hydrophilicity [99]. Various innovative methods can be used for surface modification, such as laser, plasma spray, UV photofunctionalization, and anodization [100–102]. Although materials science is fundamental with limited direct clinical applicability, the abundance of these studies and their hierarchical relation to further clinical research show that it is an integral part of modern dental implantology.

Finally, the materials and technologies discussed in the context of dental implants have implications beyond implantology. They hold relevance for various other disciplines including endodontics, orthodontics, orthognathic

surgery, craniomaxillofacial surgery, and reconstructive orthopedic onco-
logy, among others [2,4,103–105]. The precision of digital planning, its
realization, and the biocompatibility of materials are crucial factors within
this interdisciplinary field.

1.2. GUIDED IMPLANT PLACEMENT

1.2.1. REVISITING THE HISTORICAL PERSPECTIVE
IN THE LIGHT OF CURRENT UNDERSTANDING

Digital dental implant treatment planning and computer-aided surgical
guidance have become integral aspects of modern implantology, building
upon a historic development foundation [106]. There are many interconnected
terms associated with this concept: computer-aided, computer-assisted,
computer-guided, image-guided, guided, digitally/virtually planned and/or
guided, fully guided, digital surgical guides/stents/templates, static/dynamic
guidance/navigation. Many early attempts in 1980-1990 to transmit prosthetic
information for surgical procedures were constrained by guides that lacked
direct integration with radiological data [107]. In addition, some of these surgical
guiding templates were at best only limitedly linked to two-dimensional (2D)
radiographs, such as orthopantomograms [108]. Consequently, that primarily
facilitated the transfer of prosthetic information without adequately assessing
biological constraints, such as the quantity and quality of available bone [108].
These initial stents-templates functioned more as rough prosthetic orientation
transfer devices, leaving the operator a considerable degree of freedom in
selecting the position based on available bone or limiting guidance to the
pilot drill-only [109]. Therefore, it was premature to draw any conclusions
regarding the accuracy and errors of the plan during that time. Some of the
earliest proposals and prototypes of computed tomography-based surgical
stents and computer-aided planning date back to 1980-1990 [110,111]. Modica
et al. in 1991 developed a complex *in vitro* model study design requiring many
repeated CT scans for planning and various intermediate analog steps, in which
they evaluated the accuracy of the pilot drill osteotomy and were among the
first to publish on the guidance accuracy (horizontal error ranging from 0–1.5
mm, angular – 0–4 degrees) and emphasized the importance of guide stability
to avoid errors [112]. Considering the contemporary scientific perspective, this
study exhibited a significant risk of design bias, employed measurement tools
with limited precision, and possessed minimal clinical applicability. Due to the

lack of advanced and precise technologies, these limitations understandably led to low satisfaction among surgeons and created communication tensions with prosthodontists that persisted for several decades [113]. Early scientific papers provide evidence that the pursuit of enhancing collaboration between prosthodontics and surgery is of a longstanding nature [114].

1.2.2. THREE-DIMENSIONAL RADIOLOGICAL IMAGING AND PATIENT SAFETY

As evident, the pivotal point of dental implantation planning lies in 3D X-ray imaging for the comprehensive visualization of anatomical structures [115,116]. In 1980-1990, the superiority of computed tomography (CT) for surgical procedure planning over two-dimensional x-ray examinations, such as orthopantomograms, was reported [116,117]. Despite the groundbreaking impact of the invention of CT on the field of medicine, recognized by Sir Godfrey Hounsfield's Nobel Prize in 1979, a significant limitation for its applicability remained the dose of X-ray exposure experienced by patients [118–120]. The effective dose, as defined in the International Commission on Radiological Protection (ICRP) system, is a dose quantity that accounts for the tissue-weighted sum of equivalent doses in specified tissues and organs of the human body and represents the stochastic health risk (principally cancer) associated with low levels of ionizing radiation to the whole body [119,121] Brenner and Hall (2007) have suggested that CT scans alone may account for approximately 1.5–2 % of all cancer cases in the United States [122]. Today, the standard CT effective dose for dentomaxillofacial applications is 474–1160 µSv [123]. Introducing CBCT substantially reduced radiation doses for the 3D imaging [124]. CBCT imaging technology was first presented to the European market in 1998 [125]. With the increasing prevalence of 3D X-ray imaging, it is imperative for healthcare professionals to continually enhance their understanding and proficiency in radiation exposure and safety [126]. Dental CBCT adult exposure (effective dose) depending on the size of the examined field (FOV) varies widely from 5 µSv to 1073 µSv and on average is distributed as follows (according to FOV height): 212 µSv (large, >15cm), 177 µSv (medium, 10–15 cm) and 84 µSv (small, ≤10 cm) [127]. Most radiation dose is allocated to the thyroid gland, as illustrated in Table 1.

Table 1. Distribution of mean effective dose components from large FOV CBCT imaging of adult phantoms [127].

Component	Distribution
Thyroid	37 %
Salivary glands	16 %
Bone marrow	9 %
Brain	5 %
Bone surface	3 %
Esophagus	2 %
Skin	1 %
Remainder	27 %

The main factor contributing to this variability is that contemporary CBCT devices typically offer low-dose and high-resolution modes, with effective doses varying up to 15-fold [128]. Furthermore, in recent years, a dose reduction in imaging through the ultralow dose CT demonstrated the potential to reduce effective doses to 22–123 μSv per jaw scan [129]. These radiation doses are relatively similar and comparably low to those used in CBCT. However, applying low- and ultralow-dose CT and CBCT in various diagnostic tasks still requires thorough clinical evaluation [129,130]. After assessing the complete spectrum of potential CBCT doses, it can be concluded that they are higher than conventional two-dimensional dental radiographs but lower than standard CT examinations [130]. Table 2 compares radiation doses more explicitly, offering detailed measurements and values for reference. Hence, the fundamental principle persists that the advantages derived from a radiological examination should outweigh the associated risks of radiation exposure to the patient [131]. It remains critical to carefully determine the field of interest and consider the tradeoff between the resolution and exposure whenever feasible [132].

The evaluation of CT accuracy should always consider the importance of patient safety, particularly regarding the dose. The fundamental technical limiting factor of CBCT is its beam geometry, resulting in inferior image quality compared to conventional CT [135]. As implied by its name, CBCT employs divergent X-rays that form a cone-shaped beam, as opposed to a traditional CT which is occasionally referred to as a fan-beam CT [136]. Cone beam computed tomography utilizes a reconstruction principle known as "back-projection," which involves applying specific algorithms (mainly based on the Feldkamp algorithm) to reconstruct a three-dimensional volume from a collection of numerous two-dimensional X-ray projections acquired in a cir-

cular trajectory around the target object [137,138]. These inherent factors and insufficiencies of the CBCT lead to artifacts in the resulting images, which is well-known truth within the technical community [136,139]. The general artifact-causing effects are related to relatively small FOV and hardware limitation due to the costs of large flat-panel detectors [136]. A limited field of view has the region of interest which is surrounded by unreconstructed tissue, and the measured "ray-sum" includes structures outside the FOV that are traversed by the "ray", but the back-projection process does not compensate for this [140]. High hardware costs prompt manufacturers to implement smaller flat-panel detectors positioned offset to the centre of rotation, resulting in a scanning process where the central part of the reconstructed volume undergoes a complete 360° rotation while peripheral locations are scanned over a 180° half-rotation, leading to the occurrence of ring artifacts in the axial planes due to the abrupt transition between these two regions [136]. Noise and scatter are often categorized as image-deteriorating and artifact-causing factors rather than being considered artifacts themselves [141,142].

Table 2. Reported adult effective doses.

	Mean effective dose, μSv	Range of reported effective dose, μSv	Modality
Mean annual background radiation [133]	3000	-	-
Spine CT [133]	6000	1500–10000	CT
Head CT [133]	2000	900–4000	
Paranasal sinus CT [134]	200*	-	
Dentomaxillofacial CT [123]	-	474–1160	
Ultralow dose dental CT	-	22–123	
Dental CBCT: [127]	-	5–1073	CBCT
Large FOV	212	46–1073	
Medium FOV	177	9–560	
Small FOV	84	5–652	
High resolution dental CBCT [128]	126	65–171	
Low dose dental CBCT [128]	8	4–11	
Panoramic radiography	10 [133]	7-90 [133] 10–50 [124]	2D
Intraoral radiography [133]	5	0.2–10	
Cephalometric [124]	-	4.5-10	

*Median instead of mean value reported as per the original publication

Noise represents itself in inconsistent attenuation (grey) values in the projection images, and due to the lower signal-to-noise ratio compared to CT scans, CBCT images typically exhibit a high level of noise, which is expected [136]. Scatter in CBCT occurs when X-rays deviate from their intended path due to interactions with matter, and the use of larger area detectors increases the probability of capturing scattered photons, making CBCT machines more prone to image degradation caused by scattered radiation compared to highly-collimated fan-beam CTs [136,143]. Other commonly reported types of CBCT artifacts are presented in Table 3.

Table 3. Characterization of CBCT-associated artifacts [136].

Type of artefact	Reason of appearance	Appearance on image
Extinction artefacts	Highly X-ray absorbing object (metal). The signal detected in the pixels behind that material could be nearly or of zero value.	Termed as "missing value artefacts" – dark, empty area.
Beam hardening artefacts	Highly X-ray absorbing object (metal). An x-ray beam containing a range of energies passes through an object and undergoes selective attenuation of lower energy photons, leaving only higher energy photons remain to contribute to the average energy value, thus it increases (hardens).	Darks streaks/ bands.
Partial volume effect and exponential edge gradient effect	Effect appears at sharp edges with high contrast to neighboring structures.	Sharp long margin edges in the periphery of volume appears divergent and with streaks losing the precision.
Aliasing artefacts	Under-sampling due to the size of the detector elements and divergence of the cone beam	Line patterns (moire patterns), diverging from the centre to the periphery.
Ring artefacts	Due to the circular trajectory and the discrete sampling process.	Concentric rings centred around the location of the axis of rotation – most prominent in homogeneous media.
Motion artefacts (misalignment artefacts)	Misalignment of any of the three components: source, object, and detector.	Presents as double contours, blurred image.

As supported by scientific evidence, the advantageous lower radiation exposure offered by CBCT is counterbalanced by the inferior image quality, artifacts, and correspondingly reduced accuracy compared to conventional CT [144]. While most of these errors are inherent to the cone beam principle from a technological standpoint, significant efforts are dedicated to developing digital post-processing algorithms to lower some of these inaccuracies [136,145]. The requirement for high computing power limits the incorporation of specific algorithms in commercial devices [146]. Nevertheless, this constraint has been progressively reduced, along with the decrease in volume reconstruction time, thanks to the rapid advancements in computer technology observed over the past two decades [146]. Certain algorithms likely demonstrate successful performance, as indicated by scientific studies that highlight visually reduced perceived inaccuracies of metallic nature in CBCT images compared to conventional CT [147,148]. It cannot be true from a mathematical and technological standpoint; despite potential compensations through various means, CBCT inevitably possesses more distortions, as some cannot fully compensate by algorithms [136]. It is crucial to highlight that precision in patient positioning plays a significant role [149]. Ensuring that the area of interest is accurately centred within the scanned volume helps to minimize image distortions and improve measurement accuracy [149]. This is particularly important as the highest inaccuracies are typically observed at the periphery of the volume [149]. Regarding diagnostic sensitivity, the centre of the FOV demonstrated the highest values [150]. In contrast, the lowest values were observed in images acquired specifically at the posterior region, particularly when acquired with a low-resolution [150]. Unfortunately, alternative approaches to enhance the accuracy of CBCT images are constrained by either the high costs of hardware (limited by market laws), or by the increase in patient exposure (effective dose) through "high-resolution" scanning, neither of which represents a viable solution [128,136].

In comparison to CT, CBCT exhibits additional clinically relevant limitations. One of these is the absence of Hounsfield unit measurements in CBCT – at best, CBCT can provide an approximation of pseudo-Hounsfield units, but it still lacks comprehensive scientific validation [151]. Another limitation is the inadequate soft tissue contrast and lower clarity of the bone-soft tissue margin [149,152]. Dusseldorp et al. (2017) conducted a cadaver study to evaluate the influence of soft tissue presence on CBCT measurements of hard tissues, finding it to be below the clinically significant threshold of

1 mm [153]. However, the study also reported that the accuracy of CBCT may not meet the requirements for applications where high precision is of utmost importance.

The resolution of a scan is frequently connected with the size of the voxel, where a voxel serves as the volumetric equivalent of a 2D pixel [154]. The dimensions of a voxel are determined by its height, width, and depth; in CBCT, these are typically isotropic, where all three parameters are equal [125]. Voxel size and resolution exhibit an inverse relationship in which smaller voxels correspond to higher resolution, while larger voxels result in lower resolution. Nevertheless, voxel size in many CBCT units is also linked with the FOV, and opting for a smaller voxel size may inadvertently lead to increased dose due to heightened exposure [128]. Thus, combining a large FOV with high resolution (small voxel size) is seldom possible, as high-resolution imaging is typically employed for small FOVs [128]. Moreover, as the size of the FOV increases so does the scanning time and effective dose for the patient proportionally increase [127,128]. Niktash et al. (2022) provided evidence using five CBCT machines that decreasing FOV and voxel size (leading to increased resolution and radiation dose) yielded the best contrast-to-noise ratio; however, variations in exposure parameters among machines with the same FOV resulted in differences in image quality [155]. Including high-resolution scans in large FOV scenarios increases the exposure levels, reaching the upper limit within the range for CBCT and closely approaching those typically associated with conventional CT scans [124,127]. On the contrary, images obtained with smaller voxel sizes, while visually subjectively more appealing and sharper, may yield equivalent diagnostic results compared to lower-resolution images [154,156,157]. Damstra et al. (2010) evaluated CBCT measurements using scans with voxel sizes of 0.25 and 0.4 mm, comparing them to actual reference object measurements: both voxel modes demonstrated complete accuracy [158]. Some studies have reported that voxel scans with a size of 0.25 mm exhibit greater accuracy in directly measuring bone compared to 0.4 mm scans [159]. However, other research indicates no significant differences in measurement accuracy between voxel groups of 0.125 and 0.4 mm, or between voxel groups of 0.2, 0.25, 0.3, and 0.4 mm [160,161]. Measurement error values obtained from these studies are presented in Table 4. The absence of a well-defined protocol for choosing CBCT as a diagnostic tool is frequently attributed to a scarcity of evidence-based data regarding its added value in various clinical cases [154].

Table 4. Data from the studies comparing measurement error in CBCT images with different voxels and directly on the dry cadaver jaws. Mean errors and standard deviations (SD) are reported when available in the original studies.

Study	Voxel size, mm	Lowest mean error ± SD, mm	Highest mean error ± SD, mm
Sun et al, 2011	0.25	0.2 ± 0.4	0.5 ± 0.8
	0.4	0.4 ± 0.5	0.9 ± 0.8
Patcas et al, 2012	0.125	0.34 ± 0.5	0.37 ± 0.43
	0.4	0.54 ± 0.46	0.7 ± 0.84
Torres et al, 2012	0.2		
	0.25	0.68	0.72
	0.3		
	0.4		

Tanaka et al. (2021) conducted a comparative analysis of CBCT and histological measurements of buccal bone thickness and indicated that CBCT exhibited a significant overestimation of buccal bone thickness; the sensitivity of CBCT as a diagnostic tool to detect the presence or absence of buccal bone was reported to be 75 %, with a specificity of 66 % [162]. This was also illustrated by a laboratory pig jaw study demonstrating the inaccuracy of CBCT in measuring buccal bone thickness near the implant, particularly when the actual thickness was 1 mm or less [163]. According to Vanderstuyft et al. (2019) cadaver study, it was reported that CBCT is unable to detect buccal bone thickness of 0.3 mm adjacent to the implant, and the following zone of 0.45 mm is considered doubtful, resulting in a total of 0.75 mm zone of buccal bone thickness with poor accuracy in measurement [164]. Cook et al. conducted a cadaver study to assess the impact of different CBCT scan settings (long, standard, short) on buccal bone measurements [165]. They found that measurements obtained through CBCT were equally accurate compared to direct measurements [165]. Based on the available data, high-resolution scanning does not provide significant additional value in linear measurements of the jaws or evaluation of buccal bone at the teeth and implants. Therefore, lower quality and lower effective dose CBCT scanning options may be recommended for these specific purposes. Moreover, CBCT has limited utility in accurately evaluating buccal bone thickness near teeth or implants when the thickness is less than 0.75-1 mm.

Regarding computer-guided implant planning, CBCT was reported to be of equivalent value to CT while simultaneously reducing patient exposure to radiation [166]. Similar findings have been reported in the context of craniomaxillofacial image-guided surgery, where both methods CBCT have been shown to overestimate anatomical truth below 1 mm [167]. These results suggest that CBCT represents a valuable alternative to CT in this field. Upon evaluating low-dose and standard CBCT scans, it was reported that both scans yielded comparable outcomes regarding guided implant placement results [168]. In addition, Horsch et al. have reported the satisfactory application and accuracy of low-dose CBCT in the guided implantation [169]. With respect to dynamic guidance, the CBCT group exhibited superior outcomes in terms of implant placement accuracy when compared to the conventional CT group [170]. In general, European guidelines differ from American guidelines concerning the application of CBCT in the implant dentistry diagnostics [171]. The European Association for Osseointegration suggests the potential use of CBCT for treatment planning in the subsequent clinical scenarios: when standard examination and radiography are insufficient in visualizing relevant anatomy, aiming to minimize risks to important anatomical structures; in borderline situations with limited bone available; for implant positioning, aiming to optimize biomechanical, functional, and aesthetic outcomes [172]. These guidelines are in accordance with the application of CBCT for digital planning and guided implant surgery. According to the position statement of the American Academy of Oral and Maxillofacial Radiology, it is recommended to begin with panoramic and intraoral imaging as the primary imaging method; however, preoperative planning should also use cross-sectional imaging such as CBCT [173]. In this regard, American guidelines recommend using CBCT for dental implant treatment planning in all cases. It is evident that the use of CBCT in clinically indicated situations for guided implantation is justified from a rational perspective, and the application of low-dose protocols appears to be adequate in most cases.

Upon comprehensive assessment of CBCT indications associated with dental implantation, it is crucial to acknowledge that implant planning frequently constitutes a component of a broader treatment plan encompassing various dental team specialists, some of whom may necessitate X-ray examination based on their respective roles. For the extraction of mandibular third molars, in cases where the proximity to the inferior alveolar nerve canal is a concern, CBCT could provide more information than a panoramic X-ray [171]. Still,

the risk of complications remains unchanged [171]. Therefore, the primary recommendation (European Academy of DentoMaxilloFacial Radiology) is panoramic radiography, reserving CBCT for highly specific questions in individual cases [174]. In orthodontics, a small FOV is recommended [171]. The British Society of Orthodontics has included guidelines regarding the use of CBCT in cases where standard radiographs are insufficient or due to the proximity of adjacent sensitive structures: unerupted maxillary canines; dilacerated teeth; removal of unerupted or supernumerary teeth; imaging of clefts for grafting [175]. While CBCT has also been evaluated for its potential in dental caries diagnostics, it is not the preferred choice, as dental bitewing radiographs are deemed the most appropriate examination [171]. Two-dimensional radiography is generally favoured as the primary choice for periodontal diagnostics as well; however, the rationale with additional diagnostic value for using CBCT to assess complex bony defects in the molar regions (particularly in maxillary molars with furcation involvement), especially in the context of surgical treatment, has been indicated [176]. However, the American Academy of Periodontology suggests a broader range of clinical scenarios for the use of CBCT in the diagnosis of periodontitis and periimplantitis, including endo-perio lesions, cases unresponsive to localized periodontal therapy, the proximity of sensitive anatomical structures [177]. Compared to other disciplines in dentistry, the effectiveness of CBCT in diagnosing endodontic pathology is more frequently subjected to systematic review: while it exhibits an advantage over 2D radiographs in diagnosing apical periodontitis [178,179], its average sensitivity (72–78 %) and specificity (75–79 %) in detecting external root resorption and vertical root fractures are relatively low [180,181]. However, when it comes to apical periodontitis, dental radiographs are regarded as the preferred diagnostic method, and the use of CBCT should only be contemplated when there is a discrepancy between a patient's persistent symptoms and traditional diagnostic approaches [182]. The European Society of Endodontology has released a position statement regarding using CBCT in endodontics. They propose that small-volume scans are potentially appropriate in certain situations, such as evaluating and treating dentoalveolar trauma, assessing intricate root canal systems and anatomical structures before endodontic therapy, and retreatment therapy [171,183]. Additionally, CBCT may be beneficial in assessing endodontic complications like perforations and determining appropriate treatment for clinically observable root resorption [171,183]. While CBCT aids in enhancing diagnostic accuracy

for certain dental trauma cases, the implications for decision-making and patient-centred outcomes remain uncertain [171,184]. Therefore, CBCT should be employed only when two-dimensional radiography proves inadequate for the treatment selection [184]. CBCT can be employed as a diagnostic tool for facial traumas in situations where the evaluation of soft tissues is not required (in such cases, conventional CT is preferred); however, the reported impact of CBCT on treatment management is around 10 % or even lower [171]. Finally, CBCT has demonstrated favourable diagnostic efficacy in detecting changes related to sinus diseases as with conventional CT, except for evaluating soft tissues [185]. Likewise, for bone-related temporomandibular joint changes, an assessment of soft tissues should be conducted using magnetic resonance imaging (MRI) [171]. Gaining a comprehensive overview of all relevant fields, facilitates an improved comprehension of the risk-benefit ratio in the selection and rationale behind the utilization of X-ray imaging.

In the year 2020, a proof of concept was presented in case series wherein dental magnetic resonance imaging (MRI) was showcased as a viable alternative to CT/CBCT for the purpose of digitally planning guided implant placement [186]. Despite the absence of radiation usage in its medical imaging technologies, magnetic resonance imaging (MRI) is considered a component of radiology. Radiology is a specialty that uses X-rays and other forms of radiant energy to diagnose and treat disease. MRI is more advantageous in its ability to evaluate soft tissues. Its high cost and long scan time limited its applicability in dentistry for a long time [187]. Hilgenfeld et al. (2020) conducted an evaluation of the accuracy of the workflow involving dental MRI in guided implant surgery and reported that it demonstrated sufficient precision for the intended purpose [188]. Despite the potential advantages of MRI as an ionizing-radiation-free imaging technique in dentistry, its application in the field is still in its early stages. The use of MRI as an alternative to traditional radiography (CT or CBCT) in dental imaging is a novel concept that requires further research to determine its accuracy and effectiveness in implant planning, execution, and follow-up before it can be considered a reliable diagnostic method for dental clinicians [189].

In conclusion, the introduction of 3D radiographic imaging, particularly cone-beam computed tomography (CBCT), has been pivotal in laying the foundation for precise guided dental implantation. CBCT inherently exhibits a higher susceptibility to artifacts and inaccuracies when compared to conventional CT imaging. However, the paramount importance of patient

exposure and radiological safety has formed the basis for integrating CBCT examinations into dental practice. Additionally, low-dose scanning modes, which sacrifice resolution to some extent, often prove adequate for diagnostic and planning purposes. It is crucial to acknowledge that CBCT represents a fragmented (voxelized) representation of a continuous living human object, thereby introducing scientifically documented submillimetre-scale errors compared to reality. This aspect will hold significant importance in interpreting the deviations observed in digital planning and guided implant placement, and identifying their underlying sources. Notwithstanding the need to carefully assess radiation exposure's potential risks and benefits, CBCT remains a critical tool in dental implant planning. Moreover, it has indications and benefits in other domains like orthodontics or endodontics, emphasizing the importance of involving the entire dental team in its utilization and decision-making process.

1.2.3. THREE-DIMENSIONAL ORAL SURFACE IMAGING

The initial introduction of the intraoral scanner (IOS) dates back to 1980, when it was integrated into the developing CEREC® system (Sirona Dental Systems GmbH, Bensheim, Germany) [190]. Before that, since the eighteenth century, conventional impression techniques have been employed to record the three-dimensional geometry of dental tissues; however, these methods are susceptible to errors caused by volumetric changes in impression materials and the expansion of dental stone, which often necessitate compensation by the laboratory work [191]. Hence, one of the primary objectives of IOS was to improve accuracy and minimize the errors associated with conventional impression techniques [192]. The integration of the IOS device in dental practices coincided with the development of CAD/CAM technology in dentistry, providing numerous advantages for practitioners related to: reduced operative time, storage needs and overall treatment duration; enhanced treatment planning, case acceptance, communication with laboratories [193,194]. The historical development of IOS, which has significantly accelerated in the last decade, has resulted in the evolution of highly sophisticated and complex technologies that provide dentists with valuable advantages, including improved accuracy, especially digital implant planning and computer-guided surgery.

Each scanner hardware consists of three primary components: a mobile workstation to facilitate data entry, a computer monitor for user interface and

reviewing digital files, and a handheld camera device to capture scan data within the patient's oral cavity [195]. These devices are integrated via software [196]. Irrespective of the acquisition technology employed, IOS project light to capture individual images or videos, which are subsequently analysed by software to identify points of interest (POIs) and generate the 3D impression [197]. The software algorithms are crucial in defining POIs, identifying corresponding POIs across multiple images, and seamlessly combining them to create the digital intraoral impression [197]. Furthermore, the scan data undergoes processing and optimization to minimize file size while enhancing detail and resolution in specific regions indicated as significant by the software. The measurement speed, resolution, and accuracy of the scanner are determined by the technology used to capture surface data, resulting in six distinct main imaging technologies [195,196]:

1) Triangulation measures the angles and distances from known points by projecting laser light. By knowing the distance between the laser source and the sensor, and the angle, the system can calculate the angle of reflection as light bounces off the object. Using the Pythagorean theorem, the system determines the distance from the laser source to the object's surface. A thin layer of opaque powder is applied to the target tissue to ensure consistent and predictable light dispersion. This powder helps optimize the scanning process by facilitating accurate measurement and capturing detailed information.

2) Parallel confocal imaging utilizes laser light through a filtering pinhole onto the target tissue. The sensor is positioned at the confocal imaging plane, ensuring it is focused relative to the target. A small aperture in front of the sensor blocks any light from above or below the focal plane. This selective blocking allows only the focused light reflected off the target tissue to re-enter the filter and reach the sensor for further processing. By eliminating out-of-focus light or "bad data," the parallel confocal imaging technique enhances the accuracy of the scan. In a parallel confocal system, the object is tomographically sliced, and thousands of these slices are seamlessly combined through "point-and-stitch reconstruction" to generate a comprehensive picture of the scanned area.

3) Optical coherent tomography (OCT) is an interferometric imaging modality, that offers cross-sectional images of the subsurface microstructure of target objects, such as biological tissues [198]. In an

OCT scanner, the interferometer divides a broadband source field into a reference field (Er) and a sample field (Es). The sample field passes through the scanning optics and objective lens, focusing on a specific point beneath the tissue surface. The altered sample field (Es'), which scatters back from the tissue, interferes with the reference field (Er) at the surface of the photo-detector.

4) Accordion fringe interferometry (AFI) employs two light sources to project three distinct fringe patterns onto the teeth and surrounding tissues [199]. When a fringe pattern interacts with the surface, it undergoes distortion and assumes a new pattern based on the unique curvature of the object. This distortion in the fringe pattern is known as "fringe curvature." High-definition (HD) video cameras, positioned at approximately 30° offset from the projector, capture surface data points of the fringe curvature. The differential measurement of the fringe patterns allows for precise distance calculations, which remain unaffected by variations in tooth colours and materials. By leveraging these precision optical measurements, AFI enables accurate and reliable distance measurements in intraoral scanning.

5) Active Wavefront Sampling (AWS) utilizes a single camera and an AWS module [200]. In its basic configuration, the AWS module consists of an off-axis aperture that moves along a circular path around the optical axis. This movement causes the target points on the image plane to rotate in a circular pattern. The depth information of the target points can be obtained from the radius of the circular point pattern created by each point (blur-circle radii generated by the rotating AWS module). AWS imaging allows any system with a digital camera to operate in 3D, eliminating the need for multiple cameras to capture 3D geometries.

6) The three-dimensional in-motion video employs a high-definition (HD) video camera equipped with trinocular imaging, which consists of three miniature cameras positioned at the lens. These cameras capture three precise views of the tooth. Behind the cameras, a complementary metal-oxide semiconductor (CMOS) sensor converts the incoming light energy into electrical signals. The distances between two data points are calculated simultaneously from two different perspectives, allowing for the determination of accurate 3D data. These data are captured in a continuous video sequence and processed in real-time to generate a dynamic model of the scanned object. While a light dusting

of powder is required to capture surface data points, it is significantly less than the thicker coating necessary for triangulation-based methods. This technology facilitates efficient and real-time 3D imaging without compromising the accuracy of the scans.

In order to reduce the noise encountered during intraoral scanning, such as noise originating from the optical features of the target surfaces, as well as factors like wetness and random relative motions, these devices employ a combination of multiple imaging techniques quite commonly [200]. In recent years, a growing number of non-contact optical acquisition technologies have been implemented by various manufacturers in the handheld cameras of intraoral scanners [200,201]. While the six technologies discussed earlier are well-known and provide a general understanding of the underlying technology concept, it is important to note that there are more emerging technologies in this field [202]. Understanding the key principles that underlie these technologies is important to make informed clinical decisions and choosing the optimal IOS device that aligns with the practitioner's specific requirements [196]. Recent studies have demonstrated that digital impression techniques, particularly those utilizing confocal or AWS technology, offer advantages over conventional impression methods, including improved efficiency, reduced preparation and retake time, enhanced comfort, and greater patient satisfaction, making them a preferred choice for implant impressions [203,204].

Advanced IOS acquisition technologies are accompanied by even more complex reconstruction processes. The measurement of distances between distinct pictures can be achieved by using an integrated accelerometer within the camera; however, the determining the image's point of view is more commonly accomplished through similarity calculations [196]. By employing algorithms, these similarity calculations establish POIs that coincide across various images [205]. These POIs can be identified by detecting transition areas, including prominent curvatures, physical boundaries, or variations in the grey intensity [206]. Subsequently, a transformation matrix is computed to assess the similarity among all images, encompassing factors like rotation or homothety. Outliers may be statistically removed to reduce noise. The projection matrix extracts the coordinates (x, y, and z), generating a file accordingly [196]. The term "mesh" is used and it refers to a digital representation of the scanned surface, typically composed of interconnected smaller discrete cells triangles or polygons. The predominant digital format employed is the STL (Standard Tessellation Language), which is already

used in many industrial fields [207]. It represents a series of triangulated surfaces, each triangle defined by three points and an outward normal [208]. Nonetheless, alternative file formats have been devised to capture additional attributes of dental tissues, such as color, transparency, or texture, such as the Polygon File Format (PLY) [209].

When considering the quality and accuracy of scans obtained using an IOS, the practical execution of the scanning process by the dentist holds significant importance alongside the underlying technology and reconstruction techniques. Different intraoral scanning technologies, have varying hardware specifications, with some devices being preferred over others based on clinical experiences: e.g., confocal and AWS technologies handheld cameras are relatively large in size [194]. Familiarity with the ergonomics and software of each intraoral scanner contributes to operator preferences and learning curves [210]. A study comparing two scanners with the same confocal technology found that while scanning time decreased with training for both devices, one consistently had a shorter average scanning time than the other [211]. Software, powdering, and scanning path also influence handling time during the digital impressions [196]. Scan path is a specific movement of the IOS camera required during the scanning [194]. By adhering to a recommended specific movement pattern, the accuracy of the virtual model can be enhanced [212]. Standard recommendations include: positioning the scanned object at the centre of the acquisition area, fluid movement and steady distance (5–30mm), which can be challenging during axis changes (anterior-posterior) or in cases of tooth malposition [200]. Each manufacturer offers guidelines regarding the scan path, affecting the stability of the software's tracking [196]. Deviations from the recommended scan path or improper maintenance of the distance to the object can lead to loss of tracking during the impression process, resulting in software instability. Rapid or erratic movements of the IOS camera by practitioners often contribute to this issue. Manufacturers are developing strategies and software algorithms to address tracking loss during scanning by recognizing the saved geometry of the object, allowing practitioners to perform a rescan in a meaningful area without remaining stationary and providing sufficient information to the camera and software for rematching the previous POIs and completing the missed area [213]. To ensure adequate information for the software in case of tracking loss, it is important to adhere to a scan strategy that begins with areas that are easy to recognize, such as the occlusal surfaces of posterior teeth [196]. Additionally,

in the practical use of IOS, reflective surfaces in dental tissues pose challenges in achieving accurate point matching [214]. Techniques such as changing the camera orientation to increase diffuse light or using cameras with polarizing filters can help overcome this issue [215]. Additionally, some systems require a powder coating during scanning to reduce reflectivity, although this may cause patient discomfort and increase scanning time [216]. Overall, the effect of powdering on scan accuracy is not clearly differentiated in the literature [196]. Finally, it is important to consider certain basic factors during intraoral scanning: patient movement, which may inadvertently result in scanning peripheral soft tissues (e.g., tongue, buccal mucosa); the presence of blood, saliva, or gingival fluid can also distort the acquired image [206].

As the intraoral scanner software can generate files with different mesh densities, the significance of this feature is discussed. A high mesh density for the entire tooth may not be necessary due to the computational time required, but it is typically employed in areas of high curvatures such as the incisal edge or gingival sulcus [196]. Variations in mesh quality were observed among different intraoral scanning systems and lighting conditions, with photographic scanning techniques generally yielding higher quality meshes compared to video-based scanning technology [217,218]. Among the systems evaluated, TRIOS 3 demonstrated the highest consistency [217]. Also, it has been suggested that utilizing a chair light at an illuminance condition of 10,000 lux is recommended to optimize the mesh quality for this IOS system [218]. However, caution must be exercised when interpreting the data presented in the literature, as preparing and publishing scientific articles often takes time, while manufacturers frequently release updated and more advanced software for mesh construction [219].

The accuracy of IOS technologies is a topic of frequent discussion and investigation in the scientific literature [197,201,220]. According to ISO 5725, the accuracy is described by two measurement methods: trueness and precision [221]. Trueness is the extent of agreement between the average of tested results and the true or accepted reference value. Meanwhile, precision refers to the degree of agreement or consistency among test results [196]. According to both *in vitro* and *in vivo* studies, IOS technology has exhibited high accuracy [201,220,222]. In a model study, when comparing various scanners, the trueness and precision of their measurements exhibit a range from 49 ± 2 μm and 20 ± 3 μm to 106 ± 23 μm and 75 ± 44 μm [220]. Clinical studies often exhibit greater deviations compared to model studies, as evident

from the oldest study conducted in 2014, which showed the highest deviation of 1000 ± 650 μm; however subsequent studies reported data within the range of 360 ± 46 μm to 40 ± 20 μm [223]. Despite early concerns regarding the accuracy of IOS in full-arch implant scans, a recent review has shown that linear accuracy is superior to conventional impressions (mean deviations of 137.86 μm and 182.51 μm respectively) [222]. Most scanners achieve the acceptable clinical threshold of linear accuracy, typically set at 200 μm [222]. The accuracy of intraoral scanning for fully edentulous arches is influenced by various factors including the type of intraoral scanner used, the scanning technique employed, environmental conditions, implant angulation and spacing, and the material of the scan bodies [224]. The findings favoured a temperature range of 20–21 °C, air pressure 750–760 ±5 mmHg, air humidity of 45 %, implant angulation of up to 15 degrees and a spacing of 16–22 mm, as well as PEEK material for the scan body [224]. Of significance, it should be noted that the accuracy of the tested IOS was negatively affected by cutting-off and rescanning procedures, with a decrease in accuracy observed as the number and diameter of the rescanned areas increased [225,226].

Although less clinically relevant, an extraoral scanning method can be employed to acquire a three-dimensional image of the oral tissue surface. It necessitates using a laboratory (desktop) scanner and conventional impression to directly transfer the information, which introduces analog-related errors [227]. Kang. et al. in a model study (2019) compared 2 laboratory scanners and 5 IOS and concluded that laboratory scanners showed the highest accuracy (14.3 ± 0.3 μm), though this data clinically is not relevant as the model was scanned directly without taking an impression [228]. Subsequent studies by other researchers have likewise demonstrated minimal errors of laboratory scanners in model studies, with these inaccuracies considered clinically insignificant [229]. The majority of studies conducted on desktop scanners consistently report their high clinical accuracy, with some scanners even approaching the precision levels of industrial scanners, achieving a precision of 3–4 μm and trueness of 12–13 μm [230]. Kiatkroekkrai et al. (2019) demonstrated no significant difference in accuracy between guided implantation performed using IOS and impression + laboratory scanner methods [231]. Some studies have provided evidence supporting the accuracy of CBCT in the digitalization of dental plaster casts, thus enabling the utilization of their surface information [232,233]. These studies demonstrated trueness ranging from 0.09 to 0.15 mm and a precision of 0.05 ± 0.03 mm

for this method. The disadvantage of using CBCT, similar to a laboratory scanner, is that certain inaccuracies may arise due to impression techniques, plaster cast techniques, and material properties. These factors can potentially impact the quality and reliability of the CBCT scans. The notable precision demonstrated by laboratory scanners renders them suitable for facilitating the transition from analog to digital in treatment planning processes, particularly when IOS is unavailable.

A clinical trial with a one-year follow-up comparing the static guided implant positioning through the workflow using (a) laboratory scanner and (b) IOS was conducted by Cristache et al. (2021) evaluating the accuracy, labour-time and patient-reported outcomes [234]. Notably, the IOS group exhibited significantly higher implant placement accuracy compared to the laboratory scanner group, with both groups demonstrating clinically acceptable mean deviations for entry point (0.44 mm and 0.85 mm), implant apex (1.03 mm and 1.48 mm), angular deviation (2.12° and 2.48°), and depth deviation (0.45 mm and 0.68 mm) [234]. However, regarding clinical outcomes, there were no implants lost, no mechanical or biological complications, and the bone loss was minimal (0.01–0.11 mm), which was not statistically significant between groups. Patient satisfaction tended to be higher in the IOS group, along with a significantly shorter overall workflow time, as impressions and laboratory scanning took more than 2 hours (due to disinfection, transportation and pouring gypsum models), whereas IOS scanning required approximately 20 minutes [234]. This well-conducted study clarifies the rationale behind the clinical preference for the workflow employing IOS instead of impressions + laboratory scanners.

Awareness of the limitations of CBCT in capturing soft tissues and elaborately depicting tooth geometry due to low spatial resolution highlights the importance of precise surface imaging for comprehensive treatment planning. In particular, the rapid advancement of sophisticated optical technologies has led to the emergence of increasing precision intraoral scanners – a trend supported by scientific research. When assessing the scientific data regarding the accuracy of IOS, careful consideration should be given to factors such as study design, novelty (due to rapid clinically applicable advancements), and technological, environmental, and case-specific variables.

1.2.4. THREE-DIMENSIONAL IMAGE DATA MERGING

The integration of advanced and precise 3D technologies, including CBCT and IOS, has revolutionized the field of dentistry, especially prosthodontics,

by transforming treatment workflows, improving diagnostic capabilities, and optimizing clinical outcomes [7]. CBCT provides detailed three-dimensional imaging of the patient's anatomy, including bone structure and adjacent structures, while IOS captures the surface topography of the oral tissues with high precision. The fusion of CBCT and IOS data is software-dependent, necessitating careful considerations to ensure accuracy. In scientific literature, merging intraoral scans and CBCT images can be referred to using various terms, including superimposition, registration, fusion, alignment, integration, image stitching, and image overlay. This variability in terms can indeed complicate the review of the literature.

Dental CBCT segmentation is an important step in computer-aided procedures, as it allows for the generation of approximate outlines of uncertain regions, providing distinct features that enable differentiation between tooth tissues and other surrounding tissues [235]. In 2008, an automated segmentation process was described, demonstrating the technique's effectiveness in automatically classifying teeth [236]. Since then, multiple automated methods have been developed, applying various techniques in CBCT image analysis, including diverse filters, thresholds, algorithms, and other computational approaches to enhance the segmentation process [237]. In recent years, the employment of AI and deep learning has been prominent for the segmentation of CBCT images due to their high reported accuracy (0.56±0.38 mm) and significant time efficiency, being reported as 500-1800 times faster than the time required by an expert [238,239]. A recent systematic review (2023) on this topic indicated that thresholding was deemed unreliable for tooth segmentation from CBCT images, while convolutional neural networks (CNNs) emerged as the most promising approach [240]. Achieving precise delineation of teeth and bones from CBCT images is essential in digital dentistry to ensure accuracy during image merging [238].

Moreover, there is a scarcity of scientific literature regarding the acquisition settings of CBCT and the accuracy of merging it with intraoral scans (IOS). Regarding the FOV of CBCT and the merging process, it has been demonstrated that a larger FOV does not improve registration accuracy [241]. However, in scenarios with artifacts or multiple missing posterior teeth, adhering to a larger FOV is recommended. Contrary, Hamilton et al. (2022) reported that small FOV may lead to higher errors in IOS registration, the presence of sufficient well-distributed teeth within this limited FOV seems to reduce these errors [242].

The overall CBCT and IOS registration process aims to determine a transformation by taking advantage of the rigid anatomy of the jaws structures, and the partially overlapping areas of the tooth surfaces [243]. Multiple techniques have been employed to achieve registration using fiducial markers, including fabricating marker-containing devices, conducting dual CBCT scans, and performing post-processing steps for marker removal [244,245]. To simplify these procedures, alternative approaches based on virtual reference points were suggested, aiming to initially align two models and achieve a more accurate alignment by utilizing an iterative closest point (ICP) method [246–249]. The ICP method is a widely employed iterative registration technique that involves matching the closest points between two datasets and minimizing the distances between the paired points [243]. However, the ICP method heavily depends on proper initialization as it can easily get stuck in locally optimal solutions. Consequently, ICP-based methods often necessitate manual initial alignment by the user, which can be burdensome and time-consuming due to the need for manually clicking [243,250]. Becker et al. (2018) proposed that for a reliable registration, mmselecting a minimum of 10 points with a deviation below 0.5 mm is recommended, while noise exceeding 0.5 mm deteriorates the accuracy of the registration results [250]. Additionally, ICP registration may present challenges in achieving satisfactory results for patients with metallic objects or even numerous zirconia restorations [251,252]. Flügge et al. (2017) reported that more than 8 dental restorations resulted in average deviations of 1 mm for CBCT+IOS merging whereas up to 2 restorations exhibited a deviation of 0.36 mm [251]. Moreover, they observed an overall mean deviation of 0.54 mm, highlighting that the user and segmentation method had a significant impact, with default segmentation showing higher mean deviations (0.69 mm; maximum of 24.8 mm) compared to manual (0.4 mm; maximum of 9.1 mm) [251]. Another retrospective clinical study further supported this notion by demonstrating that the ratio of dental restorations has a notable impact on both the precision and time required for registering CBCT and IOS data [253]. Furthermore, in cases where there are numerous scattering (e.g., due to metal) the use of radiographic markers and fiducial markers was recommended as a potential practical solution [242,254,255]. In orthognathic surgery, the point-based superimposition of head CT scans with intraoral scans revealed deviations of up to 0.5 mm, which were deemed clinically acceptable; however, it should be noted that performing separate superimpositions for the lower and upper jaw could potentially result in a cumulative deviation of

1 mm, highlighting the importance of utilizing occlusal registration to ensure accurate alignment [256]. Surface-based registration provides another option instead of point registration, and although it has been reported to achieve acceptable accuracy, it requires expertise and training for optimal application [257]. Regarding static guided implant surgery, when comparing the fiducial registration method, surface-based registration exhibited higher inaccuracies in implant positioning, with a mean error at the implant platform of 0.83 ± 0.51 mm [258].

Recent studies suggest novel approaches based on deep learning implemented to automate the initial alignment process [259] and stitching error correction via individual tooth segmentation and identification [243]. Reported landmark and surface distance errors were 112 μm and 302 μm, respectively [243]. Interestingly, no significant advantage in registration accuracy was observed when comparing a deep learning-based platform with four different implant planning software using various registration methods (two point-based, one surface-based, and one manual registration software) [253].

Despite CBCT images not being the primary choice for surface rendering, several studies have suggested and evaluated them. Studies have affirmed that the primary concern associated with CBCT-based surface models is the presence of distortions induced by metallic or other restorations, thus indicating a requirement for artifact reduction techniques [260]. Hassan et al. (2010) evaluated the influence of CBCT scan FOV, mouth opening, voxel size, and segmentation threshold selections on the quality of the 3D surface models [261]. The quality assessment conducted by two examiners indicated a preference for the small or medium FOV, low voxel size, and open mouth scan [261]. In comparison to plaster models, modern high-resolution CBCT (0.16 mm voxel) has been suggested to yield precise surface models (0.102 ± 0.042 mm) *in vivo*, even when metal artifacts are present [262]. In contrast, dental MRI demonstrates lower accuracy (0.261 ± 0.08 mm) [262].

In some clinical cases, the fusion of two or more CBCT scans into a larger volume is applied. The accuracy of fusing two or more CBCT scans was found to be dependent on the largest voxel size of the scans, with the accuracy being approximately half the value of the voxel size (e.g., if the voxel size is 0.3 mm, the accuracy would be 0.15 mm) [149,263]. Conversely, Egbert et al. (2015) reported that the accuracy of stitched small FOV CBCT images, with a voxel size of 0.2 mm, yielded an average deviation of 0.34 ± 0.3 mm [264].

In conclusion, it is evident that in addition to the errors observed in the initial scans (CBCT and IOS), further errors arise from the merging technique employed for these scans, thus contributing to potential inaccuracies in the overall digital process. Therefore, when contemplating the errors resulting from data merging, it is crucial to acknowledge that the initial data was inherently subject to a certain level of inaccuracy, which can vary depending on the specific 3D technology employed, thus limiting the possibility of achieving absolutely accurate merging [265].

1.2.5. DIGITAL TREATMENT PLANNING

By merging bone anatomy-related volume (CBCT) with dental and soft tissue surface (IOS) a digital "patient" is created, thereby enabling digital implant planning through the specialized software. In 1993, the first software emerged, enabling the placement of virtual implants with precise dimensions on cross-sectional, axial, and panoramic views of CT images [266]. Various software options, including open-source alternatives, are available for digital implant planning, providing clinicians with diverse choices. These software applications enable clinicians to visualize and analyze bone anatomy-related data, integrate dental and soft tissue surface information, simulate prosthetic outcomes, perform virtual implant placement, and facilitate treatment planning. Although specific features and interfaces may differ, these software tools' fundamental concepts and purposes remain consistent across various options on the market.

Traditionally, prosthetic planning involved using plaster casts and conventional set-up (wax-up) techniques to aid in fabricating and visualizing the desired prosthetic restoration [267]. In terms of guided surgery, the analog workflow was done with the help of planning an implant-supported prosthesis involved fabricating a set-up on individual stone casts, transferring it to a radiographic splint with radiopaque teeth or sleeves, wearing the splint during CBCT for displaying the restoration, and subsequently modifying the splint for guided implant surgery [268]. It is evident that such an approach requires a significant amount of time, is more susceptible to human- and material-related errors at each stage, and is not fully integrated with the 3D anatomy of the bone, thereby limiting the clinical satisfaction of such a workflow. However, most digital planning software is open for integrating such a workflow [267]. Meanwhile some software working only based on a imported conventional prosthetic set-up with no other virtual option [267].

A virtual prosthetic set-up (wax-up) bypasses the requirement for an initial conventional prosthetic set-up and a radiographic splint, as all the necessary steps can be accomplished within the software [269]. Depending on the software used, the prosthetic set-up for each case can be created either individually (just a few systems available) or selected from a standardized library of teeth available within the software (majority of the systems) [267]. Alternatively, the virtual prosthetic set-up can be created individually using dental laboratory-based CAD software and imported into the implant planning software [270]. When employing a standardized library, the user can select from the available tooth options and subsequently make minor adjustments, particularly in size, to meet the approximated prosthetic information of this site [271]. Furthermore, a new method – a biogeneric design – was created that uses a mathematical algorithm and a library of different tooth shapes to design dental restorations automatically and it has already been integrated into some laboratory CAD software [272,273].

Depending on the functionalities of each software, it could incorporate and calibrate various supplementary data, improving the digital representation of the patient and enabling more precise case digitization. No implant planning software directly offers the capability to customize prosthetic elements; however, certain software platforms have integrations with external CAD programs for dental restorations [85]. One of the tools, particularly valuable for assessing aesthetics and involving patients in planning, is the virtual smile design [274]. Virtual/digital smile design is a CAD technology that creates virtual aesthetic simulations to assist dental practitioners in aligning and repositioning damaged or misaligned teeth in accordance with the appropriate facial features [85]. To accomplish this, either high-resolution dental photographs or 3D facial scans can be employed, the latter option is considered superior when it comes to evaluating aesthetics from different angles [275]. An innovative virtual simulation technology enables the direct overlay of visual 2D/3D facial data and IOS, allowing the proposed prosthetic design to be connected to this data as well [276]. Integrating facial scan and aligning it accurately poses challenges, thus developing new techniques such as using IOS-related implant scan bodies [277]. Nonetheless, there is a need for more user-friendly chairside applications for virtual smile design, as most of the existing software is difficult to use, time-consuming, unappealing for patient presentations, and challenging to integrate into the 3D workflow [276].

As virtual smile design is helpful in terms of aesthetics, likewise virtual articulators are available for functional evaluation of static and dynamic occlusion in the CAD software [267]. A virtual articulator is a computer software tool that can accurately replicate the inter-arch relationship and simulate the movement of the jaw [85]. Presently, two main types of virtual articulators exist: completely adjustable and mathematically simulated [278]. The first type is characterized by complexity and higher cost due to the electronic jaw registration system requirement and is not commonly found in clinical dental practices [278]. Another type of articulator, called a mathematically simulated virtual articulator, mimics jaw movements by using mathematical calculations to determine the paths of movement based on the settings on the articulator (e.g., e Bennett angle, horizontal condylar inclination, vertical occlusal dimension, etc.) [85]. The main drawback of mathematically simulated virtual articulators is their inability to capture and replicate personalized patient movements, but they are still widely used in dental CAD/CAM programs due to their user-friendly nature, low cost, and familiarity to dentists as a digital counterpart to commonly used semi-adjustable mechanical articulators [279]. Even though digital articulators are becoming more precise and are expected to have deviations in dynamic movements of less than 100 mm according to current evidence, utilizing the virtual articulator in conjunction with the mechanical articulator in complex cases involving alterations to the vertical dimension of occlusion is still recommended [280]. This combination allows for more comprehensive assessment and planning.

Upon evaluating the aesthetics and function of the patient, the next step following digital prosthetic wax-up is digital implant position planning. A CAD individualized or library-standard prosthetic set-up can be used for this case aligned with the IOS data. The IOS data is merged with CBCT. This allows for selecting the most favourable implant position based on prosthetic and anatomical constraints (Table 5) [267]. Regarding critical anatomical structures, the software assists in measuring distances, such as between implants (a minimum of 3 mm) and between implants and the inferior alveolar nerve canal (a minimum of 2 mm) [281]. This software typically generates a "safety zone" around the implant contour to ensure an appropriate plan relative to these structures [282]. Furthermore, the standard software also provides angular evaluation for multiple implants, including an automated implant parallelism option [283].

Table 5. Prosthetic and anatomical factors to be considered for the virtual implant planning [267].

Prosthetic factors	Anatomical factors
Final position of implant-supported prosthesis	Important structures: nerves, vessels, roots, nasal floor, sinus cavities
Crown morphology	
Occlusion	Bone quantity (horizontal, vertical)
Proximal contacts	Bone quality (cortical/cancellous)
Abutment design (pink-white aesthetics, emergence profile)	Contour/amount of soft tissue

Currently, there are numerous digital implant planning software options available. Most of these applications demonstrate high similarity in their core functionalities. However, according to a publication by Flügge et al. (2022), ImplantStudio (3Shape, Denmark) stands out with its exceptional integration of planning tools and functionalities (including external CAD software with options for virtual smile design as well as articulator) compared to other software solutions [267]. In addition, ImplantStudio has been demonstrated to have the most open library, having a wide range of implant systems with a total of 45 systems (as of 2020), surpassing other software options that typically support a lower number of systems, ranging from 1 to 26 [88]. In addition, it is beneficial for a library to encompass a variety of stock abutments, including angled options, to enable planning of angular implant placement in consideration of both bone quantity and prosthetic plan [284]. Nevertheless, it is important to acknowledge that these software applications undergo continuous development and updates, resulting in the addition of new functionalities and the inclusion of larger libraries [88,284].

In guided surgery, the software interface plays an essential role as a fundamental stage in digital implant placement planning. Nevertheless, in the present era, numerous alternatives exist with variations in their universality, functionality, integration capabilities with other software, and ease of use. While variations in additional features may exist, the fundamental core of the software remains largely consistent across different manufacturers. The virtual prosthetic set-up plays a pivotal role in determining the optimal positioning of implants within the bone, thereby contributing to the success of prosthetically driven guided implant surgery. This stage is essential for increasing the synergy between prosthodontics and surgery.

1.2.6. STATIC GUIDANCE AND ACCURACY

Static guidance systems are characterized as systems that transmit the predetermined virtual position of implants to the surgical site through a rigid surgical implant template or guide [285]. In 2002, the first software emerged, enabling digital implant planning and guide production for drilling implant osteotomies [266]. The five-year cumulative survival rates for dental implants placed using digitally-designed static surgical guides range from 94.5 % to 100 %, demonstrating comparable outcomes to the estimated general dental implant survival rate (95.6 %) over the same period [286]. An important consideration when evaluating published accuracy data is the study design, as the highest level of accuracy has been reported in the model *in vitro* studies, followed by cadaver studies, and finally clinical studies [25,287]. Despite the absence of significant differences in quality-of-life parameters and intra- or postoperative discomfort between guided and non-guided open-flap procedures, patients preferred computer technologies [288].

Guided implant surgery and static guides can be categorized according to various aspects (Fig. 2). First and foremost, it can be classified into distinct approaches: fully guided, involving both drilling and implant placement utilizing the guidance system, or partially guided, which involves the guidance system only for drilling and the implant is placed free-hand [289]. Partially guided surgery can be further divided into subcategories: either only the pilot drill or the full drilling sequence [290]. A non-computed category may also be included, assuming a guidance approach without a conventional digital planning [290]. Regarding static guides, they can be further categorized into subcategories based on the visibility and openness of the guide, specifically as open or closed guides [291]. Closed guides can be further divided into various categories based on sleeve systems, including: sleeve-in-sleeve, sleeve-in-sleeve with self-locking system, mounted sleeve-on-drill system, integrated sleeve-on-drill with metal sleeve in the guide system, integrated sleeve-on-drill without metal sleeve in the guide system [292]. Lastly, static guides can be separately categorized based on their support, including bone, mucosa, teeth, and mini-implants [25]. Furthermore, they can also be classified based on the presence or absence of pins, which are used to stabilize and fix the guide [25].
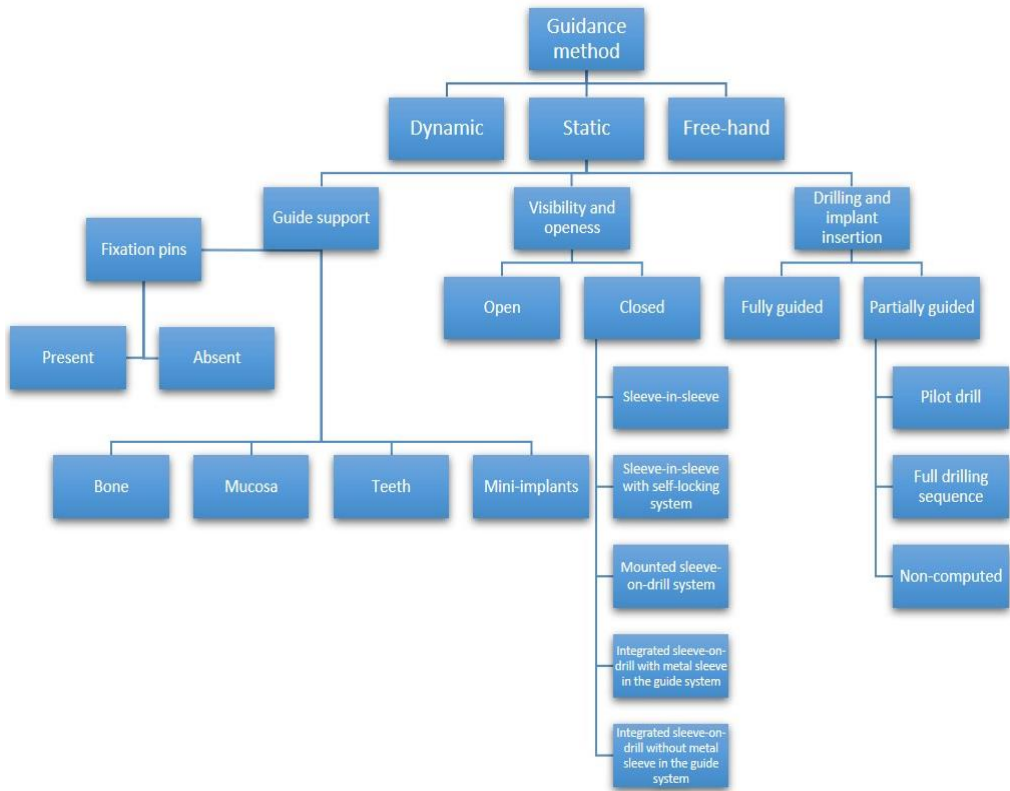
Fig. 2. Implant guidance surgery categories and static guidance subclassification.

Since a static guide is a physical template device, it necessitates production after the completion of virtual implant planning (Fig. 3). Surgical guides can be manufactured employing either subtractive (milling) or additive (printing) CAD/CAM rapid prototyping technology [266,293]. The subtractive method involves preparing a sleeve bed using a model and a laboratory-based guide-production device equipped with a drilling arm, necessitating multiple additional analog steps [266]. Ritter et al. (2014) reported the accuracy of pilot drilling for such guides to be in the range of 0.17–1.13 mm [294]. In the evaluation of CAD/CAM accuracy, it was found that a 5-axis milling machine exhibits superior accuracy compared to 3D printers, including a dental desktop stereolithography (SLA) printer, an industrial SLA printer, and an industrial fused deposition modelling (FDM) printer [295]. The accuracy of the printed model was influenced by the choice of printer, printing technology, and material used, with a dental SLA 3D printer using Bis-GMA polymer demonstrating
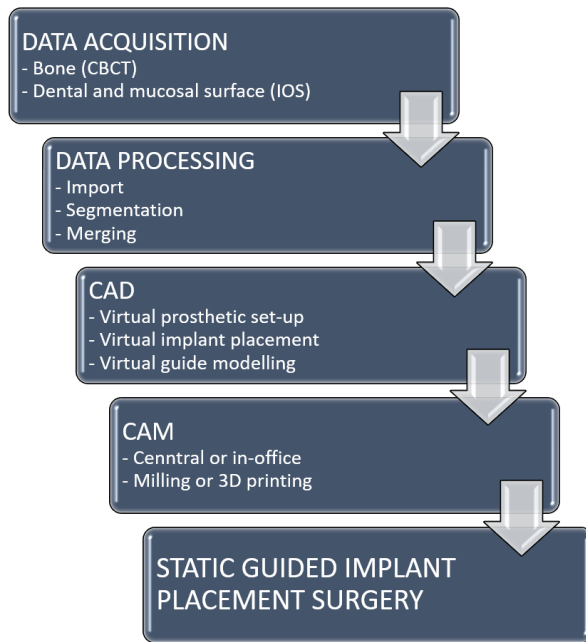
Fig. 3. Digital workflow for preoperative planning and static guide manufacture [267].

the highest accuracy in the CAD model [295]. Despite the similar guidance accuracy demonstrated by both methods, additive manufacturing offers notable advantages including high accuracy, ease of fabrication, reduced waste, and time efficiency, thereby enhancing cost-effectiveness [296]. Three-dimensional printing is the most common additive manufacturing technique used interchangeably as a synonym [266]. It is a process that involves the creation of objects by progressively adding layers of material, resulting in the desired final shape [297]. Among the wide variety of techniques available, the most commonly used 3D printing technologies for fabricating surgical guides in dental implantology include stereolithography (SLA), digital light processing (DLP), inkjet, selective laser sintering (SLS), continuous liquid interface printing (CLIP), and fused deposition modelling (FDM) [298,299]. In terms of precision, regardless of printing technique small-size guides exhibited higher levels of accuracy in 3D printing compared to full arch guides [298]. Among the reported techniques, SLA and DLP are recognized as the most accurate printing methods, while FDM is considered the least accurate [298–300]. On the contrary, a recent *in vitro* study using FDM-based guides,

incorporating different planning software and design approaches, suggested a high level implantation accuracy comparable to other fabrication methods [301]. Moreover, the SLA process has been documented to offer advantages in hardness, accuracy, and surface roughness when compared to alternative rapid prototyping techniques [302]. Adjusting the parameters of 3D printers, often performed by dental technicians, is one of the important factors in achieving the highest level of printing accuracy [298]. Finally, it has been suggested that reducing the slice thickness of the 3D printer can enhance the accuracy of the implant placement [303].

The fully-guided approach demonstrates superior implant positioning accuracy compared to free-hand and partially guided surgery [25,287,290,300,304]. Additionally, the fully-guided approach is highly compatible with flapless surgery, significantly reducing chair time, minimizing patient morbidity, and increasing patient satisfaction [290]. Regarding the drilling sequence partially guided approach, some studies have reported its comparable accuracy to fully-guided implant placement and superior accuracy to pilot drill partially guided surgery [37,305]. Younes et al. (2018) reported that partially guided implant placement using only a pilot drill demonstrated lower accuracy than the fully-guided approach, yet exhibited superior results compared to the free-hand approach [306]. Despite lacking virtual planning and exhibiting lower accuracy compared to the aforementioned methods, the non-computed approach has demonstrated higher accuracy than the free-hand approach [307]. Free-hand or mental/brain-guided approach, or conventional surgery, may or may not involve CBCT exploration for the pre-surgical planning [290]. Although free-hand surgery does not apply surgical templates, 3D planning is still recommended practice. It has been consistently reported in multiple reviews to be the least accurate approach and associated with higher patient morbidity due to the necessity of flap elevation [25,289,290,304].

The guidance's accuracy, benefits, and drawbacks can also be influenced by the guide supporting anatomical structures. Tissue support in guided implant surgery is predominantly determined by the clinical situation, specifically whether the patient presents with full or partial edentulism [289,308]. Bone-supported guides are characterized by lower accuracy, increased invasiveness by reflecting a large full-thickness flap, and subsequent higher patient morbidity and dissatisfaction [25,309,310]. These guides are frequently additionally fixed with screws or pins to enhance their stability [308]. Mucosa-supported guides are the preferred choice for flapless surgery in both partially

and fully edentulous patients, with a higher accuracy reported due to the use of 3 or 4 transmucosal fixation pins in fully edentulous or mixed tooth-mucosa support in partially edentulous cases [25,290]. Mucosa-supported guides have been observed to exhibit micromovements, even when fixation pins are used, which can potentially impact their accuracy [308,311,312]. Tooth-, mucosa-, or mixed tooth/mucosa-supported guides have been reported to exhibit superior accuracy compared to bone-supported guides [25,308,313]. Purely tooth-supported guides are infrequently reported in scientific literature, as they commonly incorporate some level of mucosa support [308]. When designing a tooth-supported guide and anticipating an open-flap approach, it is important to leave adequate space to prevent interference of the flap with the guide [314]. Fully edentulous cases, which rely on the support of mucosa or bone, exhibit lower accuracy in guided implant surgery compared to cases of partial edentulism [289,308].

Open guide design provides improved visibility and irrigation access to the surgical site [290,291]. Still, its less restrictive nature is associated with a higher likelihood of deviations during the surgical procedure [290,291]. Questions regarding the relationship and interaction between the sleeve and rotating drill, resulting in either looseness and deviations or tightness and friction, have been the subject of long-standing investigation [149]. Remarkably, the guided surgery conducted without the inclusion of a metal sleeve (i.e., having it incorporated within the plastic guide design) demonstrates similar accuracy results to that of guides with metal sleeves, thereby suggesting a metal sleeve may not be necessary [315]. Conversely, in another study, the sleeve-in-sleeve groups exhibited superior accuracy compared to the other groups, whether with or without sleeve and integrated sleeve-on-drill systems [292].

In addition to these primary categorical factors, a multitude of other influencing factors should be considered in evaluating accuracy in this context. Yeung et al. (2020) reported a high variation in vertical deviation, up to 2–3 mm, among different implant systems, suggesting a potential influence of the implant system on the dimensional and angulation accuracy [316]. This could be related to differences in implant shape design, drill design and sequence, and sleeve system variations, as discussed earlier [292]. Moreover, it was proposed that the magnitude of deviation is influenced by the size of the edentulous space and the distribution of the remaining teeth [317,318]. This is further supported by other clinical studies which indicate that an increase in the number of missing teeth was associated with decreased accuracy of

static guidance, while the use of fixation pins improved accuracy in partially edentulous cases [319]. Furthermore, a decrease in bone density (D1 > D2 > D3 > D4) and volume has been suggested to result in reduced accuracy of static guided implant placement [320,321]. In a cadaver study investigating immediate flapless implant placement in the maxillary anterior region, comparing free-hand and partially guided (drill sequence) approaches, the guided group demonstrated higher accuracy; however, both methods tended for implant position shifts towards the facial direction [322].

The most commonly reported complications predominantly involve intra-operative fractures of surgical guides, modifications to the surgical plan, early implant failure due to inadequate primary stability [266]. The main limitation of the static guidance system lies in its inability to modify the preoperative planning position during surgery, leaving freehand surgery as the only alternative for making any necessary adjustments [290]. Therefore, it is frequently recommended that proficient surgical skills and experience are highly advisable in clinical situations where there is a need to modify the surgical plan or complete the procedure without relying on the guidance system for various reasons [286,290]. This information is of significant importance, as it has been consistently observed in studies on guided surgery that the operator's experience does not significantly impact the accuracy of the procedure [291,323,324].

In addition to implant surgery, it is noteworthy that static guides have been proposed in various areas, including accurate endodontic surgery [325]. In addition, acceptable accuracy has also been demonstrated for endodontic cavity preparation, with higher deviations observed in the molar area [326,327]. Guidance has also been proposed as a precise, effective, safe, and clinically applicable strategy for accessing calcified root canals, removing fiberglass posts, and accessing teeth with developmental anomalies [328,329]. Furthermore, guided autotransplantation of teeth with custom 3D-printed surgical tooling was also proposed [330,331]. Remarkably, static guidance has been demonstrated for the placement of 3D-printed dental implants, along with individualized tooling [332]. Finally, static guides can also be utilized for bone contouring and reduction, offering the advantage of stackable guides connected to guided implant placement [333].

In conclusion, static guidance has been proven to be highly accurate, as evidenced by recent reviews recommending its use for challenging cases. In clinical scenarios characterized by narrow gaps or anatomical complexity

during dental implant placement, where the risk of damage from close proximity between teeth roots and the dental implant is present, guided implant placement is recommended as a safer approach [334]. However, there are multiple influencing factors that, at present, exhibit insufficient or heterogeneous scientific evidence regarding their impact on accuracy, thus indicating the necessity for further research in this field.

1.2.7. DYNAMIC GUIDANCE AND ACCURACY

Dynamic dental implant guidance is an emerging technology that aims to enhance the accuracy and efficiency of dental implant placement. Using real-time tracking, dynamic guidance provides continuous feedback and navigation during the surgical procedure, offering unique advantages. Dynamic navigation systems employ optical technologies, enabling real-time tracking of the patient and the handpiece, and providing visual feedback through the display on a monitor [335]. Motion tracking technology, commonly known as a micron tracker camera, enables the functionality [336]. Three essential hardware components commonly found in navigation systems include a computer with a screen, a tracking camera, and tracer attachments for both the patient and the handpiece [337]. The registration, calibration, and tracking process forms the fundamental steps in dynamically mapping the drill tip to the planned CBCT image volume of the patient in real-time [338].

Optical systems in dynamic navigation utilize either passive or active tracking arrays, with passive systems reflecting light emitted from a source back to stereo cameras, while active systems emit light that is tracked by stereo cameras [337]. Early optical navigation systems necessitated the placement of fiducial markers on the patient's arch during CBCT scanning, facilitating arch registration to the cameras through an attached array [337]. Then the registration process establishes the spatial relationship and orientation of the patient's head, linking it with the CBCT volume data in the guidance system [338]. The camera arch registration is achieved through a fiducial marker device connected to an external array/tracker [337,338]. In contrast, the implant handpiece, with its own array/tracker, allows for accurate navigation through the triangulation [337,338]. Accurate tracking of the drill and patient-mounted arrays on the monitor requires visibility within the line of sight of the overhead stereo cameras [339]. Regarding the approach presented, a significant disadvantage as it required the placement of fiducial markers for CBCT, potentially before deciding on implant placement, and it also imposed

limitations on the accessibility of that site on that specific side of the arch. Thus, registration can be achieved through various other methods, including anatomical landmarks, or surface matching techniques [339]. A recent study demonstrated the clinical applicability of a trace registration method, which replaces fiducial markers with high-contrast landmarks such as teeth, implants, or abutments [340]. Adopting these methods can eliminate the necessity of fiducial markers in CBCT scans, albeit potentially influencing registration accuracy.

The available literature on the impact of registration on navigation accuracy is limited; however, two studies indicated that cusp registration yielded comparable accuracy results to object-based registration [341,342]. Another study compared automated and manual registration methods regarding dynamic guidance accuracy and found that both approaches yielded similar results [343]. In a recent *in vitro* study conducted by Struwe et al. (2023), the impact of prefabricated and 3D-printed markers for registration on the accuracy of dynamic implant placement was evaluated [344]. The findings suggest that while both methods demonstrate comparable outcomes to static guidance, 3D-printed markers exhibit decreased accuracy levels compared to prefabricated markers. The trace-registration method showed mean deviations of 0.67 mm at the entry point and an angle discrepancy of 2.50 degrees, with improved accuracy observed when tracing 5 to 6 teeth compared to 3 to 4 teeth [345]. Schnutenhaus et al. (2021) reported a mean 3D deviation for the entry point of 1.53 ± 0.70 mm, with an angular deviation of $2.88 \pm 2.03°$, while demonstrating significant differences in various workflow parameters and highlighting the impact of the reference marker position on implant position accuracy [346].

Recent systematic reviews have shown the accuracy of dynamic navigation to be similar to static guidance and clinically acceptable [36,39,43,91,126]. Unlike static guides, dynamic navigation systems show no difference comparing *in vitro* and clinical accuracy [39,43,91]. However, Jorba-García et al. (2021) in their review reported that the overall deviations in clinical studies were 1.03 mm for the entry point and 3.68° for angular measurements, while *in vitro* model studies showed higher accuracy with deviations of 0.46 mm and 2.01° stating superior accuracy than static guidance [36]. However, it might depend on other factors, such as the number of remaining teeth used as reference objects. There is a lack of data on how the number of missing teeth and implant design could influence the accuracy of dynamic implant

navigation. Furthermore, the implant design (and drilling sequence) should also be considered an important variable [308,346]. Higher heterogeneity and a lack of clinical data on dynamic guidance accuracy exist [39]. Despite variations in components, technology, and workflow among different dynamic guidance systems, no statistically significant differences were found in the accuracy [36]. Schnutenhaus et al. (2021) have noted that most studies vary according to influencing factors in their design: fundamental differences in dynamic tracking systems, implant planning software and implant systems [39]. Thus, it is important to evaluate factors influencing the accuracy of dynamic systems.

Dynamic implant guidance has its advantages and limitations. Dynamic navigation takes less preparation time than static guides, as there is no need for guide fabrication (a single-visit approach is possible for planning and surgery). In addition, it is much more flexible and allows the surgeon to make intraoperative changes according to the situation [347]. Furthermore, it also eliminates specific static guide-related issues, such as limited field visibility, lack of drilling irrigation, and guide breakage [203,290,348]. Dynamic guidance is superior as it does not require a separate drill set or sleeves and is less challenging for patients with limited mouth opening (especially in posterior regions) [290]. It could also be considered more environmentally friendly as it leaves fewer single-use disposables than static guides. The main limitations of dynamic guidance are the high cost of the system and the learning curve [347,349,350]. Fully edentulous arches remain challenging cases, requiring additional interventions for registration and increasing costs and invasiveness, such as mini-implant placement before surgery [290,349,351]. Even though dynamic systems demonstrate improved accuracy in implant placement for partially edentulous patients compared to the conventional freehand approach, they also result in significantly increased surgical time (+ 14 minutes) without noticeable improvements in patient satisfaction or postoperative pain reduction [352,353].

Dynamic and static navigation methods exhibit similar levels of accuracy, surpassing the freehand approach, while no notable advantage in implant survival within the initial 5-year period could be observed for any particular method [126]. In a randomized controlled trial comparing static and dynamic computer-assisted implant surgery in single tooth edentulous defect, no significant difference in implant placement accuracy was observed between the two methods [354]. Another randomized controlled clinical trial comparing

static and dynamic guided implant surgery in two-implant supported fixed dental prosthesis demonstrated equal results between the two methods in terms of implant position accuracy [355]. Both dynamic and static guided implant surgery demonstrated an ease of mastery, with a learning curve effect observed only in dynamic group during *in vitro* tests conducted with beginner dental students [356].

In addition to alveolar dental implant placement, navigation systems can be applied in various other fields of dentistry. Dynamic guidance can be employed for performing the sinus lift and bone augmentation procedure, whether with or without simultaneous implant placement [357]. Moreover, it can be applied for zygomatic implants, exhibiting higher entry point deviations of 3 mm and angular deviations of 6°, and some *in vitro* studies indicating that the free-hand approach may be more accurate [358,359]. The free-hand technique for zygomatic implants has been proposed as superior to static guides, possibly due to the varying learning curves associated with each system [360]. Dynamic guidance has also been proposed as an alternative to static endodontic guidance, offering advantages such as simplicity, efficiency, precision, and reduced technique sensitivity [361]. Recently, augmented reality has emerged as a potential alternative to screen-based dynamic guidance, offering comparable accuracy results in the implant placement [362,363]. The utilization of dynamic guidance, as well as virtual and augmented reality technologies, has demonstrated enhancements in maxillofacial surgical training and planning [364]. However, limited research has been conducted to investigate the specific effects of these technologies on the quality of patient care [364].

Dynamic dental implant guidance is a promising technology that enhances accuracy and efficiency in implant placement. It involves real-time tracking and navigation, providing continuous feedback during the surgical procedure. Comparative studies have shown comparable accuracy between dynamic and static guidance systems, but further research is suggested to evaluate the impact of different influencing factors on accuracy.

1.2.8. EVALUATION OF IMPLANT PLACEMENT ACCURACY

Guided implant surgery accuracy can be assessed in precision, representing the consistency and reproducibility of the implant placement [221]. Trueness, as a measurement of accuracy, refers to how closely a result or outcome aligns with the true or intended value [196,221]. Assessing the accuracy of planned

implant position in guided implant surgery is challenging due to the complex digital planning process and lack of reliable analog alternatives for precise evaluation.

When evaluating the accuracy, commonly reported errors include angular deviations, overall 3D deviations, horizontal (lateral) deviations, and vertical (depth) deviations [365]. Other than angular deviation, discrepancies in the implant's entry and apex points can be evaluated [37]. These points include the coronal, shoulder, platform, neck, base, and insertion point for entry and tip for the apex [37]. Although apical deviation may seem more clinically important when considering adjacent anatomical structures, it is mathematically proportional and dependent on the length of the implant as a manifestation of the angular deviation [39]. The most commonly reported deviations in implant placement are the deviations at the entry point and the angular deviations [36]. From this perspective, coronal deviations hold greater clinical relevance regarding the prosthetics [39]. Horizontal and depth deviations, while still important, can be considered components of the overall 3D deviation [365]. The reporting of horizontal deviations in implant placement can vary, with measurements expressed in terms of mesiodistal (MD) or buccolingual (BL) directions, or just as a general value [321]. Due to the naturally irregular shape of the jawbones, MD and BL horizontal deviations in implant placement can be prone to researcher-related or method-related bias, as they heavily depend on the chosen reference view/position [321]. Similarly, studies that solely report on 2D deviations, often derived from an occlusal view, encounter the same limitation [36]. Vertical deviations may be reported as positive or negative values, depending on the reporter whether the implant is placed too deep or too shallow, or just as a general unsigned (absolute) value [366]. When evaluating accuracy from a clinical standpoint, considering both positive and negative values of deviations is informative, but mathematically, absolute values should be used to assess the magnitude of deviations to avoid eliminating the actual inaccuracy [366]. Implant rotation around its axis is rarely reported but has significance in the prosthetics [367]. Given the aforementioned considerations, it is evident why most studies and reviews restrict their assessment to evaluate 3D deviations and angular discrepancies related to the implant entry point [36,39]. Currently, there is a lack of a standardized index for assessing the accuracy of implant placement, leading to varying results across different methods and making comparisons between studies challenging [366].

Most studies assessing the precision of dynamic implant placement rely on post-operative CBCT images [39,43]. The method uses a digital plan (pre-operative CBCT scan with planned implant position information) being superimposed with post-operative CBCT with actual implant positions [368]. This is based on multimodality image registration by maximization of the mutual information concept [369]. One significant limitation is the requirement for additional exposure of patients to ionizing radiation (X-rays), which lacks sufficient clinical justification and practical applicability [370]. Recent literature reviews have also identified this issue, proposing of X-ray-free methods as potential alternatives [39,45,370]. It is a serious concern that a significant proportion of clinical studies fail to report the approval of the ethical committee [371]. The other challenge is that CBCT scan accuracy is limited by the voxel size as well as other settings (kVp, mA) [372–374]. Voxel and surface-based superimposition of two CBCT scans methods exhibit both accuracy and reliability, with no significant differences observed between them; nevertheless, this digital superimposition introduces a mean error in the range of 0.1–0.2 mm [375]. In most cases, post-operative implant image is not precise in CBCT scan due to metal-related scattering, artefacts and other distortions [376,377]. The last but not the least important aspect is that using this method, a researcher places a generic digital implant shape over an x-ray volume [349]. This approach raises questions regarding its limitations when reporting accuracy. All these challenges suggest looking for a safer and less human error-sensitive method for the implant position comparing and accuracy evaluation.

An *in vitro* study utilizing IOS-based evaluation demonstrated that guided surgery exhibited greater accuracy than freehand placement, yielding results comparable to those published based on CBCT superimposition in other model studies [378]. A recent publication in a model study demonstrated that the evaluation of implant position accuracy using an IOS yielded comparable accuracy results to that of a CBCT-based evaluation method [379]. This finding is further supported by another model study comparing dynamic and static guidance, which found that both IOS and CBCT evaluation methods showed comparable results, with differences measured in the micron scale [380]. Skjerven et al. (2019) in a clinical study reported that IOS and CBCT-based evaluation techniques provide similar accuracy results, with negligible mean differences between the two methods, measuring less than 0.1 mm and 0.1 degrees [381]. In a case series by Hooft et al. (2022), although most

deviations showed no significant differences, apex and shoulder BL and depth deviations were statistically significantly higher in the CBCT group by 0.1-0.3 mm, while angular deviation was 1 degree higher in the IOS group [382]. In another clinical study, the accuracy was assessed by comparing post-operative impression and plaster model-based information to CBCT-based evaluation, revealing an insignificant difference in deviations of 0.06 ± 0.75 mm at the platform and 0.007 ± 1.24 mm at the apex [383]. Recently, Ma et al. (2023) model study proposed an innovative approach for a dynamic guidance system to collect post-operative spatial data of implants through the connected handpiece position, resulting in an entry point deviation of 0.88 ± 0.37 mm and an angular deviation of 1.83 ± 0.79 degrees [384].

1.3. THE SURFACE OF PROSTHETIC MATERIALS AND SOFT TISSUE

1.3.1. PROSTHETIC MATERIALS IN IMPLANT DENTISTRY

Recently, dental implants have become a widespread treatment option for restoring partially and fully edentulous patients, with an ever-growing body of scientific evidence supporting their numerous benefits compared to a more conventional approach. After overcoming the challenges of osseointegration, most studies currently focus on peri-implant soft tissues, proving that their quantity and quality are essential for bone stability around dental implants [385]. Soft tissue integration in the transmucosal zone of implant abutments is a vital functional and biological parameter for supporting the peri-implant tissues, improving aesthetics, ensuring soft tissue seal against microorganisms and other hazardous agents, as well as preserving crestal bone loss, ultimately increasing the longevity of the implant-supported restoration [60,386–389]. The quantity and quality of soft tissue are essential for bone stability around dental implants [390,391].

The seal of soft tissue around the implant abutment and prosthesis shields the underlying tissues from the environment of the oral cavity. When this barrier of soft tissues is damaged, there is a risk that microorganisms can reach the surface of the dental implant [60,392]. Inflammation in this area might eventually lead to bone loss, compromised aesthetics, and peri-implantitis [386,393,394].

Using titanium base abutments became a standard in implant prosthodontics [395]. When placed intraorally, only a small part of this abutment and predominantly selected prosthetic material is in contact with peri-implant tissues [396]. Many prosthetic materials can be used in these situations: metal alloys, ceramics, and polymer-based materials [397]. All of them have unique advantages and disadvantages [398]. For simplicity, further in text implant abutment and prosthetic materials will be referred to as "prosthetic materials".

Among the different abutment materials, the ones based on Zirconium dioxide (ZrO_2) offer several distinct benefits. Zirconia has exceptional strength and fracture resistance, which makes it an optimal choice even in biomechanically challenging situations. Furthermore, it is corrosion-resistant and has excellent aesthetic properties [399]. The final metal-free implant-supported restoration colour strongly depends on its design and the material used for abutment fabrication [400]. The optical properties of Zirconia are favourable for the restorations' final colour and positively influence the shade of the peri-implant soft tissues when an appropriate biotype is present [401,402]. Based on colour, Zirconia can be divided into two major classes: white and pre-coloured, also called multi-layered [403]. Furthermore, ZrO_2-based abutments show better outcomes than other ceramic materials [404].

Another essential advantage of zirconia-based abutments is their excellent bio-compatibility [392]. Studies suggest a similar soft tissue blood flow around Zirconia-based abutments and natural teeth and improved microcirculation compared to other abutment materials, which could be advantageous for the immune response [405,406]. Furthermore, the inflammation infiltrates around ZrO_2 abutments are lower than around titanium ones, suggesting a better soft tissue seal with decreased bacterial invasion and reduced crestal bone loss during the first year [399,407].

Soft tissue and bone response may be influenced by the type of implant abutment material and surface properties [60,386,408]. The relationship between the material and the resulting condition of soft tissue has been reported in multiple studies [58,408–411]. Most studies have investigated the effects of titanium and zirconia materials [397,412]. However, only a few studies have been conducted on polymer-based materials, which can be used as temporary or permanent prosthetic materials. Concerns of lower biocompatibility of polymethylmethacrylate (PMMA) materials were raised in the literature (e.g., cytotoxicity of PMMA monomers, higher surface bacterial contamination compared to other materials); however, they are widely used for fabrication

of provisional restorations [413–417]. Polyetheretherketone (PEEK) materials have recently gained more attention as an alternative to titanium and ceramics [411,413,414,418,419]. Scientific evidence shows that PEEK and its modifications are favorable for fibroblast and epithelial cell response and might provide less biofilm formation [411,413,419]. A recent study evaluated a modified PEEK material and found that it positively influenced human gingival keratinocytes, contrasting with the effects of uncoated and nitride-coated titanium [420]. On the other hand, studies regarding 3D printed materials and novel polymers (e.g., polyetherketoneketone – PEKK) remain limited.

Over years of extensive research, a substantial body of knowledge has been accumulated, providing compelling evidence for the significant impact of prosthetic materials on soft tissue health at the cellular, tissue, and clinical levels. However, it should be noted that the material itself cannot fully account for the variability observed in all the soft tissue responses. Therefore, the focus has shifted towards investigating surface characteristics as well. Several other factors can influence the soft tissue response to abutments. Surface microtopography and hydrophilicity play a significant role and have been extensively studied [421–423].

1.3.2. SURFACE ROUGHNESS

A significant portion of cutting-edge dental implant research revolves around *in vitro* studies, wherein the emphasis is placed on examining new materials and their surface modifications [424]. Commonly, the surface roughness of dental implants is evaluated, and a recent meta-analysis has suggested that using rough titanium surface dental implant neck may provide superior preservation of marginal bone compared to a smooth surface [425]. Regarding soft tissue health, the surface roughness of implant abutments and prosthetic materials is a topic of discussion, particularly for two-piece bone-level implants where the implant body resides within the bone. The surface profile and roughness of prosthetic materials are influenced by dentists' or laboratories' polishing, surface finishing, and modification procedures [426].

Material surface microtopography can determine the quality of soft tissue integration around the implant abutment [60]. The tendency of rough zirconia surfaces (Ra = 0.19 ± 0.03 μm) to provide higher fibroblast content after 3 and 24 h, but lower after 48 and 72 h compared to smooth surfaces (Ra = 0.05 ± 0.01 μm) was demonstrated by recent research [427]. On the

other hand, surface roughness (Ra) higher than 0.2 μm tends to increase bacterial adhesion [428]. The formation of plaque and reproduction of bacteria depends on the characteristics of implant abutment surfaces and play an important role in the pathogenesis of infection [429–431]. In addition, higher surface roughness has been reported to reduce fibroblast proliferation and promote bacterial adhesion, biofilm formation, and associated negative consequences [432,433]. On the contrary, macro-roughened surfaces achieved through laser surface modification exhibited superior gingival morphology, proliferation, fibre orientation, and biofilm control [434]. However, the adverse effect of surfaces smoother than 0.1 μm on fibroblast function, as well as the documented association between very smooth surfaces (<0.1 μm) and increased marginal bone loss, probing depth, and bleeding on probing values, have also been reported [433,435,436]. Zirconia, titanium dioxide, and lithium disilicate materials with a surface roughness of 0.1–0.2 μm demonstrated better fibroblast attachment compared to smoother or rougher surfaces [437]. Surface roughness accounts for two important characteristics of human gingival fibroblast (HGF) proliferation and attachment—time and orientation of the fibres to the abutment surface. Results reported by different studies support the thesis that a moderately rough surface, between 1 and 2 micrometres, defined as nanotubes or directional grooves, creates optimal conditions for HGF attachment and soft tissue seal formation [438].

Different profilometry technologies and methodologies allow the evaluation of the same surfaces at different levels, which can substantially affect the surface roughness result. When interpreting research data, the profilometry method (contact or non-contact) and related parameters (tip radius, cutoff values, field of view, number of measurements per surface, etc.) need to be considered [439–442]. Quite often, inter-study discrepancies in surface roughness measurements arise due to variations in the profilometry method employed for the assessment [411,413,415,416,419].

1.3.3. SURFACE HYDROPHILICITY

The hydrophilicity of the abutment surface is another factor influencing the peri-implant tissue health [443,444]. Hydrophilicity, measured as a water contact angle (WCA) function, is among the main factors affecting protein absorption and human gingival fibroblasts' cellular attachment to implant abutments [445,446]. The material is considered hydrophilic if the contact angle of a water droplet on the surface is below 90 degrees and hydrophobic if it

exceeds 90 degrees [447]. Generally, a lower contact angle promotes fibroblast attachment [446]. Studies have demonstrated that hydrophilic abutment surfaces can promote fibroblast adhesion and proliferation and improve soft tissue attachment [443,444]. Hydrophilic surfaces and soft tissue attachment contribute to the favourable sealing of soft tissues around the implant prosthetic component [438]. On the other hand, material hydrophobicity is associated with the adhesion of certain bacteria, biofilm formation, and slower healing [448,449]. Wassmann et al. demonstrated in their study that hydrophobic surfaces are more attractive to Staphylococcus epidermidis, which exhibits cytotoxic effects on human fibroblasts and hinders smooth osseointegration and soft tissue healing [449–451].

Most polymeric materials (e.g., PMMA and PEEK) tend to be less hydrophilic than zirconia, but the correlation between their surface roughness values and water contact angle is not evident [415]. Except for novel high-performance polymer PEEK modifications, most polymeric materials typically exhibit water contact angles (WCA) in the range of 60-100 degrees [411,415]. The WCA measurements for various PMMA-based materials exhibited a 60-70 degrees range, with higher values observed after the thermocycling process [452]. PMMA modification using O_2 plasma significantly reduced WCA from approximately 95 degrees to 55 degrees, whereas CF_4 plasma treatment increased the WCA to 110 degrees [453]. For various PEEK modifications, the WCA exhibited a range of values from 63 to 85 degrees, indicating the variability in surface wettability depending on the specific PEEK modification [454].

ZrO_2-based ceramics used for abutment fabrication show a defined hydrophobic behavior, with contact angles sometimes exceeding the hydrophilic threshold of 40° by more than twice [455]. Surface plasma treatment has significantly reduced the water contact angle, resulting in highly hydrophilic surfaces in such cases [455]. Contrary to the mentioned findings, other studies have reported that zirconia is hydrophilic, with water contact angles (WCA) in the range of 50-60 degrees [456]. Other studies have reported a range of WCA values (73.8 ± 5.1 degrees) for zirconia that fall between the aforementioned findings, indicating varying degrees of hydrophilicity [457]. The combination of laser-induced microstructures, initially hydrophobic (WCA 138.4°), and subsequent argon plasma activation resulted in a switch to a hydrophilic state (WCA of 13.7°), suggesting the potential of the combination of these two techniques [458]. From the published studies, it is evident that

the hydrophilicity of zirconia ceramics varies significantly depending on the techniques used for surface modification.

The water contact angle of titanium has also been reported to vary in the range of 20-60 degrees, depending on the surface texture and roughness modifications [459]. In contrast, other studies have reported titanium to be more hydrophobic. For instance, smooth pretreatment titanium surfaces (Ti-PT) with an average roughness (Ra) of 0.45 μm and a water contact angle (WCA) of 92.4°, as well as rougher sandblasted, large grit, acid-etched treatment titanium surfaces (Ti-SLA) with a Ra of 3.3 μm and WCA of 131.8°, were tested [460].

The findings suggest that hydrophilicity, characterized by lower water contact angle (WCA) values, is influenced by the material, surface roughness, topographical elements, and other modification techniques. However, it is important to note that variations in evaluation methods may also contribute to the observed differences.

1.3.4. SURFACE CONTAMINATION

The contamination of the material surface might affect cell growth [461]. Cleaning of the implant abutment surface is important not only for decontamination but also might modify surface properties, and thus cellular response [414,462–464]. Various cleaning protocols have been suggested to improve surface biocompatibility and cell proliferation. It has been shown that ultrasonic cleaning decreases the amount of debris on implant abutments and supposedly promotes soft tissue healing [463]. The cleaning protocol used in cell proliferation research studies often differs from that used in the dental laboratory [464]. Therefore, it is unknown if the results of these studies can be applied to clinical practice. Limited data is available on the influence of surface cleaning on roughness, WCA, and biocompatibility being evaluated within the same study.

Some studies do not provide information on whether any cleaning method was employed, and in most other cases, ultrasound bath-based cleaning methods are predominantly used [413,419,465,466]. There is a lack of knowledge on the soft tissue response to polymeric materials that can be fabricated using CAD/CAM (computer-aided design and computer-aided manufacturing) or 3D printing. Moreover, it is unknown how different cleaning protocols can affect their properties.

1.3.5. THE EFFECT OF SURFACE UV TREATMENT ON ZIRCONIA-BASED CERAMIC MATERIALS

Different surface modifications have been proposed to create more favourable conditions between the implant abutment and surrounding soft tissues [423]. As mentioned earlier, plasma treatment significantly enhances the hydrophilicity of the surface. Various other methods, including but not limited to blasting, acid etching, selective infiltration etching, polishing, laser treatment, coating, biofunctionalization, and self-assembly, have been reported in scientific literature as ways of modifying zirconia surfaces [467]. Among other methods, applying UV photofunctionalization to zirconia-based materials shows promising results [427,468].

Significant alterations to the physicochemical properties of both zirconia implant surfaces being studied were evident upon implementation of the UV treatment [469]. Although the exact mechanism behind these changes is not straightforward, it is suggested that reducing surface carbon content plays a key role in influencing these alterations. The method is easy to perform chairside and brings distinct advantages, such as a substantial decrease in surface carbon content and increased wettability, proliferation, and attachment of cell structures [469,470]. However, the literature on hydrophilicity and HGF-related factors of UV-treated zirconia-based materials used for implant abutment fabrication is inconclusive. Furthermore, only a few commercially available materials have been tested previously. After undergoing UV-A and UV-C treatments, zirconia exhibited changes in colour, surface free energy, and surface chemistry; while prolonged 24-hour UV-C photofunctionalization enhanced bioactivity, it compromised the material's aesthetic appeal [471].

2. MATERIALS AND METHODS

2.1. GUIDED IMPLANT PLACEMENT ACCURACY EVALUATION

2.1.1. MODELS

Maxillary models were fabricated with polyurethane resin (Modralit® 3K Set, Dreve Dentamid GmbH, Unna, Germany), imitating bone type I (Lekholm & Zarb). These models simulated posterior edentulous defects to be restored with two-implant-supported fixed partial dentures. A single molar edentulous defect for an implant-supported crown restoration was selected as a control group. Radiopacity was adjusted by the addition of $BaSO_4$ (Barium sulphate 97 % 1–4 micron powder, Alfa Aesar, ThermoFisher (Kandel) GmbH, Germany) to approximate data (mean area Hounsfield units) from the real human CBCT. The soft tissue component was emulated by silicon gingiva (frasaco GmbH, Tettnang, Germany). Three types of models used in the study were as follows (Fig. 4):

- Kennedy I (K1) - bilateral posterior edentulous defects/areas missing molars and premolars (FDI teeth numbers: 17, 16, 15, 14 and 24, 25, 26, 27).
- Kenndy II (K2) - unilateral posterior edentulous defect/area missing right side molars and premolars (FDI teeth numbers: 17, 16, 15, 14).
- Kennedy III - two posterior defects:
  a) Left side edentulous defect (K3) missing both premolars and first molar (FDI numbers: 24, 25, 26).
  b) Single tooth edentulous defect (K3-single) on the right side missing first molar (FDI number 16).

| K1 | K2 | K3 |

Fig. 4. Models used in the study.

All of the models were securely mounted in a phantom head (ClaroNav Inc., Toronto, Ontario, Canada) to simulate a clinically relevant scenario for both dynamic and static implant placement.

The angular deviation was selected as the primary outcome variable. Sample size was calculated using G*Power 3.1 (Heinrich-Heine Universität, Düsseldorf, Germany). A total sample size of 72 was selected, considering a power of 0.80, an alpha error of 5 % and an $f2$ effect size of 0.4, based on previous studies [324,472].

2.1.2. DIGITAL PLANNING

Four computed cone beam tomography (CBCT) scans (KaVo OP3D, KaVo Dental, Biberach an der Riss, Germany) and four intraoral (IOS) scans (Trios4, 3Shape, Copenhagen, Denmark) were obtained for each model. CBCT scans were performed using a voxel size of 0.2 mm. Each CBCT scan was coded and randomly paired with one of the four IOS scans from the same model group. Using SMOP software (Swissmeda AG, Baar, Switzerland), a trained planner (H.P.) made a digital wax-up and positioned implants according to the standard implant placement requirements (confirmed virtually by the dentist):

- Prosthetically driven implant position with screw access hole in the central fossa of the crown;
- The minimal distance between the implant and the adjacent tooth is 1,5 mm;
- The minimal distance between adjacent implants is 3 mm;
- The minimal distance from a buccal/lingual wall of a resin model is 1,5 mm;
- Implants placed 1 mm subcrestally;
- 0 degree (angulation between implants).

The length and diameter of the implants per each case position are presented in Table 6.

Each plan was randomly assigned to one of the implant design groups: slightly conical self-tapping (CONELOG screw-line, Camlog Biotechnologies AG, Basel, Switzerland) (SL group) and conical self-tapping (CONELOG progressive-line, Camlog Biotechnologies AG) (PL group). This random distribution resulted in 4 implant plans per model case, exported as Standard Tessellation Language (STL) files.

Table 6. Implant parameters used in the study. CONELOG screw-line and progressive-line implant systems were used (Camlog Biotechnologies AG, Basel, Switzerland).

Position (FDI number)	Diameter	Length	Parallel
Kennedy I			
First premolar (#14)	3.8 mm	11 mm	Yes
Second molar (#17)	4.3 mm	13 mm	Yes
Kennedy II			
First premolar (#14)	3.8 mm	11 mm	Yes
Second molar (#17)	4.3 mm	13 mm	Yes
Kennedy III			
First premolar (#24)	3.8 mm	11 mm	Yes
First molar (#26)	4.3 mm	13 mm	Yes
Single			
First molar (#16)	4.3 mm	13 mm	n/a

2.1.3. STATIC GUIDED IMPLANT PLACEMENT

Based on the digital plan data a CAD design of a static surgical guide was created using ImplantStudio software (3Shape, Copenhagen, Denmark), incorporating two palatal supporting cross-bars for rigidity and occlusal windows to verify proper seating. Then the guides were 3D printed using a DLP printer Asiga Pro 4K UV385 (Asiga, Alexandria, Australia). Asiga DentaGUIDE methacrylate-based resin (Asiga Pty Ltd, Alexandria, Australia) material was used for 3D printing according to all manufacturer's instructions. The material is CE certified for the manufacture of Class I medical devices. Following the 3D printing process, the surgical guides were thoroughly washed, subjected to post-processing procedures, and finished in accordance with the instructions provided by the manufacturer (instructions for use (IFU); DentaGUIDE; Part Number / 04504). Subsequently, the guide system's guiding sleeves were inserted as planned: 3.8mm and 4.3mm (catalogue numbers J3734.3803, J3754.3801, J3734.4303, J3754.4301). A total of 36 implant guides (12 per each Kennedy case) were manufactured for the study.

Implant placement was performed following a standard guided drilling sequence for dense bone (D1), using dense bone drills (catalogue numbers J5068.3811, J5068.4313; J5068.4313, J5068.4313) in accordance with the manufacturer's instructions. Simultaneous preparation of all implant beds was carried out prior to the insertion of the implants. The implants were inserted through the guide following a fully-guided implant placement protocol,

ensuring alignment of the depth and rotation based on the sleeve and index. The insertion mounts were subsequently removed, followed by the removal of the guide, allowing the model to be further evaluated for accuracy assessment.

2.1.4. DYNAMIC GUIDED IMPLANT PLACEMENT

Navident system (ClaroNav Inc., Toronto, Ontario, Canada) was used for dynamic implant navigation. A Navident head tracker and a standard trace registration protocol using 5 points (Fig. 5) were implemented following the manufacturer's recommendations [345]. Every plan received three repetitive implant placement sessions summing up to 12 implantation sessions per model.
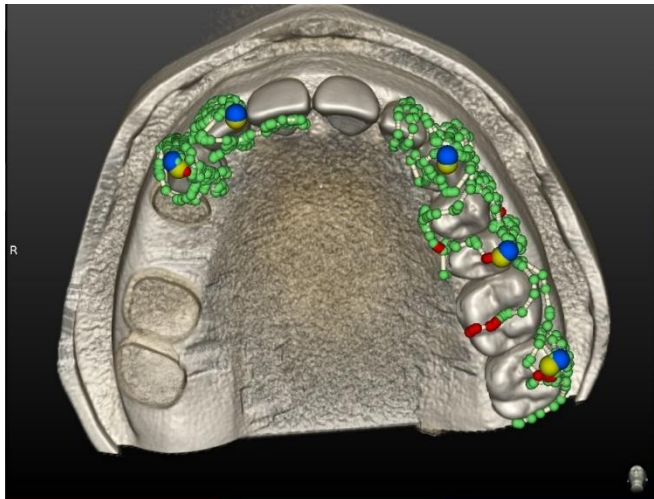
Fig. 5. Trace registration using 5 reference points in the Navident guidance system.

Implant placement used the same drills, including dense bone drills, as used in static guidance, following the same recommendations (2.1.3). The drilling sequence was adjusted specifically for the pilot drills, where only the final pilot drill of full length was calibrated and utilized instead of following the full sequence beginning with the shortest pilot drill, aligning with the standard dynamic navigation procedure. Implant placement was carried out using a fully guided approach, with the implant length calibrated based on the tip. After reaching the desired depth, the implant rotation was visually aligned to the nearest index based on the implant plan displayed on the computer screen. The insertion mounts were removed, and the model was made available for further accuracy evaluation.

2.1.5. ACCURACY EVALUATION

Post-operative implant position accuracy was evaluated using a novel IOS-based non-invasive X-ray-free method (3Shape). Implant scan bodies (catalogue number C2600.4310) were mounted on implants immediately after insertion, and registrations with IOS were taken (Trios4, 3Shape). The 3Shape software digital scan body was aligned using a three-point method, and the post-operative implant position coordinates were received (Fig. 6).

Fig. 6. A three-point alignment method is used to align of a digital scan body in the software (3shape).

Afterward, using the same software, pre-operative (planned) and post-operative implant positions were compared, and five deviation characteristics were evaluated:

- **Insertion point** – the distance between the centre points of the platforms of the two implants is the 3D displacement measure (Fig. 7-A).
- **Depth (s)** – depth deviation (signed values) shows the vertical deviation of the implant compared to the planned implant position. This is calculated by projecting the measured implant's centre to the planned implant's centre. In Fig. 7-B the axes for the implants are marked in blue, and the projected insertion point is the additional orange dot, placed using the dotted yellow line. The depth error is the distance marked by the full yellow line. It is negative if the placed implant is deeper than the planned implant. Otherwise, it is positive.
- **Depth (u)** – absolute depth deviation (unsigned values).
- **Horizontal deviation**. It is calculated by finding the shortest distance between the centre of the planned implant to the axis of the placed one. This is the distance between the top two orange dots in Fig. 7-C.
- **Angle deviation**. It is calculated in degrees by finding the smallest angle between the two implant centre axes, and this angle is marked in yellow in Fig. 7-D.

Figure 7-A   Figure 7-B   Figure 7-C   Figure 7-D
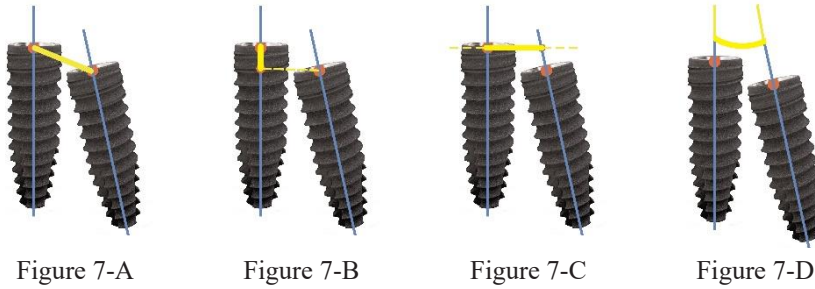
Fig. 7. Deviations measured in the study. A -insertion point; B – depth; C – horizontal; D – angle. The implant image on the left of each figure represents the planned implant position, and the image on the right – represents the post-operative implant position being evaluated.

2.1.6. DYNAMIC NAVIGATION ACCURACY
USING TWO REGISTRATION METHODS

A Kennedy Class I model, as described previously (3.1.1), was used and compared to a maxillary fully edentulous model that contained five well-defined and evenly distributed reference objects (cylinders with a diameter and length of 3 mm) positioned within the base (Fig. 8). Implant planning was conducted following the previously described protocol (3.1.2), with the exception that two implants were planned on each side for Kennedy1 class defects, resulting in a total of four implants per case (Table 7). Fully edentulous models also had four implants planned, all the same size as in the Kennedy 1 case (Table 7). Distal implants were angulated 30 degrees compared to the mesial implants (Fig. 8; as per COMFOUR™ concept) [473].
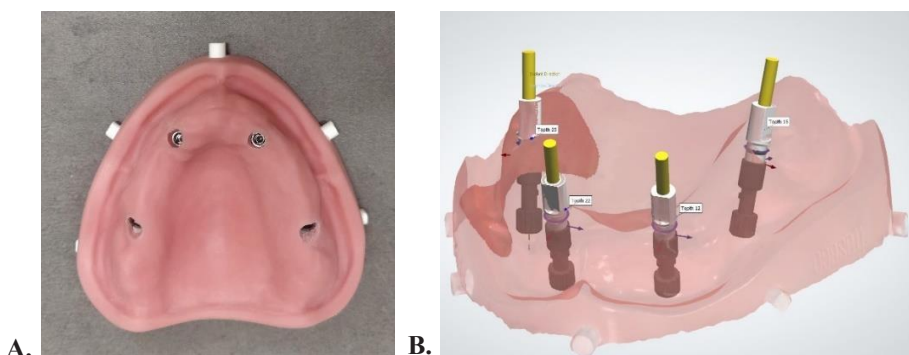
Fig. 8. An edentulous model with reference objects used in the study process. A – edentulous model after undergoing dynamically guided implant placement based on the digital plan. B – digital scan bodies that were aligned post-operatively to assess the accuracy of implant placement.

Table 7. Implant parameters were used in the study to compare dynamic guidance accuracy using two registration methods (teeth for the Kennedy1 group and reference objects for the fully edentulous group).

Position (FDI number)	Diameter	Length	Parallel
Kennedy I (teeth)			
Second right molar (#17)	4.3 mm	13 mm	Yes
First right premolar (#14)	3.8 mm	11 mm	Yes
First left premolar (#24)	3.8 mm	11 mm	Yes
Second left molar (#27)	4.3 mm	13 mm	Yes
Edentulous (reference objects)			
Second right premolar (#15)	4.3 mm	13 mm	Angulated by 30°
Second right incisor (#12)	3.8 mm	11 mm	Yes
Second left incisor (#22)	3.8 mm	11 mm	Yes
Second left premolar (#25)	4.3 mm	13 mm	Angulated by 30°

Following the manufacturer's recommendations, a Navident head tracker and a trace registration protocol utilizing five points were implemented (2.1.4) [345]. In the case of a Kennedy1 class arch defect, the anterior teeth were used to register the model's position, whereas for the edentulous case, the reference objects were employed.

Further steps for implant placement and accuracy evaluation were executed in accordance with the previously described protocol (2.1.4 and 2.1.5).

2.2. EVALUATION OF THE EFFECT OF DIFFERENT PROSTHETIC MATERIALS AND THEIR SURFACES ON THE HUMAN GINGIVAL FIBROBLASTS

Materials tested (Table 8): titanium (Ti), high translucent (ZrO-HT) and multi-layered ultra-high translucent zirconium oxide ceramics (ZrO-UTML), lithium disilicate glass-ceramics (NICE, EMAX), ZrO veneered with feldspar ceramics and glazed (ZrO-V), two types of milled (PMMA-Bre, PMMA-Ker) and 3D printed polymethylmethacrylate (PMMA-3D), polyetheretherketone (PEEK), and polyetherketoneketone (PEKK). The sample sizes for the surface and cellular experiments were determined based on a comprehensive analysis of relevant literature regarding the topic [437,474–476].

Table 8. Materials used in the study.

Abbrevia-tion	Material	Brand Name	Manufacturer
Ti (positive control)	Commercially pure grade 4 titanium	CopraTi-4	Whitepeaks Dental Solutions GmbH & Co. KG, Wesel, Germany
ZrO-HT	Zirconium oxide ceramics (3 mol % yttria-stabilized (Y2O3) tetragonal zirconia polycrystals)	KATANA™ Zirconia HT12	Kuraray Noritake, Tokyo, Japan
ZrO-UTML	Zirconium oxide ceramics (5 mol % yttria-stabilized (Y2O3) cubic zirconia polycrystals)	KATANA™ Zirconia UTML	Kuraray Noritake, Tokyo, Japan
ZrO-V	Zirconium oxide ceramic (ZrO-UTML), fired with feldspathic porcelain (potassium-aluminosilicate glass) and coated with glaze	CERABIEN™ ZR, CERABIEN™ ZR FC Paste Stain	Kuraray Noritake, Tokyo, Japan
NICE	Lithium aluminosilicate glass-ceramic reinforced with lithium disilicate	n!ce®	Straumann, Basel, Switzerland
EMAX	Lithium disilicate glass-ceramic	IPS e.max®	Ivoclar Vivadent, Schaan, Liechtenstein
PMMA-Ker	Polymethylmethacrylate	E4K PMMA Premia	Kerox Dental Ltd., St Sóskút, Hungary
PMMA-Bre	Polymethylmethacrylate composite with ceramic fillers	breCAM. multiCOM	Bredent, GmbH & Co KG, Senden, Germany
PMMA-3D	Polymethylmethacrylate (3D printed from methacrylic oligomers)	NextDent™ Crown and Bridge (C&B)	NextDent B.V., Soesterberg, The Netherlands
PEEK	Polyetheretherketone reinforced with ceramic filler	BioHPP®	Bredent, GmbH & Co KG, Senden, Germany
PEKK	Polyetherketoneketone reinforced with titanium dioxide	Pekkton® ivory	Cendres and Métaux, Biel/Bienne, Switzerland

2.2.1. SPECIMEN MANUFACTURE

Titanium specimens were milled using DATRON D5 dental mill system (DATRON AG, Mühltal, Germany). PMMA-3D specimens were printed using stereolithography technology (Form 2 printer, Formlabs, Somerville, MA, USA), and post-processed according to the manufacturer's guidelines.

All other ceramic and polymeric specimens from each group were firstly milled using a computer numeric controlled machine (Vhf S1 Impression, vhf camfacture AG, Ammerbuch, Germany) into long cylinders, which were subsequently cut into tablets. Cutting was performed using a saw microtome (Leica SP 1600, Leica Biosystems Nussloch GmbH, Nußloch, Germany) with a water-cooling agent.

ZrO groups were milled and cut larger before sintering in order to compensate for the shrinkage coefficient. The sintering procedures were performed according to the manufacturer's instructions for each material. The exact dimensions of the specimens after manufacture were 2 mm in height and 5 mm in diameter (Figure 9).

The ZrO-V group specimens were made from ZrO-UTML which were later sandblasted with 50μm alumina (Al_2O_3) particles for 15 s at 0.2 MPa pressure, an angle of 90°, and a distance of 15 mm from the surface. The air-abraded specimens were then cleaned in an ultrasonic bath with distilled water for 10 minutes (42,000 vibration/sec, Carrera 2505 PEARL Cosinus Ultrasonic Cleaner, Aquarius Deutschland GmbH, Düsseldorf, Germany) and air-dried. Subsequently the specimens were fired with feldspathic porcelain and glazed according to the manufacturer's instructions.
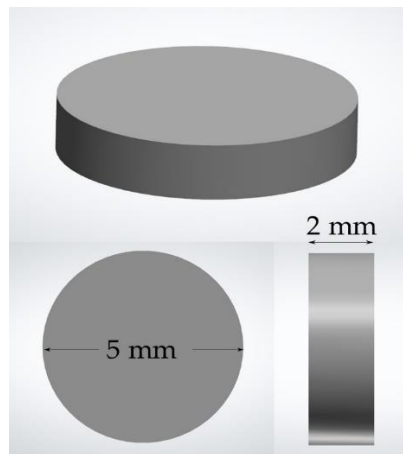
Fig. 9. Final dimensions of specimens used in the study.

2.2.2. PROFILOMETRY

Surface mean roughness (Sa) was measured using a 3D optical profiler system (PLµ 2300, Sensofar, Sensofar Group, Barcelona, Spain) with a confocal objective 50 × /0.8 A with FOV 255 × 191 µm (Nikon Lu Plan, Nikon Metrology NV, Leuven, Belgium). Five specimens from every material group were selected randomly, and 3 images of surface areas (two areas were randomly chosen on a surface periphery and one in the centre) on every selected specimen were made. The images were processed, and Sa values were measured using Gwyddion Software (Czech Metrology Institute, Jihlava, Czech Republic).

2.2.3. WATER CONTACT ANGLE MEASUREMENTS

The mean water contact angle was measured for each material group to evaluate surface hydrophilicity. After the surface cleaning samples were subsequently placed in a Krüss EasyDrop system (KRÜSS GmbH, Hamburg, Germany) and deionized water droplets (16 Ω, 2 µL) were placed on the samples, pictures were taken after 10 s and finally analysed using Krüss software (KRÜSS GmbH, Hamburg, Germany). Two measurements (one on each side of the droplet) were obtained, and the mean value was calculated. The sample chamber temperature was kept constant at 21 °C using a LabTech H50-500 water chiller (LabTech Srl, Sorisole BG, Italy). Five specimen surfaces were randomly selected from each material group resulting in 5 measurements.

2.2.4. CELL CULTURING

Cells were grown in an IMDM (Iscove's Modified Dulbecco's Medium; Gibco, Thermo Fisher Scientific, Waltham, MA, USA) with 10 % FCS (Fetal calf serum; Gibco, Thermo Fisher Scientific, Waltham, MA, USA) and antibiotics (penicillin, 100 VV/mL, and streptomycin, 100 µg/mL; Gibco, Thermo Fisher Scientific, Waltham, MA, USA) in 50 mL plastic flasks (Greiner, Greiner Bio-One GmbH, Frickenhausen, Germany). The experiments used 96 well plates (Greiner, Greiner Bio-One GmbH, Frickenhausen, Germany). Cells were grown in the incubator (Heracell™ 150i, Thermo Fisher Scientific, Waltham, MA, USA) at 37 °C, 5 % CO_2, 95 % H_2O).

Primary human gingival fibroblast (HGF) mono-layered culture was derived from healthy patient undergoing periodontal surgery using the technique described in previous research (approval of the national Bioethics committee No 158200-16-860-369) [474]. The cells from 6 to 12 passages were used in this experiment.

HGF were passaged twice a week using a 0.25% EDTA-trypsin solution following incubation at 37°C for 2-10 minutes; the dissociation of the cell monolayer was assessed under an inverted microscope, and the rounded, floating cells were suspended in a fresh growth medium with fetal bovine serum, then counted and adjusted to the desired density of 15000-30000 cells/ml before being transferred to new flasks.

In addition to human gingival fibroblasts, a spontaneously immortalized primary human gingival epithelial-like cell culture was used in this part of the study as described in previous studies [477–480]. It was received as from a clinically healthy patient. Cells from 12 to 14 passages were used in the experiments. The cells growing in suspension were harvested, centrifuged, and diluted in the growth medium, seeded and gradually frozen in freezing medium (70 % IMDM + 20 % FCS + 10 % DMSO (Sigma-Aldrich, St. Louis, MI, USA)). The culture was kept at a temperature of -80 °C. Upon thawing, the cells were seeded onto prepared samples of each material group. Human gingival epithelial-like cells adhered and grew as a monolayer.

2.2.5. CYTOTOXICITY AND PROLIFERATION ASSESSMENT

This study used 96-well plates (Greiner, Greiner Bio-One GmbH, Frickenhausen, Germany). A suspension of HGF (30×10^3 cells/mL) was prepared and poured into the plate wells with the specimens, 200 μL each, to evaluate the cytotoxicity and proliferation. For the HGF cytotoxicity evaluation, three specimens of every group were used and the number of viable cells on the specimens and the plastic control surface was registered at 12 h. The experiment was repeated three times. For the HGF proliferation assessment, three specimens from each group were used per time point (registered at 24, 48, and 72 h), respectively, and the experiment was repeated three times.

The viable cell amount was evaluated using the MTT (3-(4,5-dimetiltiazol-2-il)-2,5-diphenyltetrazolium bromide) method. At each time point, the cell growth medium was cautiously eliminated from every well, and each was filled

with 100 μL of MTT (Merck Chemicals, Merck KGaA, Darmstadt, Germany) 1 mg/mL prepared in phosphate-buffered saline (Medicago, Quabec City, Canada). MTT was removed after one hour of incubation at 37 °C, 5 % CO_2. Then, 100 μL 96 % ethanol (Vilniaus degtinė, Vilnius, Lithuania) was used to dissolve the resulting formazan crystals and 50 μL of the formed solution was poured into the new plate wells. Later, the solvent and specimens' optical density (OD) was measured spectrophotometrically at 570 nm. A spectral scanning multimode reader (Varioskan Flash, Thermo Scientific, Waltham, MA, USA) was applied for this purpose. The difference between the specimen and the mean of solvent OD was computed. The obtained OD is directly proportional to the number of viable cells. The OD, equal to the count of viable cells grown on each specimen, was described with the negative control group to compare assays. The control group was determined to be the OD, which described the number of viable cells grown on a plate well surface. For the cytotoxicity evaluation, the ratio OD of the specimen/OD of the control group at 12 h shows if the surface of a specific material inhibits the cell growth (the ratio is below 1) or, on the contrary, promotes cell proliferation (the ratio is higher than 1).

2.2.6. POLYMER-BASED MATERIALS EVALUATION

Five types of polymeric materials were included in this part of the study: polymethylmethacrylate (PMMA-Ker), polymethylmethacrylate composite (PMMA-Bre), 3D printed polymethylmethacrylate (PMMA-3D), polyetheretherketone reinforced with ceramic filler (PEEK), and polyetherketoneketone reinforced with titanium dioxide (PEKK) (Table 8). Two positive control groups were used: titanium (Ti) and zirconium oxide ceramic (ZrO-HT). In total, 84 specimens were used (12 specimens per group).

2.2.6.1. SURFACE POLISHING OF THE POLYMER-BASED SPECIMENS

Each side of the specimens was polished according to the manufacturer's protocol (Table 9). Specimens were repolished following the same protocol before every separate experiment was used in the study.

Table 9. The polishing protocols used for each material surface.

Material	Polishing Protocol per Each Surface			
Ti	EVE (R22 Item No.: 1000) White polisher 7000–10,000 min^{-1}/ 30 s EVE Ernst Vetter GmbH, Keltern, Germany	EVE (CRP-R22m) Dark blue polisher 8000–15,000 min^{-1}/ 30 s EVE Ernst Vetter GmbH, Keltern, Germany	Zircopol polishing paste and narrow brush 10,000 min^{-1}/ 30 s Feguramed GmbH, Buchen, Germany	
ZrO-HT	MPF Zmax disc (Item No. 120-0001 Zmax Large Disc 22 × 4.5 mm) 5000–10,000 min^{-1}/ 30 s MPF Brush Co., Nicosia, Cyprus	Edenta (R1530HP) StarGloss pink polisher for ceramics 5000 min^{-1}/ 30 s EDENTA AG, Au/St. Gallen, Switzerland	Edenta (R1540HP) StarGloss green polisher for ceramics 5000 min^{-1}/ 30 s EDENTA AG, Au/St. Gallen, Switzerland	Zircopol polishing paste and narrow brush 10,000 min^{-1}/ 30 s Feguramed GmbH, Buchen, Germany
PMMA-Ker, PMMA-Bre, PMMA-3D	BREDENT acrylic polisher medium grey (REF P243HM10) 10,000–15,000 min^{-1}/ 30 s Bredent medical GmbH & Co.KG, Senden, Germany	BREDENT Pumice polishing paste and narrow brush 5000–10,000 min^{-1}/ 30 s Bredent medical GmbH & Co.KG, Senden, Germany	SILADENT TEK-1 POL Diamond polishing paste and cotton brush 10,000 min^{-1}/ 30 s Siladent Dr. Böhme & Schöps GmbH, Goslar, Germany	
PEEK, PEKK	BREDENT acrylic polisher medium grey (REF P243HM10) 10,000–15,000 min^{-1}/ 30 s Bredent medical GmbH & Co.KG, Senden, Germany	Zircopol polishing paste and narrow brush 10,000 min^{-1}/ 30 s Feguramed GmbH, Buchen, Germany		

Specimens were randomly selected for each cleaning group.

Conventional cleaning protocol (CCP): specimens were disinfected in "Perform 2 %" (Schülke & Mayr GmbH, Norderstedt, Germany) solution for 10 min, then rinsed with tap water for 30 s, soaked in isopropyl alcohol (Isopropyl alcohol, ≥ 99.7 %, Sigma-Aldrich, St. Louis, MI, USA) for 10 min and washed in an ultrasonic cleaner (42,000 vibration/sec, Carrera 2505 PEARL Cosinus Ultrasonic Cleaner) with distilled water for 3 min.

Research cleaning protocol (RCP): specimens were soaked in "Decon" solution (Decon Laboratories™ Decon 90™, Fisher Scientific, NH, USA) and put on a laboratory tumbling table (Mini-Tumbling Table WT17, 25 rpm, angle of inclination 5°/10°, Biometra GmbH, Göttingen, Germany) for 24 h, rinsed with tap water 20 times, then rinsed with distilled water 10 times and soaked in 70 % ethanol for 24 h.

After washing, specimens were air-dried at room temperature for 24 h. The same protocol was repeated after every specimen polishing session before the next experiment.

2.2.7. ZIRCONIA-BASED CERAMIC MATERIALS AND PHOTOFUNCTIONALIZATION

Two materials for abutment fabrication were selected for this part of the study: ZrO-HT and ZrO-UTML (Table 8). The sample size was determined by analysing the available literature of relevant articles published on the topic. Twenty test specimens ($n = 20$) were used from each material. These were further randomly allocated to one of the groups based on surface treatment, with ten per material in each group ($n = 10$).

2.2.7.1. SURFACE FINISHING PROTOCOL OF THE ZIRCONIA-BASED SPECIMENS

All surfaces were polished according to protocols suggested by the manufacturer (Table 10). Specimens were polished each time following the exact same protocol before every separate experiment in the study. Research cleaning protocol was used for specimen cleaning (Fig. 10). Following washing, the specimens were allowed to air-dry at room temperature for 24 hours. The same surface finishing procedure (polishing and cleaning) was repeated after each session of specimen polishing, immediately before commencing the subsequent experiment.

Table 10. Polishing protocol used in the study.

Material	Polishing Protocol Used			
ZrO-HT ZrO-UTML	MPF Zmax disc (Item No. 120-0001 Zmax Large Disc 22 × 4.5 mm) 5000–10,000 min⁻¹/ 30 s MPF Brush Co., Nicosia, Cyprus	Edenta (R1530HP) StarGloss pink polisher for ceramics 5000 min⁻¹/ 30 s EDENTA AG, Au/St. Gallen, Switzerland	Edenta (R1540HP) StarGloss green polisher for ceramics 5000 min⁻¹/ 30 s EDENTA AG, Au/St. Gallen, Switzerland	Zircopol polishing paste and narrow brush 10,000 min⁻¹/ 30s Feguramed GmbH, Buchen, Germany

Fig. 10. Profilometry images for both materials included in the study based on the location: (**A**) ZrO-HT centre, (**B**) ZrO-HT periphery, (**C**) ZrO-UTML centre, (**D**) ZrO-UTML periphery.

2.2.7.2. UV PHOTOFUNCTIONALIZATION

Ten specimens per material group were selected randomly and subjected to UV surface photofunctionalization. The specimens were treated with a UV-C light system (Sylvania G15W T8 lamps, Feilo Sylvania Group, Shanghai Feilo Acoustics Co., Budapest, Hungary) with a peak wavelength of 253.7 nm for 48 h at 12 cm distance. The procedure resulted in 3.49 mW/cm^2 irradiance and was repeated between different tests. Photofunctionalization was repeated before each experiment for UV-treated groups.

2.2.8. CERAMIC MATERIALS EVALUATION

Five commercially available ceramic prosthetic materials (ZrO-HT, ZrO-UTML, ZrO-V, NICE, EMAX) and a positive Ti control group were included in this study part (Table 8). Ten test specimens (n = 10) were used from each material.

All surfaces were polished according to protocols suggested by the manufacturer (Table 11). Then research cleaning protocol (RCP) was used for

specimen cleaning. After washing, the specimens were left to air-dry at room temperature for 24 hours. Prior to each separate experiment conducted in the study, the specimens were polished and washed using the exact same protocol.

Table 11. Polishing protocol used in the study.

Material	Polishing Protocol per Each Surface			
Ti	EVE (R22 Item No.: 1000) White polisher 7000–10,000 min^{-1}/ 30 s EVE Ernst Vetter GmbH, Keltern, Germany	EVE (CRP-R22m) Dark blue polisher 8000–15,000 min^{-1}/ 30 s EVE Ernst Vetter GmbH, Keltern, Germany	Zircopol polishing paste and narrow brush 10,000 min^{-1}/30 s Feguramed GmbH, Buchen, Germany	
ZrO-HT, ZrO-UMTL, ZrO-V	MPF Zmax disc (Item No. 120-0001 Zmax Large Disc 22 × 4.5 mm) 5000–10,000 min^{-1}/ 30 s MPF Brush Co., Nicosia, Cyprus	Edenta (R1530HP) StarGloss pink polisher for ceramics 5000 min^{-1}/ 30 s EDENTA AG, Au/St. Gallen, Switzerland	Edenta (R1540HP) StarGloss green polisher for ceramics 5000 min^{-1}/ 30 s EDENTA AG, Au/St. Gallen, Switzerland	Zircopol polishing paste and narrow brush 10,000 min^{-1}/ 30 s Feguramed GmbH, Buchen, Germany
NICE, EMAX	VITA SUPRINITY polishing kit VI-SR 15m 7000-12,000 min^{-1} 30 s VITA Zahnfabrik, H. Rauter GmbH & Co. KG, Bad Säckingen, Germany	VITA SUPRINITY polishing kit VI-SR 15f 4000-8,000 min^{-1} 30 s VITA Zahnfabrik, H. Rauter GmbH & Co. KG, Bad Säckingen, Germany	Zircopol polishing paste and narrow brush 10,000 min^{-1} 30 s Feguramed GmbH, Buchen, Germany	

2.3. STATISTICAL ANALYSIS

Each step in the study that required randomization was conducted using the online tool *www.randomlists.com*.

Statistical analysis was performed using R i386 4.0.0 (Lucent Technologies, Auckland, New Zealand). The graphs were plotted using the ggplot2 plugin (Lucent Technologies, Auckland, New Zealand). The statistical significance level was set at $p < 0.05$. Data normality was tested, and parametric methods were used in case of normal data distribution; otherwise, a non-parametric analysis was performed.

Data normality and homogeneity of variance were tested by graphical analysis complemented with Shapiro-Wilks and Levene's tests. In the case of parametric analysis, the equality of variances was tested using two variances F-test (two-sided) for two groups. In the case of unequal variances, parametric tests were adjusted accordingly.

To compare the means of the two groups two-tailed independent samples *t*-test was used as a parametric test and two-sample Wilcoxon test (two-tailed with a normal approximation with continuity correction) as a non-parametric option.

In the case of parametric means comparison for more than two groups, ANOVA (either one- or two-way with interaction) were used to test the hypotheses. Where significant differences were established, appropriate post hoc and pairwise comparisons (Tukey, Games-Howell, T-test) were used. For non-parametric multiple-group means comparison Kruskal–Wallis rank-sum test and pairwise comparisons using the Wilcoxon exact rank-sum test with *p* value adjustment using Benjamini and Hochberg method were performed.

3. RESULTS

3.1. DYNAMIC GUIDED IMPLANT PLACEMENT ACCURACY

A total of 84 implants were placed, with an equal distribution of implants in each subgroup. The insertion point deviation measures ranged from 0.19 mm to 1.71 mm. Depth (s) and (u) deviations ranged from -1.47 mm to 0.74 mm and from 0.02 mm to 1.47 mm respectively. Horizontal deviation ranged from 0.09 mm to 1.37 mm. Angle deviations were in the range between 0.36° and 6.17°. Mean values and standard deviations according to Kennedy's classification of an edentulous defect and implant design are presented in Table 12. Further statistical analysis (factorial ANOVA) for each deviation type included Kennedy class, implant design, and implant position (mesial/distal) as factors. Insertion point, depth (s) and (u), horizontal and angle deviation means and standard deviations for each Kennedy class defect, implant design, and mesial/distal implant position are presented in **Fig. 11, 12, 13, 14,** and **15** respectively. The data normality exhibited minor deviations from a normal distribution, thus caution should be exercised when interpreting the results. Statistically significant factorial ANOVA (except for the single tooth edentulous defect) results between the groups are presented in brackets over the bars. Single tooth edentulous defect group means between different implant design groups were compared using a t-test, and in case of statistically significant difference, bracketed notation is provided in the figures.

Table 12. Implant placement deviations according to the edentulous defect Kennedy class and implant design (means ± SDs).

	Insertion point	Depth (s)	Depth (u)	Horizontal	Angle
Kennedy I					
Screw-Line	1.0 ± 0.3	-0.6 ± 0.5	0.6 ± 0.5	0.7 ± 0.3	1.8 ± 0.8
Progressive-Line	0.8 ± 0.4	-0.4 ± 0.7	0.6 ± 0.4	0.5 ± 0.2	2.4 ± 1.0
Kennedy II					
Screw-Line	0.9 ± 0.4	-0.1 ± 0.4	0.3 ± 0.3	0.7 ± 0.4	2.5 ± 1.4
Progressive-Line	0.8 ± 0.4	-0.3 ± 0.6	0.5 ± 0.4	0.6 ± 0.3	3.6 ± 1.6
Kennedy III					
Screw-Line	0.6 ± 0.3	-0.3 ± 0.3	0.4 ± 0.2	0.4 ± 0.3	2.0 ± 1.2
Progressive-Line	0.8 ± 0.4	-0.2 ± 0.6	0.5 ± 0.4	0.5 ± 0.3	1.9 ± 0.6
Single					
Screw-Line	0.7 ± 0.3	-0.5 ± 0.4	0.5 ± 0.3	0.5± 0.2	1.0 ± 0.5
Progressive-ne	0.7 ± 0.3	0.01 ± 0.3	0.2 ± 0.2	0.6 ± 0.3	2.0 ± 1.3

Factorial ANOVA of the insertion point data showed statistical significance for the implant design and implant position factors interaction (p = 0.018); post hoc analysis showed a statistically significant difference for the SL design implant comparing mesial and distal implant positions (p = 0.02). Kennedy's class in the factorial ANOVA was near a statistical significance level (p = 0.08). T-test analysis for a single tooth edentulous defect showed no statistically significant difference between implant design groups.

Fig. 11. Insertion point deviation means and standard deviations according to the Kennedy class of an edentulous defect, implant design, and implant position (mesial or distal).

Factorial ANOVA of the depth (s) deviation data showed statistical significance for the implant design and implant position factors interaction (p = 0.02); post hoc analysis showed a statistically significant difference for the PL design implant comparing mesial and distal implant positions (p = 0.05). T-test analysis for a single tooth edentulous defect showed a statistically significant difference between implant design groups (p = 0.029).

Fig. 12. Signed depth (depth (s)) deviation averages and standard deviations according to the Kennedy class of an edentulous defect, implant design, and implant position (mesial or distal). T-test statistics were used for a single tooth edentulous defect case two implant design group comparison.

Factorial ANOVA of the depth (u) deviation data showed statistical significance for the implant design and implant position factors interaction (p = 0.018); post hoc analysis showed implant design to have a p-value near statistical significance (p = 0.07) in a mesial implant position. The Kennedy class in the factorial ANOVA was near a statistical significance level (p = 0.07). T-test analysis for a single tooth edentulous defect showed no statistically significant difference between implant design groups.

Fig. 13. Absolute depth (depth (u)) deviation averages and standard deviations according to the Kennedy class of an edentulous defect, implant design, and implant position (mesial or distal).

Factorial ANOVA of the horizontal deviation data showed statistical significance for the implant position factor (p = 0.017). Kennedy class in the factorial ANOVA was near a statistical significance level (p = 0.066) and Kennedy class and implant design interaction (p = 0.07). T-test analysis for a single tooth edentulous defect showed no statistically significant difference between implant design groups.
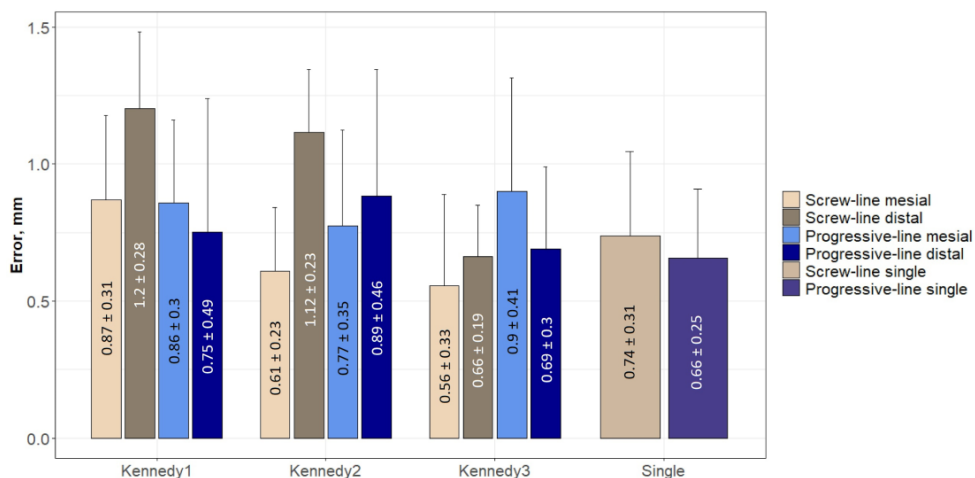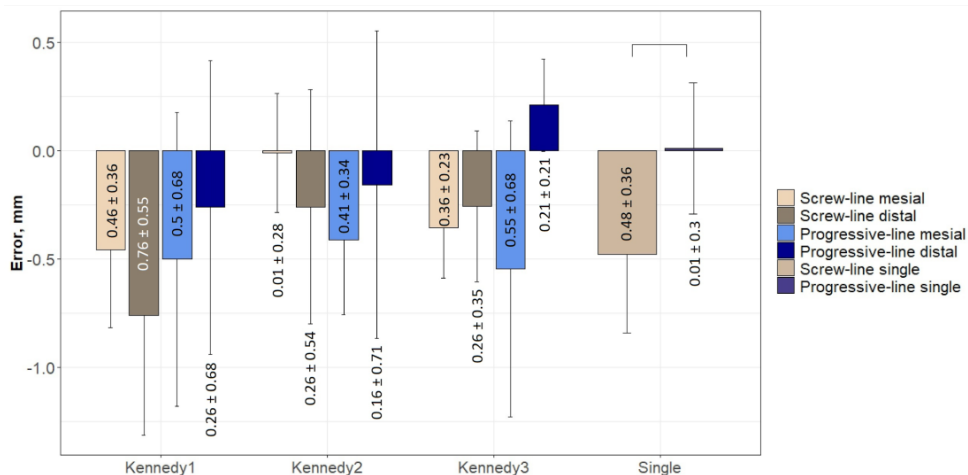

Fig. 14. Horizontal deviation averages and standard deviations according to the Kennedy class of an edentulous defect, implant design, and implant position (mesial or distal).

Factorial ANOVA of the angle deviation data showed statistical significance for every factor individually and interactions for the Kennedy class of the edentulous defect and implant position (p = 0.0008) and for all three factors (p = 0.013). K2 class had significantly (post hoc contrasts test (p-values adjusted using MVT method)) higher deviation 3.1 ± 1.6 degrees compared to K1 (2.1 ± 1.0 degrees, p = 0.001) and K3 class (2 ± 0.9 degrees, p = 0.0004) defects. The average deviations for SL and PL implant design groups were 2.1 ± 1.2 and 2.6 ± 1.3 degrees, respectively (p = 0.0243). The average deviations for implant positions were: 1.9 ± 1.0 degrees for mesial; 2.8 ± 1.3 degrees for distal (p = 0.0001). The Kennedy class of the edentulous defect and implant position interaction showed significant differences (all p values < 0.001) for the following groups: K1-K2 distal region, K2-K3 distal region, and mesial-distal in the K2 class. T-test analysis for a single tooth edentulous defect showed no statistically significant difference between implant design groups.

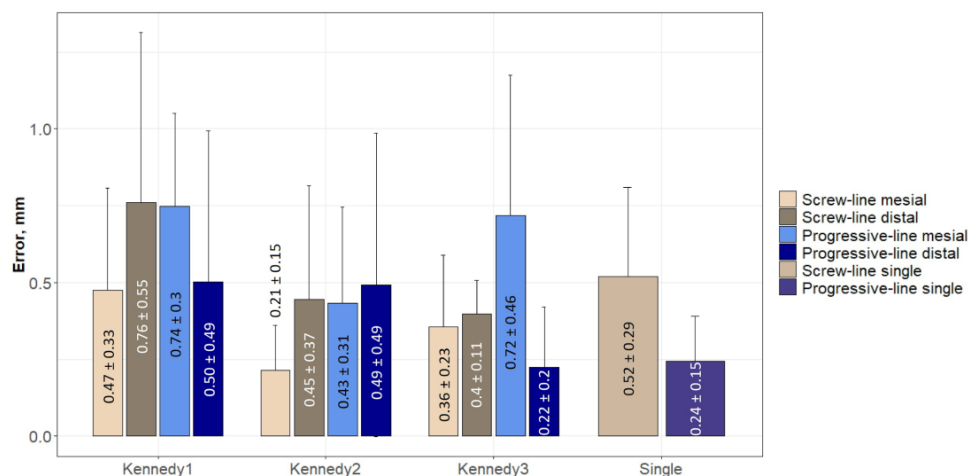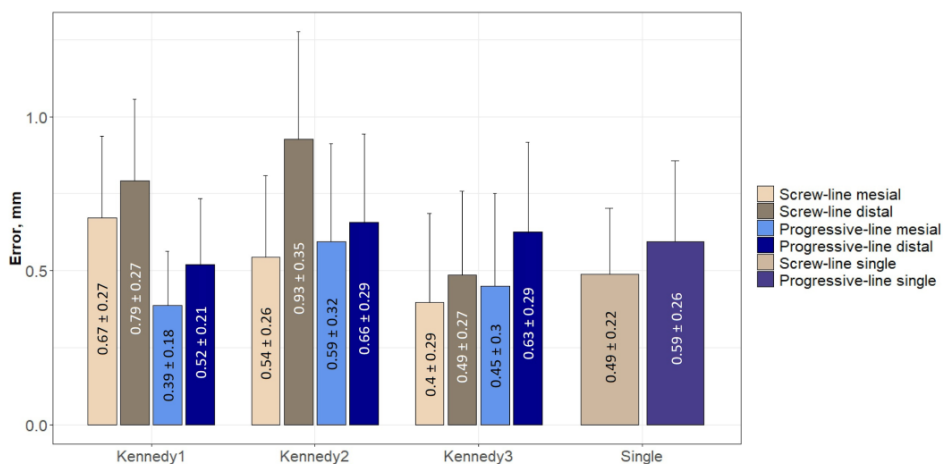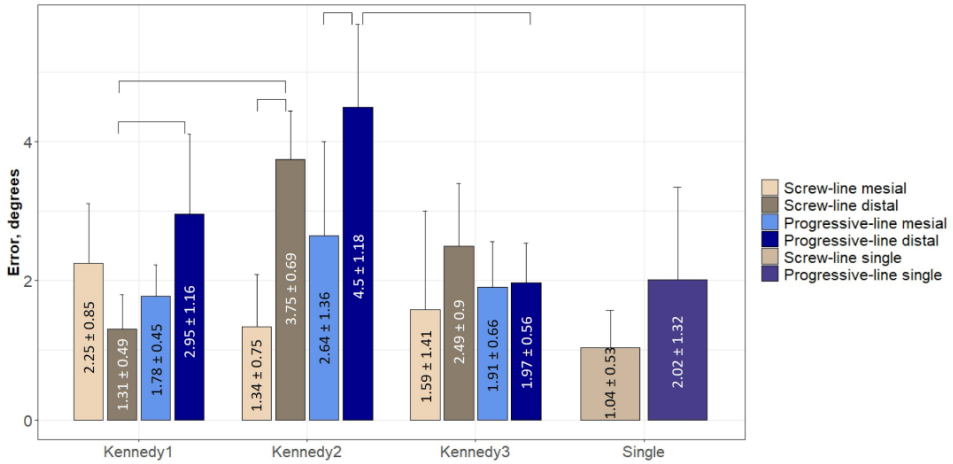**Fig. 15.** Angle deviation averages and standard deviations according to the Kennedy class of an edentulous defect, implant design, and implant position (mesial or distal). Multiway ANOVA with post hoc contrasts test (p-values adjusted using MVT* method).

*Monte-Carlo corrected p-value based on multivariate normal t-test distribution

3.2. COMPARISON OF DYNAMIC AND STATIC GUIDED IMPLANT PLACEMENT ACCURACY

A total of 168 implants were placed, with an equal distribution of 84 implants in each guidance group. The descriptive statistics of deviations for each guidance group are provided in Table 13. The average 3D insertion point deviation for static guidance was measured to be 0.52 ± 0.28 mm, while for dynamic guidance, it was found to be 0.77 ± 0.32 mm. The average angle deviation for static guidance was 2.90 ± 1.26 degrees, whereas, for dynamic guidance, it was 2.26 ± 1.26 degrees.

A total of 144 implant placements for fixed bridge prosthetic restoration were analysed using factorial (four-way) ANOVA, excluding the K3-single group. The factors included in the analysis were guidance (static, dynamic), Kennedy defect class (K1, K2, K3), implant line (SL, PL), and position (mesial, distal). The implants were evenly distributed across the different groups. Statistically significant results of factorial ANOVAs (excluding the K3 single group from the analysis) for each type of deviation are provided in Table 14. It is important to note that for some ANOVA models, the distribution of the residuals exhibited a departure from normality, indicating that the reported results should be interpreted with caution.

Table 13. The descriptive statistics of deviations for each guidance group.

		Average	SD	Min	Max	Median	IQR
Insertion point	Static	0.52	0.28	0.09	1.7	0.45	0.27
	Dynamic	0.77	0.32	0.20	1.5	0.76	0.48
Depth (s)*	Static	-0.22	0.33	-1.38	0.40	-0.18	0.35
	Dynamic	-0.27	0.48	-1.46	0.74	-0.25	0.67
Depth (u)	Static	0.29	0.27	0	1.38	0.21	0.25
	Dynamic	0.45	0.33	0.02	1.46	0.37	0.45
Horizontal	Static	0.37	0.21	0.03	0.98	0.34	0.23
	Dynamic	0.56	0.28	0.1	1.37	0.51	0.41
Angle	Static	2.9	1.3	0.5	6.3	2.8	1.6
	Dynamic	2.3	1.3	0.4	6.2	2.0	1.7

* a negative value indicates an implant placement that is too deep; a positive – is not deep enough.

Guidance was found to be a statistically significant factor for all deviations, with static guidance showing smaller deviations compared to dynamic guidance, except for the angle deviation, which was lower in the dynamic guidance group (Table 13 and Fig. 16).

Among all the significant interactions observed for the insertion point deviations, the only one involving the guidance was found in relation to the Kennedy class factor, as indicated in Table 14. Caution should be exercised when interpreting the results due to minor deviations from the assumption of normality. In the K1 and K2 groups, static guidance exhibited lower deviations compared to dynamic guidance ($p < 0.0001$ and $p = 0.0001$, respectively), while this difference was not observed in the K3 group ($p = 0.9$). For the K3 single group, factorial ANOVA revealed that the guidance factor remained statistically significant ($p = 0.009$) in terms of insertion point accuracy, favouring the static method over dynamic. However, no other factors or interactions reached statistical significance in this analysis (Fig. 17).

The analysis of signed depth deviation results showed a predominance of negative values, indicating that in the majority of cases, the implants were placed deeper than the planned position in the models (Fig. 18). Due to the counteracting nature of positive and negative values, numerical statistical analysis was not performed on the depth (s) deviation results, as it would be challenging to interpret both statistically and clinically.

Table 14. Factorial ANOVA significant results and the result of four-way interaction. Factors: Guidance (dynamic, static), Kennedy (Kennedy class group: K1, K2, K3), Implant (implant line: SL, PL), Position (mesial, distal).

Factors and interactions	Sum Sq	F value	Pr(>F)
Insertion point, 3D*			
Guidance	2.458	36.072	< 0.0001
Guidance : Kennedy	0.6995	5.133	0.007
Implant : Kennedy	0.692	5.078	0.008
Implant : Position	1.589	23.322	< 0.0001
Kennedy : Position	1.412	10.36	< 0.0001
Guidance : Implant : Kennedy : Position	0.335	2.457	0.09
Depth (u)**			
Guidance	0.698	8.025	0.005
Implant : Position	0.923	10.613	0.001
Kennedy : Position	0.767	4.407	0.01
Guidance : Implant : Kennedy : Position	0.046	0.266	0.77
Horizontal*			
Guidance	1.537	34.774	< 0.0001
Guidance : Kennedy	0.734	8.307	0.0004
Implant : Kennedy	0.304	3.438	0.04
Guidance : Position	0.424	9.592	0.002
Implant : Position	0.396	8.950	0.003
Kennedy : Position	0.494	5.585	0.005
Implant : Kennedy : Position	0.376	4.254	0.02
Guidance : Implant : Kennedy : Position	0.318	3.60	0.03
Angle			
Guidance	9.482	9.754	0.002
Position	17.283	17.778	< 0.0001
Guidance : Kennedy	22.137	11.386	< 0.0001
Guidance : Position	5.013	5.157	0.02
Kennedy : Position	20.112	10.344	< 0.0001
Guidance : Implant : Kennedy	11.008	5.662	0.004
Guidance : Kennedy : Position	11.616	5.975	0.003
Guidance : Implant : Kennedy : Position	5.165	2.657	0.07

* ANOVA model residuals Shapiro-Wilk normality test values 0.03

** ANOVA model residuals Shapiro-Wilk normality test value ≤0.001
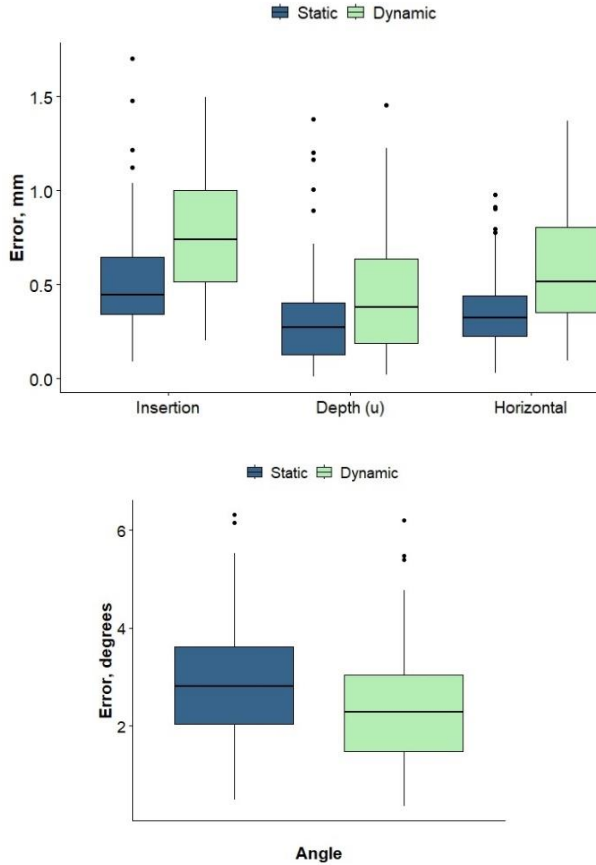
Fig. 16. Boxplot diagrams showing the deviation distributions for each guidance method for implant positioning.

The absolute depth deviations (Fig. 19), analysed using factorial ANOVA, revealed significant differences for the guidance factor (Table 13 and Fig. 16), as well as interactions between position (mesial, distal) and implant design (SL, PL), and position with Kennedy class of the defect (K1, K2, K3) (Table 14). Post hoc analysis was not performed for the interactions as they did not involve the main factor of interest (guidance), and this decision was also influenced by the violation of the normality assumption in the residuals distribution of the ANOVA model. Therefore, the results should be interpreted cautiously.

Fig. 17. Insertion point deviation according to the Kennedy class of an edentulous defect, guidance method, implant design, and implant position (mesial or distal).

Fig. 18. Signed depth (s) deviation according to the Kennedy class of an edentulous defect, guidance method, implant design, and implant position (mesial or distal).

Fig. 19. Absolute depth (depth (u)) deviation according to the Kennedy class of an edentulous defect, guidance method, implant design, and implant position (mesial or distal). Multiway ANOVA with post hoc contrasts test (p-values adjusted using MVT method) for K3 single group.

For the depth (u) analysis of the K3 single group, factorial ANOVA analysis once again supported the significant impact of the guidance on the accuracy, favouring the static approach (p = 0.002). Moreover, an interaction between guidance and implant design was observed, indicating that for screw line implants, the accuracy was significantly higher for the static than dynamic method (post hoc contrasts test, MVT adjusted p = 0.002; Fig. 19).

Factorial ANOVA analysis of horizontal deviations revealed significant effects of the guidance method (Table 13, Fig. 16) and interactions of other factors, as indicated in Table 14. The interpretation of the results should be cautiously approached due to minor deviations from the normality assumption. Post hoc analysis with contrasts test (MVT adjusted p values) for the interaction of guidance and Kennedy class revealed significant differences in accuracy between static and dynamic guidance for K1 (MVT adjusted p = 0.0005) and K2 (MVT adjusted p < 0.0001) groups, with static guidance being more accurate. Additionally, dynamic guidance demonstrated slightly higher accuracy in the K3 group compared to the K2 group (MVT adjusted p = 0.03). Regarding the interaction between guidance and position, it was observed that static guidance demonstrated greater accuracy in the distal position compared to dynamic guidance (MVT adjusted p < 0.0001), while the mesial position showed higher accuracy than the distal position in the dynamic guidance group (MVT adjusted p = 0.007). The significant differences observed in the interaction between all four factors are presented in Fig. 20.

Factorial ANOVA analysis for the K3 single group did not reveal any significant differences for any factors or interactions in relation to horizontal deviation.

In addition to guidance (Table 13, Fig. 16), the position factor also showed statistical significance for mean angle deviations, favouring the mesial position (p < 0.0001). Given the significant results obtained from the interactions of the guidance method, Kennedy class, and implant position factors (Table 14), for the sake of simplicity in reporting, a detailed post hoc analysis of the significant three-way interaction is presented (Fig. 21).

For the K3 single group, factorial ANOVA analysis demonstrated that guidance was a significant factor in relation to angle deviation, favouring the dynamic method over static (p = 0.005; Fig. 21). No other significant factors or interactions were observed in relation to angle deviation for the K3 single group.
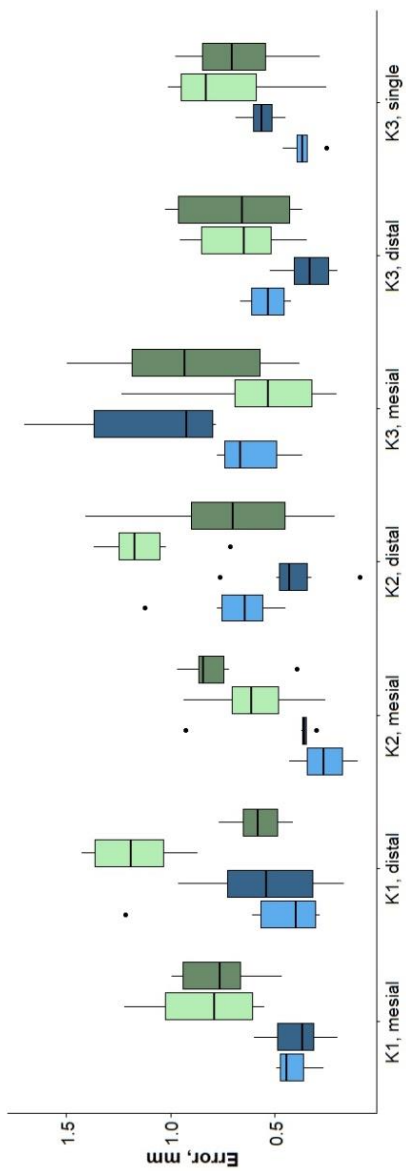
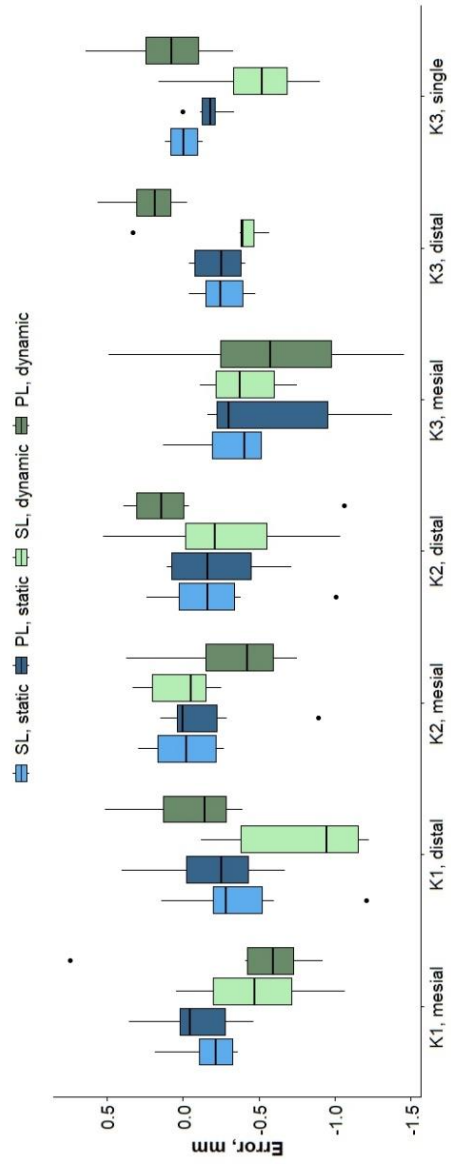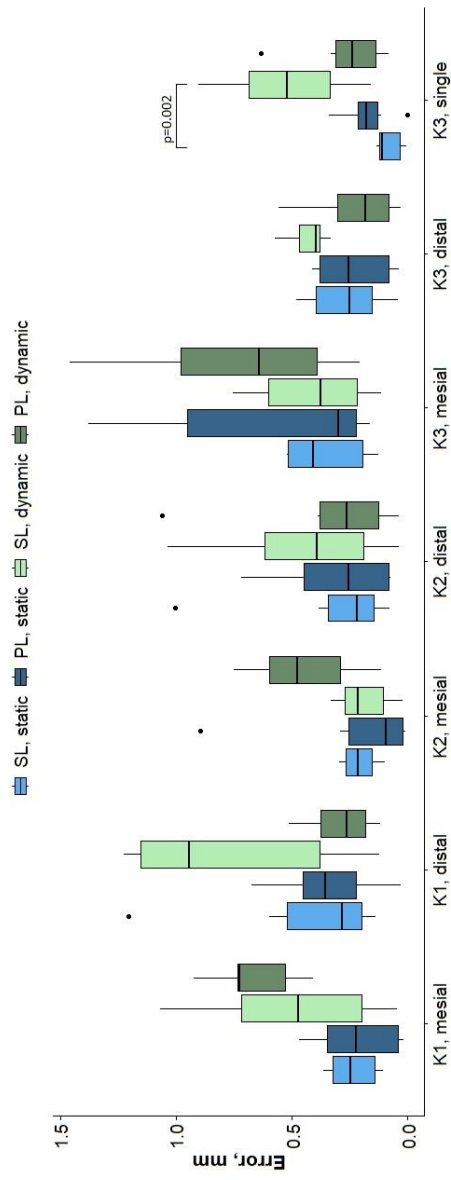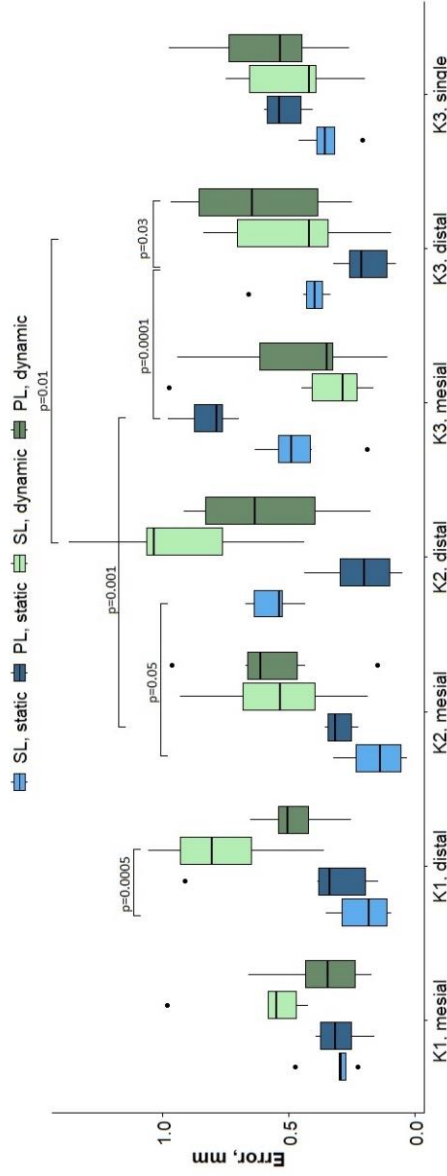**Fig. 20.** Horizontal deviation according to the Kennedy class of an edentulous defect, guidance method, implant design, and implant position (mesial or distal). Multiway ANOVA (four factors) with post hoc contrasts test (p-values adjusted using MVT method).

98
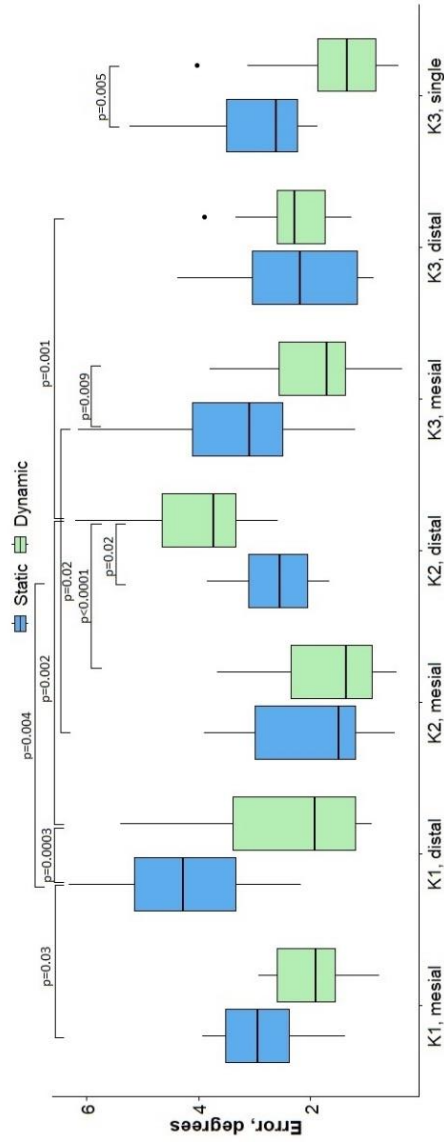
Fig. 21. Angle deviation according to the Kennedy class of an edentulous defect, guidance method, and implant position (mesial or distal). Multiway ANOVA (three factors) with post hoc contrasts test (p-values adjusted using MVT method).

3.3. DYNAMIC NAVIGATION ACCURACY
USING TWO REGISTRATION METHODS

A total of 96 implants were placed, with an equal number in each registration group, to measure accuracy in this part of the study. The main factor analysed was the registration method, categorized into two groups: registration by teeth (Kennedy1) and registration by the reference objects (edentulous). Other influencing factors analysed in this study included implant position (mesial/distal), implant design (SL/PL), and, specifically within the edentulous case, the angulation of the distal implants.
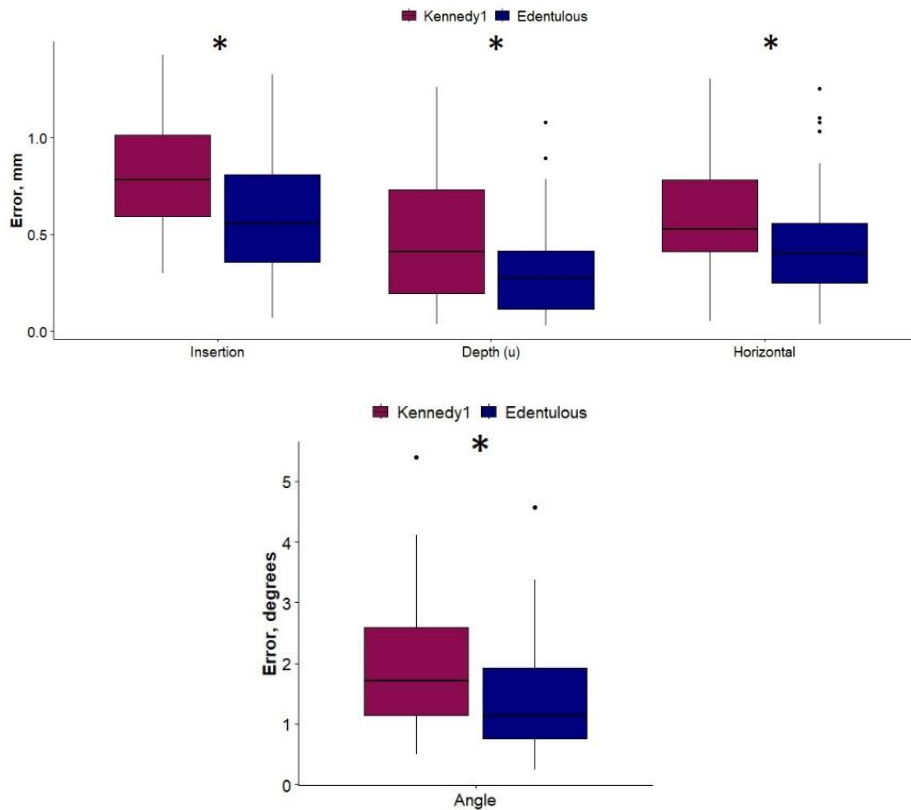
Fig. 22. Boxplot diagrams showing the deviation distributions for each guidance method for implant positioning. Kennedy1 – registration by teeth; Edentulous – registration by reference objects. Significant differences ($p < 0.05$) between means (*) were determined using a multiway ANOVA.

Factorial ANOVA revealed that trace registration by reference objects (edentulous case) to be superior in each deviation type (Fig. 22): insertion point (p = 0.0002), absolute depth (p = 0.01), horizontal (p = 0.02), and angle (p = 0.008). Although the three-way ANOVA model for the insertion point met the assumption of normality for residuals, it should be noted that the normality assumption was not met for other deviations. Therefore, caution should be exercised when interpreting the results for these deviations.

For the absolute depth deviation (u), factorial ANOVA indicated a significant interaction (p = 0.01) between implant design and position (M/D). However, it is important to note that this interaction did not include the main factor "registration method" and the post hoc analysis did not support its significance (MVT adjusted p > 0.05).

For the horizontal deviation, the implant position as a separate factor showed statistical significance (MVT adjusted p = 0.03), indicating higher accuracy for the mesial implant position (Fig. 23).
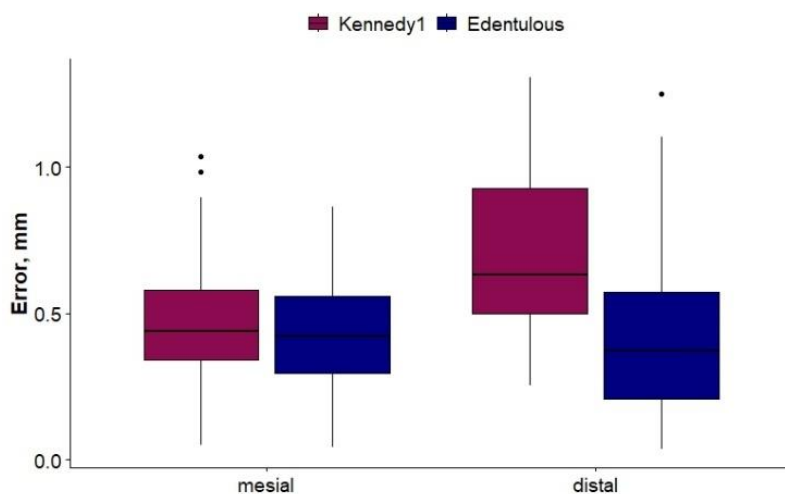
Fig. 23. Boxplot distribution of horizontal deviation by implant positions and trace registration methods. Kennedy1 – registration by teeth; Edentulous – registration by reference objects.

Factorial ANOVA for angle deviations indicated a significant interaction between implant design (SL/PL) and position (M/D), Fig. 24. Post hoc analysis showed that the SL design group had higher accuracy than the PL design group in the distal implant position (MVT adjusted p = 0.04). However, due

to the slight deviations from normality in the data, the exclusion of the main factor (trace registration), and the limited scope of the interaction, the clinical relevance of this finding is limited for further interpretation.
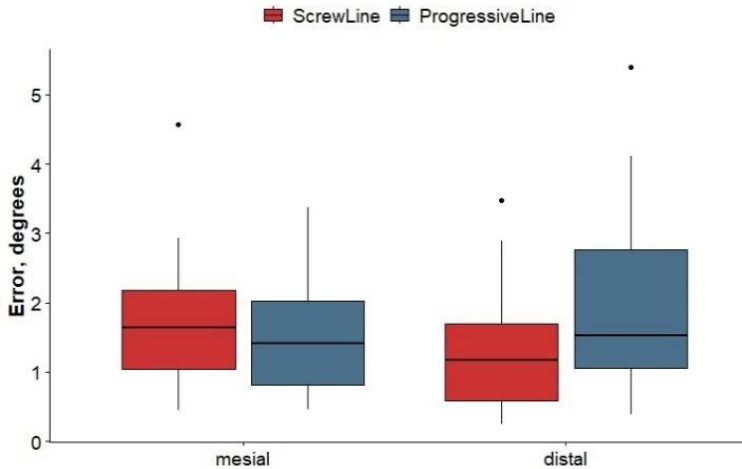
Fig. 24. Boxplot distribution of angle deviations by implant position and implant design.

For the edentulous case (reference object registration method), the comparison between mesial (parallel) and distal (30 degrees angulated) implants showed no statistically significant difference between groups.

3.4. POLYMER-BASED MATERIALS AND SURFACE CLEANING

3.4.1. SURFACE ROUGHNESS

The results of surface profilometry are presented in Table 15. In the case of the CCP, no statistically significant differences between material groups were observed. After cleaning the specimens using the RCP, ZrO-HT group surface roughness was significantly lower (Kruskal–Wallis and pairwise Wilcoxon, $p = 0.042$) compared to Ti, PMMA-Ker, PMMA-Bre, PEEK, and PEKK groups. Significant surface roughness differences for each material group comparing two surface cleaning protocols are presented in Fig. 25. Examples of material surfaces under a confocal microscope are shown in Fig. 26.

Table 15. Surface roughness (Sa) average values for each material group and cleaning protocol presented in micrometres (μm) as averages +/− standard deviations.

CCP	Material group	RCP
0.157 ± 0.049	Ti	0.146 ± 0.033
0.136 ± 0.017	ZrO-HT	0.079 ± 0.017
0.235 ± 0.079	PMMA-Ker	0.125 ± 0.016
0.208 ± 0.049	PMMA-Bre	0.155 ± 0.052
0.234 ± 0.186	PMMA-3D	0.140 ± 0.097
0.278 ± 0.103	PEEK	0.174 ± 0.055
0.228 ± 0.084	PEKK	0.129 ± 0.042

Statistically significant (Kruskal–Wallis and pairwise Wilcoxon, p-adjusted < 0.05) differences comparing material group means within each cleaning protocol are marked with a bracketed notation on the respective side of the figure. CCP—Conventional cleaning protocol; RCP—Research cleaning protocol.

Fig. 25. Sample surface roughness (Sa) values using two different cleaning protocols. The results are presented as averages +/− standard deviations. *—statistically significant differences (Wilcoxon, p < 0.05) comparing CCP and RCP for each material group. CCP—Conventional cleaning protocol; RCP—Research cleaning protocol.
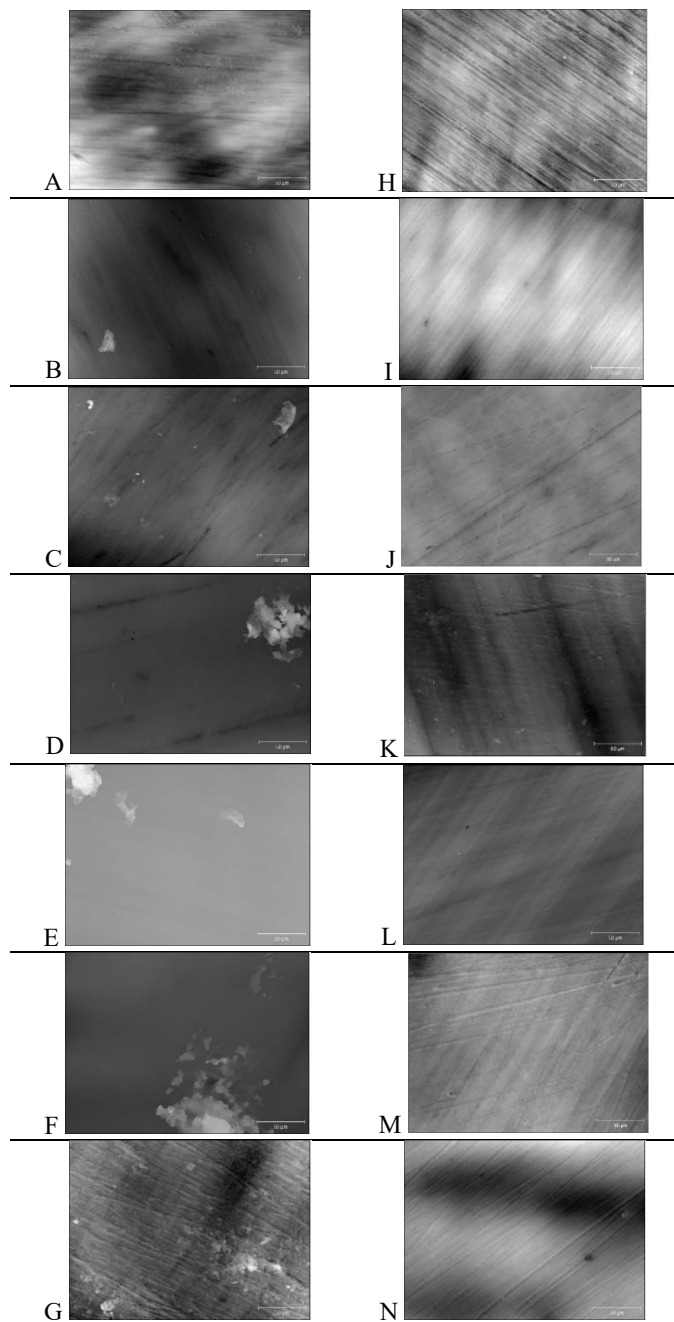
Fig. 26. Material surface images after application of CCP (**A**—Ti, **B**—ZrO-HT, **C**—PM-MA-Ker, **D**—PMMA-Bre, **E**—PMMA-3D, **F**—PEEK, **G**—PEKK) and RCP (**H, I, J, K, L, M, N** respectively) cleaning protocols obtained by confocal microscope (×50). The white bar in the lower right corner of each image represents the equivalent of 50 µm.

3.4.2. WATER CONTACT ANGLE

The results of water contact angle (WCA) measurements are presented in Table 16. In the case of CCP, the ZrO-HT group showed significantly higher (ANOVA and post hoc Tukey's Contrasts) contact angle compared to Ti ($p < 0.001$), PMMA-Bre ($p = 0.00163$), PMMA-3D ($p < 0.001$), and PEKK ($p < 0.001$) groups. Moreover, the Ti group showed a significantly lower contact angle compared to PMMA-Ker ($p = 0.00181$) and PEEK ($p < 0.001$) groups. Finally, the PMMA-3D group contact angle was significantly lower than in the PEEK group ($p = 0.03175$). In the case of surface preparation using the RCP, the ZrO-HT group showed a significantly lower contact angle compared to PMMA-Ker ($p = 0.0107$), PMMA-Bre ($p = 0.0183$), PMMA-3D ($p = 0.0131$), PEEK ($p < 0.001$), and PEKK ($p < 0.001$) groups. Furthermore, in the Ti group, the contact angle was significantly lower than the PEKK group ($p = 0.036$). Significant contact angle differences for each material group comparing two surface cleaning protocols are presented in Fig. 27. Images of water droplets used for contact angle measurement on different surfaces are presented in Fig. 28.

Table 16. Water contact angle (degrees) average values for each material group and cleaning protocol presented as averages $+/-$ standard deviations.

CCP	Material group	RCP
73.84 ± 5.18	Ti	83.24 ± 6.94
98.70 ± 4.49	ZrO-HT	69.90 ± 6.37
88.60 ± 4.03	PMMA-Ker	89.86 ± 5.32
83.76 ± 5.30	PMMA-Bre	88.74 ± 3.91
79.64 ± 2.15	PMMA-3D	89.46 ± 13.62
90.64 ± 8.73	PEEK	96.56 ± 12.41
81.34 ± 3.77	PEKK	100.6 ± 2.5

Statistically significant (ANOVA and post hoc Tukey's Contrasts, $p < 0.05$) differences comparing material group means within each cleaning protocol are marked with a bracketed notation on the respective side of the figure. CCP—Conventional cleaning protocol; RCP—Research cleaning protocol.
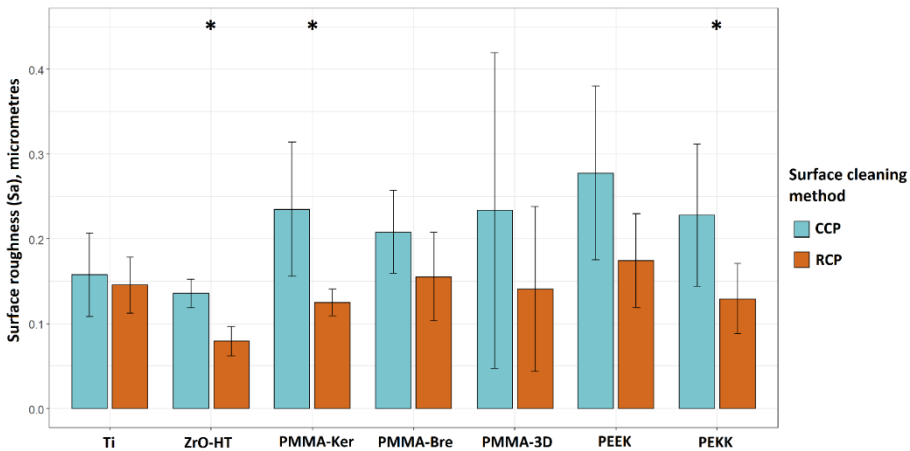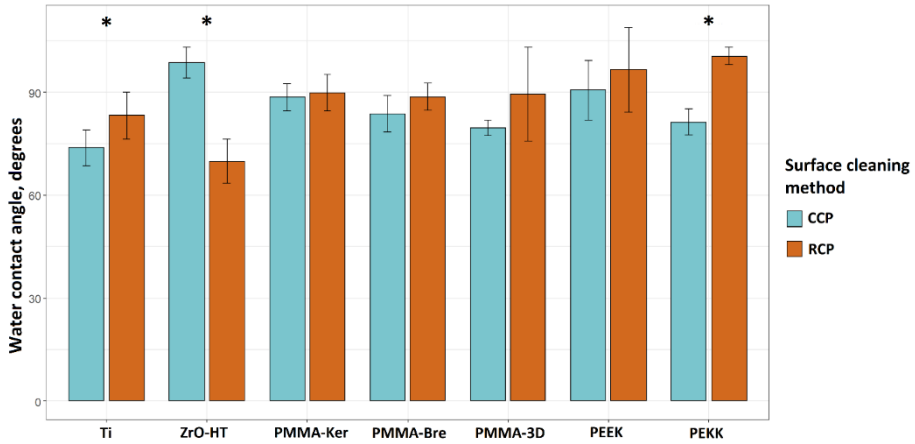
Fig. 27. Sample water contact angles using different surface cleaning protocols. The results are presented as averages +/− standard deviations. *—statistically significant differences (t-test, $p < 0.05$) comparing means of CCP and RCP for each material group. CCP—Conventional cleaning protocol; RCP—Research cleaning protocol.
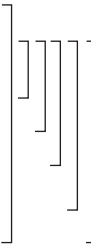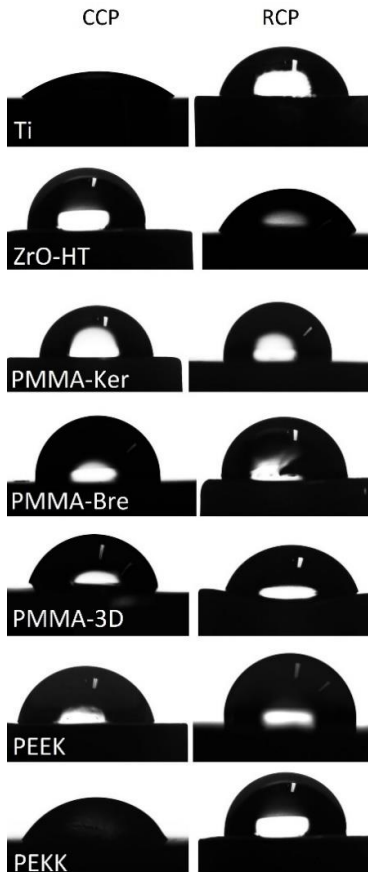

Fig. 28. Water droplets on material surfaces used for contact angle measurement. CCP – Conventional cleaning protocol; RCP – Research cleaning protocol.

3.4.3. HUMAN GINGIVAL FIBROBLAST (HGF) PROLIFERATION

Cell viability data is presented in Tables 17 and 18 for each cleaning protocol. HGF proliferation tended to increase over time for both cleaning protocols (Figure 29). Significant differences comparing both periods (t-test, $p < 0.05$) were detected for CCP in PMMA-3D, and PEKK groups. In the case of RCP, these differences were observed in Ti, PMMA-Ker groups. In the case of the CCP, data indicates more variability in HGF proliferation. After 48 h, polymeric materials (except for PMMA-Ker) cleaned by multistep RCP showed a tendency for higher cell viability (PMMA-3D, PEKK $p < 0.05$). After 72 h, cell viability tended to be higher for conventionally cleaned materials. However, due to the high dispersion of the values, the difference between two cleaning protocols at this time point was not statistically significant.

Table 17. Human gingival fibroblasts (HGF) proliferation on specimen surfaces after CCP is presented as cell viability (as a ratio of 24 h control reference).

48 hours	Material group	72 hours
1.38 ± 0.15	Control	1.82 ± 0.14
1.22 ± 0.32	Ti	1.72 ± 0.48
1.11 ± 0.34	ZrO-HT	1.51 ± 0.18
1.14 ± 0.06	PMMA-Ker	1.44 ± 0.44
0.89 ± 0.19	PMMA-Bre	1.54 ± 0.80
0.79 ± 0.03	PMMA-3D	1.17 ± 0.24
0.88 ± 0.29	PEEK	1.17 ± 0.35
0.73 ± 0.12	PEKK	1.09 ± 0.12

The results are presented as averages +/− standard deviations. Statistically significant (ANOVA and post hoc Tukey's Contrasts, $p < 0.05$) differences comparing material group means within each time period are marked with a bracketed notation on the respective side of the figure.

Table 18. HGF proliferation on specimen surfaces after the RCP is presented as cell viability (as a ratio of 24 h control reference).

48 hours	Material group	72 hours
1.20 ± 0.02	Control	1.41 ± 0.10
1.01 ± 0.04	Ti	1.13 ± 0.04
1.06 ± 0.09	ZrO-HT	1.32 ± 0.20
0.84 ± 0.05	PMMA-Ker	1.10 ± 0.11
0.98 ± 0.02	PMMA-Bre	0.88 ± 0.21
0.98 ± 0.08	PMMA-3D	0.99 ± 0.18
1.03 ± 0.02	PEEK	1.08 ± 0.08
0.96 ± 0.07	PEKK	1.08 ± 0.07

The results are presented as averages +/− standard deviations. Statistically significant (ANOVA and post hoc Tukey's Contrasts, $p < 0.05$) differences comparing material group means within each time period are marked with a bracketed notation on the respective side of the figure.
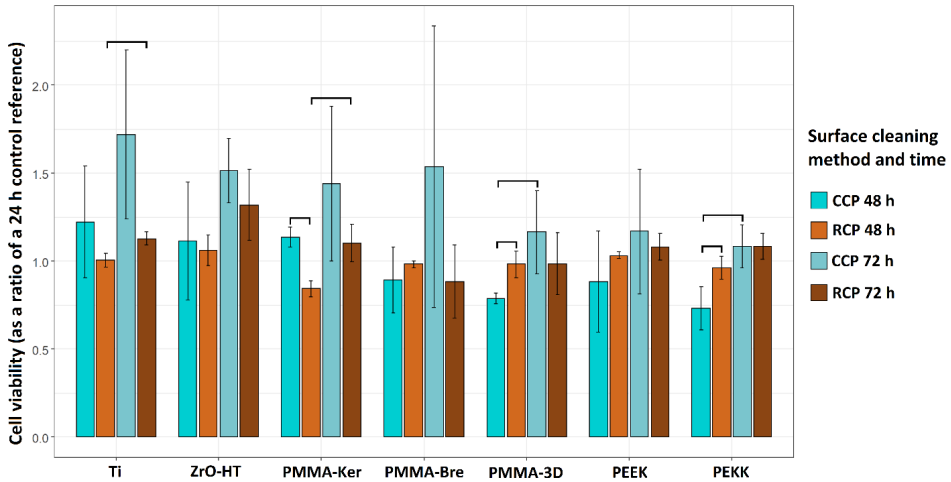
Figure 29. HGF proliferation on specimen surfaces after 48 and 72 h using two cleaning protocols. The results are presented as averages +/− standard deviations. Statistically significant differences (t-test, p < 0.05) between cleaning protocols and time periods are noted. CCP – Conventional cleaning protocol; RCP – Research cleaning protocol.

3.5. ZIRCONIA-BASED CERAMIC MATERIALS AND SURFACE UV TREATMENT

3.5.1. SURFACE ROUGHNESS

The results from the profilometry measurements (in Sa) were 0.094 ± 0.027 μm and 0.11 ± 0.036 μm for the ZrO-HT group and ZrO-UTML group, respectively. The Shapiro–Wilk normality and the homogeneity of variance tests ($p > 0.05$) allowed for evaluating any potential differences in the studied parameter using a t-test. The test showed no significant difference between the materials included in the study ($p = 0.217$). A graphical representation of the results is depicted in Figure 30. Thus, surface roughness can be assumed equal in all subsequent tests.
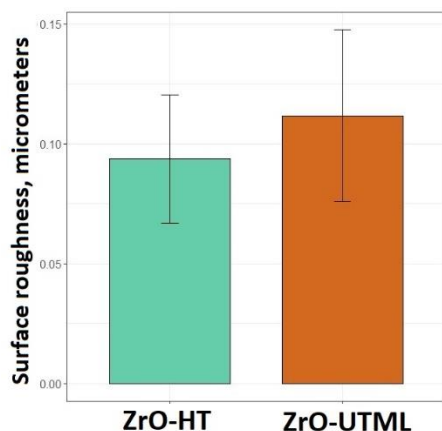
Fig. 30. Surface roughness of the two ZrO-based materials.

3.5.2. WATER CONTACT ANGLE

Hydrophilicity was assessed by measuring the water contact angle in this study. Mean values for the different groups tested are presented in Table 19.

The Shapiro–Wilk normality test and homogeneity of variance allowed for an ANOVA test usage ($p > 0.05$). UV-treated groups showed slightly increased means of contact angles compared to untreated materials. A one-way ANOVA test was used to assess the differences between the groups. The results did not reveal significant differences ($p = 0.292$).

Table 19. The water contact angle in degrees for the four groups is presented as means ± standard deviations.

Study Group	Mean	SD	F(Df)	*p*
ZrO-HT	69.9	6.4		
ZrO-HT-UV	73.7	13.9	3.50(16)	> 0.05
ZrO-UTML	79.5	12.8		
ZrO-UTML-UV	83.4	11.4		

3.5.3. HUMAN GINGIVAL FIBROBLAST CYTOTOXICITY

HGF cytotoxicity was assessed as a ratio of cell viability with a control group (value = 1) after a 12 h incubation period (Fig. 31). A one-way ANOVA test was used to compare the performance of the different groups. Nevertheless, values obtained for the UV-treated groups were higher within the same material.

109
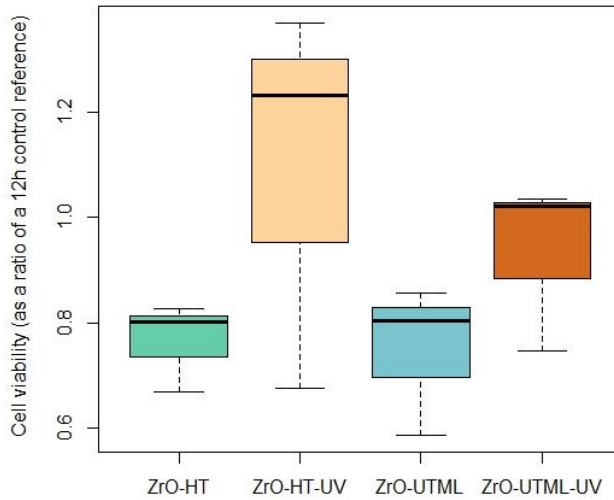
Fig. 31. Cytotoxicity assessment as a ratio of the 12-hour control reference for the four groups included in the study.

3.5.4. HUMAN GINGIVAL FIBROBLAST PROLIFERATION

HGF proliferation tended to increase over time, irrespective of the material or the UV surface treatment (Fig. 32). The highest ratio obtained for the 24 and 48 h time points was in group ZrO-HT-UV and the 72 h time point for ZrO-UTML-UV. The lowest ratio value observed for all three time points was in the ZrO-HT group.
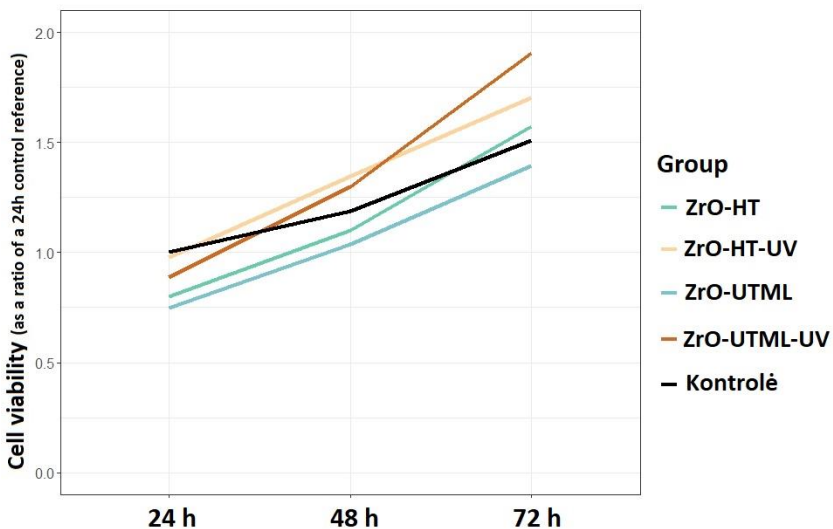
Fig. 32. The tendency of HGF proliferation in the different study groups for the tested time points at 24, 48, and 72 h.

Significant differences between groups were detected only at the 24 h time point (F(8) = 9.58, p = 0.005). The performed post hoc Tuckey analysis revealed a significant difference between ZrO-HT and Zr-HT-UV (t = 3.875, p = 0.020), as well as between ZrO-UTML and ZrO-HT-UV (t = 4.976, p = 0.005). At the 24 h time point, all values for the tested materials were lower than the control.

3.6. CERAMIC MATERIALS SURFACE EFFECT ON HGF AND EPITHELIAL-LIKE CELLS

3.6.1. SURFACE ROUGHNESS

Surface profilometry tests between the different materials are presented in Fig. 33. All materials except ZrO-V (0.69 ± 0.15 μm) had a mean Sa value below 0.25 μm. Since the variance of the data was not homogeneous, as showed by the conducted Levene test (F = 3.33, p < 0.05), a Welch one-way ANOVA test was used to test whether a significant difference exists between the surface roughness of the test samples. The results revealed a significant difference in surface roughness (Sa) between the materials (F_{Welch} = 16.68, p < 0.001). A Games-Howell post hoc pairwise analysis showed that the ZrO-V had a higher roughness than all other tested materials (p < 0.05).
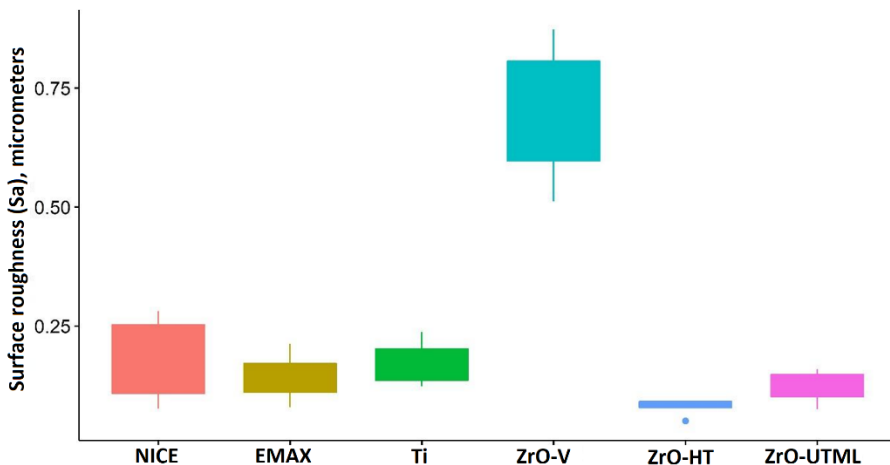
Fig. 33. Surface roughness of ceramic material.

3.6.2. WATER CONTACT ANGLE

The results from the water contact angle (WCA) measurements are presented in Table 20. The normality and homogeneity assumptions for the tested data were met; hence a One-way ANOVA test was used for the analysis (W = 0.93, p > 0.05; F_{Levene} = 2.07, p > 0.05).

Table 20. Water contact angle (WCA) in degrees for each group of materials presented as Mean and standard deviations.

Material	Mean	SD
EMAX	45.34	2.64
NICE	58.48	21.51
Ti	83.24	6.94
ZrO-V	51.56	2.16
ZrO HT	69.90	6.37
ZrO UTML	79.48	12.79

The results from the ANOVA analysis (Fig. 34) showed a significant difference between the tested samples (F = 9.70, p < 0.001). A Tukey post hoc test revealed a significant difference in contact angles between the groups TI – EMAX (p < 0.001), ZrO HT – EMAX (p < 0.05), ZrO UTML – EMAX (p < 0.001), Ti – NICE (p < 0.05), ZrO-V – Ti (p < 0.01), and ZrO UTML - ZrO-V (p < 0.01).
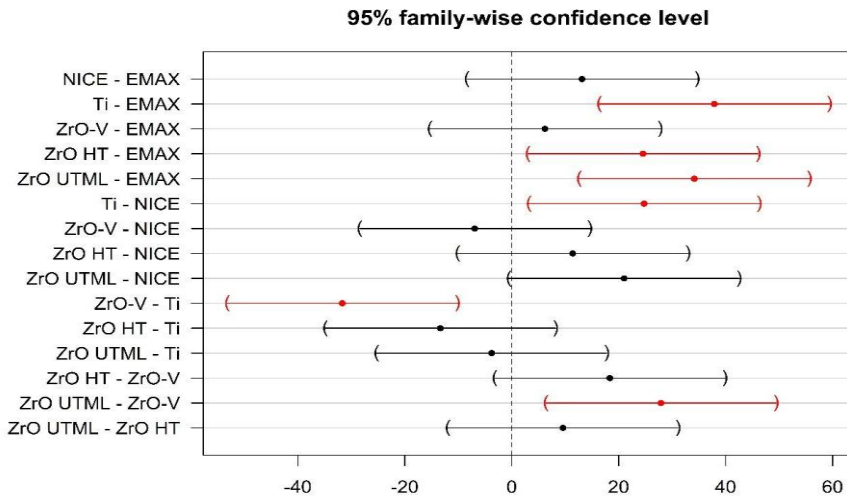
Fig. 34. A graphical representation of the mean difference for water contact angle between material groups is shown in red.

3.6.3. CYTOTOXICITY

The cytotoxicity descriptive data for both tested cell lines are presented in Table 21 as Mean ± SD. For the Epithelial-like cells, the minimum and maximum absolute values were recorded for the EMAX material (min = 0.49; max = 1.21). For the human fibroblast cells (HGF), the minimum recorded absolute values were in the NICE group (min = 0.56) and the maximum in the Ti group (max = 0.99).

Table 21. Epithelial-like cells and HGF cytotoxicity on the test sample surface is presented as cell viability (a 12-hour control reference).

| | Tested cell line | | | |
| Material | Epithelial-like cells | | Human gingival fibroblasts | |
	MEAN	SD	MEAN	SD
control	1	-	1	-
EMAX	0.84	0.36	0.80	0.06
NICE	0.80	0.11	0.65	0.16
Ti	0.71	0.14	0.77	0.20
ZrO-HT	0.73	0.24	0.76	0.08
ZrO-UTML	0.75	0.16	0.75	0.14
ZrO-V	0.67	0.21	0.75	0.13

3.6.4. PROLIFERATION

A two-way interaction analysis assessed the proliferation of epithelial-like cells and human gingival fibroblasts (HGF).

Results for epithelial like-cells proliferation are presented in Table 22 and Figure 35. It must be noted that the residuals revealed a slight departure from normality, and the reported results should be interpreted with care. There are significant differences between groups for the Material and Time variables.

Table 22. Test results for material, time, and interaction between the two variables for epithelial-like proliferation on test sample surfaces.

	Df	Sum Sq	Mean Sq	F	P
Material	6	7.56	1.26	2.25	< 0.05
Time	2	72.91	36.54	94.01	< 0.001
Material: Time	12	8.05	0.67	1.73	> 0.05
Residuals	42	16.29	0.39		

However, their interaction was insignificant (F = 1.73, p > 0.05). Furthermore, the difference in proliferation within the Material variable was only de-

tected between ZrO-V and the control group at the 72h time point (p < 0.05). There were no differences between the different test materials for all time points.

95% family-wise confidence level
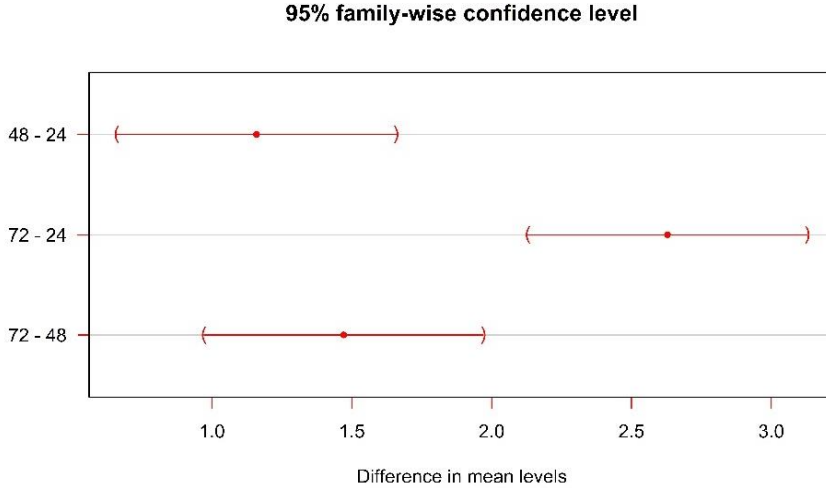
Fig. 35. A graphical representation of the mean difference for epithelial-like cell proliferation between the three observational time points shown in red.

Concerning differences in the 24h ratio of the control for the different time periods, an expected increase in the absolute values was observed (Fig. 36). Furthermore, a significant difference was observed in all tested pairs (48-24, 72-24 and 72-48), as depicted in Fig. 35.
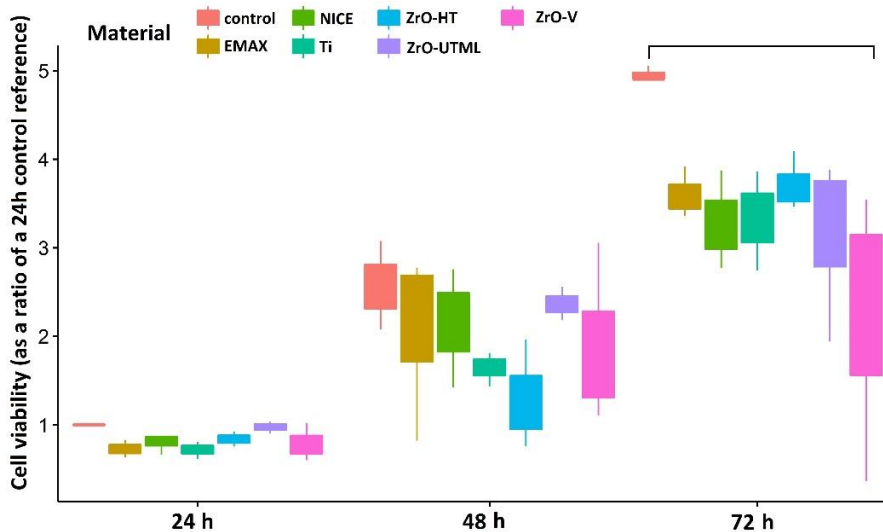
Fig. 36. Epithelial-like cell proliferation on test sample surfaces for the three tested time periods is presented as a ratio of the 24h control reference.

Results for the human gingival fibroblasts (HGF) proliferation are presented in Table 23 and Fig. 37. Significant differences exist between groups for the Material and Time variables.

Table 23. Test results for material, time, and interaction between the two variables for HGF proliferation on test sample surfaces

	Df	Sum Sq	Mean Sq	F	P
Material	6	0.28	0.05	3.64	< 0.01
Time	2	1.72	0.86	67.23	< 0.001
Material: Time	12	0.1	0.01	0.68	> 0.05
Residuals	42	0.5	0.01		

However, their interaction was insignificant (F = 0.68, p > 0.05). Furthermore, a difference in proliferation between the material variable was detected between the control group and ZrO-V at the 24h time point (p < 0.05). For the 48h timepoint, differences were observed between the control and Ti and ZrO-UTML (p < 0.05). For the 72h time point, significant differences were again observed between the control and ZrO-V (p < 0.05), NICE, and Ti (p < 0.01). HGF proliferation differed significantly between Ti and ZrO-HT at the same observation time (p < 0.05).
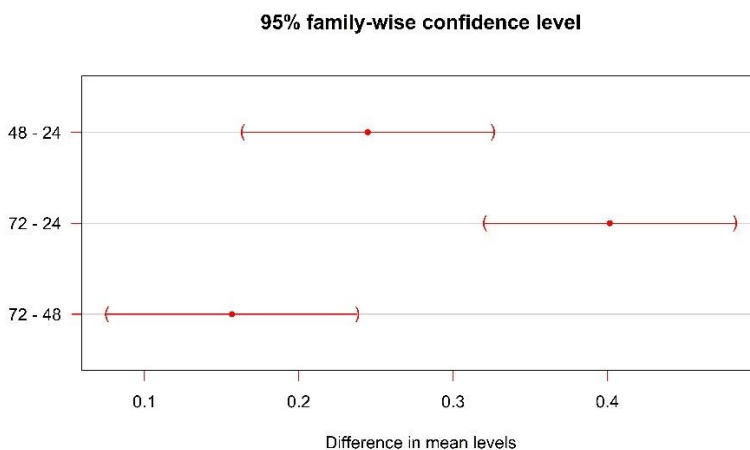
Fig. 37. A graphical representation of the mean difference for human gingival fibroblast proliferation between the three observational time points shown in red.

As with epithelial-like cells, an expected increase in the absolute values in the 24h control ratio for the different periods was observed (Fig. boxplot 38).

Moreover, a significant difference was observed between the different time points (48-24, 72-24, and 72-48), as depicted in Fig. 37.
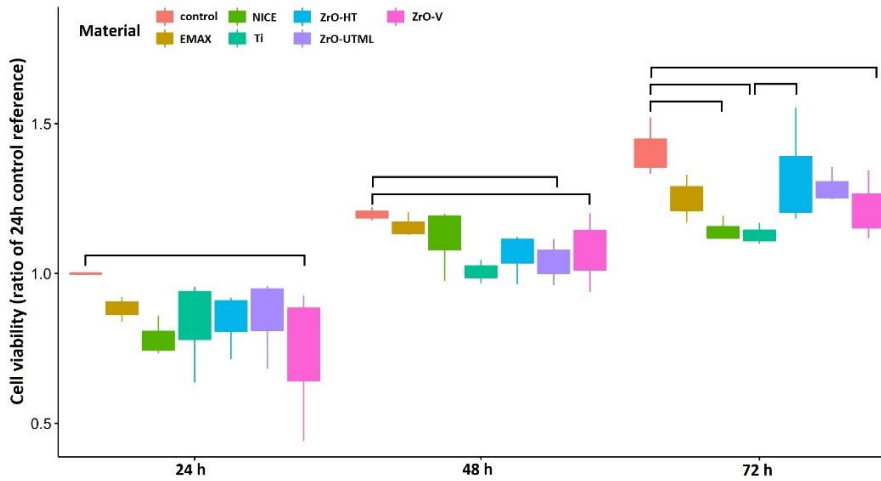
Fig. 38. Human gingival fibroblast proliferation on test sample surfaces for the three tested time periods is presented as a ratio of the 24h control reference.

4. DISCUSSION

4.1. GUIDED IMPLANT PLACEMENT ACCURACY

This study aimed to evaluate dynamic guidance's accuracy and influencing factors in a maxillary model study. As the vast majority of the other accuracy studies use CBCT based before and after comparison methods, as mentioned in the introduction, it is important to considerthis aspect when comparing the results of the current study.

This study's insertion point deviation averages are within a range of published dynamic guidance implant placement data: 0.37-1.58 mm for *in vitro* studies and 0.67-1.37 mm for clinical studies [36,39,43]. The overall insertion point 3D deviation averages ranged between 0.56 ± 0.33 (K3, SL, mesial) and 1.2 ± 0.28 mm (K1, SL, distal) for different subgroups. The data show a tendency, near statistical significance, of a decreasing insertion point deviation for an increasing number and distribution area of the teeth (increasing Kennedy class number). The latter could be explained by a larger teeth surface area and a higher spread of the reference points leading to a more accurate trace registration via teeth. Trace registration maps a CBCT scan to a real situation (in this study - a model) via the special tags (tracers). Part of dynamic guidance accuracy studies report a higher insertion point accuracy compared to the current study: 0.38 ± 0.25 mm [481], 0.41 ± 0.12 mm [482]. These studies use specific objects (fiducials) for the initial CBCT and trace registration instead of teeth surfaces [481,482]. This suggests that fiducials increase accuracy and reproducibility, but on the other hand, this method is less clinically versatile and has limitations. Contrastingly, Jorba-Garcia et al. (2019) reported slightly higher insertion point deviations using fiducials for trace registration in a Kennedy III class mandibular model study: for the novice - 1.39 ± 0.48 mm, and for an experienced surgeon - 1.19 ± 0.45 mm [472]. In the later study, the authors explain that acrylic splints for the fiducials tend to deform, thus introducing more inaccuracies and showing possible limitations. Furthermore, in the current study, the SL implant design group's distal implant position showed a significantly higher deviation than the mesial one, which was more evident in K1 and K2 cases; the deviation difference was distal-mesial, 0.3 mm, and 0.5 mm, respectively. However, these tendencies were not observed for PL design implants. Area-related differences were also rejected in a study by Kim et al. (2015): a total of 110 implants (slightly

conical design; 4.0 mm x 10 mm) were placed in 11 sites of 10 models using dynamic guidance and found no significant differences between the models and/or the sites [482]. Other studies, having implants placed in different areas, do not provide any statistical analysis regarding this aspect due to study design limitations [481,483]. Guzmán et al. (2019) placed 20 implants (conical design, 4.6 mm × 12 mm) in teeth areas #24 and #26 (K 3 class; 10 implants in each area) using dynamic guidance and found an insertion point deviation of 0.85 ± 0.48 mm [483]. This study design and the results are similar to current findings for the K3 PL group (0.8 ± 0.36 mm) [483]. Finally, Pellegrino et al. (2020) reported high insertion point deviations for fully edentulous maxillary extra-hard models study: 1.55 ± 1.08 mm (experienced) and 1.74 ± 0.64 mm (novice) [484]. The latter study findings suggest that fully edentulous and hard bone cases might influence higher deviations. In the current study, a hard bone (D1) was also simulated thus it could be related to higher deviations compared to some other studies. A 3D insertion point deviation is directly related to depth and horizontal deviations. Therefore, these deviations will be discussed separately to better understand factors influencing insertion point accuracy.

Depth (u) deviation averages for various subgroups ranged from 0.21 ± 0.15 mm to 0.76 ± 0.55 mm. These findings are similar to data provided by systematic reviews for *in vitro* studies: 0.26-1.14 mm [36,39]. Statistically significant lower deviations for mesial implant in the SL group compared to the PL group could be influenced by differences in implant and drill design. PL implant, by a rotation step of 120 degrees, changes its depth by 0.3 mm compared to 0.2 mm in SL implants [485]. For the SL group, there was a tendency for a lower mesial implant deviation compared with distal (more evident in K1 and K2 situations), which might be related to trace registration accuracy via teeth. However, there was no such tendency for the PL group. In addition, PL mesial implant deviations tended to be higher than distal, with a high deviation (0.72 ± 0.46 mm) in K3 class for PL mesial implant (3.8 x 11 mm). Similar data was also reported by Kang et al. (2014), showing higher depth deviations in the fully edentulous mandible model for the canine region (1.14 ± 1.25 mm) compared to the molar region (0.76 ± 0.84 mm) [486]. These tendencies could be better explained by analysing depth (s) data.

Depth (s) measurement reveals that in most cases, implants tended to be screwed deeper than planned, from -0.01 ± 0.28 (K2, SL, mesial) to -0.76 ± 0.55 (K1, SL, distal). The exceptions were two PL groups: K3 distal position 0.21 ± 0.21 mm and single implant defect 0.01 ± 0.3. Distal implant position

118

averages showed deviations closer to a zero for PL implant design than SL. Also, for a single tooth defect, this difference was statistically significant). PL mesial implant statistically significantly was screwed deeper than the distal implant, this relates to depth (u) data. It could be suggested that conical design shorter and narrower implants (PL 3.8 x 11 mm) in mesial position tend to be screwed 0.4-0.6 mm too deep on average. On the contrary, the SL implant (except for K3) - the distal implant tended to be screwed deeper than the mesial one. It seems that for K1 and K2 cases, depth (s) deviations are influenced by implant design, size, and position. The authors could not indicate a study where a depth (s) measurement would have been evaluated, describing the deviation size and the direction tendency of the depth deviation.

Horizontal deviations ranged from 0.39 ± 0.18 to 0.93 ± 0.35 mm for various subgroups. These findings are within the range of findings from other studies: 0.36-1.27 mm [36] and 0.33-3.03 mm [39]. In this study, distal implant position influenced a greater horizontal deviation significantly. All models studied had anterior teeth that were used for trace registration. Thus, this factor might contribute to higher horizontal accuracy for a mesial implant in a premolar-molar area. In addition, this could be supported by data showing a tendency for a higher horizontal deviation in K1 and K2 model groups (fewer teeth in the posterior region for trace registration) compared to the K3 group. Also, the mesial implant was of a smaller diameter (3.8 mm compared to 4.3 mm) and shorter (11 mm compared to 13 mm) this takes less instrumentation for implant bed preparation and might also play a role. Brief et al. (2005) reported some of the lowest horizontal deviations 0.35-0.65 mm [487]. Still, they only studied the accuracy of an implant bed preparation by a pilot drill without implant delivery in a model and it was not fixed in a mannequin. Implant placement could add more variability and higher deviations. The largest horizontal deviations were reported by Kang et al. (2014), reaching 2-3 mm (increasing for the posterior region) for fully edentulous mandibular models, thus suggesting higher deviations in fully edentulous cases [486].

Angle deviations in the present study varied from 1.04 ± 0.53 to 4.5 ± 1.18 degrees. These results are within the range for model studies of all 3 systematic reviews on dynamic guidance accuracy published in 2021: 0.89-4.45 [43]; 0.82-5.49 [36]; 1.09-12.37 [39] degrees. K2 class showed significantly higher angle deviations than K1 and K3 classes, suggesting that unilateral defects, even with a higher number of teeth, might negatively affect the angular accuracy of the dynamic guidance. Furthermore, the distal implant position

also showed a higher angle deviation compared to the mesial. Kang et al. (2014) reported contradicting findings - significantly higher angular deviation in the canine region (12.37 ± 4.18) compared to the molar (8.97 ± 3.83) [486]. The results might differ due to the involvement of the fully edentulous cases in the later study and the advancement in dental navigation systems over time. Significantly lower angular deviations for a mesial implant position were evident in both K2 class implant design subgroups. Distal implant position tended to show higher deviation in most subgroups except for K1 SL. This data is similar to horizontal deviations, both showing higher deviations for a distal implant position.

Finally, the limitations of this study should be taken into account. Even though the latest systematic review papers show no difference between model and clinical studies [36,39,43], a model study does not simulate all the possible clinical factors such as soft tissue influence, patient head movement, possible detachment of head or jaw trackers, dental assistant, limited operating field accessibility and time. In addition, this model study was designed to simulate hard bone (D I). A hard bone situation requires a well-prepared implant bed. On the other hand, a soft bone situation might lead to an easier drill or implant insertion deviation and sometimes requires much less instrumentation and changes in drill sequence (especially for bone type IV) [488]. Furthermore, this study also planned the mesial position for a smaller diameter and shorter implant. Scientific evidence shows that implant size is selected considering the anatomical situation and occlusal load in the premolar and molar areas [489–491].

4.2. POLYMER-BASED MATERIALS AND SURFACE CLEANING

This study evaluated the effect of two cleaning protocols applied to five polymeric materials. The surface roughness, hydrophilicity, and fibroblast cell culture response were analysed. In clinical practice, polymers are used as temporary or permanent prosthetic materials [492,493]. Temporary abutments are an important part of the treatment course as they form and condition soft tissues during the sensitive initial healing phase [494]. Moreover, in some cases of immediate implant placement or surgical soft tissue management procedures (especially in the esthetic area), temporary abutments might serve the entire healing period, lasting from weeks to a few months [495–497]. With

increased applications of one-stage surgery and immediate or early loading, permanent prosthetic materials can also be used during the healing phase [498–500]. The ultimate attempt during these early healing stages is to guide the cellular response of soft tissues to form the architecture and sealing around dental implant abutment similar to that around healthy natural dentition.

This part of the study aimed to evaluate the effect of five different polymer-based materials and their surface characteristics using two different cleaning protocols on HGF proliferation. The results revealed significant differences between groups' surface roughness, water contact angle, and HGF proliferation. Therefore, the null hypothesis was rejected.

Previous findings indicated that a threshold of 0.2 µm average roughness value reduces bacterial adhesion significantly [428,501–503]. In this study, the roughness values of tested polymeric materials after CCP tended to be higher than the threshold, but lower after RCP. Recent research has indicated that titanium surfaces smoother than 0.1 µm might have a negative impact on fibroblast function [435]. Surface roughness in the 0.1–0.2 µm range showed higher fibroblast adhesion than smoother or rougher surfaces for titanium, zirconium dioxide, and lithium disilicate materials [437]. In the case of CCP, only Ti and ZrO were in this range, while after RCP, all tested materials except for ZrO (0.079 +/− 0.017 µm) were in this range.

There is limited data regarding the cleaning method's influence on the surface roughness parameters. Heimer et al. found that an ultrasonic bath for 6.3 min resulted in similar material surface roughness (Ra) values (0.033 µm for PEEK and 0.066 µm for PMMA) compared to other laboratory cleaning systems operating for 15–20 min [414]. The results contradict our findings, most likely due to study design and methods differences. In the present study, polishing protocols recommended by manufacturers were applied to each material. Moreover, the CCP ultrasonic bath was used for 3 min, and finally, a non-contact surface profilometry method was used to evaluate roughness (Sa).

Average surface roughness values (Ra/Sa) in different studies range widely: PMMA 0.02–6.2 µm [413–416,465], 3D printed PMMA (SLA) 0.39–2.97 µm [465,504], PEEK 0.032–2.52 µm [411,413–415,419,465,466,505], and PEKK 0.24–3.11 µm [506,507]. In some of these studies, the cleaning protocol is either not stated or not used after polishing [419,465,504]. Most commonly, an ultrasonic bath filled either with water or alcohol (e.g., 70 % ethanol or isopropanol) with consecutive water washing was used from 3 up to 20 min [411,413,415,416,466,505,507]. There is a substantial level of heterogeneity

in the methodology employed, including variations in material specifications such as the content of inorganic fillers, surface finishing protocols, and notable differences in profilometry methods [411,413,415,416,419,465,466,504–507]. The results of the current study after both cleaning protocols are in the reported range for PMMA and PEEK but are lower for 3D-printed PMMA and PEKK. In other studies, PMMA was not polished after 3D printing, and its surface roughness varied depending on object orientation during 3D printing [504,508]. Meanwhile, PEKK abutment surfaces were roughened, and bonding strength was tested [506,507]. In the evaluation of research data, it is crucial to take into account the surface profilometry method, including whether it is contact or non-contact, as well as various parameters such as the radius of the stylus tip, the cut-off value, the field of view, and the number of measurements per surface [439–442].

Hydrophilic surfaces are known to be favourable for eucaryotic cells [443,444]. The hydrophobicity of the implant abutment surface is also reported to influence the adhesion of certain bacteria [448]. Wassmann et al. conducted an experiment demonstrating that hydrophobic surfaces are more attractive to Staphylococcus epidermidis, which causes a cytotoxic effect on human fibroblasts and therefore interferes with osseointegration and soft tissue healing [449–451]. When using CCP, ZrO and PEEK surfaces become hydrophobic, while RCP only affects polymeric materials (PMMA, PEEK, and PEKK).

A tendency for increased contact angle after the application of RCP was observed in all groups except for ZrO, with significant differences in Ti and PEKK groups. Changes in the surface hydrophilicity after using different cleaning protocols were also demonstrated in previous studies: ultrasonic bath alone resulted in the least hydrophilic surfaces for PMMA and PEEK compared to other laboratory cleaning methods [414].

Other studies reported different water contact angle measurements: PMMA 72–99º [415,416], 3D printed PMMA (SLA) 71–79º [508], PEEK 10–114º [411,415,419,466], and PEKK 64–83º [507]. The current study's findings for PMMA and PEEK are similar to those mentioned above, but PMMA-3D and PEKK showed higher contact angles after RCP. This research showed a tendency of a more thorough cleaning method (RCP) to result in a higher water contact angle for tested materials compared to CCP.

The CCP resulted in higher variability of cell proliferation and was less predictable in the outcome. Gheisarifar et al., (2020) used ultrasonic cleaning

of specimens and concluded that PEEK plasma treatment (Sa 0.68–2.14 µm, WCA 10–12º) increased HGF proliferation [411]. The present study has demonstrated that the ultrasonic cleaning-based method (CCP) of PEEK surface (Sa 0.28 ± 0.1, WCA 91 ± 9º) tends to be less favourable for HGF proliferation compared to RCP (Sa 0.17 ± 0.06 µm, WCA 97 ± 12º). This tendency was not evident at 72 h. Similar results were observed with PMMA-3D and PEKK materials. PMMA-Ker demonstrated opposite outcomes regarding HGF proliferation, favouring CCP at 48 h. Methacrylate polymers were shown to have different HGF cytotoxicity and attachment properties, depending on their composition and fabrication method [416]. This study showed similar results comparing fibroblast proliferation over time under different cleaning protocols on PMMA-Ker, PMMA-Bre, and PMMA-3D surfaces.

Another study evaluated immortalized human gingival epithelial keratinocytes (iHGEK) behaviour on smooth Ti, rough ZrO, and medium PEEK surfaces and concluded similar cellular responses to all three materials [419]. This research provides similar results with HGF culture, as there were no significant differences in terms of cell proliferation between Ti, ZrO, and PEEK groups.

Though the average proliferation values tended to be higher for the CCP after 72 h, these differences were not significant in any of the groups (including both positive controls) due to high variability. This study backs the importance of multiple repetitions (at least three independent experiments) of cell proliferation experiments to evaluate the effect of the material surface.

Furthermore, the study design's limitations must be considered as it was tested under sterile, well-controlled conditions with HGF monoculture. Under clinical conditions, immediately after the placement of implant abutment, its surface becomes a subject of fibroblasts, epithelial cells, microbial adhesion, as well as inflammatory tissue reaction. Human histology research shows that long epithelial junction predominates in contact with the transmucosal implant component [58]. Furthermore, the collagen fibres tend to be oriented parallel to the surface [509]. This can be influenced by many factors, including the implant-abutment connection, micro-gap, and "micro-trauma" due to connections and disconnections of the implant transmucosal component during the treatment [23]. The design of the current study did not allow to evaluate these circumstances. As results can be influenced by different types of materials, polishing and cleaning protocols, cell, and bacteria types used in the studies, further research is needed to provide clinical recommendations.

4.3. ZIRCONIA-BASED CERAMIC MATERIALS
AND SURFACE UV TREATMENT

This part of the study evaluated the effect of UV photofunctionalization applied to two different ZrO_2-based materials for abutment fabrication. Surface roughness, hydrophilicity, cytotoxicity, and proliferation of human gingival fibroblasts (HGF) were analysed. Zirconia-based materials have shown superior properties related to biocompatibility compared to all other materials currently in clinical use [468].

The results revealed no significant difference in the hydrophilicity, cytotoxicity, and proliferation at 48 and 72 h. Thus, the null hypothesis was accepted. At 24 h, HGF proliferation showed a significant difference only in the ZrO-HT vs ZrO-HT-UV group. Hence, the alternative hypothesis was accepted. Another significant difference between the study groups, as detected by the Tuckey HDS post hoc analysis, was between the groups ZrO-UTML and ZrO-HT-UV.

Surface morphology and roughness significantly influence bacterial and cell adhesion to abutment materials [421]. In the present study, surface finishing protocols recommended by the manufacturer were applied for the included materials. Furthermore, a cleaning procedure in an ultrasonic bath in deionised water for 1 h was also performed. Finally, a non-contact profilometry was utilised to evaluate the micro-surface characteristics. Average surface roughness is classified into four categories: smooth, minimally rough, moderately rough, and rough [426]. In addition, there is a variance in the measurement methodology for this parameter, including contact or non-contact profilometry, confocal microscopy, and SEM [427,469,470,510–513]. In the present study, minimally rough surfaces (Ra < 0.5 μm) were achieved with negligible differences in roughness, allowing for the direct comparison of both materials, disregarding these parameters' influence on the results of subsequent analyses.

Among different surface modification methods, the photofunctionalization of Zirconia-based implant abutments has increased healing potential, improved wettability, and enhanced biological seal [469,513,514]. Three main photofunctionalization methods are used based on the radiation wavelength: UV-A (100–400 nm), UV-B (290–320 nm), and UV-C (100–290 nm) [515]. In addition, mixed protocols have been used in previous studies [513]. The irradiation times vary considerably in the literature, ranging from as little as

10 min to more than 24 h [469,513–515]. In the current study, UV-C irradiation was used.

Hydrophilic surfaces are favourable for HGF adhesion, which suggests a formation of a good peri-abutment soft tissue seal [438]. Moreover, hydrophobic surfaces are associated with increased bacterial adhesion and accumulation of biofilm, slowing healing processes [449]. Previous studies have reported different contact angles evaluating Zirconia surfaces after photofunctionalization [446,510]. UV treatment has been shown to reduce carbon, increase oxygen and Zirconia surface content, and lower the WCA [469]. Since the effect of photofunctionalization is time- and dose-dependent, the average change in WCA varies considerably based on the specific experimental setting. Most studies reported a significant decrease in water contact angles after photofunctionalization. Att et al. (2009) communicated the highest untreated (100.1°) and lowest UV-treated (20.8°) WCA scores [511]. Other studies reported milder but significant increases in hydrophilicity ranging from a 10° to 50° WCA change [510,511,513]. The UV-photofunctionalization protocol used in this study did not significantly change the hydrophilicity parameters. Furthermore, an insignificant increase in the water contact angle was observed. The current study used a very thorough and detailed specimen cleaning protocol which reduced surface impurities, thus likely reducing the effect of UV towards the WCA.

During the soft tissue healing process around implant abutments, the adhesion proliferation and contact of HGFs to the materials' surface would affect the biological seal. Furthermore, it was found that the inner surface adjacent to the biomaterial has a higher fibroblast count [516]. It was suggested that conditioning abutment surfaces with UV light would affect hydrophilicity, reduce the hydrocarbon content, and enhance surface electro-positivity, promoting protein adsorption and cellular adhesion [469,517]. The results of this study can partially confirm these suggestions. The change in the 24–48–72 h proliferation curve for HGF between the UV-treated and non-treated groups suggests that the former performs better. These results might be due to the decontamination properties of UV irradiation or the type of material used, since most other factors have been eliminated as covariates [469]. This is also evident in the cytotoxicity test where a notable difference between the UV-treated and non-treated groups was observed for both tested materials, albeit a non-significant one.

This study has several limitations. All experiments were performed *in vitro* in sterile and well-controlled conditions using an HGF monoculture.

In a clinical setting, the abutment surface is contaminated during placement and subjected to microbial adhesion and contact with inflammation fluids, blood, and different types of cells. The study design does not include these conditions. Furthermore, the macroscopic design of the specimens and test assembly deviates from the clinical conditions. Thus, a 2D experimental model was used instead of a 3D (organotypic) model [513,518]. As changes can further influence design parameters and materials, further investigation is appropriate to assert the current results and provide clinical recommendations. The authors should discuss the results and how they can be interpreted from the perspective of previous studies and the working hypotheses. The findings and their implications should be discussed in the broadest context possible. Future research directions may also be highlighted.

4.4. CERAMIC MATERIALS SURFACE INFLUENCE ON HUMAN GINGIVAL FIBROBLASTS AND EPITHELIAL-LIKE CELLS

Several material-dependent factors contribute to forming a stable mucosal seal around implant abutments or final restorations that come in contact with the oral soft tissues, such as surface roughness (Sa), chemistry and hydrophilicity. All of the aforementioned are suggested to be of significant importance for both epithelial and fibroblast cell attachment as well as bacterial adhesion and biofilm formation [394,428,432,456,475,476,503,519–525].

The surface roughness of ceramic materials is governed by the clinician or laboratory's finishing and surface modification procedures. Three levels of surface roughness are discussed in the literature – macro (Ra ~ 10 μm), micro (Ra ~ 1 μm) and nano (Ra ~ 0.2 μm) [432,526]. As previously stated, a reported "threshold value" of 0.2 μm is suggested to facilitate the formation of a favorable soft-tissue seal. Furthermore, machined stock titanium abutments for most systems seem to be near this value ranging from Ra 0.15-0.24 μm [527,528]. In the current study, the specific polishing, cleaning, and surface modification protocol yielded a desirable surface roughness in all studied ceramic materials except ZrO-V, with a value of 0.69 ± 0.14 μm. The resulting standard deviations from the Sa tests demonstrate that the protocol employed in the study can predictably achieve a surface roughness value between 0.1 μm and 0.2 μm for most materials. An increased surface roughness might reduce fibroblast proliferation and induce better bacterial adhesion, biofilm formation

and related adverse effects [432,433]. A clinical study reported that a surface roughness of 0.8 μm increased biofilm's volume and pathogenicity 25 times [436]. The current study did not show a significant difference between the varying surface roughness, cytotoxicity, and proliferation of fibroblasts, except for the ZrO-V material at the 24h observation period. However, this parameter seems to influence the proliferation of epithelial-like cells (ZrO-V, control; $p < 0.05$).

On another note, very smooth surfaces < 0.1 μm have been reported to increase attachment loss, probing depth and BOP values [433,436]. The results of the current study did not find a significant difference in cytotoxicity and proliferation for both tested cell types between the ~ 0.2 μm (NICE, Ti) and the smoother ~ 0.1 μm (ZrO HT, ZrO UTML, EMAX) materials. Moreover, macro-rough surfaces of ~ 8 μm produced by laser modifications of the surface with specific texture (Laser Lok) demonstrated superior properties in terms of gingival morphology, proliferation, fibre orientation, as well as the effectiveness of biofilm control [434,529,530]. The findings suggest that relying solely on surface roughness as a predictor for soft tissue seal formation and *in vivo* cell behaviour may be unreliable.

It should be noted that most of the studies cited above use a different (two-dimensional, profile) roughness parameter (Ra). In contrast, our study deemed an areal roughness parameter (Sa) more adequate, which should be considered when interpreting the influence of Sa on both cell cultures and comparing the results with other published articles.

Another important parameter for cell and bacterial adhesion to prosthetic materials is the surface free energy (SFE), represented as the water contact angle. The tested materials showed variable WCA ranging from 45.34 ± 2.64° to 79 ± 12.79° (Table – desc. WCA). A more pronounced hydrophilic surface was observed in NICE, EMAX and ZrO-V, while the other ZrO-based materials included in the study and Ti showed more hydrophobic surfaces. These results seem to align with other water contact angles reported for Ti and ZrO-based materials having a broad range based on the surface finishing and modification protocols [524]. It has been proven that super-hydrophobic surfaces of ~ 150° have distinct antibacterial properties [523]. However, the current finishing protocol resulted in much lower average WCA angles (64.67 ± 17.40°). Hence it might be proposed that WCA below and around the hydrophilic threshold (90°) do not significantly influence oral cell adhesion. It has been suggested that fibroblast spreading is greater on hydrophilic surfaces.

However, this parameter seems only to influence initial attachment but not proliferation or cytosquelette organisation [531]. The current results for the tested cell lines in contact with materials with varying WCA confirm these findings since no difference was found between the tested materials at the 72-hour time point.

Fibroblasts and epithelial-like cells do not show a time-stable selective affinity towards different classes of permanent prosthetic materials [394,475,476,520]. Our results confirm these findings since no statistically significant difference was observed between different materials in the HGF and epithelial-like cell proliferation tests. However, achieving a faster adhesion, forming a stable connection between human oral cells and the implant or abutment surfaces and creating a mucosal seal is important for the long-term success of the treatment [432,433]. An optimal outcome of surface treatment procedures would forming a stable connective tissue layer which limits the down growth of epithelial cells, bacterial adhesion, and the subsequent development of biofilm. The current study's results show significant time-related differences in the proliferation parameters for both tested cell types. The epithelial-like cells showed a significant difference in proliferation for all three tested time periods, with a gradual increase in the 24-hour control ratio denoting a tendency for increased proliferation from 24 to 48 and 72 hours. Except for ZrO-V and the control group ($p < 0.05$), differences between materials were insignificant. Previous studies reported similar results [394,456,522]. The latter further confirms that the tested materials have no cytotoxic effects on the tested cell line. Results for the HGF had a similar tendency. A significant difference was observed for the 24-48 and 72-24 hours tests ($p < 0.05$, $p < 0.001$). However, there were no cytotoxic effects and proliferation differences for the different tested materials. Considering the varying WCA, the differences in surface roughness and the different chemistry of the samples, our results show poor discrimination between micro and nano-surface roughness and different SFE.

A limitation of the current study is the *in vitro* design. The experiments were conducted in sterile, well-controlled conditions using monocultures for HGF and epithelial-like cells. Thus, the clinical conditions – the presence of multiple competing cell types, bacteria and exposure to saliva and inflammatory tissue products, were not recreated. Several human histology studies show that various materials and surface treatments provide significantly different results for cell and bacterial adhesion [532,533]. Furthermore, the difference

seems quantitative and qualitative, including area coverage, cell morphology and fibre orientation [532–535]. Hence, these conditions must be considered when translating the results into clinical scenarios. Moreover, well-controlled experiments with few observations per group often lead to slight departures from a normal distribution. Substantial evidence shows that ANOVA analyses and related pairwise comparisons are robust in non-normally distributed data [536]. Nevertheless, results from tests in such conditions must be interpreted carefully.

No single factor can explain cell behaviour. However, combining multiple favourable aspects achieved through the correct choice of material with surface treatment protocol might positively influence an early formation and a stable mucosal seal between the abutment and oral soft tissues.

CONCLUSIONS

Considering study limitations, the following conclusions can be drawn:

1. The intraoral scan-based accuracy evaluation provides a valuable alternative and proves the high accuracy of the fully-guided implant placement procedure concerning edentulous defect Kennedy class, implant design and position.

2. Static guidance demonstrated greater accuracy in all aspects except for angle deviations compared to dynamic guidance.

3. The use of reference objects can enhance the accuracy of dynamic guidance for implant placement.

4. Cleaning protocols for polymer-based materials affect roughness, contact angle, and cell proliferation. A more detailed cleaning protocol reduces surface roughness, and promotes cellular proliferation on polyetherketoneketone and 3D-printed polymethylmethacrylate surfaces.

5. UV surface activation of zirconia-based materials can positively impact human gingival fibroblast viability and proliferation.

6. Glazing and veneering zirconia ceramic surfaces result in a noticeable increase in roughness and negatively affects cellular viability.

PRACTICAL RECOMMENDATIONS AND FUTURE PERSPECTIVES

1. It is recommended to prioritize using of intraoral scan-based accuracy evaluation methods as they provide a safe and accurate alternative to traditional computed tomography-based X-ray methods for assessing implant placement accuracy.

2. Prosthetically driven digitally planned fully-guided implant placement is recommended as an accurate treatment modality with regards to various edentulous defect modifications, implant design, and position.

3. Applying well-defined and distributed reference objects to the dynamic navigation method can provide higher accuracy, specifically in cases characterized by minimal remaining dentition or fully edentulous situations.

4. A thorough cleaning protocol is recommended in clinical practice to promote a favourable soft tissue response.

5. UV surface photofunctionalization might be a cost-effective activation method for zirconia-based ceramics and might enhance soft tissue health.

6. Veneered and glazed ceramics are not recommended in areas where soft tissue cellular attachment is expected.

ORCID
Rokas Borusevicius https://orcid.org/0000-0003-0341-9045
Vygandas Rutkunas https://orcid.org/0000-0001-5740-4573

CURRICULUM VITAE

Name	Rokas
Surname	Borusevičius
Date of birth	1990 11 14
Place of birth	Klaipėda, Lietuva
E-mail	rokas.borusevicius@gmail.com

Research activities website	https://www.researchgate.net/profile/Rokas-Borusevicius-3

Education

1997–2005	Vydūnas Secondary School, Klaipėda, Lithuania
	Certificate of primary education
2005–2009	"Ąžuolynas" gymnasium, Klaipėda, Lithuania
	Certificate of basic education
	General certificate of secondary education with award
2009–2014	Vilnius University, Faculty of Medicine, Institute of Odontology, Vilnius, Lithuania
	Master's Diploma
2014–2017	Vilnius University, Faculty of Medicine, Institute of Odontology, Vilnius, Lithuania
	Certificate of Specialist in Periodontology

Work experience

2014–2017	Dentist General Practitioner, Public practice
2017–2019	Periodontist, Public and private practice
2019–present	Periodontist, Private practice
2019–present	Member of a scientific group DIGITORUM

Licences

2014–present	Dentist General Practitioner, OPL-04400
2017–present	Periodontist, OPL-05053

SUPPLEMENTAL MATERIAL

Approval of the Ethics Committee

VILNIAUS UNIVERSITETO MEDICINOS FAKULTETAS
Viešoji įstaiga, Universiteto g. 3, LT- 01513 Vilnius, tel. (8 5) 268 7001, faks. (8 5) 272 8646, el. p. infor@cr.vu.lt.
Duomenys kaupiami ir saugomi Juridinių asmenų registre, kodas 211950810.
Fakulteto duomenys: M.K. Čiurlionio g. 21/27, LT-03101 Vilnius, tel. (8 5) 239 8701, (8 5) 239 7800, faks. (8 5) 239 8705,
el. p. mf@mf.vu.lt
VILNIAUS REGIONINIS BIOMEDICININIŲ TYRIMŲ ETIKOS KOMITETAS
M.K. Čiurlionio g. 21/27, LT-03101 Vilnius, tel. (8 5) 268 6998, el. p. rbtek@mf.vu.lt

LEIDIMAS
ATLIKTI BIOMEDICININĮ TYRIMĄ

2016-07-12   Nr.158200-16-860-369

Tyrimo pavadinimas:
Protezinių medžiagų biosuderinamumo bei 3D spausdinimo technologijų audinių regeneracijai in vitro ir in vivo vertinimas

Protokolo Nr.:	1
Versija:	002
Data:	2016-06-27
Asmens informavimo ir informuoto asmens sutikimo forma:	In vitro
Versija:	2a
Data:	2016-06-28
Asmens informavimo ir informuoto asmens sutikimo forma:	In vivo
Versija:	2b
Data:	2016-06-28
Pagrindinis tyrėjas:	**Vygandas Rutkūnas**
Įstaigos pavadinimas:	VšĮ VUL Žalgirio klinika
Adresas:	Žalgirio g. 117, Vilnius
Įstaigos pavadinimas:	UAB „Prodentum"
Adresas:	Kalvarijų g. 128A, Vilnius
Leidimas galioja iki:	**2019-09-01**

Leidimas išduotas Vilniaus regioninio biomedicininių tyrimų etikos komiteto posėdžio (protokolas Nr. 158200-2016/07), vykusio 2016 m. liepos 12 d. sprendimu.

	Vilniaus regioninio biomedicininių	tyrimų etikos komiteto ekspertų grupės	nariai
Nr.	Vardas, pavardė	veiklos sritis	dalyvavo posėdyje
1	doc. dr. Laimutė Jakavonytė	filosofija	taip
2	prof.dr. Jolanta Dadonienė	epidemiologija, medicina	taip
3	doc.dr. Jaunius Gumbis	teisė	ne
4	Genovaitė Bulzgytė	slauga	taip
5	prof.dr. Augustina Jankauskienė	medicina	ne
6	dr. Laura Malinauskienė	medicina	taip
7	Eglė Zubienė	psichologija	taip
8	prof. Saulius Vosylius	medicina	taip
9	Ugnė Šakūnienė	pacientų teisės	ne

Pirmininkė   Laura Malinauskienė

133

VILNIAUS REGIONINIS BIOMEDICININIŲ TYRIMŲ ETIKOS KOMITETAS
sui generis darinys prie VILNIAUS UNIVERSITETO

Biomedicininio tyrimo „Protezinių medžiagų biosuderinamumo bei 3D   2019-09-19 Nr. 2019-LP-37
spausdinimo technologijų audinių regeneracijai in vitro ir in vivo
vertinimas"
pagrindiniam tyrėjui Vygandui Rutkūnui

Dėl leidimo Nr. 158200-16-860-369 papildymo Nr. 1

PRITARIMAS

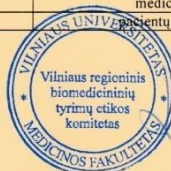Vilniaus regioninis biomedicininių tyrimų etikos komitetas išnagrinėjo Jūsų prašymą keisti/papildyti biomedicininio tyrimo „*Protezinių medžiagų biosuderinamumo bei 3D spausdinimo technologijų audinių regeneracijai in vitro ir in vivo vertinimas*", leidimą Nr. 158200-16-860-369, išduotą 2016-07-12 d. Ekspertai pritaria:

- Tyrimo pratęsimui iki 2025-09-01 d.;
- Atnaujintam protokolui (versijos Nr. 003, data 2019-06-27 d.);
- Atnaujintų informuoto asmens sutikimo formų teikimui (donorų grupė – versijos Nr. 4, data 2019-08-16 d. ir regeneracijos klinikinio tyrimo grupė - versijos Nr. 4, data 2019-08-16 d.).

Pirmininkas   prof. dr. (HP) Saulius Vosylius

BIBLIOGRAPHY

[1]   Rutkūnas V, Gedrimienė A, Auškalnis L, Admakin O, Mangano F. Accuracy of Fixed Implant-Supported Dental Prostheses Additively Manufactured by Metal, Ceramic, or Polymer: A Systematic Review. J Prosthodont 2022;31:70–87. https://doi.org/10.1111/jopr.13449.

[2]   Tel A, Arboit L, De Martino M, Isola M, Sembronio S, Robiony M. Systematic review of the software used for virtual surgical planning in craniomaxillofacial surgery over the last decade. Int J Oral Maxillofac Surg 2022:S0901-5027(22)00461-1. https://doi.org/10.1016/j.ijom.2022.11.011.

[3]   Huang S, Wei H, Li D. Additive manufacturing technologies in the oral implant clinic: A review of current applications and progress. Front Bioeng Biotechnol 2023;11:1100155. https://doi.org/10.3389/fbioe.2023.1100155.

[4]   Apostolakis D, Michelinakis G, Kamposiora P, Papavasiliou G. The current state of computer assisted orthognathic surgery: A narrative review. J Dent 2022;119:104052. https://doi.org/10.1016/j.jdent.2022.104052.

[5]   Glas HH, Vosselman N, de Visscher SAHJ. The use of 3D virtual surgical planning and computer aided design in reconstruction of maxillary surgical defects. Curr Opin Otolaryngol Head Neck Surg 2020;28:122–8. https://doi.org/10.1097/MOO.0000000000000618.

[6]   Romandini M, Ruales-Carrera E, Sadilina S, Hämmerle CHF, Sanz M. Minimal invasiveness at dental implant placement: A systematic review with meta-analyses on flapless fully guided surgery. Periodontol 2000 2022. https://doi.org/10.1111/prd.12440.

[7]   Pletkus J, Rutkūnas V, Gendvilienė I, Borusevičius R, Gedrimienė A, Auškalnis A, et al. Model-free digital workflow and immediate functional loading of implant-supported monolithic glass-ceramic crowns: A case series. J Dent 2022;125:104270. https://doi.org/10.1016/j.jdent.2022.104270.

[8]   Alauddin MS, Baharuddin AS, Mohd Ghazali MI. The Modern and Digital Transformation of Oral Health Care: A Mini Review. Healthcare (Basel) 2021;9:118. https://doi.org/10.3390/healthcare9020118.

[9]   Fokas G, Vaughn VM, Scarfe WC, Bornstein MM. Accuracy of linear measurements on CBCT images related to presurgical implant treatment planning: A systematic review. Clin Oral Implants Res 2018;29 Suppl 16:393–415. https://doi.org/10.1111/clr.13142.

[10] Manicone PF, De Angelis P, Rella E, Damis G, D'addona A. Patient preference and clinical working time between digital scanning and conventional impression making for implant-supported prostheses: A systematic review and meta-analysis. J Prosthet Dent 2022;128:589–96. https://doi.org/10.1016/j.prosdent.2020.11.042.

[11] Mühlemann S, Kraus RD, Hämmerle CHF, Thoma DS. Is the use of digital technologies for the fabrication of implant-supported reconstructions more efficient and/or more effective than conventional techniques: A systematic review. Clin Oral Implants Res 2018;29 Suppl 18:184–95. https://doi.org/10.1111/clr.13300.

[12] Bedrossian EA. Complete digital workflow for complete arch implant therapy: Fact or fiction? J Prosthet Dent 2022;127:821–2. https://doi.org/10.1016/j.prosdent.2022.04.021.

[13] Ekelund J-A, Lindquist LW, Carlsson GE, Jemt T. Implant treatment in the edentulous mandible: a prospective study on Brånemark system implants over more than 20 years. Int J Prosthodont 2003;16:602–8.

[14] Chappuis V, Buser R, Brägger U, Bornstein MM, Salvi GE, Buser D. Long-term outcomes of dental implants with a titanium plasma-sprayed surface: a 20-year prospective case series study in partially edentulous patients. Clin Implant Dent Relat Res 2013;15:780–90. https://doi.org/10.1111/cid.12056.

[15] Lini F, Poli PP, Beretta M, Cortinovis I, Maiorana C. Long-term retrospective observational cohort study on the survival rate of stepped screw titanium implants followed up to 20 years. Int J Oral Maxillofac Implants 2019;34:999–1006. https://doi.org/10.11607/jomi.7007.

[16] Basu B, Gowtham NH, Xiao Y, Kalidindi SR, Leong KW. Biomaterialomics: Data science-driven pathways to develop fourth-generation biomaterials. Acta Biomater 2022;143:1–25. https://doi.org/10.1016/j.actbio.2022.02.027.

[17] Darriba I, Seidel A, Moreno F, Botelho J, Machado V, Mendes JJ, et al. Influence of low insertion torque values on survival rate of immediately loaded dental implants: A systematic review and meta-analysis. J Clin Periodontol 2023;50:158–69. https://doi.org/10.1111/jcpe.13733.

[18] Fan R, Quinton HA, Golberg MB, Portnof JE. Immediate Implants. Dent Clin North Am 2021;65:89–102. https://doi.org/10.1016/j.cden.2020.09.007.

[19] Dioguardi M, Spirito F, Quarta C, Sovereto D, Basile E, Ballini A, et al. Guided Dental Implant Surgery: Systematic Review. J Clin Med 2023;12:1490. https://doi.org/10.3390/jcm12041490.

[20] Chokaree P, Poovarodom P, Chaijareenont P, Yavirach A, Rungsiyakull P. Biomaterials and Clinical Applications of Customized Healing Abutment-A Narrative Review. J Funct Biomater 2022;13:291. https://doi.org/10.3390/jfb13040291.

[21] Perrotti V, Zhang D, Liang A, Wong J, Quaranta A. The Effect of One-Abutment at One-Time on Marginal Bone Loss Around Implants Placed in Healed Bone: A Systematic Review of Human Studies. Implant Dent 2019;28:603–12. https://doi.org/10.1097/ID.0000000000000931.

[22] Tallarico M, Caneva M, Meloni SM, Xhanari E, Covani U, Canullo L. Definitive Abutments Placed at Implant Insertion and Never Removed: Is It an Effective Approach? A Systematic Review and Meta-Analysis of Randomized Controlled Trials. J Oral Maxillofac Surg 2018;76:316–24. https://doi.org/10.1016/j.joms.2017.08.025.

[23] Laleman I, Lambert F. Implant connection and abutment selection as a predisposing and/or precipitating factor for peri-implant diseases: A review. Clin Implant Dent Relat Res 2023. https://doi.org/10.1111/cid.13185.

[24] Chackartchi T, Romanos GE, Parkanyi L, Schwarz F, Sculean A. Reducing errors in guided implant surgery to optimize treatment outcomes. Periodontol 2000 2022;88:64–72. https://doi.org/10.1111/prd.12411.

[25] Tahmaseb A, Wismeijer D, Coucke W, Derksen W. Computer technology applications in surgical implant dentistry: a systematic review. Int J Oral Maxillofac Implants 2014;29 Suppl:25–42. https://doi.org/10.11607/jomi.2014suppl.g1.2.

[26] Ebenezer S, Kumar VV, Thor A. Basics of Dental Implantology for the Oral Surgeon. In: Bonanthaya K, Panneerselvam E, Manuel S, Kumar VV, Rai A, editors. Oral and Maxillofacial Surgery for the Clinician, Singapore: Springer Nature; 2021, p. 385–405. https://doi.org/10.1007/978-981-15-1346-6_18.

[27] Kageyama I, Maeda S, Takezawa K. Importance of anatomy in dental implant surgery. J Oral Biosci 2021;63:142–52. https://doi.org/10.1016/j.job.2021.01.002.

[28] Chen ST, Buser D, Sculean A, Belser UC. Complications and treatment errors in implant positioning in the aesthetic zone: Diagnosis and possible solutions. Periodontol 2000 2023. https://doi.org/10.1111/prd.12474.

[29] Cooper LF, De Kok IJ, Thalji G, Bryington MS. Prosthodontic Management of Implant Therapy: Esthetic Complications. Dent Clin North Am 2019;63:199–216. https://doi.org/10.1016/j.cden.2018.11.003.

[30] Renouard F, Amalberti R, Renouard E. Are "Human Factors" the Primary Cause of Complications in the Field of Implant Dentistry? Int J Oral Maxillofac Implants 2017;32:e55–61. https://doi.org/10.11607/jomi.2017.2.e.

[31] Revilla-León M, Yilmaz B, Kois JC, Att W. Prevention of peri-implant disease in edentulous patients with fixed implant rehabilitations. Clinical Implant Dentistry and Related Research n.d.;n/a. https://doi.org/10.1111/cid.13182.

[32] Tatakis DN, Chien H-H, Parashis AO. Guided implant surgery risks and their prevention. Periodontol 2000 2019;81:194–208. https://doi.org/10.1111/prd.12292.

[33] Pimkhaokham A, Jiaranuchart S, Kaboosaya B, Arunjaroensuk S, Subbalekha K, Mattheos N. Can computer-assisted implant surgery improve clinical outcomes and reduce the frequency and intensity of complications in implant dentistry? A critical review. Periodontol 2000 2022;90:197–223. https://doi.org/10.1111/prd.12458.

[34] Zhang F, Gao X, Ye Z-Y, Xu D-Q, Ding X. The clinical accuracy of the implant digital surgical guide: A meta-analysis. Am J Dent 2020;33:296–304.

[35] Guentsch A, Sukhtankar L, An H, Luepke PG. Precision and trueness of implant placement with and without static surgical guides: An in vitro study. J Prosthet Dent 2020. https://doi.org/10.1016/j.prosdent.2020.06.015.

[36] Jorba-García A, González-Barnadas A, Camps-Font O, Figueiredo R, Valmaseda-Castellón E. Accuracy assessment of dynamic computer-aided implant placement: a systematic review and meta-analysis. Clin Oral Investig 2021. https://doi.org/10.1007/s00784-021-03833-8.

[37] Block MS, Emery RW, Cullum DR, Sheikh A. Implant Placement Is More Accurate Using Dynamic Navigation. J Oral Maxillofac Surg 2017;75:1377–86. https://doi.org/10.1016/j.joms.2017.02.026.

[38] Al Yafi F, Camenisch B, Al-Sabbagh M. Is Digital Guided Implant Surgery Accurate and Reliable? Dent Clin North Am 2019;63:381–97. https://doi.org/10.1016/j.cden.2019.02.006.

[39] Schnutenhaus S, Edelmann C, Knipper A, Luthardt R. Accuracy of Dynamic Computer-Assisted Implant Placement: A Systematic Review and Meta-Analysis of Clinical and In Vitro Studies. Journal of Clinical Medicine 2021;10:704. https://doi.org/10.3390/jcm10040704.

[40] Afrashtehfar KI, Jurado CA, Moshaverinia A. Dynamic navigation may be used for most implant surgery scenarios due to its satisfactory accuracy.

J Evid Based Dent Pract 2022;22:101797. https://doi.org/10.1016/j.jebdp.2022.101797.

[41] Parra-Tresserra A, Marquès-Guasch J, Ortega-Martínez J, Basilio-Monné J, Hernández-Alfaro F. Current state of dynamic surgery. A literature review. Med Oral Patol Oral Cir Bucal 2021;26:e576–81. https://doi.org/10.4317/medoral.24566.

[42] Pyo S-W, Lim Y-J, Koo K-T, Lee J. Methods Used to Assess the 3D Accuracy of Dental Implant Positions in Computer-Guided Implant Placement: A Review. J Clin Med 2019;8:54. https://doi.org/10.3390/jcm8010054.

[43] Wei S-M, Zhu Y, Wei J-X, Zhang C-N, Shi J-Y, Lai H-C. Accuracy of dynamic navigation in implant surgery: A systematic review and meta-analysis. Clin Oral Implants Res 2021. https://doi.org/10.1111/clr.13719.

[44] Sawicki P, Zawadzki PJ, Regulski P. The Impact of Cone-Beam Computed Tomography Exposure Parameters on Peri-Implant Artifacts: A Literature Review. Cureus 2022;14:e23035. https://doi.org/10.7759/cureus.23035.

[45] Schnutenhaus S, Edelmann C, Rudolph H, Luthardt RG. Retrospective study to determine the accuracy of template-guided implant placement using a novel nonradiologic evaluation method. Oral Surg Oral Med Oral Pathol Oral Radiol 2016;121:e72-79. https://doi.org/10.1016/j.oooo.2015.12.012.

[46] Gonçalves GSY, de Magalhães KMF, Rocha EP, Dos Santos PH, Assunção WG. Oral health-related quality of life and satisfaction in edentulous patients rehabilitated with implant-supported full dentures all-on-four concept: a systematic review. Clin Oral Investig 2022;26:83–94. https://doi.org/10.1007/s00784-021-04213-y.

[47] Garcia-Sanchez R, Dopico J, Kalemaj Z, Buti J, Pardo Zamora G, Mardas N. Comparison of clinical outcomes of immediate versus delayed placement of dental implants: A systematic review and meta-analysis. Clin Oral Implants Res 2022;33:231–77. https://doi.org/10.1111/clr.13892.

[48] Eini E, Yousefimanesh H, Ashtiani AH, Saki-Malehi A, Olapour A, Rahim F. Comparing success of immediate versus delay loading of implants in fresh sockets: a systematic review and meta-analysis. Oral Maxillofac Surg 2022;26:185–94. https://doi.org/10.1007/s10006-021-00983-7.

[49] Zhao G, Zhou Y, Shi S, Liu X, Zhang S, Song Y. Long-term clinical outcomes of immediate loading versus non-immediate loading in single-implant restorations: a systematic review and meta-analysis. Int J Oral Maxillofac Surg 2022;51:1345–54. https://doi.org/10.1016/j.ijom.2022.03.057.

[50] Brånemark PI. Osseointegration and its experimental background. J Prosthet Dent 1983;50:399–410. https://doi.org/10.1016/s0022-3913(83)80101-2.

[51] Kreve S, Ferreira I, da Costa Valente ML, Dos Reis AC. Relationship between dental implant macro-design and osseointegration: a systematic review. Oral Maxillofac Surg 2022. https://doi.org/10.1007/s10006-022-01116-4.

[52] Bassetti RG, Stähli A, Bassetti MA, Sculean A. Soft tissue augmentation around osseointegrated and uncovered dental implants: a systematic review. Clin Oral Investig 2017;21:53–70. https://doi.org/10.1007/s00784-016-2007-9.

[53] Tavelli L, Barootchi S, Avila-Ortiz G, Urban IA, Giannobile WV, Wang H-L. Peri-implant soft tissue phenotype modification and its impact on peri-implant health: A systematic review and network meta-analysis. J Periodontol 2021;92:21–44. https://doi.org/10.1002/JPER.19-0716.

[54] Monje A, González-Martín O, Ávila-Ortiz G. Impact of peri-implant soft tissue characteristics on health and esthetics. J Esthet Restor Dent 2023;35:183–96. https://doi.org/10.1111/jerd.13003.

[55] Bressan E, Guazzo R, Tomasi C, Peña TG, Galindo-Moreno P, Caponio VCA, et al. Influence of soft tissue thickness on marginal bone level around dental implants: A systematic review with meta-analysis and trial-sequential analysis. Clin Oral Implants Res 2023. https://doi.org/10.1111/clr.14032.

[56] Mattheos N, Vergoullis I, Janda M, Miseli A. The Implant Supracrestal Complex and Its Significance for Long-Term Successful Clinical Outcomes. Int J Prosthodont 2021;34:88–100. https://doi.org/10.11607/ijp.7201.

[57] Sutariya PV, Mehta SP, Upadhyay HH, Pathan MR, Patel SR, Bhatia YA. The soft tissue esthetic outcome with and without immediate provisionalization in immediate implants: A systematic review and meta-analysis. J Indian Prosthodont Soc 2022;22:2–12. https://doi.org/10.4103/jips.jips_227_21.

[58] Atsuta I, Ayukawa Y, Kondo R, Oshiro W, Matsuura Y, Furuhashi A, et al. Soft tissue sealing around dental implants based on histological interpretation. J Prosthodont Res 2016;60:3–11. https://doi.org/10.1016/j.jpor.2015.07.001.

[59] Sanz M, Schwarz F, Herrera D, McClain P, Figuero E, Molina A, et al. Importance of keratinized mucosa around dental implants: Consensus report of group 1 of the DGI/SEPA/Osteology Workshop. Clin Oral Implants Res 2022;33 Suppl 23:47–55. https://doi.org/10.1111/clr.13956.

[60] Al Rezk F, Trimpou G, Lauer H-C, Weigl P, Krockow N. Response of soft tissue to different abutment materials with different surface topographies: a review of the literature. Gen Dent 2018;66:18–25.

[61] Zol SM, Alauddin MS, Said Z, Mohd Ghazali MI, Hao-Ern L, Mohd Farid DA, et al. Description of Poly(aryl-ether-ketone) Materials (PAEKs), Polyetheretherketone (PEEK) and Polyetherketoneketone (PEKK) for Application as a Dental Material: A Materials Science Review. Polymers (Basel) 2023;15:2170. https://doi.org/10.3390/polym15092170.

[62] Alagatu A, Dhapade D, Gajbhiye M, Panjrekar R, Raut A. Review of different material and surface modification techniques for dental implants. Materials Today: Proceedings 2022;60:2245–9. https://doi.org/10.1016/j.matpr.2022.03.338.

[63] Brånemark PI, Hansson BO, Adell R, Breine U, Lindström J, Hallén O, et al. Osseointegrated implants in the treatment of the edentulous jaw. Experience from a 10-year period. Scand J Plast Reconstr Surg Suppl 1977;16:1–132.

[64] Palmquist A. A multiscale analytical approach to evaluate osseointegration. J Mater Sci Mater Med 2018;29:60. https://doi.org/10.1007/s10856-018-6068-y.

[65] Papaspyridakos P, Chen C-J, Singh M, Weber H-P, Gallucci GO. Success criteria in implant dentistry: a systematic review. J Dent Res 2012;91:242–8. https://doi.org/10.1177/0022034511431252.

[66] Linkevicius T, Puisys A, Linkeviciene L, Peciuliene V, Schlee M. Crestal Bone Stability around Implants with Horizontally Matching Connection after Soft Tissue Thickening: A Prospective Clinical Trial. Clin Implant Dent Relat Res 2015;17:497–508. https://doi.org/10.1111/cid.12155.

[67] Sailer I, Karasan D, Todorovic A, Ligoutsikou M, Pjetursson BE. Prosthetic failures in dental implant therapy. Periodontol 2000 2022;88:130–44. https://doi.org/10.1111/prd.12416.

[68] Messias A, Karasan D, Nicolau P, Pjetursson BE, Guerra F. Rehabilitation of full-arch edentulism with fixed or removable dentures retained by root-form dental implants: A systematic review of outcomes and outcome measures used in clinical research in the last 10 years. Clin Oral Implants Res 2023;34 Suppl 25:38–54. https://doi.org/10.1111/clr.13931.

[69] Feine J, Abou-Ayash S, Al Mardini M, de Santana RB, Bjelke-Holtermann T, Bornstein MM, et al. Group 3 ITI Consensus Report: Patient-reported outcome measures associated with implant dentistry. Clin Oral Implants Res 2018;29 Suppl 16:270–5. https://doi.org/10.1111/clr.13299.

[70] Thoma DS, Strauss FJ, Mancini L, Gasser TJW, Jung RE. Minimal invasiveness in soft tissue augmentation at dental implants: A systematic review and meta-analysis of patient-reported outcome measures. Periodontol 2000 2023;91:182–98. https://doi.org/10.1111/prd.12465.

[71]   Marković A, Mišić T, Janjić B, Šćepanović M, Trifković B, Ilić B, et al. Immediate Vs Early Loading of Bone Level Tapered Dental Implants With Hydrophilic Surface in Rehabilitation of Fully Edentulous Maxilla: Clinical and Patient Centered Outcomes. J Oral Implantol 2022;48:358–69. https://doi.org/10.1563/aaid-joi-D-21-00045.

[72]   Esposito M, Grusovin MG, Chew YS, Coulthard P, Worthington HV. WITHDRAWN: Interventions for replacing missing teeth: 1- versus 2-stage implant placement. Cochrane Database Syst Rev 2018;5:CD006698. https://doi.org/10.1002/14651858.CD006698.pub3.

[73]   Gulati M, Govila V, Verma S, Rajkumar B, Anand V, Aggarwal A, et al. In Vivo Evaluation of Two-Piece Implants Placed Following One-Stage and Two-Stage Surgical Protocol in Posterior Mandibular Region. Assessment of Alterations in Crestal Bone Level. Clin Implant Dent Relat Res 2015;17:854–61. https://doi.org/10.1111/cid.12186.

[74]   Gotfredsen K, Hosseini M, Rimborg S, Özhayat E. Patient's perception of timing concepts in implant dentistry: A systematic review. Clin Oral Implants Res 2021;32 Suppl 21:67–84. https://doi.org/10.1111/clr.13861.

[75]   Alfadda SA, Chvartszaid D, Tulbah HI, Finer Y. Immediate versus conventional loading of mandibular implant-supported fixed prostheses in edentulous patients: 10-year report of a randomised controlled trial. Int J Oral Implantol (Berl) 2019;12:431–46.

[76]   Abdunabi A, Morris M, Nader SA, Souza RF de. Impact of immediately loaded implant-supported maxillary full-arch dental prostheses: a systematic review. J Appl Oral Sci 2019;27:e20180600. https://doi.org/10.1590/1678-7757-2018-0600.

[77]   Slagter KW, Raghoebar GM, Hentenaar DFM, Vissink A, Meijer HJA. Immediate placement of single implants with or without immediate provisionalization in the maxillary aesthetic region: A 5-year comparative study. J Clin Periodontol 2021;48:272–83. https://doi.org/10.1111/jcpe.13398.

[78]   Huynh-Ba G, Oates TW, Williams MAH. Immediate loading vs. early/conventional loading of immediately placed implants in partially edentulous patients from the patients' perspective: A systematic review. Clin Oral Implants Res 2018;29 Suppl 16:255–69. https://doi.org/10.1111/clr.13278.

[79]   Francisco H, Marques D, Pinto C, Aiquel L, Caramês J. Is the timing of implant placement and loading influencing esthetic outcomes in single-tooth implants?-A systematic review. Clin Oral Implants Res 2021;32 Suppl 21:28–55. https://doi.org/10.1111/clr.13811.

[80] Puisys A, Auzbikaviciute V, Vindasiute-Narbute E, Pranskunas M, Razukevicus D, Linkevicius T. Immediate implant placement vs. early implant treatment in the esthetic area. A 1-year randomized clinical trial. Clin Oral Implants Res 2022;33:634–55. https://doi.org/10.1111/clr.13924.

[81] Lang NP, Pun L, Lau KY, Li KY, Wong MCM. A systematic review on survival and success rates of implants placed immediately into fresh extraction sockets after at least 1 year. Clin Oral Implants Res 2012;23 Suppl 5:39–66. https://doi.org/10.1111/j.1600-0501.2011.02372.x.

[82] Blanco J, Carral C, Argibay O, Liñares A. Implant placement in fresh extraction sockets. Periodontol 2000 2019;79:151–67. https://doi.org/10.1111/prd.12253.

[83] Akin R, Chapple AG. Clinical Advantages of Immediate Posterior Implants With Custom Healing Abutments: Up to 8-Year Follow-Up of 115 Cases. J Oral Maxillofac Surg 2022;80:1952–65. https://doi.org/10.1016/j.joms.2022.08.014.

[84] Corrado F, Marconcini S, Cosola S, Giammarinaro E, Covani U. Immediate Implant and Customized Healing Abutment Promotes Tissues Regeneration: a 5-year Clinical Report. J Oral Implantol 2023. https://doi.org/10.1563/aaid-joi-D-21-00224.

[85] Watanabe H, Fellows C, An H. Digital Technologies for Restorative Dentistry. Dent Clin North Am 2022;66:567–90. https://doi.org/10.1016/j.cden.2022.05.006.

[86] Cervino G, Fiorillo L, Arzukanyan AV, Spagnuolo G, Cicciù M. Dental Restorative Digital Workflow: Digital Smile Design from Aesthetic to Function. Dent J (Basel) 2019;7:30. https://doi.org/10.3390/dj7020030.

[87] Revilla-León M, Kois DE, Zeitler JM, Att W, Kois JC. An overview of the digital occlusion technologies: Intraoral scanners, jaw tracking systems, and computerized occlusal analysis devices. J Esthet Restor Dent 2023. https://doi.org/10.1111/jerd.13044.

[88] Kernen F, Kramer J, Wanner L, Wismeijer D, Nelson K, Flügge T. A review of virtual planning software for guided implant surgery - data import and visualization, drill guide design and manufacturing. BMC Oral Health 2020;20:251. https://doi.org/10.1186/s12903-020-01208-1.

[89] Bishti S, Tuna T, Rittich A, Wolfart S. Patient-reported outcome measures (PROMs) of implant-supported reconstructions using digital workflows: A systematic review and meta-analysis. Clin Oral Implants Res 2021;32 Suppl 21:318–35. https://doi.org/10.1111/clr.13846.

[90]   Schepke U. [A PhD completed. Innovations in restorative dentistry: necessary or superfluous?]. Ned Tijdschr Tandheelkd 2018;125:403–6. https://doi.org/10.5177/ntvt.2018.07/08.18135.

[91]   Wang F, Wang Q, Zhang J. Role of Dynamic Navigation Systems in Enhancing the Accuracy of Implant Placement: A Systematic Review and Meta-Analysis of Clinical Studies. J Oral Maxillofac Surg 2021;79:2061–70. https://doi.org/10.1016/j.joms.2021.06.005.

[92]   Edelhoff D, Stimmelmayr M, Schweiger J, Ahlers MO, Güth J-F. Advances in materials and concepts in fixed prosthodontics: a selection of possible treatment modalities. Br Dent J 2019;226:739–48. https://doi.org/10.1038/s41415-019-0265-z.

[93]   Cai H, Xu X, Lu X, Zhao M, Jia Q, Jiang H-B, et al. Dental Materials Applied to 3D and 4D Printing Technologies: A Review. Polymers (Basel) 2023;15:2405. https://doi.org/10.3390/polym15102405.

[94]   Gendviliene I, Simoliunas E, Alksne M, Dibart S, Jasiuniene E, Cicenas V, et al. Effect of extracellular matrix and dental pulp stem cells on bone regeneration with 3D printed PLA/HA composite scaffolds. Eur Cell Mater 2021;41:204–15. https://doi.org/10.22203/eCM.v041a15.

[95]   Cevik P, Schimmel M, Yilmaz B. New generation CAD-CAM materials for implant-supported definitive frameworks fabricated by using subtractive technologies. Biomed Res Int 2022;2022:3074182. https://doi.org/10.1155/2022/3074182.

[96]   Schünemann FH, Galárraga-Vinueza ME, Magini R, Fredel M, Silva F, Souza JCM, et al. Zirconia surface modifications for implant dentistry. Mater Sci Eng C Mater Biol Appl 2019;98:1294–305. https://doi.org/10.1016/j.msec.2019.01.062.

[97]   van Oirschot BAJA, Zhang Y, Alghamdi HS, Cordeiro JM, Nagay BE, Barao VAR, et al. Surface Engineering for Dental Implantology: Favoring Tissue Responses Along the Implant. Tissue Eng Part A 2022;28:555–72. https://doi.org/10.1089/ten.TEA.2021.0230.

[98]   Shah KK, Sivaswamy V. A Literature Review on Implant Abutment Types, Materials, and Fabrication Processes. J Long Term Eff Med Implants 2022;33:57–66. https://doi.org/10.1615/JLongTermEffMedImplants.2022042720.

[99]   Rupp F, Liang L, Geis-Gerstorfer J, Scheideler L, Hüttig F. Surface characteristics of dental implants: A review. Dent Mater 2018;34:40–57. https://doi.org/10.1016/j.dental.2017.09.007.

[100] Tzanakakis E-GC, Skoulas E, Pepelassi E, Koidis P, Tzoutzas IG. The Use of Lasers in Dental Materials: A Review. Materials (Basel) 2021;14:3370. https://doi.org/10.3390/ma14123370.

[101] Pesce P, Menini M, Santori G, Giovanni ED, Bagnasco F, Canullo L. Photo and Plasma Activation of Dental Implant Titanium Surfaces. A Systematic Review with Meta-Analysis of Pre-Clinical Studies. J Clin Med 2020;9:2817. https://doi.org/10.3390/jcm9092817.

[102] Chopra D, Gulati K, Ivanovski S. Understanding and optimizing the antibacterial functions of anodized nano-engineered titanium implants. Acta Biomater 2021;127:80–101. https://doi.org/10.1016/j.actbio.2021.03.027.

[103] Peña-Bengoa F, Valenzuela M, Flores MJ, Dufey N, Pinto KP, Silva EJNL. Effectiveness of guided endodontics in locating calcified root canals: a systematic review. Clin Oral Investig 2023;27:2359–74. https://doi.org/10.1007/s00784-023-04863-0.

[104] Bianchi J, Mendonca G, Gillot M, Oh H, Park J, Turkestani NA, et al. Three-dimensional digital applications for implant space planning in orthodontics: A narrative review. J World Fed Orthod 2022;11:207–15. https://doi.org/10.1016/j.ejwf.2022.10.006.

[105] Burke ZDC, Blumstein GW, Zoller SD, Park HY, Bernthal NM. Reconstructive Science in Orthopedic Oncology. Tech Orthop 2018;33:175–82. https://doi.org/10.1097/BTO.0000000000000282.

[106] Buser D, Sennerby L, De Bruyn H. Modern implant dentistry based on osseointegration: 50 years of progress, current trends and open questions. Periodontol 2000 2017;73:7–21. https://doi.org/10.1111/prd.12185.

[107] Edge MJ. Surgical placement guide for use with osseointegrated implants. J Prosthet Dent 1987;57:719–22. https://doi.org/10.1016/0022-3913(87)90371-4.

[108] Burns DR, Crabtree DG, Bell DH. Template for positioning and angulation of intraosseous implants. J Prosthet Dent 1988;60:479–83. https://doi.org/10.1016/0022-3913(88)90253-3.

[109] Orenstein IH. The surgical template: a prescription for implant success. Implant Dent 1992;1:182–4. https://doi.org/10.1097/00008505-199200130-00003.

[110] Engelman MJ, Sorensen JA, Moy P. Optimum placement of osseointegrated implants. J Prosthet Dent 1988;59:467–73. https://doi.org/10.1016/0022-3913(88)90044-3.

[111] Kraut RA. Utilization of 3D/Dental software for precise implant site selection: clinical reports. Implant Dent 1992;1:134–9. https://doi.org/10.1097/00008505-199205000-00005.

[112] Modica F, Fava C, Benech A, Preti G. Radiologic-prosthetic planning of the surgical phase of the treatment of edentulism by osseointegrated implants: an in vitro study. J Prosthet Dent 1991;65:541–6. https://doi.org/10.1016/0022-3913(91)90297-a.

[113] Binon PP. Treatment planning complications and surgical miscues. J Oral Maxillofac Surg 2007;65:73–92. https://doi.org/10.1016/j.joms.2007.03.014.

[114] Zinner ID, Small SA, Panno FV. Presurgical prosthetics and surgical templates. Dent Clin North Am 1989;33:619–33.

[115] Eckerdal O, Kvint S. Presurgical planning for osseointegrated implants in the maxilla. A tomographic evaluation of available alveolar bone and morphological relations in the maxilla. Int J Oral Maxillofac Surg 1986;15:722–6. https://doi.org/10.1016/s0300-9785(86)80113-2.

[116] Verstreken K, Van Cleynenbreugel J, Martens K, Marchal G, van Steenberghe D, Suetens P. An image-guided planning system for endosseous oral implants. IEEE Trans Med Imaging 1998;17:842–52. https://doi.org/10.1109/42.736056.

[117] Tal H, Moses O. A comparison of panoramic radiography with computed tomography in the planning of implant surgery. Dentomaxillofac Radiol 1991;20:40–2. https://doi.org/10.1259/dmfr.20.1.1884852.

[118] Hounsfield GN. Computerized transverse axial scanning (tomography). 1. Description of system. Br J Radiol 1973;46:1016–22. https://doi.org/10.1259/0007-1285-46-552-1016.

[119] Jacobi W. The concept of the effective dose a proposal for the combination of organ doses. Radiat Environ Biophys 1975;12:101–9. https://doi.org/10.1007/BF01328971.

[120] McCullough EC, Payne JT. Patient dosage in computed tomography. Radiology 1978;129:457–63. https://doi.org/10.1148/129.2.457.

[121] ICRP n.d. https://www.icrp.org/page.asp?id=382 (accessed June 4, 2023).

[122] Brenner DJ, Hall EJ. Computed tomography--an increasing source of radiation exposure. N Engl J Med 2007;357:2277–84. https://doi.org/10.1056/NEJMra072149.

[123] Loubele M, Bogaerts R, Van Dijck E, Pauwels R, Vanheusden S, Suetens P, et al. Comparison between effective radiation dose of CBCT and MSCT scanners for dentomaxillofacial applications. Eur J Radiol 2009;71:461–8. https://doi.org/10.1016/j.ejrad.2008.06.002.

[124] Bornstein MM, Scarfe WC, Vaughn VM, Jacobs R. Cone beam computed tomography in implant dentistry: a systematic review focusing on

guidelines, indications, and radiation dose risks. Int J Oral Maxillofac Implants 2014;29 Suppl:55–77. https://doi.org/10.11607/jomi.2014suppl.g1.4.

[125] Hatcher DC. Operational principles for cone-beam computed tomography. J Am Dent Assoc 2010;141 Suppl 3:3S-6S. https://doi.org/10.14219/jada.archive.2010.0359.

[126] Kunzendorf B, Naujokat H, Wiltfang J. Indications for 3-D diagnostics and navigation in dental implantology with the focus on radiation exposure: a systematic review. Int J Implant Dent 2021;7:52. https://doi.org/10.1186/s40729-021-00328-9.

[127] Ludlow JB, Timothy R, Walker C, Hunter R, Benavides E, Samuelson DB, et al. Effective dose of dental CBCT-a meta analysis of published data and additional data for nine CBCT units. Dentomaxillofac Radiol 2015;44:20140197. https://doi.org/10.1259/dmfr.20140197.

[128] Ludlow JB, Walker C. Assessment of phantom dosimetry and image quality of i-CAT FLX cone-beam computed tomography. Am J Orthod Dentofacial Orthop 2013;144:802–17. https://doi.org/10.1016/j.ajodo.2013.07.013.

[129] Widmann G, Al-Ekrish AA. Ultralow Dose MSCT Imaging in Dental Implantology. Open Dent J 2018;12:87–93. https://doi.org/10.2174/1874210601812010087.

[130] Yeung AWK, Jacobs R, Bornstein MM. Novel low-dose protocols using cone beam computed tomography in dental medicine: a review focusing on indications, limitations, and future possibilities. Clin Oral Investig 2019;23:2573–81. https://doi.org/10.1007/s00784-019-02907-y.

[131] McGuigan MB, Duncan HF, Horner K. An analysis of effective dose optimization and its impact on image quality and diagnostic efficacy relating to dental cone beam computed tomography (CBCT). Swiss Dent J 2018;128:297–316.

[132] da Silva Moura W, Chiqueto K, Pithon GM, Neves LS, Castro R, Henriques JFC. Factors influencing the effective dose associated with CBCT: a systematic review. Clin Oral Investig 2019;23:1319–30. https://doi.org/10.1007/s00784-018-2561-4.

[133] Mettler FA, Huda W, Yoshizumi TT, Mahesh M. Effective doses in radiology and diagnostic nuclear medicine: a catalog. Radiology 2008;248:254–63. https://doi.org/10.1148/radiol.2481071451.

[134] van der Molen AJ, Schilham A, Stoop P, Prokop M, Geleijns J. A national survey on radiation dose in CT in The Netherlands. Insights Imaging 2013;4:383–90. https://doi.org/10.1007/s13244-013-0253-9.

[135] Endo M, Tsunoo T, Nakamori N, Yoshida K. Effect of scattered radiation on image noise in cone beam CT. Med Phys 2001;28:469–74. https://doi.org/10.1118/1.1357457.

[136] Schulze R, Heil U, Groβ D, Bruellmann D, Dranischnikow E, Schwanecke U, et al. Artefacts in CBCT: a review. Dentomaxillofac Radiol 2011;40:265–73. https://doi.org/10.1259/dmfr/30642039.

[137] Yu L, Pan X, Pelizzari CA. Image reconstruction with a shift-variant filtration in circular cone-beam CT. International Journal of Imaging Systems and Technology 2004;14:213–21. https://doi.org/10.1002/ima.20026.

[138] Feldkamp L, Davis LC, Kress J. Practical Cone-Beam Algorithm. J Opt Soc Am 1984;1:612–9.

[139] Sharp GC, Kandasamy N, Singh H, Folkert M. GPU-based streaming architectures for fast cone-beam CT image reconstruction and demons deformable registration. Phys Med Biol 2007;52:5771–83. https://doi.org/10.1088/0031-9155/52/19/003.

[140] Siltanen S, Kolehmainen V, Järvenpää S, Kaipio JP, Koistinen P, Lassas M, et al. Statistical inversion for medical x-ray tomography with few radiographs: I. General theory. Phys Med Biol 2003;48:1437–63. https://doi.org/10.1088/0031-9155/48/10/314.

[141] Strid KG. Significance of quantum fluctuations in roentgen imaging. Acta Radiol Oncol 1980;19:129–38. https://doi.org/10.3109/02841868009130144.

[142] Altunbas MC, Shaw CC, Chen L, Lai C, Liu X, Han T, et al. A post-reconstruction method to correct cupping artifacts in cone beam breast computed tomography. Med Phys 2007;34:3109–18. https://doi.org/10.1118/1.2748106.

[143] Tofts PS, Gore JC. Some sources of artefact in computed tomography. Phys Med Biol 1980;25:117–27. https://doi.org/10.1088/0031-9155/25/1/011.

[144] Szabo B, Dobai A, Dobo C. Cone-Beam Computed Tomography in Dentomaxillofacial Radiology, 2020. https://doi.org/10.5772/intechopen.90932.

[145] Prell D, Kyriakou Y, Kalender WA. Comparison of ring artifact correction methods for flat-detector CT. Phys Med Biol 2009;54:3881–95. https://doi.org/10.1088/0031-9155/54/12/018.

[146] Xu F, Mueller K. Accelerating popular tomographic reconstruction algorithms on commodity PC graphics hardware. IEEE Transactions on Nuclear Science 2005;52:654–63. https://doi.org/10.1109/TNS.2005.851398.

[147] Stuehmer C, Essig H, Bormann K-H, Majdani O, Gellrich N-C, Rücker M. Cone beam CT imaging of airgun injuries to the craniomaxillofacial region. Int J Oral Maxillofac Surg 2008;37:903–6. https://doi.org/10.1016/j.ijom.2008.07.007.

[148] Hsieh J, Molthen RC, Dawson CA, Johnson RH. An iterative approach to the beam hardening correction in cone beam CT. Med Phys 2000;27:23–9. https://doi.org/10.1118/1.598853.

[149] Verhamme LM, Meijer GJ, Boumans T, Schutyser F, Bergé SJ, Maal TJJ. A clinically relevant validation method for implant placement after virtual planning. Clin Oral Implants Res 2013;24:1265–72. https://doi.org/10.1111/j.1600-0501.2012.02565.x.

[150] Fakhar HB, Mallahi M, Panjnoush M, Kashani PM. Effect of Voxel Size and Object Location in the Field of View on Detection of Bone Defects in Cone Beam Computed Tomography. J Dent (Tehran) 2016;13:279–86.

[151] Eguren M, Holguin A, Diaz K, Vidalon J, Linan C, Pacheco-Pereira C, et al. Can gray values be converted to Hounsfield units? A systematic review. Dentomaxillofac Radiol 2022;51:20210140. https://doi.org/10.1259/dmfr.20210140.

[152] Scarfe WC, Farman AG. What is cone-beam CT and how does it work? Dent Clin North Am 2008;52:707–30, v. https://doi.org/10.1016/j.cden.2008.05.005.

[153] Dusseldorp JK, Stamatakis HC, Ren Y. Soft tissue coverage on the segmentation accuracy of the 3D surface-rendered model from cone-beam CT. Clin Oral Investig 2017;21:921–30. https://doi.org/10.1007/s00784-016-1844-x.

[154] Spin-Neto R, Gotfredsen E, Wenzel A. Impact of voxel size variation on CBCT-based diagnostic outcome in dentistry: a systematic review. J Digit Imaging 2013;26:813–20. https://doi.org/10.1007/s10278-012-9562-7.

[155] Niktash A, Mehralizadeh S, Talaeipour A. The Effect of Different Field of View Sizes on Contrast-to-Noise Ratio of Cone-Beam Computed Tomography Units: An In-Vitro Study. Front Dent 2022;19:32. https://doi.org/10.18502/fid.v19i32.10804.

[156] Palomo JM, Rao PS, Hans MG. Influence of CBCT exposure conditions on radiation dose. Oral Surg Oral Med Oral Pathol Oral Radiol Endod 2008;105:773–82. https://doi.org/10.1016/j.tripleo.2007.12.019.

[157] Davies J, Johnson B, Drage N. Effective doses from cone beam CT investigation of the jaws. Dentomaxillofac Radiol 2012;41:30–6. https://doi.org/10.1259/dmfr/30177908.

[158] Damstra J, Fourie Z, Huddleston Slater JJR, Ren Y. Accuracy of linear measurements from cone-beam computed tomography-derived surface models of different voxel sizes. Am J Orthod Dentofacial Orthop 2010;137:16.e1-6; discussion 16-17. https://doi.org/10.1016/j.ajodo.2009.06.016.

[159] Sun Z, Smith T, Kortam S, Kim D-G, Tee BC, Fields H. Effect of bone thickness on alveolar bone-height measurements from cone-beam computed tomography images. Am J Orthod Dentofacial Orthop 2011;139:e117-127. https://doi.org/10.1016/j.ajodo.2010.08.016.

[160] Patcas R, Müller L, Ullrich O, Peltomäki T. Accuracy of cone-beam computed tomography at different resolutions assessed on the bony covering of the mandibular anterior teeth. Am J Orthod Dentofacial Orthop 2012;141:41–50. https://doi.org/10.1016/j.ajodo.2011.06.034.

[161] Torres MGG, Campos PSF, Segundo NPN, Navarro M, Crusoé-Rebello I. Accuracy of linear measurements in cone beam computed tomography with different voxel sizes. Implant Dent 2012;21:150–5. https://doi.org/10.1097/ID.0b013e31824bf93c.

[162] Tanaka Y, Dutra V, Lin W-S, Levon J, Hamada Y. Evaluation of the accuracy of buccal bone thickness measurement from cone beam computed tomography compared with histologic analysis. J Prosthet Dent 2021:S0022-3913(21)00499-6. https://doi.org/10.1016/j.prosdent.2021.08.026.

[163] Domic D, Bertl K, Ahmad S, Schropp L, Hellén-Halme K, Stavropoulos A. Accuracy of cone-beam computed tomography is limited at implant sites with a thin buccal bone: A laboratory study. J Periodontol 2021;92:592–601. https://doi.org/10.1002/JPER.20-0222.

[164] Vanderstuyft T, Tarce M, Sanaan B, Jacobs R, de Faria Vasconcelos K, Quirynen M. Inaccuracy of buccal bone thickness estimation on cone-beam CT due to implant blooming: An ex-vivo study. J Clin Periodontol 2019;46:1134–43. https://doi.org/10.1111/jcpe.13183.

[165] Cook VC, Timock AM, Crowe JJ, Wang M, Covell DA. Accuracy of alveolar bone measurements from cone beam computed tomography acquired using varying settings. Orthod Craniofac Res 2015;18 Suppl 1:127–36. https://doi.org/10.1111/ocr.12072.

[166] Poeschl PW, Schmidt N, Guevara-Rojas G, Seemann R, Ewers R, Zipko HT, et al. Comparison of cone-beam and conventional multislice computed tomography for image-guided dental implant planning. Clin Oral Investig 2013;17:317–24. https://doi.org/10.1007/s00784-012-0704-6.

[167] Dings JP, Verhamme L, Merkx MA, Xi T, Meijer GJ, Maal TJ. Reliability and accuracy of cone beam computed tomography versus conventional multidetector computed tomography for image-guided craniofacial implant planning: An in vitro study. Int J Oral Maxillofac Implants 2019;34:665–72. https://doi.org/10.11607/jomi.6915.

150

[168] Unger S, Penzenstadler M, Husain AA-H, Wiedemeier D, Stadlinger B, Valdec S. Comparison of Geometric Accuracy of Low-Dose and Standard-Dose Dental CBCT Imaging Protocols in CAD/CAM-Guided Dental Implant Surgery. Int J Oral Maxillofac Implants 2023;38:287–94. https://doi.org/10.11607/jomi.9851.

[169] Horsch L, Labis C, Trebing CT, Kronsteiner D, Hilgenfeld T, Rammelsberg P, et al. Predictability and image quality of low-dose cone-beam computed tomography in computer-guided implantology: An experimental study. J Dent 2021;112:103744. https://doi.org/10.1016/j.jdent.2021.103744.

[170] Tao B, Shen Y, Sun Y, Huang W, Wang F, Wu Y. Comparative accuracy of cone-beam CT and conventional multislice computed tomography for real-time navigation in zygomatic implant surgery. Clin Implant Dent Relat Res 2020;22:747–55. https://doi.org/10.1111/cid.12958.

[171] Schulze RKW, Drage NA. Cone-beam computed tomography and its applications in dental and maxillofacial radiology. Clin Radiol 2020;75:647–57. https://doi.org/10.1016/j.crad.2020.04.006.

[172] Harris D, Horner K, Gröndahl K, Jacobs R, Helmrot E, Benic GI, et al. E.A.O. guidelines for the use of diagnostic imaging in implant dentistry 2011. A consensus workshop organized by the European Association for Osseointegration at the Medical University of Warsaw. Clin Oral Implants Res 2012;23:1243–53. https://doi.org/10.1111/j.1600-0501.2012.02441.x.

[173] Tyndall DA, Price JB, Tetradis S, Ganz SD, Hildebolt C, Scarfe WC, et al. Position statement of the American Academy of Oral and Maxillofacial Radiology on selection criteria for the use of radiology in dental implantology with emphasis on cone beam computed tomography. Oral Surg Oral Med Oral Pathol Oral Radiol 2012;113:817–26. https://doi.org/10.1016/j.oooo.2012.03.005.

[174] Matzen LH, Berkhout E. Cone beam CT imaging of the mandibular third molar: a position paper prepared by the European Academy of DentoMaxilloFacial Radiology (EADMFR). Dentomaxillofac Radiol 2019;48:20190039. https://doi.org/10.1259/dmfr.20190039.

[175] Isaacson K, Thom AR. Orthodontic radiography guidelines. Am J Orthod Dentofacial Orthop 2015;147:295–6. https://doi.org/10.1016/j.ajodo.2014.12.005.

[176] Walter C, Schmidt JC, Dula K, Sculean A. Cone beam computed tomography (CBCT) for diagnosis and treatment planning in periodontology: A systematic review. Quintessence Int 2016;47:25–37. https://doi.org/10.3290/j.qi.a34724.

[177] Mandelaris GA, Scheyer ET, Evans M, Kim D, McAllister B, Nevins ML, et al. American Academy of Periodontology Best Evidence Consensus Statement on Selected Oral Applications for Cone-Beam Computed Tomography. J Periodontol 2017;88:939–45. https://doi.org/10.1902/jop.2017.170234.

[178] Leonardi Dutra K, Haas L, Porporatti AL, Flores-Mir C, Nascimento Santos J, Mezzomo LA, et al. Diagnostic Accuracy of Cone-beam Computed Tomography and Conventional Radiography on Apical Periodontitis: A Systematic Review and Meta-analysis. J Endod 2016;42:356–64. https://doi.org/10.1016/j.joen.2015.12.015.

[179] Hilmi A, Patel S, Mirza K, Galicia JC. Efficacy of imaging techniques for the diagnosis of apical periodontitis: A systematic review. Int Endod J 2023. https://doi.org/10.1111/iej.13921.

[180] Baena-de la Iglesia T, Yañez-Vico RM, Iglesias-Linares A. DIAGNOSTIC PERFORMANCE OF CONE-BEAM COMPUTED TOMOGRAPHY TO DIAGNOSE IN VIVO/IN VITRO ROOT RESORPTION: A SYSTEMATIC REVIEW AND META-ANALYSIS. J Evid Based Dent Pract 2023;23:101803. https://doi.org/10.1016/j.jebdp.2022.101803.

[181] Habibzadeh S, Ghoncheh Z, Kabiri P, Mosaddad SA. Diagnostic efficacy of cone-beam computed tomography for detection of vertical root fractures in endodontically treated teeth: a systematic review. BMC Med Imaging 2023;23:68. https://doi.org/10.1186/s12880-023-01024-3.

[182] Special Committee to Revise the Joint AAE/AAOMR Position Statement on use of CBCT in Endodontics. AAE and AAOMR Joint Position Statement: Use of Cone Beam Computed Tomography in Endodontics 2015 Update. Oral Surg Oral Med Oral Pathol Oral Radiol 2015;120:508–12. https://doi.org/10.1016/j.oooo.2015.07.033.

[183] Patel S, Brown J, Semper M, Abella F, Mannocci F. European Society of Endodontology position statement: Use of cone beam computed tomography in Endodontics: European Society of Endodontology (ESE) developed by. Int Endod J 2019;52:1675–8. https://doi.org/10.1111/iej.13187.

[184] Kullman L, Al Sane M. Guidelines for dental radiography immediately after a dento-alveolar trauma, a systematic literature review. Dent Traumatol 2012;28:193–9. https://doi.org/10.1111/j.1600-9657.2011.01099.x.

[185] Fakhran S, Alhilali L, Sreedher G, Dohatcu AC, Lee S, Ferguson B, et al. Comparison of simulated cone beam computed tomography to conventional helical computed tomography for imaging of rhinosinusitis. Laryngoscope 2014;124:2002–6. https://doi.org/10.1002/lary.24603.

[186] Flügge T, Ludwig U, Hövener J-B, Kohal R, Wismeijer D, Nelson K. Virtual implant planning and fully guided implant surgery using magnetic resonance imaging-Proof of principle. Clin Oral Implants Res 2020;31:575–83. https://doi.org/10.1111/clr.13592.

[187] Reda R, Zanza A, Mazzoni A, Cicconetti A, Testarelli L, Di Nardo D. An Update of the Possible Applications of Magnetic Resonance Imaging (MRI) in Dentistry: A Literature Review. J Imaging 2021;7:75. https://doi.org/10.3390/jimaging7050075.

[188] Hilgenfeld T, Juerchott A, Jende JME, Rammelsberg P, Heiland S, Bendszus M, et al. Use of dental MRI for radiation-free guided dental implant planning: a prospective, in vivo study of accuracy and reliability. Eur Radiol 2020;30:6392–401. https://doi.org/10.1007/s00330-020-07262-1.

[189] de Carvalho E Silva Fuglsig JM, Wenzel A, Hansen B, Lund TE, Spin-Neto R. Magnetic Resonance Imaging for the Planning, Execution, and Follow-up of Implant-Based Oral Rehabilitation: Systematic Review. Int J Oral Maxillofac Implants 2021;36:432–41. https://doi.org/10.11607/jomi.8536.

[190] Mörmann WH. The evolution of the CEREC system. J Am Dent Assoc 2006;137 Suppl:7S-13S. https://doi.org/10.14219/jada.archive.2006.0398.

[191] Chen LC, Xu ZQ. Innovative 3D Dental Measurement for Tooth Model Restoration. Key Engineering Materials 2005;295–296:145–50. https://doi.org/10.4028/www.scientific.net/KEM.295-296.145.

[192] Duret F. [Toward a new symbolism in the fabrication of prosthetic design]. Cah Prothese 1985;13:65–71.

[193] Alghazzawi TF. Advancements in CAD/CAM technology: Options for practical implementation. J Prosthodont Res 2016;60:72–84. https://doi.org/10.1016/j.jpor.2016.01.003.

[194] Zimmermann M, Mehl A, Mörmann WH, Reich S. Intraoral scanning systems - a current overview. Int J Comput Dent 2015;18:101–29.

[195] Kravitz N, Groth C, Jones P, Graham J, Redmond W. Intraoral digital scanners. Journal of Clinical Orthodontics : JCO 2014;48:337–47.

[196] Richert R, Goujat A, Venet L, Viguie G, Viennot S, Robinson P, et al. Intraoral Scanner Technologies: A Review to Make a Successful Impression. J Healthc Eng 2017;2017:8427595. https://doi.org/10.1155/2017/8427595.

[197] Anh J-W, Park J-M, Chun Y-S, Kim M, Kim M. A comparison of the precision of three-dimensional images acquired by 2 digital intraoral scanners: effects of tooth irregularity and scanning direction. Korean J Orthod 2016;46:3–12. https://doi.org/10.4041/kjod.2016.46.1.3.

[198] Schmitt JM. Optical coherence tomography (OCT): a review. IEEE Journal of Selected Topics in Quantum Electronics 1999;5:1205–15. https://doi.org/10.1109/2944.796348.

[199] Bloss R. Accordion fringe interferometry: a revolutionary new digital shape-scanning technology. Sensor Review - SENS REV 2008;28:22–6. https://doi.org/10.1108/02602280810849983.

[200] Logozzo S, Zanetti EM, Franceschini G, Kilpelä A, Mäkynen A. Recent advances in dental optics – Part I: 3D intraoral scanners for restorative dentistry. Optics and Lasers in Engineering 2014;54:203–21. https://doi.org/10.1016/j.optlaseng.2013.07.017.

[201] Giuliodori G, Rappelli G, Aquilanti L. Intraoral Scans of Full Dental Arches: An In Vitro Measurement Study of the Accuracy of Different Intraoral Scanners. International Journal of Environmental Research and Public Health 2023;20:4776. https://doi.org/10.3390/ijerph20064776.

[202] Kachhara S, Nallaswamy D, Ganapathy DM, Sivaswamy V, Rajaraman V. Assessment of intraoral scanning technology for multiple implant impressions - A systematic review and meta-analysis. J Indian Prosthodont Soc 2020;20:141–52. https://doi.org/10.4103/jips.jips_379_19.

[203] Joda T, Derksen W, Wittneben JG, Kuehl S. Static computer-aided implant surgery (s-CAIS) analysing patient-reported outcome measures (PROMs), economics and surgical complications: A systematic review. Clinical Oral Implants Research 2018;29:359–73. https://doi.org/10.1111/clr.13136.

[204] Burhardt L, Livas C, Kerdijk W, van der Meer WJ, Ren Y. Treatment comfort, time perception, and preference for conventional and digital impression techniques: A comparative study in young patients. Am J Orthod Dentofacial Orthop 2016;150:261–7. https://doi.org/10.1016/j.ajodo.2015.12.027.

[205] Hong-Seok P, Chintal S. Development of High Speed and High Accuracy 3D Dental Intra Oral Scanner. Procedia Engineering 2015;100:1174–81. https://doi.org/10.1016/j.proeng.2015.01.481.

[206] Aubreton O, Bajard A, Verney B, Truchetet F. Infrared system for 3D scanning of metallic surfaces. Machine Vision and Applications 2013;24:1513–24. https://doi.org/10.1007/s00138-013-0487-z.

[207] Jurrens KK. Standards for the rapid prototyping industry. Rapid Prototyping Journal 1999;5:169–78. https://doi.org/10.1108/13552549910295514.

[208] Szilvśi-Nagy M, Mátyási Gy. Analysis of STL files. Mathematical and Computer Modelling 2003;38:945–60. https://doi.org/10.1016/S0895-7177(03)90079-3.

[209] Cevidanes LHS, Ruellas ACO, Jomier J, Nguyen T, Pieper S, Budin F, et al. Incorporating 3-dimensional models in online articles. Am J Orthod Dentofacial Orthop 2015;147:S195-204. https://doi.org/10.1016/j.ajodo.2015.02.002.

[210] Yuzbasioglu E, Kurt H, Turunc R, Bilir H. Comparison of digital and conventional impression techniques: evaluation of patients' perception, treatment comfort, effectiveness and clinical outcomes. BMC Oral Health 2014;14:10. https://doi.org/10.1186/1472-6831-14-10.

[211] Kim J, Park J-M, Kim M, Heo S-J, Shin IH, Kim M. Comparison of experience curves between two 3-dimensional intraoral scanners. J Prosthet Dent 2016;116:221–30. https://doi.org/10.1016/j.prosdent.2015.12.018.

[212] Müller P, Ender A, Joda T, Katsoulis J. Impact of digital intraoral scan strategies on the impression accuracy using the TRIOS Pod scanner. Quintessence Int 2016;47:343–9. https://doi.org/10.3290/j.qi.a35524.

[213] Mao Z, Park K, Lee K, Li X. Robust surface reconstruction of teeth from raw pointsets. Int J Numer Method Biomed Eng 2014;30:382–96. https://doi.org/10.1002/cnm.2608.

[214] Lim J-H, Mangal U, Nam N-E, Choi S-H, Shim J-S, Kim J-E. A Comparison of Accuracy of Different Dental Restorative Materials between Intraoral Scanning and Conventional Impression-Taking: An In Vitro Study. Materials (Basel) 2021;14:2060. https://doi.org/10.3390/ma14082060.

[215] Burgner J, Simpson AL, Fitzpatrick JM, Lathrop RA, Herrell SD, Miga MI, et al. A study on the theoretical and practical accuracy of conoscopic holography-based surface measurements: toward image registration in minimally invasive surgery. Int J Med Robot 2013;9:190–203. https://doi.org/10.1002/rcs.1446.

[216] Patzelt SBM, Lamprinos C, Stampf S, Att W. The time efficiency of intraoral scanners: an in vitro comparative study. J Am Dent Assoc 2014;145:542–51. https://doi.org/10.14219/jada.2014.23.

[217] Revilla-León M, Jiang P, Sadeghpour M, Piedra-Cascón W, Zandinejad A, Özcan M, et al. Intraoral digital scans: Part 2-influence of ambient scanning light conditions on the mesh quality of different intraoral scanners. J Prosthet Dent 2020;124:575–80. https://doi.org/10.1016/j.prosdent.2019.06.004.

[218] Revilla-León M, Subramanian SG, Özcan M, Krishnamurthy VR. Clinical Study of the Influence of Ambient Lighting Conditions on the Mesh Quality of an Intraoral Scanner. J Prosthodont 2020;29:651–5. https://doi.org/10.1111/jopr.13205.

[219] Mangano F, Gandolfi A, Luongo G, Logozzo S. Intraoral scanners in dentistry: a review of the current literature. BMC Oral Health 2017;17:149. https://doi.org/10.1186/s12903-017-0442-x.

[220] Imburgia M, Logozzo S, Hauschild U, Veronesi G, Mangano C, Mangano FG. Accuracy of four intraoral scanners in oral implantology: a comparative in vitro study. BMC Oral Health 2017;17:92. https://doi.org/10.1186/s12903-017-0383-4.

[221] Menditto A, Patriarca M, Magnusson B. Understanding the meaning of accuracy, trueness and precision. Accred Qual Assur 2007;12:45–7. https://doi.org/10.1007/s00769-006-0191-z.

[222] Floriani F, Lopes GC, Cabrera A, Duarte W, Zoidis P, Oliveira D, et al. Linear Accuracy of Intraoral Scanners for Full-Arch Impressions of Implant-Supported Prostheses: A Systematic Review and Meta-Analysis. Eur J Dent 2023. https://doi.org/10.1055/s-0042-1758798.

[223] Schmidt A, Wöstmann B, Schlenz MA. Accuracy of digital implant impressions in clinical studies: A systematic review. Clin Oral Implants Res 2022;33:573–85. https://doi.org/10.1111/clr.13951.

[224] Carneiro Pereira AL, Souza Curinga MR, Melo Segundo HV, da Fonte Porto Carreiro A. Factors that influence the accuracy of intraoral scanning of total edentulous arches rehabilitated with multiple implants: A systematic review. J Prosthet Dent 2023;129:855–62. https://doi.org/10.1016/j.prosdent.2021.09.001.

[225] Revilla-León M, Quesada-Olmo N, Gómez-Polo M, Sicilia E, Farjas-Abadia M, Kois JC. Influence of rescanning mesh holes on the accuracy of an intraoral scanner: An in vivo study. J Dent 2021;115:103851. https://doi.org/10.1016/j.jdent.2021.103851.

[226] Ali IE, Hattori M, Sumita YI, Wakabayashi N. Effect of cut-out rescan procedures on the accuracy of an intraoral scanner used for digitizing an ear model: An in vitro study. J Prosthodont 2022. https://doi.org/10.1111/jopr.13591.

[227] Runkel C, Güth J-F, Erdelt K, Keul C. Digital impressions in dentistry—accuracy of impression digitalisation by desktop scanners. Clin Oral Invest 2020;24:1249–57. https://doi.org/10.1007/s00784-019-02995-w.

[228] Kang B, Son K, Lee K. Accuracy of Five Intraoral Scanners and Two Laboratory Scanners for a Complete Arch: A Comparative In Vitro Study. Applied Sciences 2020;10:74. https://doi.org/10.3390/app10010074.

[229] Alalwan R, Alessa R, Alghurairi N, Alaqail H, Awawdeh M, Masuadi E. Accuracy, Precision, and Efficiency of Three-Dimensional (3D) Dental

Lab Scanners: A Comparative Study of Two Systems. The Open Dentistry Journal 2022;16. https://doi.org/10.2174/18742106-v16-e221020-2022-33.

[230] Borbola D, Berkei G, Simon B, Romanszky L, Sersli G, DeFee M, et al. In vitro comparison of five desktop scanners and an industrial scanner in the evaluation of an intraoral scanner accuracy. Journal of Dentistry 2023;129:104391. https://doi.org/10.1016/j.jdent.2022.104391.

[231] Kiatkroekkrai P, Takolpuckdee C, Subbalekha K, Mattheos N, Pimkhaokham A. Accuracy of implant position when placed using static computer-assisted implant surgical guides manufactured with two different optical scanning techniques: a randomized clinical trial. Int J Oral Maxillofac Surg 2020;49:377–83. https://doi.org/10.1016/j.ijom.2019.08.019.

[232] Emara A, Sharma N, Halbeisen FS, Msallem B, Thieringer FM. Comparative Evaluation of Digitization of Diagnostic Dental Cast (Plaster) Models Using Different Scanning Technologies. Dent J (Basel) 2020;8:79. https://doi.org/10.3390/dj8030079.

[233] Becker K, Schmücker U, Schwarz F, Drescher D. Accuracy and eligibility of CBCT to digitize dental plaster casts. Clin Oral Investig 2018;22:1817–23. https://doi.org/10.1007/s00784-017-2277-x.

[234] Cristache CM, Burlibasa M, Tudor I, Totu EE, Di Francesco F, Moraru L. Accuracy, Labor-Time and Patient-Reported Outcomes with Partially versus Fully Digital Workflow for Flapless Guided Dental Implants Insertion-A Randomized Clinical Trial with One-Year Follow-Up. J Clin Med 2021;10:1102. https://doi.org/10.3390/jcm10051102.

[235] Kakehbaraei S, Seyedarabi H, Zenouz AT. Dental Segmentation in Cone-beam Computed Tomography Images Using Watershed and Morphology Operators. J Med Signals Sens 2018;8:119–24.

[236] Momeni M, Aghaeizadeh Zoroofi R. Automated dental recognition by wavelet descriptors in CT multi-slices data. Int J CARS 2008;3:533–42. https://doi.org/10.1007/s11548-008-0255-0.

[237] H A, Zoroofi R, Shirani G. Rapid Automatic Segmentation and Visualization of Teeth in CT-Scan Data. Journal of Applied Sciences 2009;9. https://doi.org/10.3923/jas.2009.2031.2044.

[238] Cui Z, Fang Y, Mei L, Zhang B, Yu B, Liu J, et al. A fully automatic AI system for tooth and alveolar bone segmentation from cone-beam CT images. Nat Commun 2022;13:2096. https://doi.org/10.1038/s41467-022-29637-2.

[239] Shaheen E, Leite A, Alqahtani KA, Smolders A, Van Gerven A, Willems H, et al. A novel deep learning system for multi-class tooth segmentation

and classification on cone beam computed tomography. A validation study. J Dent 2021;115:103865. https://doi.org/10.1016/j.jdent.2021.103865.

[240] Polizzi A, Quinzi V, Ronsivalle V, Venezia P, Santonocito S, Lo Giudice A, et al. Tooth automatic segmentation from CBCT images: a systematic review. Clin Oral Investig 2023. https://doi.org/10.1007/s00784-023-05048-5.

[241] Pieralli S, Beyer C, Wesemann C, Vach K, Russe MF, Kernen F, et al. Impact of radiographic field-of-view volume on alignment accuracy during virtual implant planning: A noninterventional retrospective pilot study. Clin Oral Implants Res 2022;33:1021–9. https://doi.org/10.1111/clr.13983.

[242] Hamilton A, Jamjoom F, Doliveux S, Gallucci GO, Friedland B. Radiographic markers for merging virtual data sets. The Journal of Prosthetic Dentistry 2019;122:5–9. https://doi.org/10.1016/j.prosdent.2018.08.007.

[243] Jang T, Yun HS, Kim J-E, Lee S-H, Seo JK. Fully automatic integration of dental CBCT images and full-arch intraoral impressions with stitching error correction via individual tooth segmentation and identification. ArXiv 2021.

[244] Gateno J, Xia J, Teichgraeber JF, Rosen A. A new technique for the creation of a computerized composite skull model. J Oral Maxillofac Surg 2003;61:222–7. https://doi.org/10.1053/joms.2003.50033.

[245] Uechi J, Okayama M, Shibata T, Muguruma T, Hayashi K, Endo K, et al. A novel method for the 3-dimensional simulation of orthognathic surgery by using a multimodal image-fusion technique. Am J Orthod Dentofacial Orthop 2006;130:786–98. https://doi.org/10.1016/j.ajodo.2006.03.025.

[246] Kim BC, Lee CE, Park W, Kang SH, Zhengguo P, Yi CK, et al. Integration accuracy of digital dental models and 3-dimensional computerized tomography images by sequential point- and surface-based markerless registration. Oral Surg Oral Med Oral Pathol Oral Radiol Endod 2010;110:370–8. https://doi.org/10.1016/j.tripleo.2010.03.036.

[247] Lin H-H, Chiang W-C, Lo L-J, Sheng-Pin Hsu S, Wang C-H, Wan S-Y. Artifact-resistant superimposition of digital dental models and cone-beam computed tomography images. J Oral Maxillofac Surg 2013;71:1933–47. https://doi.org/10.1016/j.joms.2013.06.199.

[248] Hernández-Alfaro F, Guijarro-Martínez R. New protocol for three-dimensional surgical planning and CAD/CAM splint generation in orthognathic surgery: an in vitro and in vivo study. Int J Oral Maxillofac Surg 2013;42:1547–56. https://doi.org/10.1016/j.ijom.2013.03.025.

[249] Besl P, McKay HD. A method for registration of 3-D shapes. IEEE Trans Pattern Anal Mach Intell. Pattern Analysis and Machine Intelligence, IEEE Transactions On 1992;14:239–56. https://doi.org/10.1109/34.121791.

[250] Becker K, Wilmes B, Grandjean C, Drescher D. Impact of manual control point selection accuracy on automated surface matching of digital dental models. Clin Oral Investig 2018;22:801–10. https://doi.org/10.1007/s00784-017-2155-6.

[251] Flügge T, Derksen W, te Poel J, Hassan B, Nelson K, Wismeijer D. Registration of cone beam computed tomography data and intraoral surface scans – A prerequisite for guided implant surgery with CAD/CAM drilling guides. Clin Oral Implants Res 2017;28:1113–8. https://doi.org/10.1111/clr.12925.

[252] Alaidrous M, Finkelman M, Kudara Y, Campos HC, Kim Y, De Souza AB. Influence of zirconia crown artifacts on cone beam computed tomography scans and image superimposition of tomographic image and tooth surface scan: An in vitro study. The Journal of Prosthetic Dentistry 2021;125:684.e1-684.e8. https://doi.org/10.1016/j.prosdent.2020.06.028.

[253] Piao X-Y, Park J-M, Kim H, Kim Y, Shim J-S. Evaluation of different registration methods and dental restorations on the registration duration and accuracy of cone beam computed tomography data and intraoral scans: a retrospective clinical study. Clin Oral Investig 2022;26:5763–71. https://doi.org/10.1007/s00784-022-04533-7.

[254] Wu Q, Wu J, Tan Y, Sun J, Yu H. A chairside digital radiographic guide for registering digital casts to cone beam computed tomography scans with strong metallic artifacts. The Journal of Prosthetic Dentistry 2023. https://doi.org/10.1016/j.prosdent.2022.11.025.

[255] Yang W-M, Ho C-T, Lo L-J. Automatic Superimposition of Palatal Fiducial Markers for Accurate Integration of Digital Dental Model and Cone Beam Computed Tomography. Journal of Oral and Maxillofacial Surgery 2015;73:1616.e1-1616.e10. https://doi.org/10.1016/j.joms.2015.04.004.

[256] Lin X, Chen T, Liu J, Jiang T, Yu D, Shen SGF. Point-based superimposition of a digital dental model on to a three-dimensional computed tomographic skull: an accuracy study in vitro. Br J Oral Maxillofac Surg 2015;53:28–33. https://doi.org/10.1016/j.bjoms.2014.09.007.

[257] Zou B, Kim J-H, Kim S-H, Choi T-H, Shin Y, Kook Y-A, et al. Accuracy of a surface-based fusion method when integrating digital models and the cone beam computed tomography scans with metal artifacts. Sci Rep 2022;12:8034. https://doi.org/10.1038/s41598-022-11677-9.

[258] Han Y-T, Lin W-C, Fan F-Y, Chen C-L, Lin C-C, Cheng H-C. Comparison of Dental Surface Image Registration and Fiducial Marker Registration: An In Vivo Accuracy Study of Static Computer-Assisted Implant Surgery. J Clin Med 2021;10:4183. https://doi.org/10.3390/jcm10184183.

[259] Chung M, Lee J, Song W, Song Y, Yang I-H, Lee J, et al. Automatic Registration Between Dental Cone-Beam CT and Scanned Surface via Deep Pose Regression Neural Networks and Clustered Similarities. IEEE Transactions on Medical Imaging 2020;39:3900–9. https://doi.org/10.1109/TMI.2020.3007520.

[260] Nabha W, Hong Y-M, Cho J-H, Hwang H-S. Assessment of metal artifacts in three-dimensional dental surface models derived by cone-beam computed tomography. Korean J Orthod 2014;44:229–35. https://doi.org/10.4041/kjod.2014.44.5.229.

[261] Hassan B, Couto Souza P, Jacobs R, de Azambuja Berti S, van der Stelt P. Influence of scanning and reconstruction parameters on quality of three-dimensional surface models of the dental arches from cone beam computed tomography. Clin Oral Invest 2010;14:303–10. https://doi.org/10.1007/s00784-009-0291-3.

[262] Hilgenfeld T, Juerchott A, Deisenhofer UK, Weber D, Rues S, Rammelsberg P, et al. In vivo accuracy of tooth surface reconstruction based on CBCT and dental MRI-A clinical pilot study. Clin Oral Implants Res 2019;30:920–7. https://doi.org/10.1111/clr.13498.

[263] Nada RM, Maal TJJ, Breuning KH, Bergé SJ, Mostafa YA, Kuijpers-Jagtman AM. Accuracy and reproducibility of voxel based superimposition of cone beam computed tomography models on the anterior cranial base and the zygomatic arches. PLoS One 2011;6:e16520. https://doi.org/10.1371/journal.pone.0016520.

[264] Egbert N, Cagna DR, Ahuja S, Wicks RA. Accuracy and reliability of stitched cone-beam computed tomography images. Imaging Sci Dent 2015;45:41–7. https://doi.org/10.5624/isd.2015.45.1.41.

[265] Komuro A, Yamada Y, Uesugi S, Terashima H, Kimura M, Kishimoto H, et al. Accuracy and dimensional reproducibility by model scanning, intraoral scanning, and CBCT imaging for digital implant dentistry. Int J Implant Dent 2021;7:63. https://doi.org/10.1186/s40729-021-00343-w.

[266] D'haese J, Ackhurst J, Wismeijer D, De Bruyn H, Tahmaseb A. Current state of the art of computer-guided implant surgery. Periodontology 2000 2017;73:121–33. https://doi.org/10.1111/prd.12175.

[267] Flügge T, Kramer J, Nelson K, Nahles S, Kernen F. Digital implantology—a review of virtual planning software for guided implant surgery. Part II: Prosthetic set-up and virtual implant planning. BMC Oral Health 2022;22:23. https://doi.org/10.1186/s12903-022-02057-w.

[268] Basten CH. The use of radiopaque templates for predictable implant placement. Quintessence Int 1995;26:609–12.

[269] Ganz SD. Restoratively driven implant dentistry utilizing advanced software and CBCT: realistic abutments and virtual teeth. Dent Today 2008;27:122, 124, 126–7.

[270] Abrera-Crum L, D'Affronte LC, Platia CL, Yimer LK. Challenges in the workflow of a digital diagnostic wax-up: a case report. Gen Dent 2020;68:56–60.

[271] Flügge TV, Nelson K, Schmelzeisen R, Metzger MC. Three-dimensional plotting and printing of an implant drilling guide: simplifying guided implant surgery. J Oral Maxillofac Surg 2013;71:1340–6. https://doi.org/10.1016/j.joms.2013.04.010.

[272] Mehl A, Blanz V, Hickel R. Biogeneric tooth: a new mathematical representation for tooth morphology in lower first molars. Eur J Oral Sci 2005;113:333–40. https://doi.org/10.1111/j.1600-0722.2005.00224.x.

[273] Wang F, Tang Q, Xi S, Liu R, Niu L. Comparison and evaluation of the morphology of crowns generated by biogeneric design technique with CEREC chairside system. PLoS One 2020;15:e0227050. https://doi.org/10.1371/journal.pone.0227050.

[274] Zimmermann M, Mehl A. Virtual smile design systems: a current review. Int J Comput Dent 2015;18:303–17.

[275] Lin W-S, Harris BT, Phasuk K, Llop DR, Morton D. Integrating a facial scan, virtual smile design, and 3D virtual patient for treatment with CAD-CAM ceramic veneers: A clinical report. The Journal of Prosthetic Dentistry 2018;119:200–5. https://doi.org/10.1016/j.prosdent.2017.03.007.

[276] Coachman C, Georg R, Bohner L, Rigo LC, Sesma N. Chairside 3D digital design and trial restoration workflow. The Journal of Prosthetic Dentistry 2020;124:514–20. https://doi.org/10.1016/j.prosdent.2019.10.015.

[277] Nuytens P, Li J, Lepidi L. Face oriented digital workflow for transferring intraoral and extraoral data of edentulous arch rehabilitated with multiple implants: A clinical technique. The Journal of Prosthetic Dentistry 2023. https://doi.org/10.1016/j.prosdent.2023.02.023.

[278] Koralakunte PR, Aljanakh M. The role of virtual articulator in prosthetic and restorative dentistry. J Clin Diagn Res 2014;8:ZE25-28. https://doi.org/10.7860/JCDR/2014/8929.4648.

[279] Lepidi L, Galli M, Mastrangelo F, Venezia P, Joda T, Wang H-L, et al. Virtual Articulators and Virtual Mounting Procedures: Where Do We Stand? J Prosthodont 2021;30:24–35. https://doi.org/10.1111/jopr.13240.

[280] Hsu MR, Driscoll CF, Romberg E, Masri R. Accuracy of Dynamic Virtual Articulation: Trueness and Precision. J Prosthodont 2019;28:436–43. https://doi.org/10.1111/jopr.13035.

[281] Stevens M, Frazier K. Preoperative implant evaluation and virtual treatment planning. Clinical Dentistry Reviewed 2021;5. https://doi.org/10.1007/s41894-021-00110-5.

[282] Greenstein G, Tarnow D. The mental foramen and nerve: clinical and anatomical factors related to dental implant placement: a literature review. J Periodontol 2006;77:1933–43. https://doi.org/10.1902/jop.2006.060197.

[283] Scolozzi P, Michelini F, Crottaz C, Perez A. Computer-Aided Design and Computer-Aided Modeling (CAD/CAM) for Guiding Dental Implant Surgery: Personal Reflection Based on 10 Years of Real-Life Experience. J Pers Med 2023;13:129. https://doi.org/10.3390/jpm13010129.

[284] Mora MA, Chenin DL, Arce RM. Software Tools and Surgical Guides in Dental-Implant-Guided Surgery. Dental Clinics 2014;58:597–626. https://doi.org/10.1016/j.cden.2014.04.001.

[285] Jung RE, Schneider D, Ganeles J, Wismeijer D, Zwahlen M, Hämmerle CHF, et al. Computer technology applications in surgical implant dentistry: a systematic review. Int J Oral Maxillofac Implants 2009;24 Suppl:92–109.

[286] Walker-Finch K, Ucer C. Five-year survival rates for implants placed using digitally-designed static surgical guides: a systematic review. Br J Oral Maxillofac Surg 2020;58:268–76. https://doi.org/10.1016/j.bjoms.2019.12.007.

[287] Bover-Ramos F, Viña-Almunia J, Cervera-Ballester J, Peñarrocha-Diago M, García-Mira B. Accuracy of Implant Placement with Computer-Guided Surgery: A Systematic Review and Meta-Analysis Comparing Cadaver, Clinical, and In Vitro Studies. Int J Oral Maxillofac Implants 2018;33:101–15. https://doi.org/10.11607/jomi.5556.

[288] Sancho-Puchades M, Alfaro FH, Naenni N, Jung R, Hämmerle C, Schneider D. A Randomized Controlled Clinical Trial Comparing Conventional And Computer-Assisted Implant Planning and Placement in Partially Edentulous Patients. Part 2: Patient Related Outcome Measures. Int J

Periodontics Restorative Dent 2019;39:e99–110. https://doi.org/10.11607/prd.4145.

[289] Gargallo-Albiol J, Barootchi S, Marqués-Guasch J, Wang H-L. Fully Guided Versus Half-Guided and Freehand Implant Placement: Systematic Review and Meta-analysis. Int J Oral Maxillofac Implants 2020;35:1159–69. https://doi.org/10.11607/jomi.7942.

[290] Gargallo-Albiol J, Barootchi S, Salomó-Coll O, Wang H. Advantages and disadvantages of implant navigation surgery. A systematic review. Annals of Anatomy - Anatomischer Anzeiger 2019;225:1–10. https://doi.org/10.1016/j.aanat.2019.04.005.

[291] Hinckfuss S, Conrad HJ, Lin L, Lunos S, Seong W-J. Effect of surgical guide design and surgeon's experience on the accuracy of implant placement. J Oral Implantol 2012;38:311–23. https://doi.org/10.1563/AAID-JOI-D-10-00046.

[292] Sittikornpaiboon P, Arunjaroensuk S, Kaboosaya B, Subbalekha K, Mattheos N, Pimkhaokham A. Comparison of the accuracy of implant placement using different drilling systems for static computer-assisted implant surgery: A simulation-based experimental study. Clin Implant Dent Relat Res 2021;23:635–43. https://doi.org/10.1111/cid.13032.

[293] Zivanovic S, Popovic M, Nikola V, Pjevic M, Slavković N. An Overview of Rapid Prototyping Technologies using Subtractive, Additive and Formative Processes. FME Transactions 2020;48:246–53. https://doi.org/10.5937/fmet2001246Z.

[294] Ritter L, Palmer J, Bindl A, Irsen S, Cizek J, Karapetian V-E, et al. Accuracy of chairside-milled CAD/CAM drill guides for dental implants. Int J Comput Dent 2014;17:115–24.

[295] Anadioti E, Kane B, Zhang Y, Bergler M, Mante F, Blatz MB. Accuracy of Dental and Industrial 3D Printers. J Prosthodont 2022;31:30–7. https://doi.org/10.1111/jopr.13470.

[296] Henprasert P, Dawson DV, El-Kerdani T, Song X, Couso-Queiruga E, Holloway JA. Comparison of the Accuracy of Implant Position Using Surgical Guides Fabricated by Additive and Subtractive Techniques. Journal of Prosthodontics 2020;29:534–41. https://doi.org/10.1111/jopr.13161.

[297] Stavropoulos P, Foteinopoulos P. Modelling of additive manufacturing processes: a review and classification. Manufacturing Rev 2018;5:2. https://doi.org/10.1051/mfreview/2017014.

[298] Rouzé l'Alzit F, Cade R, Naveau A, Babilotte J, Meglioli M, Catros S. Accuracy of commercial 3D printers for the fabrication of surgical guides

163

in dental implantology. Journal of Dentistry 2022;117:103909. https://doi.org/10.1016/j.jdent.2021.103909.

[299] Yeager B, Çakmak G, Zheng F, Johnston WM, Yilmaz B. Error analysis of stages involved in CBCT-guided implant placement with surgical guides when different printing technologies are used. J Prosthet Dent 2023:S0022-3913(22)00744-2. https://doi.org/10.1016/j.prosdent.2022.11.018.

[300] Bencharit S, Staffen A, Yeung M, Whitley D, Laskin DM, Deeb GR. In Vivo Tooth-Supported Implant Surgical Guides Fabricated With Desktop Stereolithographic Printers: Fully Guided Surgery Is More Accurate Than Partially Guided Surgery. J Oral Maxillofac Surg 2018;76:1431–9. https://doi.org/10.1016/j.joms.2018.02.010.

[301] Rothlauf S, Pieralli S, Wesemann C, Burkhardt F, Vach K, Kernen F, et al. Influence of planning software and template design on the accuracy of static computer assisted implant surgery performed using guides fabricated with material extrusion technology: An in vitro study. Journal of Dentistry 2023;132:104482. https://doi.org/10.1016/j.jdent.2023.104482.

[302] Kim GD, Oh YT. A benchmark study on rapid prototyping processes and machines: Quantitative comparisons of mechanical properties, accuracy, roughness, speed, and material cost. Proceedings of the Institution of Mechanical Engineers, Part B: Journal of Engineering Manufacture 2008;222:201–15. https://doi.org/10.1243/09544054JEM724.

[303] Panjnoush M, Kheirandish Y, Sharifi R, Mirjalili F. Effect of slice thickness of 3D printer in fabrication of surgical guide on the accuracy of dental implant placement. J Oral Implantol 2023. https://doi.org/10.1563/aaid-joi-D-21-00179.

[304] Tattan M, Chambrone L, González-Martín O, Avila-Ortiz G. Static computer-aided, partially guided, and free-handed implant placement: A systematic review and meta-analysis of randomized controlled trials. Clin Oral Implants Res 2020;31:889–916. https://doi.org/10.1111/clr.13635.

[305] Kühl S, Zürcher S, Mahid T, Müller-Gerbl M, Filippi A, Cattin P. Accuracy of full guided vs. half-guided implant surgery. Clin Oral Implants Res 2013;24:763–9. https://doi.org/10.1111/j.1600-0501.2012.02484.x.

[306] Younes F, Cosyn J, De Bruyckere T, Cleymaet R, Bouckaert E, Eghbali A. A randomized controlled study on the accuracy of free-handed, pilot-drill guided and fully guided implant surgery in partially edentulous patients. J Clin Periodontol 2018;45:721–32. https://doi.org/10.1111/jcpe.12897.

[307] Noharet R, Pettersson A, Bourgeois D. Accuracy of implant placement in the posterior maxilla as related to 2 types of surgical guides: a pilot

study in the human cadaver. J Prosthet Dent 2014;112:526–32. https://doi. org/10.1016/j.prosdent.2013.12.013.

[308] Tahmaseb A, Wu V, Wismeijer D, Coucke W, Evans C. The accuracy of static computer-aided implant surgery: A systematic review and meta-analysis. Clin Oral Implants Res 2018;29 Suppl 16:416–35. https://doi. org/10.1111/clr.13346.

[309] Vercruyssen M, De Laat A, Coucke W, Quirynen M. An RCT comparing patient-centred outcome variables of guided surgery (bone or mucosa supported) with conventional implant placement. J Clin Periodontol 2014;41:724–32. https://doi.org/10.1111/jcpe.12257.

[310] Pozzi A, Tallarico M, Marchetti M, Scarfò B, Esposito M. Computer-guided versus free-hand placement of immediately loaded dental implants: 1-year post-loading results of a multicentre randomised controlled trial. Eur J Oral Implantol 2014;7:229–42.

[311] Cassetta M, Stefanelli LV, Giansanti M, Di Mambro A, Calasso S. Accuracy of a computer-aided implant surgical technique. Int J Periodontics Restorative Dent 2013;33:317–25. https://doi.org/10.11607/prd.1019.

[312] Cassetta M, Di Mambro A, Giansanti M, Stefanelli LV, Cavallini C. The intrinsic error of a stereolithographic surgical template in implant guided surgery. Int J Oral Maxillofac Surg 2013;42:264–75. https://doi. org/10.1016/j.ijom.2012.06.010.

[313] Raico Gallardo YN, da Silva-Olivio IRT, Mukai E, Morimoto S, Sesma N, Cordaro L. Accuracy comparison of guided surgery for dental implants according to the tissue of support: a systematic review and meta-analysis. Clin Oral Implants Res 2017;28:602–12. https://doi.org/10.1111/clr.12841.

[314] Arisan V, Karabuda CZ, Ozdemir T. Implant surgery using bone- and mucosa-supported stereolithographic guides in totally edentulous jaws: surgical and post-operative outcomes of computer-aided vs. standard techniques. Clin Oral Implants Res 2010;21:980–8. https://doi.org/10.1111/ j.1600-0501.2010.01957.x.

[315] Adams CR, Ammoun R, Deeb GR, Bencharit S. Influence of Metal Guide Sleeves on the Accuracy and Precision of Dental Implant Placement Using Guided Implant Surgery: An In Vitro Study. Journal of Prosthodontics 2023;32:62–70. https://doi.org/10.1111/jopr.13503.

[316] Yeung M, Abdulmajeed A, Carrico CK, Deeb GR, Bencharit S. Accuracy and precision of 3D-printed implant surgical guides with different implant systems: An in vitro study. J Prosthet Dent 2020;123:821–8. https://doi. org/10.1016/j.prosdent.2019.05.027.

[317] Behneke A, Burwinkel M, Knierim K, Behneke N. Accuracy assessment of cone beam computed tomography-derived laboratory-based surgical templates on partially edentulous patients. Clin Oral Implants Res 2012;23:137–43. https://doi.org/10.1111/j.1600-0501.2011.02176.x.

[318] Schnutenhaus S, Edelmann C, Rudolph H, Dreyhaupt J, Luthardt RG. 3D accuracy of implant positions in template-guided implant placement as a function of the remaining teeth and the surgical procedure: a retrospective study. Clin Oral Investig 2018;22:2363–72. https://doi.org/10.1007/s00784-018-2339-8.

[319] Matsumura A, Nakano T, Ono S, Kaminaka A, Yatani H, Kabata D. Multivariate analysis of causal factors influencing accuracy of guided implant surgery for partial edentulism: a retrospective clinical study. International Journal of Implant Dentistry 2021;7:28. https://doi.org/10.1186/s40729-021-00313-2.

[320] Quispe-López N, Flores-Fraile J, Pardal-Peláez B, Delgado-Martínez J, Montero J. Factors Influencing the Accuracy of Guided Surgery: An In Vitro Trial. Int J Oral Maxillofac Implants 2023;38:120–9. https://doi.org/10.11607/jomi.9794.

[321] Putra RH, Yoda N, Iikubo M, Kataoka Y, Yamauchi K, Koyama S, et al. Influence of bone condition on implant placement accuracy with computer-guided surgery. International Journal of Implant Dentistry 2020;6:62. https://doi.org/10.1186/s40729-020-00249-z.

[322] Chen Z, Li J, Sinjab K, Mendonca G, Yu H, Wang H-L. Accuracy of flapless immediate implant placement in anterior maxilla using computer-assisted versus freehand surgery: A cadaver study. Clin Oral Implants Res 2018;29:1186–94. https://doi.org/10.1111/clr.13382.

[323] Lin C-C, Ishikawa M, Huang B-H, Huang M-S, Cheng H-C, Maida T, et al. In Vitro Accuracy of Static Guided Implant Surgery Measured by Optical Scan: Examining the Impact of Operator Experience. Applied Sciences 2020;10:2718. https://doi.org/10.3390/app10082718.

[324] Park S-J, Leesungbok R, Cui T, Lee SW, Ahn S-J. Reliability of a CAD/CAM Surgical Guide for Implant Placement: An In Vitro Comparison of Surgeons' Experience Levels and Implant Sites. Int J Prosthodont 2017;30:367–169. https://doi.org/10.11607/ijp.5179.

[325] Ackerman S, Aguilera FC, Buie JM, Glickman GN, Umorin M, Wang Q, et al. Accuracy of 3-dimensional-printed Endodontic Surgical Guide: A Human Cadaver Study. J Endod 2019;45:615–8. https://doi.org/10.1016/j.joen.2019.02.005.

[326] Su Y, Chen C, Lin C, Lee H, Chen K, Lin Y, et al. Guided endodontics: accuracy of access cavity preparation and discrimination of angular and linear deviation on canal accessing ability—an ex vivo study. BMC Oral Health 2021;21:606. https://doi.org/10.1186/s12903-021-01936-y.

[327] Zubizarreta-Macho Á, Valle Castaño S, Montiel-Company JM, Mena-Álvarez J. Effect of Computer-Aided Navigation Techniques on the Accuracy of Endodontic Access Cavities: A Systematic Review and Meta-Analysis. Biology (Basel) 2021;10:212. https://doi.org/10.3390/biology10030212.

[328] Decurcio DA, Bueno MR, Silva JA, Loureiro MAZ, Damião Sousa-Neto M, Estrela C. Digital Planning on Guided Endodontics Technology. Braz Dent J 2021;32:23–33. https://doi.org/10.1590/0103-6440202104740.

[329] Anderson J, Wealleans J, Ray J. Endodontic applications of 3D printing. Int Endod J 2018;51:1005–18. https://doi.org/10.1111/iej.12917.

[330] Anssari Moin D, Verweij JP, Waars H, van Merkesteyn R, Wismeijer D. Accuracy of Computer-Assisted Template-Guided Autotransplantation of Teeth With Custom Three-Dimensional Designed/Printed Surgical Tooling: A Cadaveric Study. J Oral Maxillofac Surg 2017;75:925.e1-925.e7. https://doi.org/10.1016/j.joms.2016.12.049.

[331] Anssari Moin D, Derksen W, Verweij JP, van Merkesteyn R, Wismeijer D. A Novel Approach for Computer-Assisted Template-Guided Autotransplantation of Teeth With Custom 3D Designed/Printed Surgical Tooling. An Ex Vivo Proof of Concept. J Oral Maxillofac Surg 2016;74:895–902. https://doi.org/10.1016/j.joms.2016.01.033.

[332] Anssari Moin D, Derksen W, Waars H, Hassan B, Wismeijer D. Computer-assisted template-guided custom-designed 3D-printed implant placement with custom-designed 3D-printed surgical tooling: an in-vitro proof of a novel concept. Clin Oral Implants Res 2017;28:582–5. https://doi.org/10.1111/clr.12838.

[333] Mijiritsky E, Ben Zaken H, Shacham M, Cinar IC, Tore C, Nagy K, et al. Variety of Surgical Guides and Protocols for Bone Reduction Prior to Implant Placement: A Narrative Review. Int J Environ Res Public Health 2021;18:2341. https://doi.org/10.3390/ijerph18052341.

[334] Han H, Kim P-J, Kim K-T, Kim S, Ku Y, Cho Y-D. Dental implant proximity to adjacent teeth: A retrospective study. Clinical Implant Dentistry and Related Research 2022;24:733–9. https://doi.org/10.1111/cid.13132.

[335] Bouchard C, Magill JC, Nikonovskiy V, Byl M, Murphy BA, Kaban LB, et al. Osteomark: a surgical navigation system for oral and maxillofacial

surgery. International Journal of Oral and Maxillofacial Surgery 2012;41:265–70. https://doi.org/10.1016/j.ijom.2011.10.017.

[336] Luebbers H-T, Messmer P, Obwegeser JA, Zwahlen RA, Kikinis R, Graetz KW, et al. Comparison of different registration methods for surgical navigation in cranio-maxillofacial surgery. J Craniomaxillofac Surg 2008;36:109–16. https://doi.org/10.1016/j.jcms.2007.09.002.

[337] Block MS, Emery RW. Static or Dynamic Navigation for Implant Placement—Choosing the Method of Guidance. Journal of Oral and Maxillofacial Surgery 2016;74:269–77. https://doi.org/10.1016/j.joms.2015.09.022.

[338] Mandelaris GA, Stefanelli LV, DeGroot BS. Dynamic Navigation for Surgical Implant Placement: Overview of Technology, Key Concepts, and a Case Report. Compend Contin Educ Dent 2018;39:614–21; quiz 622.

[339] Ewers R, Schicho K, Undt G, Wanschitz F, Truppe M, Seemann R, et al. Basic research and 12 years of clinical experience in computer-assisted navigation technology: a review. International Journal of Oral and Maxillofacial Surgery 2005;34:1–8. https://doi.org/10.1016/j.ijom.2004.03.018.

[340] Scheyer ET, Mandelaris GA, McGuire MK, AlTakriti MA, Stefanelli LV. Implant Placement Under Dynamic Navigation Using Trace Registration: Case Presentations. Int J Periodontics Restorative Dent 2020;40:e241–8. https://doi.org/10.11607/prd.4479.

[341] Ma F, Sun F, Wei T, Ma Y. Comparison of the accuracy of two different dynamic navigation system registration methods for dental implant placement: A retrospective study. Clinical Implant Dentistry and Related Research 2022;24:352–60. https://doi.org/10.1111/cid.13090.

[342] Wei T, Ma F, Sun F, Ma Y. Assessment of the Accuracy of Two Different Dynamic Navigation System Registration Methods for Dental Implant Placement in the Posterior Area: An In Vitro Study. J Pers Med 2023;13:139. https://doi.org/10.3390/jpm13010139.

[343] Wu B-Z, Xue F, Ma Y, Sun F. Accuracy of automatic and manual dynamic navigation registration techniques for dental implant surgery in posterior sites missing a single tooth: A retrospective clinical analysis. Clinical Oral Implants Research 2023;34:221–32. https://doi.org/10.1111/clr.14034.

[344] Struwe M, Leontiev W, Connert T, Kühl S, Filippi A, Herber V, et al. Accuracy of a dynamic navigation system for dental implantation with two different workflows and intraoral markers compared to static-guided implant surgery: An in-vitro study. Clinical Oral Implants Research 2023;34:196–208. https://doi.org/10.1111/clr.14030.

[345] Stefanelli LV, Mandelaris GA, DeGroot BS, Gambarini G, De Angelis F, Di Carlo S. Accuracy of a Novel Trace-Registration Method for Dynamic Navigation Surgery. Int J Periodontics Restorative Dent 2020;40:427–35. https://doi.org/10.11607/prd.4420.

[346] Schnutenhaus S, Knipper A, Wetzel M, Edelmann C, Luthardt R. Accuracy of Computer-Assisted Dynamic Navigation as a Function of Different Intraoral Reference Systems: An In Vitro Study. Int J Environ Res Public Health 2021;18:3244. https://doi.org/10.3390/ijerph18063244.

[347] Kalaivani G, Balaji VR, Manikandan D, Rohini G. Expectation and reality of guided implant surgery protocol using computer-assisted static and dynamic navigation system at present scenario: Evidence-based literature review. J Indian Soc Periodontol 2020;24:398–408. https://doi.org/10.4103/jisp.jisp_92_20.

[348] Boa K, Barrak I, Varga E, Joob-Fancsaly A, Varga E, Piffko J. Intraosseous generation of heat during guided surgical drilling: an ex vivo study of the effect of the temperature of the irrigating fluid. Br J Oral Maxillofac Surg 2016;54:904–8. https://doi.org/10.1016/j.bjoms.2016.06.004.

[349] Stefanelli LV, DeGroot BS, Lipton DI, Mandelaris GA. Accuracy of a Dynamic Dental Implant Navigation System in a Private Practice. Int J Oral Maxillofac Implants 2019;34:205–13. https://doi.org/10.11607/jomi.6966.

[350] Golob Deeb J, Bencharit S, Carrico CK, Lukic M, Hawkins D, Rener-Sitar K, et al. Exploring training dental implant placement using computer-guided implant navigation system for predoctoral students: A pilot study. Eur J Dent Educ 2019;23:415–23. https://doi.org/10.1111/eje.12447.

[351] Wang M, Eitan M, Zhan Y, Shen H, Liu F. Digital workflow for prosthetically driven implant navigation surgery in a fully edentulous patient: a case report. Int J Comput Dent 2021;24:303–15.

[352] Jorba-García A, Bara-Casaus JJ, Camps-Font O, Sánchez-Garcés MÁ, Figueiredo R, Valmaseda-Castellón E. Accuracy of dental implant placement with or without the use of a dynamic navigation assisted system: A randomized clinical trial. Clin Oral Implants Res 2023;34:438–49. https://doi.org/10.1111/clr.14050.

[353] Kunavisarut C, Santivitoonvong A, Chaikantha S, Pornprasertsuk-Damrongsri S, Joda T. Patient-reported outcome measures comparing static computer-aided implant surgery and conventional implant surgery for single-tooth replacement: A randomized controlled trial. Clin Oral Implants Res 2022;33:278–90. https://doi.org/10.1111/clr.13886.

[354] Kaewsiri D, Panmekiate S, Subbalekha K, Mattheos N, Pimkhaokham A. The accuracy of static vs. dynamic computer-assisted implant surgery in single tooth space: A randomized controlled trial. Clin Oral Implants Res 2019;30:505–14. https://doi.org/10.1111/clr.13435.

[355] Yimarj P, Subbalekha K, Dhanesuan K, Siriwatana K, Mattheos N, Pimkhaokham A. Comparison of the accuracy of implant position for two-implants supported fixed dental prosthesis using static and dynamic computer-assisted implant surgery: A randomized controlled clinical trial. Clin Implant Dent Relat Res 2020;22:672–8. https://doi.org/10.1111/cid.12949.

[356] Wang W, Zhuang M, Li S, Shen Y, Lan R, Wu Y, et al. Exploring training dental implant placement using static or dynamic devices among dental students. European Journal of Dental Education n.d.;n/a. https://doi.org/10.1111/eje.12825.

[357] Stefanelli LV, Pranno N, De Angelis F, La Rosa S, Polimeni A, Di Carlo S. Navigated Antral Bone Expansion (NABE): a prospective study on 35 patients with 4 months of follow-up post implant loading. BMC Oral Health 2020;20:273. https://doi.org/10.1186/s12903-020-01268-3.

[358] Bhalerao A, Marimuthu M, Wahab A, Ayoub A. Dynamic navigation for zygomatic implant placement: A randomized clinical study comparing the flapless versus the conventional approach. J Dent 2023;130:104436. https://doi.org/10.1016/j.jdent.2023.104436.

[359] González Rueda JR, García Ávila I, de Paz Hermoso VM, Riad Deglow E, Zubizarreta-Macho Á, Pato Mourelo J, et al. Accuracy of a Computer-Aided Dynamic Navigation System in the Placement of Zygomatic Dental Implants: An In Vitro Study. J Clin Med 2022;11:1436. https://doi.org/10.3390/jcm11051436.

[360] González Rueda JR, Galparsoro Catalán A, de Paz Hermoso VM, Riad Deglow E, Zubizarreta-Macho Á, Pato Mourelo J, et al. Accuracy of computer-aided static and dynamic navigation systems in the placement of zygomatic dental implants. BMC Oral Health 2023;23:150. https://doi.org/10.1186/s12903-023-02856-9.

[361] D GT, Saxena P, Gupta S. Static vs. dynamic navigation for endodontic microsurgery - A comparative review. J Oral Biol Craniofac Res 2022;12:410–2. https://doi.org/10.1016/j.jobcr.2022.04.010.

[362] Ma L, Jiang W, Zhang B, Qu X, Ning G, Zhang X, et al. Augmented reality surgical navigation with accurate CBCT-patient registration for dental implant placement. Med Biol Eng Comput 2019;57:47–57. https://doi.org/10.1007/s11517-018-1861-9.

[363] Mai H-N, Dam VV, Lee D-H. Accuracy of Augmented Reality-Assisted Navigation in Dental Implant Surgery: Systematic Review and Meta-analysis. J Med Internet Res 2023;25:e42040. https://doi.org/10.2196/42040.

[364] Ayoub A, Pulijala Y. The application of virtual reality and augmented reality in Oral & Maxillofacial Surgery. BMC Oral Health 2019;19:238. https://doi.org/10.1186/s12903-019-0937-8.

[365] Dreiseidler T, Tandon D, Ritter L, Neugebauer J, Mischkowski RA, Scheer M, et al. Accuracy of a newly developed open-source system for dental implant planning. Int J Oral Maxillofac Implants 2012;27:128–37.

[366] Huang L, Zhang X, Mo A. A Retrospective Study on the Transferring Accuracy of a Fully Guided Digital Template in the Anterior Zone. Materials (Basel) 2021;14:4631. https://doi.org/10.3390/ma14164631.

[367] Platzer S, Bertha G, Heschl A, Wegscheider WA, Lorenzoni M. Three-dimensional accuracy of guided implant placement: indirect assessment of clinical outcomes. Clin Implant Dent Relat Res 2013;15:724–34. https://doi.org/10.1111/j.1708-8208.2011.00406.x.

[368] Van Assche N, Van Steenberghe D, Guerrero ME, Hirsch E, Schutyser F, Quirynen M, et al. Accuracy of implant placement based on pre-surgical planning of three-dimensional cone-beam images: a pilot study. Journal of Clinical Periodontology 2007;34:816–21. https://doi.org/10.1111/j.1600-051X.2007.01110.x.

[369] Maes F, Collignon A, Vandermeulen D, Marchal G, Suetens P. Multimodality image registration by maximization of mutual information. IEEE Trans Med Imaging 1997;16:187–98. https://doi.org/10.1109/42.563664.

[370] Derksen W, Wismeijer D, Flügge T, Hassan B, Tahmaseb A. The accuracy of computer-guided implant surgery with tooth-supported, digitally designed drill guides based on CBCT and intraoral scanning. A prospective cohort study. Clinical Oral Implants Research 2019;30:1005–15. https://doi.org/10.1111/clr.13514.

[371] Naeini EN, Atashkadeh M, De Bruyn H, D'Haese J. Narrative review regarding the applicability, accuracy, and clinical outcome of flapless implant surgery with or without computer guidance. Clin Implant Dent Relat Res 2020;22:454–67. https://doi.org/10.1111/cid.12901.

[372] Maret D, Telmon N, Peters OA, Lepage B, Treil J, Inglèse JM, et al. Effect of voxel size on the accuracy of 3D reconstructions with cone beam CT. Dentomaxillofac Radiol 2012;41:649–55. https://doi.org/10.1259/dmf/81804525.

[373] Dong T, Xia L, Cai C, Yuan L, Ye N, Fang B. Accuracy of in vitro mandibular volumetric measurements from CBCT of different voxel sizes with different segmentation threshold settings. BMC Oral Health 2019;19:206. https://doi.org/10.1186/s12903-019-0891-5.

[374] Eliliwi M, Bazina M, Palomo JM. kVp, mA, and voxel size effect on 3D voxel-based superimposition. Angle Orthod 2020;90:269–77. https://doi.org/10.2319/012719-52.1.

[375] Han G, Li J, Wang S, Wang L, Zhou Y, Liu Y. A comparison of voxel- and surface-based cone-beam computed tomography mandibular superimposition in adult orthodontic patients. J Int Med Res 2021;49:0300060520982708. https://doi.org/10.1177/0300060520982708.

[376] Gupta J, Ali SP. Cone beam computed tomography in oral implants. Natl J Maxillofac Surg 2013;4:2–6. https://doi.org/10.4103/0975-5950.117811.

[377] Rinkel J, Gerfault L, Estève F, Dinten J-M. A new method for x-ray scatter correction: first assessment on a cone-beam CT experimental setup. Phys Med Biol 2007;52:4633–52. https://doi.org/10.1088/0031-9155/52/15/018.

[378] Tan PLB, Layton DM, Wise SL. In vitro comparison of guided versus freehand implant placement: use of a new combined TRIOS surface scanning, Implant Studio, CBCT, and stereolithographic virtually planned and guided technique. Int J Comput Dent 2018;21:87–95.

[379] Yi C, Li S, Wen A, Wang Y, Zhao Y, Zhang Y. Digital versus radiographic accuracy evaluation of guided implant surgery: an in vitro study. BMC Oral Health 2022;22:540. https://doi.org/10.1186/s12903-022-02585-5.

[380] Franchina A, Stefanelli LV, Maltese F, Mandelaris GA, Vantaggiato A, Pagliarulo M, et al. Validation of an Intra-Oral Scan Method Versus Cone Beam Computed Tomography Superimposition to Assess the Accuracy between Planned and Achieved Dental Implants: A Randomized In Vitro Study. Int J Environ Res Public Health 2020;17:9358. https://doi.org/10.3390/ijerph17249358.

[381] Skjerven H, Olsen-Bergem H, Rønold HJ, Riis UH, Ellingsen JE. Comparison of postoperative intraoral scan versus cone beam computerised tomography to measure accuracy of guided implant placement-A prospective clinical study. Clin Oral Implants Res 2019;30:531–41. https://doi.org/10.1111/clr.13438.

[382] van Hooft J, Kielenstijn G, Liebregts J, Baan F, Meijer G, D'haese J, et al. Intraoral Scanning as an Alternative to Evaluate the Accuracy of Dental Implant Placements in Partially Edentate Situations: A Prospective Clinical Case Series. J Clin Med 2022;11:5876. https://doi.org/10.3390/jcm11195876.

[383] Carini F, Coppola G, Saggese V. Comparison between CBCT superimposition protocol and S.T.A.P. method to evaluate the accuracy in implant insertion in guided surgery. Minerva Dent Oral Sci 2022;71:223–32. https://doi.org/10.23736/S2724-6329.21.04469-1.

[384] Ma F, Liu M, Liu X, Wei T, Liu L, Sun F. Proposal and Validation of a New Nonradiological Method for Postoperative Three-Dimensional Implant Position Analysis Based on the Dynamic Navigation System: An In Vitro Study. J Pers Med 2023;13:362. https://doi.org/10.3390/jpm13020362.

[385] Chien H-H, Schroering RL, Prasad HS, Tatakis DN. Effects of a new implant abutment design on peri-implant soft tissues. J Oral Implantol 2014;40:581–8. https://doi.org/10.1563/AAID-JOI-D-12-00313.

[386] Chai WL, Razali M, Ngeow WC. Dimension and Structures of Biological Seal of Peri-Implant Tissues. IntechOpen; 2016. https://doi.org/10.5772/63950.

[387] Dhir S, Mahesh L, Kurtzman GM, Vandana KL. Peri-implant and periodontal tissues: a review of differences and similarities. Compend Contin Educ Dent 2013;34:e69-75.

[388] Neiva R, Neiva K, Oh T-J, Wang H. Clinical and morphological aspects of the implant / soft tissue interface, 2010.

[389] Welander M. Soft tissue integration to dental implants 2008.

[390] Rezaei Esfahrood Z, Kadkhodazadeh M, Gholamin P, Amid R, Passanezi E, Hosein Zadeh H. Biologic Width around Dental Implants: An Updated Review. Journal of Dental Materials and Techniques 2016;5:68–81. https://doi.org/10.22038/jdmt.2016.6616.

[391] Suárez-López Del Amo F, Lin G-H, Monje A, Galindo-Moreno P, Wang H-L. Influence of Soft Tissue Thickness on Peri-Implant Marginal Bone Loss: A Systematic Review and Meta-Analysis. J Periodontol 2016;87:690–9. https://doi.org/10.1902/jop.2016.150571.

[392] Sanz-Martín I, Sanz-Sánchez I, Carrillo de Albornoz A, Figuero E, Sanz M. Effects of modified abutment characteristics on peri-implant soft tissue health: A systematic review and meta-analysis. Clin Oral Implants Res 2018;29:118–29. https://doi.org/10.1111/clr.13097.

[393] Furuhashi A, Ayukawa Y, Atsuta I, Okawachi H, Koyano K. The difference of fibroblast behavior on titanium substrata with different surface characteristics. Odontology 2012;100:199–205. https://doi.org/10.1007/s10266-011-0029-y.

[394] Canullo L, Genova T, Gross Trujillo E, Pradies G, Petrillo S, Muzzi M, et al. Fibroblast Interaction with Different Abutment Surfaces: In Vitro Study. Int J Mol Sci 2020;21:1919. https://doi.org/10.3390/ijms21061919.

[395] Afrashtehfar KI, Weber A, Abou-Ayash S. Titanium-base abutments may have similar long-term peri-implant effects as non-bonded one-piece abutments. Evid Based Dent 2022;23:134–5. https://doi.org/10.1038/s41432-022-0835-9.

[396] Cinquini C, Marchio V, Di Donna E, Alfonsi F, Derchi G, Nisi M, et al. Histologic Evaluation of Soft Tissues around Dental Implant Abutments: A Narrative Review. Materials (Basel) 2022;15:3811. https://doi.org/10.3390/ma15113811.

[397] Canullo L, Annunziata M, Pesce P, Tommasato G, Nastri L, Guida L. Influence of abutment material and modifications on peri-implant soft-tissue attachment: A systematic review and meta-analysis of histological animal studies. J Prosthet Dent 2021;125:426–36. https://doi.org/10.1016/j.prosdent.2020.01.025.

[398] Sampatanukul T, Serichetaphongse P, Pimkhaokham A. Histological evaluations and inflammatory responses of different dental implant abutment materials: A human histology pilot study. Clin Implant Dent Relat Res 2018;20:160–9. https://doi.org/10.1111/cid.12562.

[399] Bharate V, Kumar Y, Koli D, Pruthi G, Jain V. Effect of different abutment materials (zirconia or titanium) on the crestal bone height in 1 year. J Oral Biol Craniofac Res 2020;10:372–4. https://doi.org/10.1016/j.jobcr.2019.10.001.

[400] Dede DÖ, Armağanci A, Ceylan G, Celik E, Cankaya S, Yilmaz B. Influence of implant abutment material on the color of different ceramic crown systems. J Prosthet Dent 2016;116:764–9. https://doi.org/10.1016/j.prosdent.2016.04.004.

[401] Sala L, Bascones-Martínez A, Carrillo-de-Albornoz A. Impact of abutment material on peri-implant soft tissue color. An in vitro study. Clin Oral Investig 2017;21:2221–33. https://doi.org/10.1007/s00784-016-2015-9.

[402] Tabatabaian F, Jafari A, Namdari M, Mahshid M. Influence of coping and veneer thickness on the color of zirconia-based restorations on different implant abutment backgrounds. J Prosthet Dent 2019;121:327–32. https://doi.org/10.1016/j.prosdent.2018.02.022.

[403] Alqutaibi AY, Ghulam O, Krsoum M, Binmahmoud S, Taher H, Elmalky W, et al. Revolution of Current Dental Zirconia: A Comprehensive Review. Molecules 2022;27:1699. https://doi.org/10.3390/molecules27051699.

[404] Atash R, Boularbah M-R, Sibel C. Color variation induced by abutments in the superior anterior maxilla: an in vitro study in the pig gingiva. J Adv Prosthodont 2016;8:423–32. https://doi.org/10.4047/jap.2016.8.6.423.

[405] Kajiwara N, Masaki C, Mukaibo T, Kondo Y, Nakamoto T, Hosokawa R. Soft tissue biological response to zirconia and metal implant abutments compared with natural tooth: microcirculation monitoring as a novel bioindicator. Implant Dent 2015;24:37–41. https://doi.org/10.1097/ID.0000000000000167.

[406] Barwacz CA, Brogden KA, Stanford CM, Dawson DV, Recker EN, Blanchette D. Comparison of pro-inflammatory cytokines and bone metabolism mediators around titanium and zirconia dental implant abutments following a minimum of 6 months of clinical function. Clin Oral Implants Res 2015;26:e35–41. https://doi.org/10.1111/clr.12326.

[407] Degidi M, Artese L, Scarano A, Perrotti V, Gehrke P, Piattelli A. Inflammatory infiltrate, microvessel density, nitric oxide synthase expression, vascular endothelial growth factor expression, and proliferative activity in peri-implant soft tissues around titanium and zirconium oxide healing caps. J Periodontol 2006;77:73–80. https://doi.org/10.1902/jop.2006.77.1.73.

[408] Rompen E, Domken O, Degidi M, Pontes AEF, Piattelli A. The effect of material characteristics, of surface topography and of implant components and connections on soft tissue integration: a literature review. Clin Oral Implants Res 2006;17 Suppl 2:55–67. https://doi.org/10.1111/j.1600-0501.2006.01367.x.

[409] Nascimento C do, Pita MS, Santos E de S, Monesi N, Pedrazzi V, Albuquerque Junior RF de, et al. Microbiome of titanium and zirconia dental implants abutments. Dent Mater 2016;32:93–101. https://doi.org/10.1016/j.dental.2015.10.014.

[410] Sadowsky SJ. Has zirconia made a material difference in implant prosthodontics? A review. Dent Mater 2020;36:1–8. https://doi.org/10.1016/j.dental.2019.08.100.

[411] Gheisarifar M, Thompson GA, Drago C, Tabatabaei F, Rasoulianboroujeni M. In vitro study of surface alterations to polyetheretherketone and titanium and their effect upon human gingival fibroblasts. J Prosthet Dent 2021;125:155–64. https://doi.org/10.1016/j.prosdent.2019.12.012.

[412] Sanz-Sánchez I, Sanz-Martín I, Carrillo de Albornoz A, Figuero E, Sanz M. Biological effect of the abutment material on the stability of peri-implant marginal bone levels: A systematic review and meta-analysis. Clin Oral Implants Res 2018;29 Suppl 18:124–44. https://doi.org/10.1111/clr.13293.

[413] Hahnel S, Wieser A, Lang R, Rosentritt M. Biofilm formation on the surface of modern implant abutment materials. Clin Oral Implants Res 2015;26:1297–301. https://doi.org/10.1111/clr.12454.

[414] Heimer S, Schmidlin PR, Stawarczyk B. Effect of different cleaning methods of polyetheretherketone on surface roughness and surface free energy properties. J Appl Biomater Funct Mater 2016;14:e248-255. https://doi.org/10.5301/jabfm.5000291.

[415] Sturz CRC, Faber F-J, Scheer M, Rothamel D, Neugebauer J. Effects of various chair-side surface treatment methods on dental restorative materials with respect to contact angles and surface roughness. Dent Mater J 2015;34:796–813. https://doi.org/10.4012/dmj.2014-098.

[416] Shim JS, Kim HC, Park SI, Yun HJ, Ryu JJ. Comparison of Various Implant Provisional Resin Materials for Cytotoxicity and Attachment to Human Gingival Fibroblasts. Int J Oral Maxillofac Implants 2019;34:390–6. https://doi.org/10.11607/jomi.6707.

[417] Pituru SM, Greabu M, Totan A, Imre M, Pantea M, Spinu T, et al. A Review on the Biocompatibility of PMMA-Based Dental Materials for Interim Prosthetic Restorations with a Glimpse into their Modern Manufacturing Techniques. Materials (Basel) 2020;13:2894. https://doi.org/10.3390/ma13132894.

[418] Najeeb S, Zafar MS, Khurshid Z, Siddiqui F. Applications of polyetheretherketone (PEEK) in oral implantology and prosthodontics. J Prosthodont Res 2016;60:12–9. https://doi.org/10.1016/j.jpor.2015.10.001.

[419] Ramenzoni LL, Attin T, Schmidlin PR. In Vitro Effect of Modified Polyetheretherketone (PEEK) Implant Abutments on Human Gingival Epithelial Keratinocytes Migration and Proliferation. Materials (Basel) 2019;12:1401. https://doi.org/10.3390/ma12091401.

[420] Bagchi P, Alfawzan AA, Magar SM, Priya R, Kochhar AS, Agrawal S, et al. An In vitro Evaluation of Effect of Implant Abutment on Human Gingival Epithelial Keratinocytes. Ann Afr Med 2022;21:217–22. https://doi.org/10.4103/aam.aam_116_20.

[421] Rausch MA, Shokoohi-Tabrizi H, Wehner C, Pippenger BE, Wagner RS, Ulm C, et al. Impact of Implant Surface Material and Microscale Roughness on the Initial Attachment and Proliferation of Primary Human Gingival Fibroblasts. Biology (Basel) 2021;10:356. https://doi.org/10.3390/biology10050356.

[422] Yamano S, Al-Sowygh ZH, Gallucci GO, Wada K, Weber H-P, Sukotjo C. Early peri-implant tissue reactions on different titanium surface topographies. Clin Oral Implants Res 2011;22:815–9. https://doi.org/10.1111/j.1600-0501.2010.02059.x.

[423] Gibbs S, Roffel S, Meyer M, Gasser A. Biology of soft tissue repair: gingival epithelium in wound healing and attachment to the tooth and abutment surface. Eur Cell Mater 2019;38:63–78. https://doi.org/10.22203/eCM. v038a06.

[424] Kirmanidou Y, Sidira M, Drosou M-E, Bennani V, Bakopoulou A, Tsouknidas A, et al. New Ti-Alloys and Surface Modifications to Improve the Mechanical Properties and the Biological Response to Orthopedic and Dental Implants: A Review. Biomed Res Int 2016;2016:2908570. https:// doi.org/10.1155/2016/2908570.

[425] Zhang Q, Yue X. Marginal Bone Loss around Machined Smooth Neck Implants Compared to Rough Threaded Neck Implants: A Systematic Review and Meta-Analysis. J Prosthodont 2021;30:401–11. https://doi. org/10.1111/jopr.13333.

[426] Albrektsson T, Wennerberg A. Oral implant surfaces: Part 1--review focusing on topographic and chemical properties of different surfaces and in vivo responses to them. Int J Prosthodont 2004;17:536–43.

[427] Yang Y, Zhou J, Liu X, Zheng M, Yang J, Tan J. Ultraviolet light-treated zirconia with different roughness affects function of human gingival fibroblasts in vitro: the potential surface modification developed from implant to abutment. J Biomed Mater Res B Appl Biomater 2015;103:116– 24. https://doi.org/10.1002/jbm.b.33183.

[428] Bollen CM, Papaioanno W, Van Eldere J, Schepers E, Quirynen M, van Steenberghe D. The influence of abutment surface roughness on plaque accumulation and peri-implant mucositis. Clin Oral Implants Res 1996;7:201–11. https://doi.org/10.1034/j.1600-0501.1996.070302.x.

[429] Grössner-Schreiber B, Herzog M, Hedderich J, Dück A, Hannig M, Griepentrog M. Focal adhesion contact formation by fibroblasts cultured on surface-modified dental implants: an in vitro study. Clin Oral Implants Res 2006;17:736–45. https://doi.org/10.1111/j.1600-0501.2006.01277.x.

[430] Teughels W, Van Assche N, Sliepen I, Quirynen M. Effect of material characteristics and/or surface topography on biofilm development. Clin Oral Implants Res 2006;17 Suppl 2:68–81. https://doi.org/10.1111/j.1600-0501.2006.01353.x.

[431] Fürst MM, Salvi GE, Lang NP, Persson GR. Bacterial colonization immediately after installation on oral titanium implants. Clin Oral Implants Res 2007;18:501–8. https://doi.org/10.1111/j.1600-0501.2007.01381.x.

[432] Pacha-Olivenza MÁ, Tejero R, Fernández-Calderón MC, Anitua E, Troya M, González-Martín ML. Relevance of Topographic Parameters

on the Adhesion and Proliferation of Human Gingival Fibroblasts and Oral Bacterial Strains. Biomed Res Int 2019;2019:8456342. https://doi.org/10.1155/2019/8456342.

[433] Bollen CM, Lambrechts P, Quirynen M. Comparison of surface roughness of oral hard materials to the threshold surface roughness for bacterial plaque retention: a review of the literature. Dent Mater 1997;13:258–69. https://doi.org/10.1016/s0109-5641(97)80038-3.

[434] Esfahanizadeh N, Motalebi S, Daneshparvar N, Akhoundi N, Bonakdar S. Morphology, proliferation, and gene expression of gingival fibroblasts on Laser-Lok, titanium, and zirconia surfaces. Lasers Med Sci 2016;31:863–73. https://doi.org/10.1007/s10103-016-1927-6.

[435] Migita S, Okuyama S, Araki K. Sub-micrometer scale surface roughness of titanium reduces fibroblasts function. J Appl Biomater Funct Mater 2016;14:e65-69. https://doi.org/10.5301/jabfm.5000260.

[436] Quirynen M, van der Mei HC, Bollen CM, Schotte A, Marechal M, Doornbusch GI, et al. An in vivo study of the influence of the surface roughness of implants on the microbiology of supra- and subgingival plaque. J Dent Res 1993;72:1304–9. https://doi.org/10.1177/0022034593 0720090801.

[437] Mehl C, Kern M, Schütte A-M, Kadem LF, Selhuber-Unkel C. Adhesion of living cells to abutment materials, dentin, and adhesive luting cement with different surface qualities. Dent Mater 2016;32:1524–35. https://doi.org/10.1016/j.dental.2016.09.006.

[438] Paul S, Hanisch O, Nesic D. Human gingival fibroblast proliferation on materials used for dental implant abutments: a systematic review. Int J Prosthodont 2021;34:811–28. https://doi.org/10.11607/ijp.7388.

[439] Jaturunruangsri S. Evaluation of material surface profiling methods: contact versus non-contact, 2015.

[440] Miyoshi K. Surface Characterization Techniques: An Overview 2002.

[441] Arman S, Ungar P, Brown C, DeSantis L, Schmidt C, Prideaux G. Minimizing inter-microscope variability in dental microwear texture analysis. Surface Topography: Metrology and Properties 2016;4:024007. https://doi.org/10.1088/2051-672X/4/2/024007.

[442] Donoso MG, Méndez-Vilas A, Bruque JM, González-Martin ML. On the relationship between common amplitude surface roughness parameters and surface area: Implications for the study of cell–material interactions. International Biodeterioration & Biodegradation 2007;59:245–51. https://doi.org/10.1016/j.ibiod.2006.09.011.

[443] Gittens RA, Scheideler L, Rupp F, Hyzy SL, Geis-Gerstorfer J, Schwartz Z, et al. A review on the wettability of dental implant surfaces II: Biological and clinical aspects. Acta Biomater 2014;10:2907–18. https://doi.org/10.1016/j.actbio.2014.03.032.

[444] Sartoretto SC, Alves ATNN, Resende RFB, Calasans-Maia J, Granjeiro JM, Calasans-Maia MD. Early osseointegration driven by the surface chemistry and wettability of dental implants. J Appl Oral Sci 2015;23:279–87. https://doi.org/10.1590/1678-775720140483.

[445] Barberi J, Spriano S. Titanium and Protein Adsorption: An Overview of Mechanisms and Effects of Surface Features. Materials (Basel) 2021;14:1590. https://doi.org/10.3390/ma14071590.

[446] Kim Y-S, Shin S-Y, Moon S-K, Yang S-M. Surface properties correlated with the human gingival fibroblasts attachment on various materials for implant abutments: a multiple regression analysis. Acta Odontol Scand 2015;73:38–47. https://doi.org/10.3109/00016357.2014.949845.

[447] Albrektsson T, Wennerberg A. On osseointegration in relation to implant surfaces. Clin Implant Dent Relat Res 2019;21 Suppl 1:4–7. https://doi.org/10.1111/cid.12742.

[448] Subramani K, Jung RE, Molenberg A, Hammerle CHF. Biofilm on dental implants: a review of the literature. Int J Oral Maxillofac Implants 2009;24:616–26.

[449] Wassmann T, Kreis S, Behr M, Buergers R. The influence of surface texture and wettability on initial bacterial adhesion on titanium and zirconium oxide dental implants. Int J Implant Dent 2017;3:32. https://doi.org/10.1186/s40729-017-0093-3.

[450] Otto M. Staphylococcus epidermidis--the "accidental" pathogen. Nat Rev Microbiol 2009;7:555–67. https://doi.org/10.1038/nrmicro2182.

[451] Li X, Liu Z, Liu H, Chen X, Liu Y, Tan H. Photodynamic inactivation of fibroblasts and inhibition of Staphylococcus epidermidis adhesion and biofilm formation by toluidine blue O. Mol Med Rep 2017;15:1816–22. https://doi.org/10.3892/mmr.2017.6184.

[452] Atalay S, Çakmak G, Fonseca M, Schimmel M, Yilmaz B. Effect of thermocycling on the surface properties of CAD-CAM denture base materials after different surface treatments. Journal of the Mechanical Behavior of Biomedical Materials 2021;121:104646. https://doi.org/10.1016/j.jmbbm.2021.104646.

[453] Sui S, Li L, Shen J, Ni G, Xie H, Lin Q, et al. Plasma treatment of polymethyl methacrylate to improve surface hydrophilicity and antifouling

performance. Polymer Engineering & Science 2021;61:506–13. https://doi.org/10.1002/pen.25595.

[454] Montaño-Machado V, Chevallier P, Bonilla-Gameros L, Copes F, Quarta C, Kú-Herrera J de J, et al. Development of Multifunctional Materials Based on Poly(ether ether ketone) with Improved Biological Performances for Dental Applications. Materials (Basel) 2021;14:1047. https://doi.org/10.3390/ma14041047.

[455] Matthes R, Jablonowski L, Holtfreter B, Gerling T, von Woedtke T, Kocher T. Fibroblast Growth on Zirconia Ceramic and Titanium Disks After Application with Cold Atmospheric Pressure Plasma Devices or with Antiseptics. Int J Oral Maxillofac Implants 2019;34:809–18. https://doi.org/10.11607/jomi.7285.

[456] Kim Y-S, Ko Y, Kye S-B, Yang S-M. Human gingival fibroblast (HGF-1) attachment and proliferation on several abutment materials with various colors. Int J Oral Maxillofac Implants 2014;29:969–75. https://doi.org/10.11607/jomi.3704.

[457] Rozeik AS, Chaar MS, Sindt S, Wille S, Selhuber-Unkel C, Kern M, et al. Cellular properties of human gingival fibroblasts on novel and conventional implant-abutment materials. Dent Mater 2022;38:540–8. https://doi.org/10.1016/j.dental.2021.12.139.

[458] Staehlke S, Oster P, Seemann S, Kruse F, Brief J, Nebe B. Laser Structured Dental Zirconium for Soft Tissue Cell Occupation—Importance of Wettability Modulation. Materials (Basel) 2022;15:732. https://doi.org/10.3390/ma15030732.

[459] Petrini M, Pierfelice T, D'Amico E, Pietro N, Pandolfi A, D'Arcangelo C, et al. Influence of Nano, Micro and Macro Topography of Dental Implant Surfaces on Human Gingival Fibroblasts. International Journal of Molecular Sciences 2021;22:9871. https://doi.org/10.3390/ijms22189871.

[460] Martínez-Hernández M, Hannig M, García-Pérez VI, Olivares-Navarrete R, Fecher-Trost C, Almaguer-Flores A. Roughness and wettability of titanium implant surfaces modify the salivary pellicle composition. J Biomed Mater Res B Appl Biomater 2021;109:1017–28. https://doi.org/10.1002/jbm.b.34766.

[461] Happe A, Sielker S, Hanisch M, Jung S. The Biological Effect of Particulate Titanium Contaminants of Dental Implants on Human Osteoblasts and Gingival Fibroblasts. Int J Oral Maxillofac Implants 2019;34:673–80. https://doi.org/10.11607/jomi.6929.

[462] Canullo L, Micarelli C, Lembo-Fazio L, Iannello G, Clementini M. Microscopical and microbiologic characterization of customized titanium abutments after different cleaning procedures. Clin Oral Implants Res 2014;25:328–36. https://doi.org/10.1111/clr.12089.

[463] Gehrke P, Tabellion A, Fischer C. Microscopical and chemical surface characterization of CAD/CAM zircona abutments after different cleaning procedures. A qualitative analysis. J Adv Prosthodont 2015;7:151–9. https://doi.org/10.4047/jap.2015.7.2.151.

[464] Nakajima K, Odatsu T, Shinohara A, Baba K, Shibata Y, Sawase T. Effects of cleaning methods for custom abutment surfaces on gene expression of human gingival fibroblasts. J Oral Sci 2017;59:533–9. https://doi.org/10.2334/josnusd.16-0681.

[465] Heimer S, Schmidlin PR, Roos M, Stawarczyk B. Surface properties of polyetheretherketone after different laboratory and chairside polishing protocols. J Prosthet Dent 2017;117:419–25. https://doi.org/10.1016/j.prosdent.2016.06.016.

[466] Elawadly T, Radi IAW, El Khadem A, Osman RB. Can PEEK Be an Implant Material? Evaluation of Surface Topography and Wettability of Filled Versus Unfilled PEEK With Different Surface Roughness. J Oral Implantol 2017;43:456–61. https://doi.org/10.1563/aaid-joi-D-17-00144.

[467] Karthigeyan S, Ravindran AJ, Bhat RTR, Nageshwarao MN, Murugesan SV, Angamuthu V. Surface Modification Techniques for Zirconia-Based Bioceramics: A Review. J Pharm Bioallied Sci 2019;11:S131–4. https://doi.org/10.4103/JPBS.JPBS_45_19.

[468] Guo L, Smeets R, Kluwe L, Hartjen P, Barbeck M, Cacaci C, et al. Cytocompatibility of Titanium, Zirconia and Modified PEEK after Surface Treatment Using UV Light or Non-Thermal Plasma. Int J Mol Sci 2019;20:5596. https://doi.org/10.3390/ijms20225596.

[469] Tuna T, Wein M, Swain M, Fischer J, Att W. Influence of ultraviolet photofunctionalization on the surface characteristics of zirconia-based dental implant materials. Dent Mater 2015;31:e14-24. https://doi.org/10.1016/j.dental.2014.10.008.

[470] Yang Y, Zheng M, Liao Y, Zhou J, Li H, Tan J. Different behavior of human gingival fibroblasts on surface modified zirconia: A comparison between ultraviolet (UV) light and plasma. Dent Mater J 2019;38:756–63. https://doi.org/10.4012/dmj.2018-101.

[471] Han A, Ding H, Tsoi JKH, Imazato S, Matinlinna JP, Chen Z. Prolonged UV-C Irradiation is a Double-Edged Sword on the Zirconia Surface. ACS Omega 2020;5:5126–33. https://doi.org/10.1021/acsomega.9b04123.

[472] Jorba-García A, Figueiredo R, González-Barnadas A, Camps-Font O, Valmaseda-Castellón E. Accuracy and the role of experience in dynamic computer guided dental implant surgery: An in-vitro study. Med Oral Patol Oral Cir Bucal 2019;24:e76–83. https://doi.org/10.4317/medoral.22785.

[473] Gollner MG. Digital transformation: analog expertise and digital optimization. Int J Comput Dent 2022;25:407–19. https://doi.org/10.3290/j.ijcd.b3555715.

[474] Rutkunas V, Bukelskiene V, Sabaliauskas V, Balciunas E, Malinauskas M, Baltriukiene D. Assessment of human gingival fibroblast interaction with dental implant abutment materials. J Mater Sci Mater Med 2015;26:169. https://doi.org/10.1007/s10856-015-5481-8.

[475] Fischer NG, Wong J, Baruth A, Cerutis DR. Effect of Clinically Relevant CAD/CAM Zirconia Polishing on Gingival Fibroblast Proliferation and Focal Adhesions. Materials (Basel) 2017;10:1358. https://doi.org/10.3390/ma10121358.

[476] Kimura Y, Matsuzaka K, Yoshinari M, Inoue T. Initial attachment of human oral keratinocytes cultured on zirconia or titanium. Dent Mater J 2012;31:346–53. https://doi.org/10.4012/dmj.2011-189.

[477] Dickson MA, Hahn WC, Ino Y, Ronfard V, Wu JY, Weinberg RA, et al. Human keratinocytes that express hTERT and also bypass a p16(INK4a)-enforced mechanism that limits life span become immortal yet retain normal growth and differentiation characteristics. Mol Cell Biol 2000;20:1436–47. https://doi.org/10.1128/MCB.20.4.1436-1447.2000.

[478] Salo T, Lyons JG, Rahemtulla F, Birkedal-Hansen H, Larjava H. Transforming growth factor-beta 1 up-regulates type IV collagenase expression in cultured human keratinocytes. J Biol Chem 1991;266:11436–41.

[479] Mäkelä M, Salo T, Larjava H. MMP-9 from TNF alpha-stimulated keratinocytes binds to cell membranes and type I collagen: a cause for extended matrix degradation in inflammation? Biochem Biophys Res Commun 1998;253:325–35. https://doi.org/10.1006/bbrc.1998.9641.

[480] Grenade C, De Pauw-Gillet M-C, Pirard C, Bertrand V, Charlier C, Vanheusden A, et al. Biocompatibility of polymer-infiltrated-ceramic-network (PICN) materials with Human Gingival Keratinocytes (HGKs). Dent Mater 2017;33:333–43. https://doi.org/10.1016/j.dental.2017.01.001.

[481] Emery RW, Merritt SA, Lank K, Gibbs JD. Accuracy of Dynamic Navigation for Dental Implant Placement-Model-Based Evaluation. J Oral Implantol 2016;42:399–405. https://doi.org/10.1563/aaid-joi-D-16-00025.

[482] Kim S-G, Lee W-J, Lee S-S, Heo M-S, Huh K-H, Choi S-C, et al. An advanced navigational surgery system for dental implants completed in a single visit: an in vitro study. J Craniomaxillofac Surg 2015;43:117–25. https://doi.org/10.1016/j.jcms.2014.10.022.

[483] Mediavilla Guzmán A, Riad Deglow E, Zubizarreta-Macho Á, Agustín-Panadero R, Hernández Montero S. Accuracy of Computer-Aided Dynamic Navigation Compared to Computer-Aided Static Navigation for Dental Implant Placement: An In Vitro Study. J Clin Med 2019;8. https://doi.org/10.3390/jcm8122123.

[484] Pellegrino G, Bellini P, Cavallini PF, Ferri A, Zacchino A, Taraschi V, et al. Dynamic Navigation in Dental Implantology: The Influence of Surgical Experience on Implant Placement Accuracy and Operating Time. An in Vitro Study. Int J Environ Res Public Health 2020;17. https://doi.org/10.3390/ijerph17062153.

[485] CONELOG Implant System by Camlog: the conical connection n.d. https://www.camlog.com/en/products/implant-systems/conelog/ (accessed November 29, 2021).

[486] Kang S-H, Lee J-W, Lim S-H, Kim Y-H, Kim M-K. Verification of the usability of a navigation method in dental implant surgery: in vitro comparison with the stereolithographic surgical guide template method. J Craniomaxillofac Surg 2014;42:1530–5. https://doi.org/10.1016/j.jcms.2014.04.025.

[487] Brief J, Edinger D, Hassfeld S, Eggers G. Accuracy of image-guided implantology. Clin Oral Implants Res 2005;16:495–501. https://doi.org/10.1111/j.1600-0501.2005.01133.x.

[488] García-Vives N, Andrés-García R, Rios-Santos V, Fernández-Palacín A, Bullón-Fernández P, Herrero-Climent M, et al. In vitro evaluation of the type of implant bed preparation with osteotomes in bone type IV and its influence on the stability of two implant systems. Med Oral Patol Oral Cir Bucal 2009;14:e455-460.

[489] Farina R, Pramstaller M, Franceschetti G, Pramstaller C, Trombelli L. Alveolar ridge dimensions in maxillary posterior sextants: a retrospective comparative study of dentate and edentulous sites using computerized tomography data. Clin Oral Implants Res 2011;22:1138–44. https://doi.org/10.1111/j.1600-0501.2010.02087.x.

[490] Padhye NM, Bhatavadekar NB. Quantitative Assessment of the Edentulous Posterior Maxilla for Implant Therapy: A Retrospective Cone Beam Computed Tomographic Study. J Maxillofac Oral Surg 2020;19:125–30. https://doi.org/10.1007/s12663-019-01236-7.

[491] Shemtov-Yona K. Quantitative assessment of the jawbone quality classification: A meta-analysis study. PLoS One 2021;16:e0253283. https://doi.org/10.1371/journal.pone.0253283.

[492] Papathanasiou I, Kamposiora P, Papavasiliou G, Ferrari M. The use of PEEK in digital prosthodontics: A narrative review. BMC Oral Health 2020;20:217. https://doi.org/10.1186/s12903-020-01202-7.

[493] de Araújo Nobre M, Moura Guedes C, Almeida R, Silva A, Sereno N. Hybrid Polyetheretherketone (PEEK)-Acrylic Resin Prostheses and the All-on-4 Concept: A Full-Arch Implant-Supported Fixed Solution with 3 Years of Follow-Up. J Clin Med 2020;9:2187. https://doi.org/10.3390/jcm9072187.

[494] Beretta M, Poli PP, Pieriboni S, Tansella S, Manfredini M, Cicciù M, et al. Peri-Implant Soft Tissue Conditioning by Means of Customized Healing Abutment: A Randomized Controlled Clinical Trial. Materials (Basel) 2019;12:3041. https://doi.org/10.3390/ma12183041.

[495] Lin C-Y, Chen Z, Pan W-L, Wang H-L. Impact of timing on soft tissue augmentation during implant treatment: A systematic review and meta-analysis. Clin Oral Implants Res 2018;29:508–21. https://doi.org/10.1111/clr.13148.

[496] Mijiritsky E. Plastic temporary abutments with provisional restorations in immediate loading procedures: a clinical report. Implant Dent 2006;15:236–40. https://doi.org/10.1097/01.id.0000230306.93399.d0.

[497] Mijiritsky E, Mardinger O, Mazor Z, Chaushu G. Immediate provisionalization of single-tooth implants in fresh-extraction sites at the maxillary esthetic zone: up to 6 years of follow-up. Implant Dent 2009;18:326–33. https://doi.org/10.1097/ID.0b013e31819ecaaa.

[498] Ghoul WE, Chidiac JJ. Prosthetic requirements for immediate implant loading: a review. J Prosthodont 2012;21:141–54. https://doi.org/10.1111/j.1532-849X.2011.00819.x.

[499] Gallucci GO, Hamilton A, Zhou W, Buser D, Chen S. Implant placement and loading protocols in partially edentulous patients: A systematic review. Clin Oral Implants Res 2018;29 Suppl 16:106–34. https://doi.org/10.1111/clr.13276.

[500] Chaushu L, Naishlos S, Rosner O, Zenziper E, Glikman A, Lavi D, et al. Changing Preference of One- Vs. Two-Stage Implant Placement in Partially Edentulous Individuals: An 18-Year Retrospective Study. Applied Sciences 2020;10:7060. https://doi.org/10.3390/app10207060.

[501] Drake DR, Paul J, Keller JC. Primary bacterial colonization of implant surfaces. Int J Oral Maxillofac Implants 1999;14:226–32.

[502] Quirynen M, Bollen CM, Papaioannou W, Van Eldere J, van Steenberghe D. The influence of titanium abutment surface roughness on plaque accumulation and gingivitis: short-term observations. Int J Oral Maxillofac Implants 1996;11:169–78.

[503] Bürgers R, Gerlach T, Hahnel S, Schwarz F, Handel G, Gosau M. In vivo and in vitro biofilm formation on two different titanium implant surfaces. Clin Oral Implants Res 2010;21:156–64. https://doi.org/10.1111/j.1600-0501.2009.01815.x.

[504] Dikova T, Dzhendov DA, Ivanov D, Bliznakova K. Dimensional accuracy and surface roughness of polymeric dental bridges produced by different 3D printing processes. Archives of Materials Science and Engineering 2018;2:65–75. https://doi.org/10.5604/01.3001.0012.8660.

[505] Kurahashi K, Matsuda T, Ishida Y, Ichikawa T. Effect of polishing protocols on the surface roughness of polyetheretherketone. J Oral Sci 2020;62:40–2. https://doi.org/10.2334/josnusd.18-0473.

[506] Fokas G, Guo CY, Tsoi JKH. The effects of surface treatments on tensile bond strength of polyether-ketone-ketone (PEKK) to veneering resin. J Mech Behav Biomed Mater 2019;93:1–8. https://doi.org/10.1016/j.jmbbm.2019.01.015.

[507] Lee K-S, Shin M-S, Lee J-Y, Ryu J-J, Shin S-W. Shear bond strength of composite resin to high performance polymer PEKK according to surface treatments and bonding materials. J Adv Prosthodont 2017;9:350–7. https://doi.org/10.4047/jap.2017.9.5.350.

[508] Shim JS, Kim J-E, Jeong SH, Choi YJ, Ryu JJ. Printing accuracy, mechanical properties, surface characteristics, and microbial adhesion of 3D-printed resins with various printing orientations. J Prosthet Dent 2020;124:468–75. https://doi.org/10.1016/j.prosdent.2019.05.034.

[509] Ivanovski S, Lee R. Comparison of peri-implant and periodontal marginal soft tissues in health and disease. Periodontol 2000 2018;76:116–30. https://doi.org/10.1111/prd.12150.

[510] Han Y, Yan Y, Lu C. Ultraviolet-enhanced bioactivity of ZrO2 films prepared by micro-arc oxidation. Thin Solid Films 2009;517:1577–81. https://doi.org/10.1016/j.tsf.2008.09.064.

[511] Att W, Takeuchi M, Suzuki T, Kubo K, Anpo M, Ogawa T. Enhanced osteoblast function on ultraviolet light-treated zirconia. Biomaterials 2009;30:1273–80. https://doi.org/10.1016/j.biomaterials.2008.11.024.

[512] Watanabe H, Saito K, Kokubun K, Sasaki H, Yoshinari M. Change in surface properties of zirconia and initial attachment of osteoblastlike cells with hydrophilic treatment. Dent Mater J 2012;31:806–14. https://doi.org/10.4012/dmj.2012-069.

[513] Razali M, Ngeow WC, Omar RA, Chai WL. An In-Vitro Analysis of Peri-Implant Mucosal Seal Following Photofunctionalization of Zirconia Abutment Materials. Biomedicines 2021;9:78. https://doi.org/10.3390/biomedicines9010078.

[514] Al Qahtani WMS, Schille C, Spintzyk S, Al Qahtani MSA, Engel E, Geis-Gerstorfer J, et al. Effect of surface modification of zirconia on cell adhesion, metabolic activity and proliferation of human osteoblasts. Biomed Tech (Berl) 2017;62:75–87. https://doi.org/10.1515/bmt-2015-0139.

[515] Flanagan D. Photofunctionalization of Dental Implants. J Oral Implantol 2016;42:445–50. https://doi.org/10.1563/aaid-joi-D-15-00145.

[516] Moon IS, Berglundh T, Abrahamsson I, Linder E, Lindhe J. The barrier between the keratinized mucosa and the dental implant. An experimental study in the dog. J Clin Periodontol 1999;26:658–63. https://doi.org/10.1034/j.1600-051x.1999.261005.x.

[517] Ogawa T. Ultraviolet photofunctionalization of titanium implants. Int J Oral Maxillofac Implants 2014;29:e95-102. https://doi.org/10.11607/jomi.te47.

[518] Roffel S, Wu G, Nedeljkovic I, Meyer M, Razafiarison T, Gibbs S. Evaluation of a novel oral mucosa in vitro implantation model for analysis of molecular interactions with dental abutment surfaces. Clin Implant Dent Relat Res 2019;21 Suppl 1:25–33. https://doi.org/10.1111/cid.12750.

[519] Riivari S, Shahramian K, Kangasniemi I, Willberg J, Narhi T. TiO2-Modified Zirconia Surface Improves Epithelial Cell Attachment. The International Journal of Oral & Maxillofacial Implants 2019;34:313–9. https://doi.org/10.11607/jomi.6862.

[520] Rigolin MSM, de Avila ED, Basso FG, Hebling J, de S Costa CA, Mollo Junior F de A. Effect of different implant abutment surfaces on OBA-09

epithelial cell adhesion. Microsc Res Tech 2017. https://doi.org/10.1002/jemt.22941.

[521] Sabaliauskas V, Juciute R, Bukelskiene V, Rutkunas V, Trumpaite-Vanagiene R, Puriene A. In vitro evaluation of cytotoxicity of permanent prosthetic materials. Stomatologija 2011;13:75–80.

[522] Baltriukienė D, Sabaliauskas V, Balčiūnas E, Melninkaitis A, Liutkevičius E, Bukelskienė V, et al. The effect of laser-treated titanium surface on human gingival fibroblast behavior. J Biomed Mater Res A 2014;102:713–20. https://doi.org/10.1002/jbm.a.34739.

[523] Echeverria C, Torres MDT, Fernández-García M, de la Fuente-Nunez C, Muñoz-Bonilla A. Physical methods for controlling bacterial colonization on polymer surfaces. Biotechnology Advances 2020;43:107586. https://doi.org/10.1016/j.biotechadv.2020.107586.

[524] Zhao B, van der Mei HC, Subbiahdoss G, de Vries J, Rustema-Abbing M, Kuijer R, et al. Soft tissue integration versus early biofilm formation on different dental implant materials. Dent Mater 2014;30:716–27. https://doi.org/10.1016/j.dental.2014.04.001.

[525] Barbour ME, O'Sullivan DJ, Jenkinson HF, Jagger DC. The effects of polishing methods on surface morphology, roughness and bacterial colonisation of titanium abutments. J Mater Sci Mater Med 2007;18:1439–47. https://doi.org/10.1007/s10856-007-0141-2.

[526] Verran J, Boyd RD. The relationship between substratum surface roughness and microbiological and organic soiling: A review. Biofouling 2001;17:59–71. https://doi.org/10.1080/08927010109378465.

[527] Happe A, Röling N, Schäfer A, Rothamel D. Effects of different polishing protocols on the surface roughness of Y-TZP surfaces used for custom-made implant abutments: a controlled morphologic SEM and profilometric pilot study. J Prosthet Dent 2015;113:440–7. https://doi.org/10.1016/j.prosdent.2014.12.005.

[528] Sawase T, Wennerberg A, Hallgren C, Albrektsson T, Baba K. Chemical and topographical surface analysis of five different implant abutments. Clin Oral Implants Res 2000;11:44–50. https://doi.org/10.1034/j.1600-0501.2000.011001044.x.

[529] Martins de Barros RR, Provinciatti MM, Muglia VA, Novaes AB. The Effect of Laser-Lok Abutments on Fiber Orientation and Buccal Bone Remodeling: A Histomorphometric Study. Int J Periodontics Restorative Dent 2020;40:73–81. https://doi.org/10.11607/prd.4426.

[530] John G, Schwarz F, Kravchenko A, Ommerborn MA, Becker J. Effectivity of homecare and professional biofilm removal procedures on initial supragingival biofilm on laser-microtextured implant surfaces in an ex vivo model. Int J Implant Dent 2021;7:51. https://doi.org/10.1186/s40729-021-00326-x.

[531] Ponsonnet L, Reybier K, Jaffrezic N, Comte V, Lagneau C, Lissac M, et al. Relationship between surface properties (roughness, wettability) of titanium and titanium alloys and cell behaviour. Materials Science and Engineering: C 2003;23:551–60. https://doi.org/10.1016/S0928-4931(03)00033-X.

[532] Garcia B, Camacho F, Peñarrocha D, Tallarico M, Perez S, Canullo L. Influence of plasma cleaning procedure on the interaction between soft tissue and abutments: a randomized controlled histologic study. Clin Oral Implants Res 2017;28:1269–77. https://doi.org/10.1111/clr.12953.

[533] Blázquez-Hinarejos M, Ayuso-Montero R, Álvarez-López J-M, Manzanares-Céspedes M-C, López-López J. Histological differences in the adherence of connective tissue to laser-treated abutments and standard abutments for dental implants. An experimental pilot study in humans. Med Oral Patol Oral Cir Bucal 2017;22:e774–9. https://doi.org/10.4317/medoral.21949.

[534] Ghinassi B, D'Addazio G, Di Baldassarre A, Femminella B, Di Vincenzo G, Piattelli M, et al. Immunohistochemical Results of Soft tissues Around a New Implant Healing-Abutment Surface: A Human Study. J Clin Med 2020;9:1009. https://doi.org/10.3390/jcm9041009.

[535] Schwarz F, Mihatovic I, Becker J, Bormann KH, Keeve PL, Friedmann A. Histological evaluation of different abutments in the posterior maxilla and mandible: an experimental study in humans. J Clin Periodontol 2013;40:807–15. https://doi.org/10.1111/jcpe.12115.

[536] Blanca MJ, Alarcón R, Arnau J, Bono R, Bendayan R. Non-normal data: Is ANOVA still a valid option? Psicothema 2017;29:552–7. https://doi.org/10.7334/psicothema2016.383.

[537] Stünkel R, Zeller A-N, Bohne T, Böhrnsen F, Wedi E, Raschke D, et al. Accuracy of intraoral real-time navigation versus static, CAD/CAM-manufactured pilot drilling guides in dental implant surgery: an in vitro study. Int J Implant Dent 2022;8:41. https://doi.org/10.1186/s40729-022-00430-6.

[538] Stefanelli LV, Mandelaris GA, Franchina A, Di Nardo D, Galli M, Pagliarulo M, et al. Accuracy Evaluation of 14 Maxillary Full Arch Implant Treatments Performed with Da Vinci Bridge: A Case Series. Materials (Basel) 2020;13:2806. https://doi.org/10.3390/ma13122806.

SANTRAUKA

SANTRUMPŲ SĄRAŠAS

CAD/CAM – kompiuterinis modeliavimo ir gamybos metodas
CCP – įprastas plovimo protokolas
D – distalinis
DICOM – skaitmeninis vaizdavimas ir ryšiai medicinoje
DLP – skaitmeninis šviesos apdorojimas
DMSO – dimetilsulfoksidas
EMAX – ličio disilikato stiklo keramika „e.max"
FCS – fetalinis veršelio serumas
FDI – pasaulio odontologų federacija (prac. *Fédération Dentaire Internationale*)
FDM – lydyto nusėdimo modeliavimas
FOV – matymo laukas
HD – aukštos raiškos
HGF – žmogaus dantenų fibroblastai
IMDM – Iskovo modifikuota Dulbeco terpė (angl. *Iscove's Modified Dulbecco's Medium*)
IOS – intraoralinis skeneris (skenavimas)
KT – kompiuterinė tomografija
K1 – *Kennedy* I klasės defektas
K2 – *Kennedy* II klasės defektas
K3 – *Kennedy* III klasės defektas
M – mezialinis
MD – meziodistalinis
MRI – magnetinio rezonanso vaizdavimas (tyrimas)
MTT – 3-(4,5-dimetiltiazol-2-il-)-2,5-difeniltetrazolio bromidas
MVT – Monte Karlo metodas, skirtas p reikšmės korekcijai
NICE – ličio disilikato stiklo keramika „n!ce"
OD – optinis tankis (angl. *optical density*)
PEEK – polietereterketonas
PEKK – polieterketonketonas
PL – „*Porgressive-line*" implantų dizainas
PMMA – polimetilmetakrilatas
PMMA-Bre – frezuojamas „*Bredent*" polimetilmetakrilatas

PMMA-Ker – frezuotas „*Kerox*" polimetilmetakrilatas
PMMA-3D – trimačiu būdu spausdintas polimetilmetakrilatas
POI – dominantis taškas
RCP – tyrimo plovimo protokolas
Sa – vidutinis paviršiaus ploto šiurkštumas
SN – standartinis nuokrypis (angl. *SD*)
SL – „*Screw-line*" implantų dizainas
SLA – stereolitografija
SLS – selektyvus lazerinis sukepinimas
STL – standartinė šablonų biblioteka, standartinė trikampio kalba, stereolitografija
Ti – titanas
TKT – tūrinė kompiuterinė tomografija
UV-C – ultravioletinė spinduliuotė, kurios bangos ilgis 200–290 nm
WCA – vandens kontaktinis kampas
ZrO – cirkonio oksido (ZrO_2, arba tiesiog cirkonio) keramika
ZrO-HT – didelio skaidrumo cirkonio oksido keramika
ZrO-UTML – ypač skaidri daugiasluoksnė cirkonio oksido keramika
ZrO-V – lauko špatu dengta cirkonio oksido keramika
ŽDF – žmogaus dantenų fibroblastai
3D – trimatis

ĮVADAS

IŽANGA

Sparčiai besivystančių technologijų dėka, mes gyvename itin įdomiu ir dinamišku laikotarpiu. Šiuolaikinė odontologija ir medicina ne tik siekia stabdyti ligą ir naikinti jos padarinius, bet kartu ir atkurti paciento gyvenimo kokybę, įskaitant funkciją ir estetiką. Tokia tendencija stebima įvairiose tarpusavyje susijusiose galvos ir kaklo medicinos disciplinose, įskaitant, bet neapsiribojant, burnos, veido ir žandikaulių chirurgija, ortognatine chirurgija, odontologija, ortopedija, onkologija. Bendras siekis skatina mažinti tarpdisciplininį barjerą, dalintis žiniomis, tobulinti gydymo protokolus ir jų įgyvendinimą. Todėl vis labiau tampa akivaizdi gydymo planavimo, kaip atskiro etapo, svarba ir tiksliausias įmanomas to plano įgyvendinimas. Tai dažnai reikalauja gebėjimo sklandžiai jungti gydymo etapus, kurie istoriškai buvo atskirti pagal klasikinę nomenklatūrą. Taigi, šiuolaikinio mokslo šviesoje svarbūs tampa ne tik atskiri įrodymais pagrįsti dėmenys, bet ir visas vientisas gydymo procesas – nuo chirurgijos iki funkcijos ir estetikos.

Trimatės (3D) skaitmeninės technologijos atveria naujas galimybes odontologijoje ir medicinoje šiems tikslams pasiekti [1–5]. Šiandien inovacijos sparčiai vystosi ir įsilieja į kasdieninę gydytojo praktiką, nešdamos naudą tiek pacientui, tiek ir gydytojui [6–8]. Tūrinė kompiuterinė tomografija (TKT), intraoralinis skenavimas (IOS), kompiuterinis modeliavimo ir gamybos metodas (*CAD/CAM*) jau tapo įprastos technologijos praktikoje, siekiant didesnio tikslumo, laiko našumo, paciento saugumo ir estetinių lūkesčių išpildymo [1,9–12]. Be to, dantų implantacija jau tapo plačiai taikoma ir patikima gydymo metodika tiek dalinai, tiek pilnai bedančių pacientų reabilitacijai, kurios ilgalaikio funkcionavimo rodikliai siekia iki 99 % [13–15]. Skaitmeninės technologijos gali būti taikomos įvairiuose paciento gydymo dantų implantais etapuose: nuo diagnostikos, planavimo ir chirurgijos iki protezavimo ir gydymo tikslumo vertinimo [1,3]. Negana to, įvairios pažangios technologijos įtraukiamos ir į aukšto biologinio suderinamumo medžiagų vystymą, kurio galutinis pritaikymo tikslas yra į pacientą orientuotos aukščiausios kokybės sveikatos priežiūros paslaugos [16]. Taigi, akivaizdu, technologinis progresas ne tik apima pavienius aspektus, bet ir iš esmės didina bendrą sinergiją tarp chirurginio ir restauracinio gydymo etapų. Tai tiek idėjiškai, tiek ir praktiškai lemia augančius gydymo standartus, mažėjančią atskirtį tarp implantų įsriegimo ir sėkmingo jų protezavimo. Ši auganti sinergija stebima ne tik mokslinių

tyrimų tendencijose, bet ir praktikoje: nuo vienmomentės implantacijos ir ne-atidėliotino protezavimo, tęsiant skaitmeniniu būdu suplanuota implantacija ir baigiant individualizuotomis gijimo galvutėmis bei vienu-kartu viena-atrama (angl. *one-time one-abutment*) koncepcijomis [17–23].

Visa tai kartu įgalina tikslių skaitmeninių dantų implantologijos ir protezavimo protokolų kūrimą, skiriant ypatingą dėmesį biologijai, funkcijai ir estetikai. Nepaisant labai greito technologijų tobulėjimo, šių protokolų klinikinis taikymas reikalauja mokslu pagrįstų įrodymų [12]. Daugeliu atvejų publikuoti tyrimai vertina tik vieną protokolo aspektą arba mažą visos gydymo eigos dalį [24]. Taip pat neretai nurodoma, jog netikslumai tokiame, skaitmena pagrįstame, procese gali kilti tiek kiekviename individualiame žingsnyje, tiek jų sąveikoje [25]. Šie pastebėjimai pabrėžia tyrimų svarbą ir poreikį, kartu siekiant išaiškinti ir galimus įtaką darančius veiksnius. Šio tyrimo tikslas yra įvertinti du esminius tokios darbo eigos etapus: skaitmeniniu būdu suplanuoto implantų pozicionavimo 3D tikslumą ir minkštųjų audinių ląstelių reakciją į protezinio komponento medžiagas.

Vienas iš svarbiausių kriterijų, lemiančių sėkmingą dantų implantų įsriegimą, yra teisingas implantų padėties parinkimas kauliniame audinyje, atsižvelgiant į biologines ir anatomines sąlygas [26]. Ypač svarbu atsižvelgti į pažeidimams jautrias gretimas anatomines struktūras (nervai, gretimi dantys, prienosiniai ančiai, kraujagyslės ir pan.) [27]. Neteisingai parinkta dantų implantų 3D padėtis yra neretai pasitaikanti klaida, kuri kai kuriais atvejais gali lemti sudėtingas komplikacijas, įskaitant estetines, ir iššūkius ieškant jų sprendimo [28–30]. Todėl pastaraisiais dešimtmečiais vis didesnis dėmesys skiriamas dantų implantų padėčiai, vadovaujantis ne tik biologiniais, bet ir protezavimo kriterijais [31]. Navigavimas dantų implantologijoje tampa vis labiau įprastu įrankiu, siekiant užtikrinti tikslią implantų padėtį, o kartu ir paciento saugumą [32,33]. Dantų implantacija, taikant naviguojančias priemones, užtikrina kur kas tikslesnius implanto padėties rezultatus, lyginant su implantavimu laisva ranka [34–37]. Išskiriami du pagrindiniai navigavimo būdai: statinis ir dinaminis [24]. Pirmasis, statinis, metodas yra dažniau sutinkamas praktikoje ir yra pagrįstas *CAD/CAM* būdu pagamintu (dažniausiai 3D spausdintu) chirurginiu šablonu (gidu) [38]. Antrasis metodas pagrįstas grąžto sekimu (dažniausiai ekrane) realiuoju laiku su grįžtamuoju ryšiu, naudojant paciento TKT vaizdus [39]. Abiem atvejais galima tiek pilnai naviguota (su implanto įsriegimu), tiek ir belopė implantacija [6]. Dinaminis navigavimas yra santykinai nauja technologija klinikinėje praktikoje, lyginant su statiniais gidais [24]. Tačiau jis turi unikalų pranašumą – nuolatinį sekimą

realiu laiku ir galimybę keisti pradinį planą, atsižvelgiant į chirurginės procedūros metu galimai paaiškėjusias nenumatytas aplinkybes [40]. Nors vis daugiau tyrimų nagrinėja gidinės implantacijos tikslumą, tik nedidelė dalis jų vertina veiksnius, darančius įtaką šiam tikslumui [40,41].

Dauguma tyrimų, vertinančių implantų pozicijos tikslumą, naudoja pooperacinę TKT [39,42,43]. Priešoperacinis TKT skenavimas su numatyta implantų padėties informacija (planas) yra sulygiuojamas su pooperaciniu TKT skenavimu, kuriame matoma reali implantų padėtis [42]. Tačiau metodas turi trūkumų. Pagrindinis – papildomos paciento apšvitos jonizuojančia spinduliuote (rentgeno spinduliais) poreikis, kuris turi menką klinikinį pagrįstumą ar naudą pacientui [42,44]. Rizikos ir naudos santykis yra ypač svarbus bioetikos, o kartu ir gydymo principas – pirmiausia nepakenkti (lot. *primum non nocere*). Be to, taikant šį metodą, implantų pooperacinės padėties nustatymo tikslumas yra neigiamai veikiamas periimplantinių vaizdo artefaktų [44]. Visa tai taip pat pastebėta ir naujausiose literatūros apžvalgose – siūloma ieškoti implantų pozicionavimo tikslumo vertinimo metodų, nereikalaujančių rentgeno apšvitos [39,42,45].

Palanki implantų padėtis įgalina neatidėliotiną protezavimą, kuris gerina pacientų gyvenimo kokybę ir kartu jau tapo viena iš sėkmingo gydymo siekiamybių, atsižvelgiant į situaciją [46–49]. Naujausi moksliniai tyrimai patvirtina tokį protezavimą, kaip kliniškai sėkmingą [17,47–49]. Kaulinio audinio atsakas į danties implantą ir osteointegracijos procesas yra išsamiai nagrinėtos temos, todėl šiuo metu vis daugiau tyrimų skiriama implantus supantiems minkštiesiems audiniams, kaip svarbiai dedamajai, siekiant užtikrinti norimus ilgalaikius estetinius ir funkcinius rezultatus [50–54]. Įrodyta, kad minkštųjų audinių kiekis ir kokybė yra svarbus veiksnys kaulo stabilumui aplink implantus [55]. Šiuo metu periimplantinių minkštųjų audinių sveikatos tema patiria esminį pokytį – vis daugiau dėmesio skiriama visam virškauliniam kompleksui, susidedančiam iš minkštųjų audinių ir implanto transmukozinio elemento [23,56]. Klinikinių tyrimų duomenys pagrindžia neatidėliotino implanto protezavimo svarbą siekiant palankiausio estetinio rezultato [57]. Sveiki minkštieji audiniai (daugiausia dantenos) formuoja barjerą, kuris saugo implantą supantį kaulą nuo žalingų veiksnių ir sukuria sąlygas pacientui užtikrinti gerą asmeninę higieną [58]. Jei šis barjeras pažeidžiamas, galiausiai tai lemia kaulinio audinio netekimą, prastėjančią estetiką ir netgi implanto praradimą kraštutiniu atveju [54,59].

Skirtingos medžiagos ir jų paviršiai turi nevienodas minkštųjų audinių biologinio suderinamumo savybes [60]. Šiuo metu rinkoje atsiranda vis

daugiau protezinių medžiagų, įskaitant ir naujos kartos polimerus bei 3D spausdintas medžiagas [20,61]. Šių medžiagų paviršiai yra įvairiais būdais modifikuojami: skirtingi paviršiaus poliravimo protokolai, įvairūs plovimo metodai, fotofunkcionalizacija naudojant ultravioletinę spinduliuotę, aktyvavimas plazma, lazerinis apdorojimas ir dar daug kitų metodų [62]. Esama nedaug tyrimų, kurie vienoda metodika vertina skirtingas neatidėliotino protezavimo medžiagas bei paviršius, jų savybes ir tuo pačiu biologinį suderinamumą su minkštaisiais audiniais. Trūkstant palyginamų bazinių tyrimų rezultatų, sudėtinga toliau interpretuoti ir aptarti šių medžiagų klinikinį pritaikomumą. Taigi, siekiant užtikrinti palankų gijimą ir galutinį gydymo rezultatą, duomenys apie minkštųjų audinių atsaką į protezines medžiagas yra ne mažiau svarbūs nei tiksli implanto 3D padėtis kaule.

TYRIMO TIKSLAI

I. Ištirti ir įvertinti skaitmeniniu būdu suplanuoto dantų implantavimo tikslumą.

II. Įvertinti žmogaus dantenų fibroblastų reakciją į medžiagas, skirtas neatidėliotinam implantų protezavimui.

TYRIMO UŽDAVINIAI

1. Ištirti dinaminės navigacijos technologijos 3D tikslumą skaitmeniniu būdu suplanuotam dantų implantavimui, įvertinant dantų implantų dizaino, dantų lanko bedančio defekto konfigūracijos ir implantų pozicijos įtaką.

2. Įvertinti dinaminiu ir statiniu metodais nukreipiamo dantų implantų pozicionavimo 3D tikslumą.

3. Įvertinti dinaminės navigacijos implantacijos 3D tikslumą, lyginant sekimo registravimą naudojant dantis ir atskaitos objektus.

4. Ištirti žmogaus dantenų fibroblastų atsaką į neatidėliotinam protezavimui skirtas polimerines medžiagas, įvertinant jų paviršiaus šiurkštumą, hidrofiliškumą ir plovimo protokolo įtaką.

5. Ištirti žmogaus dantenų fibroblastų atsaką į keramines medžiagas, skirtas neatidėliotinam protezavimui, įvertinant jų paviršiaus šiurkštumą ir hidrofiliškumą.

6. Ištirti cirkonio oksido keramikos paviršiaus aktyvavimo UV spinduliuote įtaką žmogaus dantenų fibroblastų atsakui.

Tyrime pagrindinis dėmesys skiriamas dantų implantacijos chirurginio ir protezavimo etapų sinergijai. Tai apima dvi modernaus gydymo eigos temas: tikslų 3D implantų pozicionavimą ir po to sekančio neatidėliotino protezavimo medžiagų biologinį suderinamumą. Šie aspektai yra svarbūs nuo pat pirmųjų implantacijos minučių, pirminio žaizdos gijimo, iki ilgalaikės supančių kietųjų bei minkštųjų audinių sveikatos ir stabilumo. Tokia kompleksinė tema atspindi gydymo eigos konceptualumą bei pabrėžia klasikinę biologijos ir anatomijos svarbą, tačiau taip pat siekia pažangaus gydymo, skirto savalaikiam paciento funkcijos ir estetikos atkūrimui.

Atliekamas tyrimas taiko ir vertina inovatyvias skaitmenines 3D technologijas, atitinkančias naujausias mokslinių tyrimų ir klinikinės praktikos tendencijas. Šis tyrimas nagrinėja skaitmeninių įrankių pritaikomumo ir tikslumo klausimus. Rezultatai reikšmingai prisideda prie įrodymais pagrįsto naujų technologijų naudojimo implantologijoje ir protezavime. Svarbu paminėti, jog moksliniame darbe vertinami įvairūs veiksniai, lemiantys nukreiptos implantacijos tikslumą: navigavimo metodas (statinis ir dinaminis), dinaminio metodo registravimo būdas (dantys ar atskaitos objektai), bedančio defekto konfigūracija (*Kennedy* I, II ir III klasės), implantų dizainas (mažiau ir daugiau kūginis), implantų pozicija (mezialinė ir distalinė). Tai yra vienas esminių tyrimo naujumo aspektų. Didelė dalis šių veiksnių anksčiau nebuvo nagrinėta. Todėl iki šiol duomenų šioje srityje trūko ir jie buvo nevienareikšmiai, ribojantys klinikinių žinių gilinimą. Mokslinis tyrimas leidžia įvertinti tikslumo klausimą pagal vientisą protokolą, užtikrinant nuoseklumą ir objektyvumą. Toks požiūris svariai prisideda prie palankiausios gydymo strategijos nustatymo pacientui.

Didelė dalis atliktų sisteminių apžvalgų pabrėžia implantacijos tikslumo vertinimo metodų poreikį, kurie būtų orientuoti į paciento radiacinę saugą. Šis tyrimas yra vienas iš pirmųjų, vertinančių pilnai naviguojamos implantacijos tikslumą IOS pagrindu. Toks tikslumo vertinimo metodas yra racionalesnis ir saugesnis pacientui, lyginant su iki šiol naudotais metodais. Neabejotinai tai yra svarbi ateities odontologijos dedamoji.

Tyrimo aktualumą papildo žmogaus dantenų fibroblastų atsako į protezinių komponentų medžiagas vertinimas, atsižvelgiant į jų paviršiaus parametrus. Tai papildo odontologinėje praktikoje vyraujančią tendenciją, kai siekiant išvengti antro chirurginio etapo pasirenkamas neatidėliotinas proteazavimas

arba fiksuojamas dantenas formuojantis transmukozinis elementas. Tai įmanoma tik esant tiksliai implanto padėčiai ir palankiai klinikinei situacijai. Vienas iš pagrindinių šio darbo naujumo kriterijų yra tai, jog tiriamas labai didelis protezinių medžiagų skaičius, nuo polimerų (įskaitant inovatyvius, 3D spausdintus bei aukštos kokybės polimerus) iki titano ir įvairių keramikos rūšių. Nors esama publikacijų, kuriose vertinama viena ar kelios medžiagos ir vienas ar keli paviršiaus kriterijai, tačiau retai įtraukiamas minkštųjų audinių ląstelių atsako vertinimas. Šis tyrimas vienu metu vertina paviršiaus paruošimą ir jo įtaką šiurkštumui, vandens kontaktiniam kampui, žmogaus dantenų fibroblastų gyvybingumui bei proliferacijai. Šios žinios įgalina išsamesnį neatidėliotinos protezinės medžiagos pasirinkimo klinikinėje praktikoje vaizdą, atsižvelgiant į mažiau ištirtą minkštųjų audinių ląstelių reakciją.

Darbe taip pat vertinama protezinių medžiagų paviršių plovimo metodo, o taip pat ir paviršiaus aktyvavimo ultravioletu (fotofunkcionalizacija) įtaka. Abu aspektai yra mažai nagrinėti kituose moksliniuose tyrimuose ir prisideda prie šio tyrimo naujumo.

Apibendrinant, tyrimas yra reikšmingas indėlis į naujų skaitmeninių 3D technologijų tikslumo implantologijos srityje ir neatidėliotino protezavimo medžiagų biologinio suderinamumo aspektus. Tyrimas svariai prisideda prie įrodymais pagrįsto tikslaus skaitmeniniu būdu planuotos dantų implantacijos ir protezavimo sampratos bei klinikinių protokolų tobulinimo.

GINAMIEJI TEIGINIAI

1. Statinė ir dinaminė dantų implantacijos navigacija pasižymi aukštu dantų implantų pozicionavimo tikslumu.

2. Dinaminės navigacijos registravimas atskaitos objektų pagrindu yra palanki alternatyva tiksliai implantų padėčiai pasiekti.

3. Neatidėliotino protezavimo medžiaga ir paviršius turi įtakos žmogaus dantenų fibroblastų atsakui.

4. Protezinės medžiagos paviršiaus plovimo protokolas turi įtakos paviršiaus šiurkštumui, vandens kontaktiniam kampui ir žmogaus dantenų fibroblastų gyvybingumui.

5. Cirkonio oksido keramikos paviršiaus modifikavimas aktyvuojant UV spinduliais yra potencialus būdas keisti žmogaus dantenų fibroblastų atsaką.

1. MEDŽIAGOS IR METODAI

1.1. IMPLANTŲ POZICIONAVIMO, TAIKANT NAVIGACIJĄ, TIKSLUMO VERTINIMAS

1.1.1. MODELIAI

Viršutinio žandikaulio modeliai, imituojantys I tipo kaulinį audinį (D1 pagal *Lekholm ir Zarb*), buvo pagaminti poliuretano dervos pagrindu (*Modralit® 3K Set, Dreve Dentamid GmbH*, Unna, Vokietija). Šiuose modeliuose buvo simuliuojami galinių dantų grupės bedančiai defektai, kurių atstatymui reikalinga dviejų implantų atrama daliniam fiksuotam protezui. Vieno bedančio krūminio danties defektas, atstatomas pavieniu vainikėliu ant implanto, buvo pasirinktas kaip kontrolinė grupė. Modelių medžiagos rentgeno kontrastiškumas buvo koreguotas pridedant BaSO4 (97 %, milteliai 1–4 mikronų, *Alfa Aesar, ThermoFisher (Kandel) GmbH*, Vokietija) maksimaliai imituojant gyvo žmogaus TKT skenavimo duomenis (vidutinio ploto Hounsfildo vienetai). Minkštųjų audinių komponentas buvo imituotas silikoninėmis dantenomis (*frasaco GmbH, Tettnang*, Vokietija). Šioje tyrimo dalyje buvo naudoti trijų tipų modeliai (1 pav.):

- *Kennedy* I (K1) – abipusių galinių bedančių defektų sritys, apimančios prieškrūminius ir krūminius dantis (FDI dantų numeriai: 17, 16, 15, 14 ir 24, 25, 26, 27).
- *Kennedy* II (K2) – vienpusio galinio bedančio defekto sritis, apimanti dešinės pusės prieškrūminius ir krūminius dantis (FDI dantų numeriai: 17, 16, 15, 14).
- *Kennedy* III – dvi galinių bedančių defektų sritys:
  a) Kairės pusės bedančio defekto sritis (K3), apimanti abu prieškrūminius ir pirmąjį krūminį dantį (FDI dantų numeriai: 24, 25, 26).
  b) Vieno dešinės pusės pirmojo krūminio danties (K3, *single*) bedantis defektas (FDI danties numeris 16).

Visi modeliai eksperimentų metu buvo tvirtai įmontuoti fantomo galvoje (*ClaroNav Inc., Toronto, Ontario*, Kanada), siekiant simuliuoti kliniškai artimesnį implantavimo scenarijų tek dinaminei, tiek ir statinei navigacijai.

| K1 | K2 | K3 |

1 pav. Tyrime naudoti viršutinio žandikaulio modeliai.

Kampo paklaida (angl. *angle*) buvo pasirinkta kaip pagrindinis rezultato kintamasis, siekiant apskaičiuoti imties dydį. Jis buvo apskaičiuotas naudojant G*Power 3.1 (*Heinrich-Heine Universität, Düsseldorf*, Vokietija). Visos imties dydis buvo nustatytas 72, atsižvelgiant į 0,80 dydžio statistinę galią, 5 % alfa paklaidą ir 0,4 efekto dydį pagal ankstesnius tyrimus [324,472].

1.1.2. SKAITMENINIS PLANAVIMAS

Kiekvienam modeliui buvo atlikti keturi TKT skenavimai (*KaVo OP3D, KaVo Dental, Biberach an der Riss*, Vokietija) ir keturi IOS skenavimai (*Trios4, 3Shape, Copenhagen*, Danija). TKT skenavimas buvo atliekamas taikant 0,2 mm vokselio dydį. Kiekviena TKT buvo užkoduota ir atsitiktinai suporuota su vienu iš keturių IOS skenavimų. Patyręs technikas (H.P.), taikant *SMOP* programinę įrangą (*Swissmeda AG, Baar*, Šveicarija), atliko implantų pozicijų planavimą, atsižvelgdamas į standartinius implantų padėties santykio reikalavimus (skaitmeniniu būdu patvirtintus odontologo):

- Planuojamo protezo padiktuota implanto padėtis su implanto varžto išėjimo anga per centrinę duobutę būsimame vainike;
- Minimalus atstumas tarp implanto ir gretimo danties 1,5 mm;
- Minimalus atstumas tarp dviejų implantų 3 mm;
- Minimalus atstumas nuo žandinės/liežuvinės dervinio modelio sienelės 1,5 mm;
- Implantai pozicionuojami ~ 1 mm žemiau kaulo lygio;
- Paraleli implantų numatytų tiltiniam protezui tarpusavio padėtis (0 laipsnių).

Tyrimui parinktų implantų parametrai, ilgis ir diametras, yra aprašyti lentelėje (1 lentelė).

1 lentelė. Implantų, taikytų tyrime, parametrai. Naudotos *CONELOG Screw-line* ir *Progressive-line* implantų sistemos (*Camlog Biotechnologies AG,* Bazelis, Šveicarija).

Pozicija (FDI numeris)	Diametras	Ilgis	Lygiagretumas
***Kennedy* I klasės defektas**			
Pirmas prieškrūminis (#14)	3.8 mm	11 mm	Taip
Antras krūminis (#17)	4.3 mm	13 mm	Taip
***Kennedy* II klasės defektas**			
Pirmas prieškrūminis (#14)	3.8 mm	11 mm	Taip
Antras krūminis (#17)	4.3 mm	13 mm	Taip
***Kennedy* III klasės defektas**			
Pirmas prieškrūminis (#24)	3.8 mm	11 mm	Taip
Pirmas krūminis (#26)	4.3 mm	13 mm	Taip
***Kennedy* III klasės vieno danties defektas**			
Pirmas krūminis (#16)	4.3 mm	13 mm	-

Kiekvienas planas buvo atsitiktinai paskirtas vienai implantų dizaino grupei:

- Mažo kūgio savisriegis (*CONELOG Screw-line, Camlog Biotechnologies AG*, Bazelis, Šveicarija) – SL grupė;
- Didesnio kūgio savisriegis (*CONELOG Progressive-line, Camlog Biotechnologies AG*) – PL grupė.

Tokiu būdu kiekvienai modelio situacijai (*Kennedy* klasei) buvo sudaryti 4 skirtingi skaitmeniniai implantacijos planai, kurie buvo išsaugoti kaip stereolitografiniai (STL) failai.

1.1.3. IMPLANTŲ POZICIONAVIMAS
### TAIKANT STATINĘ NAVIGACIJĄ

Naudojant skaitmeninio plano informaciją, statinės navigacijos chirurginio gido *CAD* dizainas buvo sukurtas su *ImplantStudio* programine įranga (*3Shape*, Kopenhaga, Danija), įtraukiant skersines sijas tvirtumui ir okliuzinius langus nusėdimo tikslumui įvertinti. Tuomet gidai buvo atspausdinti 3D būdu su *DLP* tipo spausdintuvu *Asiga Pro* 4K UV385 (*Asiga, Alexandria*, Australija). Dervinė medžiaga metakrilato pagrindu *Asiga DentaGUIDE* (*Asiga Pty Ltd, Alexandria*, Australija) naudota 3D spausdinimui, laikantis visų gamintojo nurodymų. Ši medžiaga yra CE sertifikuota I klasės medicinos prietaisų gamybai. Atlikus 3D spausdinimo procesą, chirurginiai gidai buvo toliau kruopščiai nuplauti, apdoroti ir baigti pagal gamintojo pateiktas instrukcijas (*Instructions for use (IFU); DentaGUIDE; Part Number / 04504*). Vėliau,

atsižvelgiant į skaitmeninį planą buvo įdėtos nukreipiančiosios gido metalinės movos: 3,8 mm ir 4,3 mm dydžio atitinkamai planui (katalogo numeriai J3734.3803, J3754.3801; J3734.4303, J3754.4301). Iš viso tyrimui buvo pagaminti 36 statinės navigacijos gidai (12 kiekvienam *Kennedy* atvejui).

Implantacijos procedūra toliau buvo atlikta laikantis gamintojo instrukcijose nurodomos standartinės gidinės grąžtų sekos, skirtos kieto kaulinio audinio (D1) atvejams, įskaitant ir grąžtus, skirtus tankiam kaului (katalogo numeriai J5068.3811, J5068.4313; J5068.4313, J5068.4313). Prieš įvedant implantus, vienu metu buvo paruoštos visos implantų ložės. Implantai buvo įsriegti per gidą pagal pilnai nukreipiantį implantacijos protokolą, užtikrinantį gylio ir rotacijos padėtį pagal movą ir joje esančią žymę. Įsriegus visus implantus, buvo nusuktos įvedimo detalės ir išimtos kartu su gidu, tokiu būdu įgalinant tolimesnį modelio ir implantų pozicijų vertinimą.

1.1.4. IMPLANTŲ POZICIONAVIMAS TAIKANT DINAMINĘ NAVIGACIJĄ

Dinaminei navigacijai taikyta *Navident* sistema (*ClaroNav Inc., Toronto, Ontario*, Kanada). Buvo naudojamas ant fantomo fiksuojamas *Navident* sistemos galvos žymeklis (angl. *head tracker*) ir standartinis penkių taškų sekimo registravimo protokolas (2 pav.), remiantis gamintojo instrukcijomis [345]. Pagal kiekvieną implantacijos planą buvo pakartojamos 3 dinaminės navigacijos implantacijos sesijos, taigi bendras modelio *Kennedy* situacijai tenkančių sesijų skaičius buvo 12.
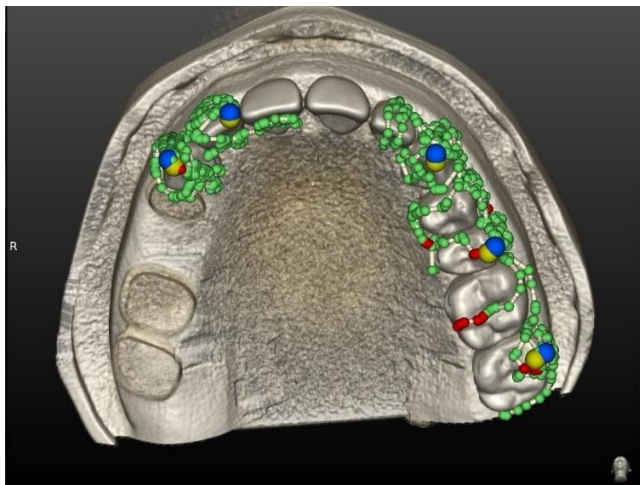
2 pav. Sekimo registravimas *Navident* navigacijos sistema, naudojant 5 atskaitos taškus (pažymėti mėlyna spalva).

Implantų ložės paruošimui iš esmės laikytasi tų pačių gamintojų instrukcijų ir taikyti tie patys grąžtai kaip ir statinės navigacijos metodo atveju (2.1.3), įskaitant ir tankaus kaulo grąžtus. Vienintelė išimtis buvo taikoma pradiniams (pilotiniams, angl. *pilot*) grąžtams: vietoje pilnos sekos (nuo trumpiausio iki viso ilgio), buvo taikomas iš karto viso ilgio sukalibruotas pradinis grąžtas, remiantis standartinės dinaminės navigacijos procedūros principais. Implanto sriegimas taip pat buvo atliekamas naudojant dinaminę navigaciją sukalibravus jo viršūnę, taigi išpildant pilnai nukreiptos implantacijos koncepciją. Pasiekus suplanuotą implanto gylį, rotacija buvo vizualiai sugretinama atsižvelgiant į artimiausią įvedėjo žymę ir implantacijos planą kompiuterio ekrane. Tuomet visos įvedimo detalės buvo nuimtos ir modelis toliau analizuotas tikslumo vertinimo etape.

1.1.5. TIKSLUMO VERTINIMAS

Pooepracinių implantų padėčių tikslumas buvo vertinamas taikant inovatyvų neinvazinį ir nereikalaujantį rentgeno apšvitos metodą IOS pagrindu (*3Shape*). Pirmiausia implantų skenavimo kūnai (katalogo numeris C2600.4310) buvo fiksuojami ant implantų iš karto po jų įsriegimo, o po to sekė skenavimas IOS (*Trios4, 3Shape*). Tuomet *3Shape* programinės įrangos pagalba skaitmeninis skenavimo kūnas buvo sulygiuojamas taikant standartinį trijų taškų metodą, tokiu būdu buvo užfiksuojama informacija apie pooperacines implantų padėtis (3 pav.).


3 pav. Trijų taškų metodas skirtas skaitmeninio skenavimo kūno sulygiavimui su pooperaciniu IOS vaizdu ir tokiu būdu gaunama informacija apie realizuotas implantų padėtis skaitmeninės įrangos pagalba (*3shape*).

Vėliau suplanuota (priešoperacinė) implantų padėties informacija buvo lyginama su įgyvendinta (pooperacine) implantų padėties informacija taikant tą pačią programinę įrangą. Viso buvo apskaičiuojamos penkių tipų paklaidos:
- **Įvesties taško** (angl. *insertion point*) – atstumas tarp dviejų implantų platformų centro taškų. Tai 3D nuokrypio įvertis (4-A pav.).

- **Gylio (r)** (angl. *depth (s)*) – gylio nuokrypis (teigiamos ir neigiamos vertės) parodo vertikalią implanto paklaidą, lyginant su suplanuota implanto padėtimi. Apskaičiuojama projektuojant implanto platformos centrą ant suplanuoto implanto centro ašies. Paveiksle 4-B implantų ašys pavaizduotos mėlynomis linijomis, projektuojamas (geltona punktyrinė linija) įvesties taškas pažymėtas papildomu oranžiniu tašku ir matuojamas atstumas (gylio klaida) pažymėtas ištisine geltona linija suplanuotos implanto padėties ašyje. Jei įsriegtas implantas giliau nei suplanuota – klaida įgyja neigiamą vertę, priešingu atveju – teigiamą.
- **Gylio (a)** (angl. *depth (u)*) – absoliuti gylio nuokrypio vertė (tik teigiamos vertės).
- **Horizontali paklaida** (angl. *horizontal*). Apskaičiuojama randant trumpiausią atstumą tarp suplanuoto implanto platformos centro ir realios implanto padėties centro ašies. Tai atstumas tarp dviejų oranžinių taškų pažymėtas ištisine geltona linija 4-C paveiksle.
- **Kampo paklaida** (angl. *angle*). Apskaičiuojama randant mažiausią kampą tarp dviejų implantų centro ašių. Šis kampas pažymėtas 4-D paveiksle.


| Figure 7-A | Figure 7-B | Figure 7-C | Figure 7-D |
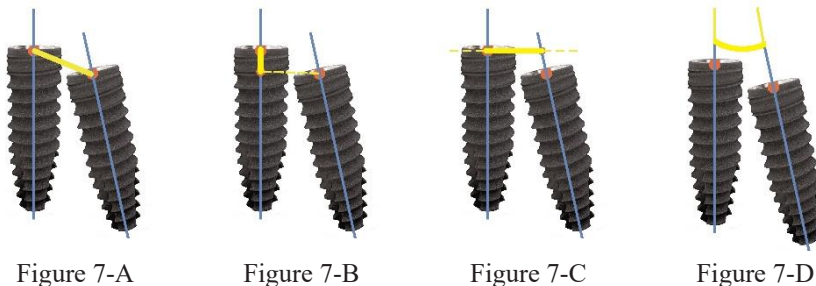
4 pav. Tyrime vertintos paklaidų rūšys. A – įvesties taško; B – gylio; C – horizontali; D – kampo. Implanto iliustracija kairėje kiekvieno paveikslo dalyje atspindi suplanuotą implanto poziciją, o dešinėje – po operacijos realizuotą implanto poziciją, kuri yra vertinama.

1.1.6. DINAMINĖS NAVIGACIJOS TIKSLUMO VERTINIMAS TAIKANT DU SKIRTINGUS REGISTRAVIMO METODUS

Kennedy I klasės (Kennedy1) modelis buvo naudotas kaip aprašyta anksčiau (3.1.1) ir lygintas su pilnai bedančio viršutinio žandikaulio modelio situacija, kurio pagrinde buvo fiksuoti penki tikslios apibrėžties ir tolygiai paskirstyti atskaitos objektai – 3 mm skersmens ir 3 mm ilgio cilindrai (5 pav.). Implantų padėties planavimas Kennedy1 grupei buvo atliktas pagal tą patį anksčiau

aprašytą protokolą (2.1.2), tačiau šiuo atveju buvo planuojamas abipusis atstatymas, todėl viso suplanuoti 4 implantai kiekvienam atvejui (2 lentelė). Pilnai bedančio modelio situacijai taip pat buvo planuojami 4 implantai tokių pačių matmenų kaip ir Kennedy1 grupei (2 lentelė). Tačiau galiniai implantai buvo palenkti 30 laipsnių kampu priekinių implantų atžvilgiu (5 pav.; atitinkamai pagal *COMFOUR™* koncepciją) [473].
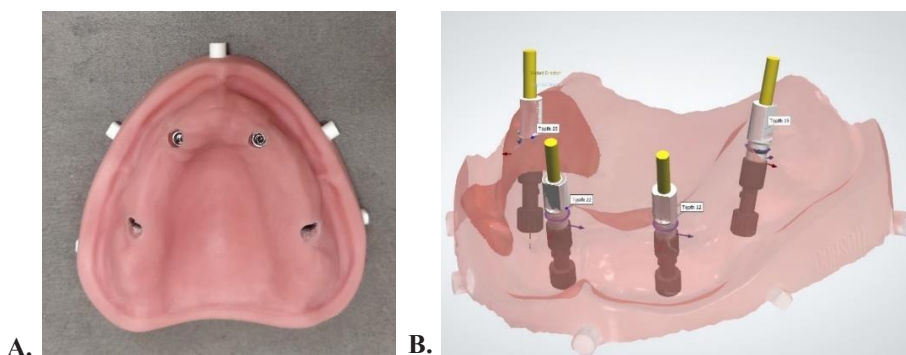
5 pav. Tyrime naudotas bedantis modelis su atskaitos objektais. A – bedantis modelis su implantais, įsriegtais dinaminės navigacijos pagalba. B – IOS gautas vaizdas su skaitmeniniais skenavimo kūnais sulygiuotais po implantacijos, siekiant įvertinti procedūros tikslumą.

2 lentelė. Dinaminės navigacijos tikslumo tyrimo dalyje naudotų implantų matmenys, taikant du skirtingus sekimo registravimo metodus (dantys – Kennedy1 grupėje ir atskaitos objektai – pilnai bedančio modelio grupėje).

Pozicija (FDI numeris)	Diametras	Ilgis	Lygiagretumas
Kennedy I klasės defektas (atskaita – dantys)			
Antras dešinys krūminis (#17)	4,3 mm	13 mm	Taip
Pirmas dešinys prieškrūminis (#14)	3,8 mm	11 mm	Taip
Pirmas kairys prieškrūminis (#24)	3,8 mm	11 mm	Taip
Antras kairys krūminis (#27)	4,3 mm	13 mm	Taip
Bedantis (atskaitos objektai)			
Antras dešinys prieškrūminis (#15)	4,3 mm	13 mm	Palenktas 30° kampu
Antras dešinys kandis (#12)	3,8 mm	11 mm	Taip
Antras kairys kandis (#22)	3,8 mm	11 mm	Taip
Antras kairys prieškrūminis (#25)	4,3 mm	13 mm	Palenktas 30° kampu

Navident galvos žymeklis ir sekimo registravimas pagal penkis taškus buvo naudojami (2.1.4), atsižvelgiant į gamintojo nurodomą protokolą [345]. Kennedy1 grupės atveju priekiniai dantys buvo naudoti registracijos procesui, o tuo tarpu bedančio žandikaulio atveju – atskaitos objektai. Tolesni implantavimo ir tikslumo vertinimo žingsniai atitiko anksčiau aprašytą protokolą (3.1.4 ir 3.1.5).

1.2. SKIRTINGŲ PROTEZINIŲ MEDŽIAGŲ IR JŲ PAVIRŠIŲ BEI ŽMOGAUS DANTENŲ LĄSTELIŲ ATSAKO VERTINIMAS

Tirtos medžiagos (lentelė 3): titanas (Ti), aukšto skaidrumo (ZrO-HT) ir ypač aukšto skaidrumo daugiasluoksnė (ZrO-UTML) cirkonio oksido keramikos, ličio disilikato stiklo keramikos (NICE, EMAX), cirkonio oksido keramika dengta lauko špato keramika ir glazūra (ZrO-V), du tipai frezuojamo (PMMA-Bre, PMMA-Ker) ir 3D spausdintas polimetilmetakrilatas (PMMA-3D), polietereterketonas (PEEK) ir polieterketonketonas (PEKK). Imčių dydžiai šioje tyrimo dalyje buvo parinkti atsižvelgiant į išsamią literatūros analizę šia tema [437,474–476].

1.2.1. MĖGINIŲ RUOŠIMAS

Titano mėginiai buvo frezuojami naudojant *DATRON D5* odontologinę frezavimo sistemą (*DATRON AG, Mühltal*, Vokietija). PMMA-3D mėginiai buvo atspausdinti naudojant stereolitografinę (SLA) technologiją (*Form 2 printer, Formlabs, Somerville, MA,* JAV), ir toliau apdoroti pagal gamintojo instrukcijas.

Kiti keraminių ir polimerinių medžiagų grupių mėginiai pirmiausia buvo išfrezuoti į ilgus cilindrus, naudojant kompiuterinį skaitmeninio valdymo frezavimo apartą (*Vhf S1 Impression, vhf camfacture AG, Ammerbuch*, Vokietija), o toliau jie buvo supjaustyti trumpais tabletės formos cilindrais. Pjovimas atliktas taikant pjūklinį mikrotomą, aušinamą vandeniu (*Leica SP 1600, Leica Biosystems Nussloch GmbH, Nußloch*, Vokietija).

Cirkonio oksido keramikos grupės buvo išfrezuotos ir supjaustytos didesnio pradinio dydžio prieš sinterizavimą, siekiant kompensuoti dydžio pokytį atsižvelgiant į medžiagos susitraukimo koeficientą. ZrO ir EMAX grupių sinterizavimas krosnyje buvo atliekamas laikantis gamintojo instrukcijų. Tikslūs galutiniai mėginių matmenys po visų ruošimo etapų buvo: 2 mm aukščio ir 5 mm pločio cilindrai (6 pav.).

3 lentelė. Tyrime naudotos medžiagos.

Trumpi-nys	Medžiaga	Firminis pavadinimas	Gamintojas
Ti (teigiama kontrolė)	Komerciškai grynas 4 klasės titanas	CopraTi-4	*Whitepeaks Dental Solutions GmbH & Co. KG, Wesel*, Vokietija
ZrO-HT	Cirkonio oksido keramika (3 mol % itriu stabilizuoti (Y_2O_3) tetragoniniai cirkonio polikristalai)	KATANA™ Zirconia HT12	*Kuraray Noritake, Tokyo*, Japonija
ZrO-UTML	Cirkonio oksido keramika (5 mol % itriu stabilizuoti (Y_2O_3) tetragoniniai cirkonio polikristalai)	KATANA™ Zirconia UTML	*Kuraray Noritake, Tokyo*, Japonija
ZrO-V	Cirkonio oksido keramika (ZrO-UTML), užkepta lauko špato porcelianu (kalio-aluminosilikato stiklu) ir padengta glazūra	CERABIEN™ ZR , CERABIEN™ ZR FC Paste Stain	*Kuraray Noritake, Tokyo*, Japonija
NICE	Ličio aliuminosilikato stiklo keramika, sustiprina ličio disilikatu	n!ce®	*Straumann, Basel*, Šveicarija
EMAX	Ličio disilikato stiklo keramika	IPS e.max®	*Ivoclar Vivadent, Schaan*, Lichtenšteinas
PMMA-Ker	Polimetilmetakrilatas	E4K PMMA Premia	*Kerox Dental Ltd., St Sóskút*, Vengrija
PMMA-Bre	Polimetilmetakrilato kompozitas su keraminiais užpildais	breCAM. multiCOM	*Bredent, GmbH & Co KG, Senden*, Vokietija
PMMA-3D	Polimetilmetakrilatas (3D būdu atspausdintas iš metakrilinių oligomerų)	NextDent™ Crown and Bridge (C&B)	*NextDent B.V., Soesterberg*, Nyderlandai
PEEK	Polietereterketonas, sustiprintas keramikiniu užpildu	BioHPP®	*Bredent, GmbH & Co KG, Senden*, Vokietija
PEKK	Polieterketonketonas, sustiprintas titano dioksidu	Pekkton® ivory	*Cendres and Métaux, Biel/Bienne*, Šveicarija

ZrO-V grupės mėginiai buvo pagaminti iš ZrO-UTML, kuris toliau buvo veikiamas oro-abrazijos būdu su 50μm aliuminio (Al$_2$O$_3$) dalelėmis, veikiant 15 sekundžių 0,2 MPa spaudimu, 90° kampu ir 15 mm atstumu nuo paviršiaus. Nusmėliuoti mėginiai buvo nuplauti ultragarsinėje vonelėje (42000 vibracijų/sek, *Carrera 2505 PEARL Cosinus Ultrasonic Cleaner, Aquarius Deutschland GmbH, Düsseldorf*, Vokietija) su distiliuotu vandeniu (10 minučių) ir išdžiovinti ore. Po to jie buvo užkepti lauko špato keramika ir padengti glazūra pagal gamintojo nurodymus.
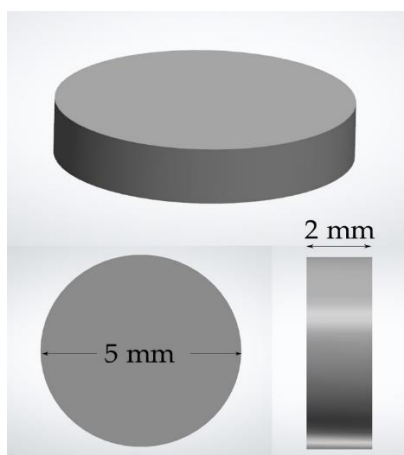
6 pav. Galutiniai mėginių, naudotų tyrime, matmenys.

1.2.2. PROFILOMETRIJA

Mėginių vidutinis paviršiaus šiurkštumas (Sa) buvo matuojamas 3D optiniu profilometru (*PLμ 2300, Sensofar, Sensofar Group, Barcelona*, Ispanija) su konfokaliniu objektyvu 50 × /0,8 A, matymo laukas (FOV) 255 × 191 μm (*Nikon Lu Plan, Nikon Metrology NV, Leuven*, Belgija). Tai buvo atliekama po visų paviršiaus apdorojimo ir plovimo procedūrų. Penki mėginiai iš kiekvienos grupės buvo atsitiktinai atrinkti ir kiekvieno mėginio 3 sričių atsitiktiniai vaizdai buvo fiksuojami (dvi sritys atsitiktinai pasirinktos mėginio periferijoje ir viena – centre). Mėginių vaizdai buvo apdoroti ir Sa vertės pamatuotos naudojant *Gwyddion* programinę įrangą (*Czech Metrology Institute, Jihlava*, Čekija).

1.2.3. VANDENS KONTAKTINIO KAMPO MATAVIMAS

Siekiant įvertinti paviršiaus hidrofiliškumą, vidutinis vandens kontaktinis kampas buvo pamatuotas kiekvienai medžiagos mėginių grupei. Po paviršių

apdorojimo ir plovimo mėginiai buvo patalpinti *Krüss EasyDrop* kontaktinio kampo testavimo įrenginyje (*KRÜSS GmbH, Hamburg*, Vokietija) ir dejonizuoto vandens lašeliai (16 Ω, 2 μL) buvo užlašinami ant mėginių. Lašelių nuotraukos ant paviršių fiksuotos po 10 sekundžių ir įvertintos naudojant *Krüss* programinę įrangą (*KRÜSS GmbH, Hamburg*, Vokietija). Kiekvienu atveju du matavimai (po vieną iš abejų lašo pusių) buvo pamatuoti ir apskaičiuotas jų vidurkis. Mėginių kameros temperatūra buvo nuolat palaikoma 21 °C naudojant *LabTech H50-500* vandens šaldytuvą (*LabTech Srl, Sorisole BG*, Italija). Penki mėginių paviršiai buvo atsitiktine tvarka parinkti iš kiekvienos medžiagos grupės, taigi viso gauti 5 matavimų rezultatai kiekvienai grupei.

1.2.4. ŽMOGAUS DANTENŲ LĄSTELĖS

Ląstelių kultūros augintos *IMDM* (Iskovo modifikuota Dulbeco terpė; *Gibco, Thermo Fisher Scientific, Waltham, MA*, JAV) su 10 % *FCS* (fetalinis veršelio serumas; *Gibco, Thermo Fisher Scientific, Waltham, MA*, JAV) ir antibiotikais (penicilinas, 100 VV/mL, ir streptomicinas, 100 μg/mL; *Gibco, Thermo Fisher Scientific, Waltham*, MA, JAV) 50 mL tūrio plastikiniuose flakonėliuose (*Greiner, Greiner Bio-One GmbH, Frickenhausen*, Vokietija). ŽDF ląstelės buvo auginamos inkubatoriuje (*Heracell™ 150i, Thermo Fisher Scientific, Waltham, MA*, JAV) at 37 °C, 5 % CO_2, 95 % H_2O).

Tyrime naudota pirminė monosluoksnė žmogaus dantenų fibroblastų (ŽDF; angl. *HGF*) kultūra. Šios ląstelės buvo gautos iš sveiko paciento, kuriam buvo atliekama standartinė periodontologinė chirurginė procedūra (Bioetikos komiteto leidimas NR. 158200-16-860-369). Ši metodika ir operacinė technika aprašyta ir naudota ankstesniuose tyrimuose [474]. Eksperimentuose naudoti ŽDF tarp 6 ir 12 pasažų. Ląstelės buvo persėjamos du kartus per savaitę, monosluoksnį disperguojant 0,25% EDTA-tripsino (etilendiamintetraacto rūgštis) tirpalu ir inkubuojant 37°C 2–10 min. Įvertinus mikroskopu suapvalėjusios ląstelės suspenduotos šviežioje augimo terpėje, apskaičiuotas tankis ir 15000–30000 ląstelių/mL persėtos į naujus flakonėlius.

Į epitelines panašių (angl. *epithelial-like*) žmogaus dantenų ląstelių pirminė kultūra buvo gauta iš kliniškai sveiko paciento ir spontaniškai imortalizuota, remiantis ankstesniuose moksliniuose tyrimuose publikuota metodika [477–480]. Į epitelines panašios žmogaus dantenų ląstelės prilipo ir augo vienu sluoksniu. Eksperimentuose naudotos ląstelės tarp 12 ir 14 pasažų. Palaipsniui užšaldytos šaldymo terpėje (70 % *IMDM* + 20 % *FCS* + 10 % DMSO (dimetilsulfoksidas, *Sigma-Aldrich, St. Louis, MI*, JAV)) ląstelės

laikytos -80 °C temperatūroje, šaldiklyje. Vėliau atšildžius, ląstelės užsėtos ant paruoštų kiekvienos medžiagos grupės mėginių.

1.2.5. CITOTOKSIŠKUMO IR PROLIFERACIJOS VERTINIMAS

Eksperimentams naudotos 96 šulinėlių plokštelės (*Greiner, Greiner Bio-One GmbH, Frickenhausen*, Vokietija). Paruošta ląstelių suspensija (30 × 10^3 ląstelių/mL) buvo pilama po 200 µL į kiekvieną plokštelės šulinėlį su paruoštais mėginiais (plačiau 2.2.6–2.2.8 skyriai). Citotoksiškumo vertinimui trys mėginiai iš kiekvienos medžiagos grupės buvo naudoti gyvybingų ląstelių skaičiui įvertinti po 12 valandų, lyginant santykį su tuo pačiu laiku užregistruotu neigiamos kontrolinės grupės (tuščias plastiko šulinėlis) skaičiumi. Proliferacijos vertinimui, trys mėginiai iš kiekvienos medžiagos grupės buvo naudojami kiekviename laiko taške (fiksuojama po 24, 48 ir 72 val.) ir taip pat naudojamas santykis su 24 val. neigiamos kontrolinės grupės skaičiumi. Tiek citotoksiškumo, tiek proliferacijos eksperimentai buvo kartojami 3 kartus.

Gyvybingų ląstelių kiekis buvo įvertinamas MTT (3-(4,5-dimetiltiazol-2-il-)-2,5-difeniltetrazolio bromidas) kolorimetrijos metodu. Kiekviename laiko atskaitos taške, ląstelių augimo terpė buvo atsargiai bei kruopščiai nusiurbta ir pašalinta iš kiekvieno šulinėlio, tuomet jis užpildytas 100 µL 1 mg/mL MTT (*Merck Chemicals, Merck KGaA, Darmstadt*, Vokietija), ištirpinto fosfatiniame buferiniame tirpale (*Medicago, Quabec City*, Kanada). Po 1 valandos inkubacijos termostate (37 °C, 5 % CO2) MTT nusiurbtas, o susidarę formazano kristalai ištirpinti 100 µl 96 % etanolyje (Vilniaus degtinė, Vilnius, Lietuva), tuomet 50 µl susidariusio tirpalo perkelta į švarius šulinėlius, kuriuose matuojamas optinis tankis (OD). Matavimai atlikti spektrofotometru (*Varioskan Flash, Thermo Scientific,, altham, MA*, JAV), naudojant 570 nm bangos ilgį tiek mėginiams, tiek ir tirpikliui (fonas). Iš gautų reikšmių apskaičiuotas skirtumas tarp tiriamojo mėginio bei tirpiklio OD. Gauta reikšmė yra proporcinga gyvų ląstelių kiekiui ant tiriamojo mėginio. Norint palyginti bandymus tarpusavyje, kiekvienos medžiagų grupės duobučių OD vidurkio reikšmė padalinta iš neigiamos kontrolinės grupės vidurkio (citotoksiškumo vertinime – 12 val.; proliferacijos – 24 val.).

Kai mėginio/kontrolės OD santykis (12 val. arba 24 val.) mažesnis už 1, tai rodo medžiagos slopinantį poveikį ląstelių augimui ir kuo žemesnė vertė – tuo stipresnis citotoksinis poveikis. Jei santykio vertė didesnė nei 1 – medžiaga skatina ląstelių augimą ir laikoma palankia bei necitotoksiška.

1.2.6. POLIMERINIŲ MEDŽIAGŲ VERTINIMAS

Penkių tipų polimerinės medžiagos vertintos šioje tyrimo dalyje: polimetilmetakrilatas (PMMA-Ker), polimetilmetakrilato kompozitas (PMMA-Bre), 3D spausdintas polimetilmetakrilatas (PMMA-3D), polietereterketonas su keramikiniu užpildu (PEEK) ir polieterketonketonas su titano dioksidu (PEKK) (3 lentelė). Naudotos dvi teigiamos kontrolinės grupės: titanas (Ti) ir cirkonio oksido keramika (ZrO-HT). Viso buvo naudoti 84 mėginiai (12 mėginių kiekvienai grupei). Medžiagų paviršių vertinimui matuotas paviršiaus šiurkštumas (Sa), vandens kontaktinis kampas (*WCA*) ir žmogaus dantenų fibroblastų (ŽDF) proliferacija.

1.2.6.1. POLIMERINIŲ MEDŽIAGŲ PAVIRŠIAUS POLIRAVIMAS

Kiekvienas mėginio paviršius buvo poliruojamas vadovaujantis gamintojo protokolu (4 lentelė). Prieš kiekvieną tolimesnį tyrimo eksperimentą, mėginiai buvo iš naujo poliruojami pagal tą patį protokolą.

1.2.6.2. POLIMERINIŲ MEDŽIAGŲ PAVIRŠIAUS PLOVIMAS

Po poliravimo kiekvienos grupės mėginiai atsitiktinai paskirsčius plauti dviem skirtingais plovimo metodais siekiant pašalinti paviršiaus užterštumą.

Standartinis plovimo protokolas (*CCP*): 10 minučių dezinfekuota „*Perform* 2 %" (*Schülke & Mayr GmbH, Norderstedt*, Vokietija) tirpale, 30 sekundžių plauta vandentiekio vandeniu, 10 minučių veikta izopropanoliu (*Isopropyl alcohol (C_3H_8O), $\geq$ 99,7 %, Sigma-Aldrich, St. Louis, MI*, JAV), 3 minutes plauta ultragarsinėje vonelėje (42,000 vibracijų/sekundę, *Carrera 2505 PEARL Cosinus Ultrasonic Cleaner*) su distiliuotu vandeniu.

Tyrimo plovimo protokolas (*RCP*): mėginius išdėliojus į plokštelės duobutes ir į kiekvieną įpylus po 5 ml 10% „*Decon*" (*Decon Laboratories™ Decon 90™, Fisher Scientific, NH,* JAV) tirpalo vartyklėje (*Mini-Tumbling Table WT17, 25 rpm,* inklinacija 5°/10°, *Biometra GmbH, Göttingen*, Vokietija) purtyta 24 valandas, 20 kartų plauta vandentiekio vandeniu, 10 kartų distiliuotu vandeniu, 24 valandas veikta 70 % etanolio tirpalu.

Po plovimo mėginiai 24 valandas džiovinti kambario temperatūroje. Tie patys abiejų plovimo protokolų žingsniai kartoti prieš kiekvieną naują bandymą kiekvienam mėginiui.

**4 lentelė.** Medžiagų paviršių poliravimo protokolai taikyti kiekvienam mėginio paviršiui.

Medžiaga	Kiekvieno paviršiaus poliravimo protokolas			
Ti	*EVE (R22 Item No.: 1000)* baltas polyras 7000–10,000 min^{-1}/ 30 s *EVE Ernst Vetter GmbH, Keltern*, Vokietija	*EVE (CRP-R22m)* tamsiai mėlynas polyras 8000–15,000 min^{-1}/ 30 s *EVE Ernst Vetter GmbH*	*Zircopol* poliravimo pasta ir šepetėlis 10,000 min^{-1}/ 30 s *Feguramed GmbH, Buchen*, Vokietija	
ZrO-HT	*MPF Zmax* diskas (*Item No. 120-0001 Zmax Large Disc 22 × 4.5 mm*) 5000–10,000 min^{-1}/ 30 s *MPF Brush Co., Nicosia*, Kipras	*Edenta* (*R1530HP*) *StarGloss* rožinis keramikos polyras 5000 min^{-1}/ 30 s *EDENTA AG, Au/St. Gallen*, Šveicarija	Edenta (R1540HP) *StarGloss* žalias keramikos polyras 5000 min^{-1}/ 30 s *EDENTA AG*	*Zircopol* poliravimo pasta ir šepetėlis 10,000 min^{-1}/ 30 s *Feguramed GmbH*
PMMA-Ker, PMMA-Bre, PMMA-3D	*BREDENT* vidutinio šiurkštumo pilkas polyras (*REF P243HM10*) 10,000–15,000 min^{-1}/ 30 s *Bredent medical GmbH & Co.KG, Senden*, Vokietija	*BREDENT* pemza ir šepetėlis 5000–10,000 min^{-1}/ 30 s *Bredent medical GmbH & Co.KG*	*SILADENT TEK-1 POL* deimantinė poliravimo pasta ir medvilninis šepetėlis 10,000 min^{-1}/ 30 s *Siladent Dr. Böhme & Schöps GmbH, Goslar*, Vokietija	
PEEK, PEKK	*BREDENT* vidutinio šiurkštumo pilkas polyras (*REF P243HM10*) 10,000–15,000 min^{-1}/ 30 s *Bredent medical GmbH & Co.KG*	*Zircopol* poliravimo pasta ir šepetėlis 10,000 min^{-1}/ 30 s *Feguramed GmbH*		

1.2.7. CIRKONIO PAGRINDO KERAMINĖS MEDŽIAGOS
IR FOTOFUNKCIONALIZAVIMAS

Dvi ZrO protezinės medžiagos pasirinktos šiai tyrimo daliai: ZrO-HT ir ZrO-UTML (3 lentelė). Kiekvienos tiriamos medžiagos buvo įtraukta po dvidešimt mėginių. Jie toliau atsitiktinai priskirti vienai iš grupių, remiantis paviršiaus apdorojimu, taigi viso po dešimt medžiagų kiekvienoje grupėje. Šioje tyrimo dalyje vertintas paruoštų paviršių šiurkštumas (Sa), vandens kontaktinis kampas (*WCA*) ir žmogaus dantenų fibroblastų (ŽDF) proliferacija.

1.2.7.1. CIRKONIO PAGRINDO KERAMINIŲ
MEDŽIAGŲ PAVIRŠIAUS PARUOŠIMAS

Visi paviršiai buvo poliruojami remiantis gamintojo nurodytais protokolais (5 lentelė). Prieš kiekvieną naują eksperimentą mėginiai buvo poliruojami iš naujo tuo pačiu protokolu. Tyrimo plovimo protokolas (*RCP*; 2.2.6.2) buvo taikytas po poliravimo mėginių plovimui, siekiant užtikrinti švarius paviršius (7 pav.). Po to mėginiai 24 valandas džiovinti kambario temperatūroje. Toks pat plovimo protokolas taikytas kaskart pieš naują tyrimo eksperimentą.
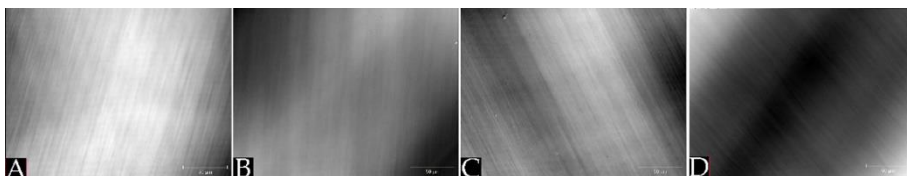
7 pav. Abiejų tirtų medžiagų paviršių profilometrijos vaizdai, demonstruojantys švarius paviršius be priemaišų. Medžiagos ir vaizdo lokacija: (**A**) ZrO-HT centre, (**B**) ZrO-HT periferijoje, (**C**) ZrO-UTML centre, (**D**) ZrO-UTML periferijoje.

1.2.7.2. PAVIRŠIAUS AKTYVAVIMAS UV SPINDULIUOTE

Dešimt mėgininių iš kiekvienos medžiagos grupės buvo atsitiktinai atrinkti ir jų paviršius aktyvuotas (fotofunkcionalizuotas, angl. *photofunctionalization*) UV spinduliais. Po plovimo mėginiai veikti UV-C šviesa (*Sylvania G15W T8* lempos*, Feilo Sylvania Group, Shanghai Feilo Acoustics Co., Budapest*, Vengrija) 253,7 nm bangos ilgiu 48 valandas 12 cm atstumu, vidutinė apšvita siekė 3,49 mW/cm^2. Prieš kiekvieną eksperimentą fotofunkcionalizacija buvo kartojama šioms dviem grupėms tuo pačiu protokolu.

1.2.8. KERAMINIŲ MEDŽIAGŲ VERTINIMAS

Šioje tyrimo dalyje vertintos penkios komercinės keraminės protezavimo medžiagos (ZrO-HT, ZrO-UTML, ZrO-V, NICE, EMAX) ir teigiamos kontrolės (Ti) grupė (3 lentelė). Viso buvo tiriama po 10 mėginių iš kiekvienos medžiagos grupės. Šioje tyrimo dalyje taip pat vertinta paruoštų paviršių Sa, *WCA* ir ŽDF proliferacija ir citotoksiškumas. Papildomai vertintas į epitelines panašių žmogaus dantenų ląstelių pirminės kultūros atsakas (proliferacija ir citotoksiškumas) į tiriamas protezines medžiagas.

Visi paviršiai buvo poliruoti laikantis gamintojų nurodytų protokolų (5 lentelė). Po to paviršiai buvo nuplauti taikant tyrimo plovimo protokolą (*RCP*; 2.2.6.2) ir mėginiai buvo palikti 24 valandas džiūti ore kambario temperatūroje. Prieš kiekvieną naują eksperimentą paviršiaus poliravimas ir plovimas buvo kartojamas tiksliai pagal tą patį protokolą.

5 lentelė. Titano ir keraminių medžiagų paviršių poliravimo protokolai naudoti tyrime.

Medžiaga	Kiekvieno paviršiaus poliravimo protokolas			
Ti	*EVE* (*R22 Item No.: 1000*) baltas polyras 7000–10000 min^{-1} 30 s *EVE Ernst Vetter GmbH, Keltern*, Vokietija	EVE (CRP-R22m) tamsiai mėlynas polyras 8000–15000 min^{-1} 30 s *EVE Ernst Vetter GmbH*	*Zircopol* poliravimo pasta ir šepetėlis 10000 min^{-1} 30 s *Feguramed GmbH, Buchen,* Vokietija	
ZrO-HT, ZrO-UMTL, ZrO-V	*MPF Zmax* diskas (*Item No. 120-0001 Zmax Large Disc 22 × 4.5 mm*) 5000–10000 min^{-1} 30 s *MPF Brush Co., Nicosia*, Kipras	*Edenta* (*R1530HP*) *StarGloss* rožinis keramikos polyras 5000 min^{-1} 30 s *EDENTA AG, Au/St. Gallen*, Šveicarija	*Edenta* (*R1540HP*) *StarGloss* žalias keramikos polyras 5000 min^{-1} 30 s *EDENTA AG*	*Zircopol* poliravimo pasta ir šepetėlis 10000 min^{-1} 30 s *Feguramed GmbH*
NICE, EMAX	*VITA SUPRINITY* poliravimo rinkinys *VI-SR 15m* 7000-12000 min^{-1} 30 s *VITA Zahnfabrik, H. Rauter GmbH & Co. KG, Bad Säckingen,* Vokietija	*VITA SUPRINITY* poliravimo rinkinys *VI-SR 15f* 4000-8000 min^{-1} 30 s *VITA Zahnfabrik, H. Rauter GmbH & Co. KG*	*Zircopol* poliravimo pasta ir šepetėlis 10000 min^{-1} 30 s *Feguramed GmbH*	

1.3. STATISTINĖ ANALIZĖ

Kiekvienam tyrimo etapui, kuriam buvo reikalingas atsitiktinis pasiskirstymas, buvo taikomas atviros prieigos internetinis instrumentas *www.randomlists.com*.

Statistinė analizė atlikta naudojant *R i386 4.0.0* programinę įrangą (*Lucent Technologies, Auckland*, Naujoji Zelandija). Grafikai buvo kuriami naudojant *ggplot2* įskiepį (*Lucent Technologies, Auckland,* Naujoji Zelandija). Statistinis reikšmingumo lygmuo buvo nustatytas $p < 0,05$. Duomenų normalumas buvo patikrintas ir parametriniai metodai buvo naudojami normalaus duomenų pasiskirstymo atveju; kitu atveju, buvo taikomi neparametriniai analizės metodai.

Duomenų normalumas ir dispersijos homogeniškumas buvo patikrinti grafiniu analizės metodu, papildant Šapiro–Vilko (angl. *Shapiro-Wilk*), Livyno (angl. *Levene*) ir F (angl. *F-test*) kriterijais. Nelygių dispersijų atveju, parametriniai testai buvo atitinkamai pritaikyti (pvz. *Welch ANOVA* ir *Games-Howell post hoc* kriterijus).

Norint palyginti dviejų grupių vidurkius, parametrinės analizės atveju buvo naudojamas dviejų nepriklausomų imčių dvipusis t-testas (angl. *independent samples t-test, two-tailed*). Neparametrinės dviejų grupių palyginimo analizės atveju taikytas dvipusis Vilkoksono rangų sumų kriterijus su normalumo aproksimacija (angl. *two-sample Wilcoxon test, two-tailed, with a normal approximation with continuity correction*).

Trijų ir daugiau grupių parametrinė analizė atlikta taikant vienfaktorinę arba daugiafaktorinę ANOVA (angl. *one-way; multi-way/ factorial ANOVA*). Nustačius reikšmingus skirtumus, buvo taikomi atitinkami *post hoc* ir porinių palyginimų metodai: Tjuko (angl. *Tukey*) ar poriniai kontrastai su p verčių Monte Karlo korekcija, pagrįsta daugiamačiu normaliuoju t-testo skirstiniu (MVT, angl. *pair-wise contrasts with Monte-Carlo corrected p-value based on multivariate normal t-test distribution*). Jei lygintos trys ir daugiau grupės neparametriškai, tuomet taikytas Kruskalio-Voliso (angl. *Kruskal-Wallis*) testas, vėliau jei nustatomi reikšmingi skirtumai – atliktas porinis palyginimas naudojant Vilkoksono rangų sumų kriterijų su p reikšmės koregavimu naudojant *Benjamini ir Hochberg* metodą.

2. REZULTATAI

2.1. IMPLANTŲ POZICIONAVIMO, TAIKANT DINAMINĘ NAVIGACIJĄ, TIKSLUMAS

Viso buvo įsriegti 84 implantai su vienodu skaičiaus pasiskirstymu visose grupėse. Įvesties taško paklaidos matavimai varijavo (ekstremumai) nuo 0,19 mm iki 1,71 mm. Gylio (r) paklaidų matavimai varijavo nuo -1,47 mm iki 0,74 mm. Gylio (a) – nuo 0,02 mm iki 1,47 mm. Horizontalios paklaidos matavimai varijavo nuo 0,09 mm iki 1,37 mm. Kampo paklaidos matavimai buvo pasiskirstę tarp 0,36° ir 6,17°. Vidutinės paklaidų vertės ir standartiniai nuokrypiai pagal bedančio defekto *Kennedy* klasės ir implanto dizaino grupes pateikiamos 6 lentelėje. Tolimesnė statistinė analizė (daugiafaktorinė ANOVA) kiekvienai paklaidos rūšiai buvo vertinama įtraukiant šiuos faktorius: *Kennedy* klasę (K1, K2, K3), implanto dizainas (SL, PL) ir pozicija (M, D). Įvesties taško, gylio (r) ir (a), horizontalios ir kampo paklaidų vidurkiai bei standartiniai nuokrypiai (SD) atitinkamai pavaizduoti 8, 9, 10, 11, 12 paveiksluose. Duomenų normalumas pasižymėjo nedideliais nuokrypiais nuo normaliojo skirstinio, todėl rezultatus reikėtų vertinti atsižvelgiant į tai. Statistiškai reikšmingi daugiafaktorinės ANOVA su post hoc porinių kontrastų (neįtraukiant K3 vieno danties defekto grupės) skirtumai ($p < 0.05$) pavaizduoti laužtiniais skliaustais virš grupių. Vieno danties defekto grupės (K3, *single*) duomenys tarp skirtingų implanto dizaino grupių buvo palyginti taikant t-testą ir statistiškai reikšmingi skirtumai pažymėti grafikuose tuo pačiu būdu.

Įvesties taško paklaidų analizė daugiafaktorine ANOVA parodė statistiškai reikšmingą sąveiką tarp implanto dizaino (SL, PL) ir pozicijos faktorių (M, D) ($p = 0,018$); post hoc analizė identifikavo, jog SL dizaino atveju mezialinė implanto padėtis lemia statistiškai reikšmingai mažesnes paklaidas nei distalinė ($p = 0,02$). *Kennedy* klasės faktoriaus įtaka buvo arti statistinio reikšmingumo lygmens ($p = 0,08$) daugiafaktorinėje ANOVA. Vieno danties defekto (*single*) implanto dizaino grupių vidurkių palyginimas t-testu neatskleidė reikšmingo skirtumo.

6 lentelė. Implanto padėties paklaidos atsižvelgiant į bedančių defektų *Kennedy* klasę ir implanto dizainą (vidurkiai ir standartiniai nuokrypiai). *Screw-line* (SL) – mažiau išreikšto kūgio implanto dizainas; *Progressive-line* (PL) – daugiau išreikšto.

Implanto dizaino grupė	Įvesties taško	Gylio (r)	Gylio (a)	Horizon-tali	Kampo
Kennedy **I klasės defektas**					
SL	1.0 ± 0.3	-0.6 ± 0.5	0.6 ± 0.5	0.7 ± 0.3	1.8 ± 0.8
PL	0.8 ± 0.4	-0.4 ± 0.7	0.6 ± 0.4	0.5 ± 0.2	2.4 ± 1.0
Kennedy **II klasės defektas**					
SL	0.9 ± 0.4	-0.1 ± 0.4	0.3 ± 0.3	0.7 ± 0.4	2.5 ± 1.4
PL	0.8 ± 0.4	-0.3 ± 0.6	0.5 ± 0.4	0.6 ± 0.3	3.6 ± 1.6
Kennedy **III klasės defektas**					
SL	0.6 ± 0.3	-0.3 ± 0.3	0.4 ± 0.2	0.4 ± 0.3	2.0 ± 1.2
PL	0.8 ± 0.4	-0.2 ± 0.6	0.5 ± 0.4	0.5 ± 0.3	1.9 ± 0.6
Kennedy **III klasės vieno danties defektas**					
SL	0.7 ± 0.3	-0.5 ± 0.4	0.5 ± 0.3	0.5± 0.2	1.0 ± 0.5
PL	0.7 ± 0.3	0.01 ± 0.3	0.2 ± 0.2	0.6 ± 0.3	2.0 ± 1.3
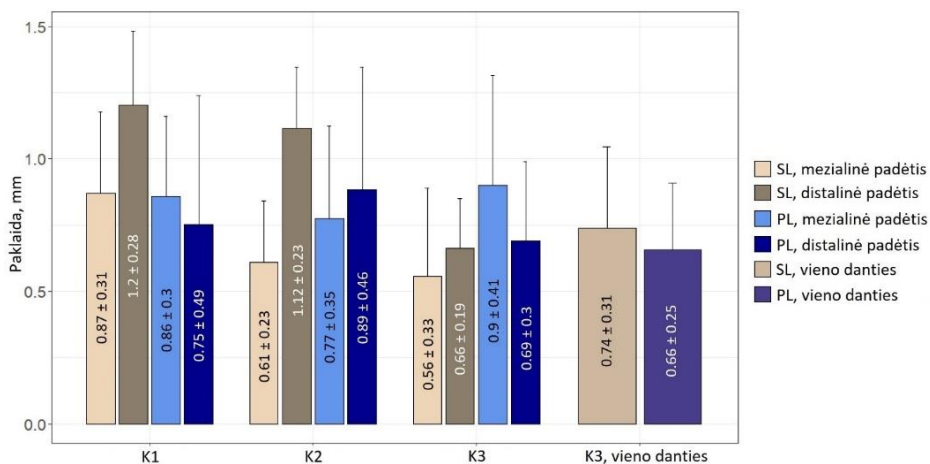
8 pav. Įvesties taško paklaidos (vidurkiai ir standartiniai nuokrypiai) atsižvelgiant į bedančių defektų *Kennedy* klasę, implanto dizainą (SL ir PL grupės) ir implanto pa-dėtį (mezialinė ir distalinė).

Gylio (r) paklaidos demonstruoja neigiamų verčių tendenciją – implantai dažnu atveju buvo įsukami giliau nei suplanuota (9 pav.). Vidurkių statistinė analizė turėtų būti vertinama saikingai, nes teigiamos ir neigiamos vertės

maskuoja pilną paklaidos mastą. Gylio (r) paklaidų duomenų daugiafaktorinė ANOVA taip pat atskleidė implanto dizaino ir padėties faktorių sąveikos reikšmingą grupių skirtumą (p = 0,02); post hoc analizė identifikavo, jog PL dizaino grupėje distalinė implanto padėtis pasižymėjo mažesne gylio (r) paklaida nei mezialinė (p = 0,05). Vieno danties defekto implanto dizaino grupių gylio (r) paklaidos analizė t-testu atskleidė statistiškai reikšmingai mažesnį vidurkį SL grupėje (p = 0,029).
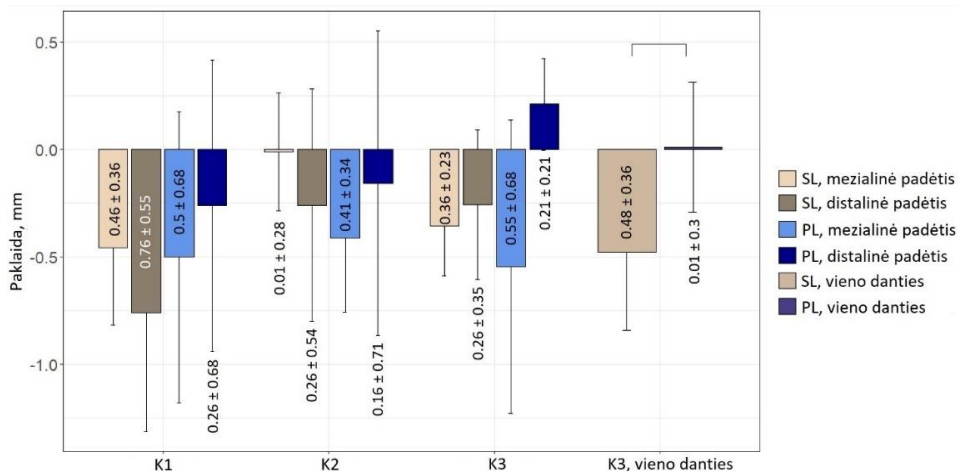
9 pav. Gylio (r) paklaidos (vidurkiai ir standartiniai nuokrypiai) atsižvelgiant į bedančių defektų *Kennedy* klasę, implanto dizainą (SL ir PL grupės) ir implanto padėtį (mezialinė ir distalinė). Vienos danties defekto (*single*) grupių palyginimas atliktas taikant t-testą.

Gylio (a) paklaidų daugiafaktorinė ANOVA analizė taip pat atskleidė statistiškai reikšmingą implanto dizaino ir pozicijos sąveiką (p = 0,018). Post hoc analizė identifikavo, jog SL implanto dizainas turėjo įtakos mažesnei gylio paklaidai nei PL mezialinėje implanto padėtyje arti statistiškai reikšmingo skirtumo (p = 0,07). Taip pat daugiafaktorinė ANOVA analizė nurodė, jog defekto *Kennedy* klasės grupių skirtumas buvo arti statistinio reikšmingumo lygmens (p = 0,07). Vieno danties defekto gylio (a) paklaidų tarp implanto dizaino grupių t-testo analizė statistiškai reikšmingo skirtumo neidentifikavo.
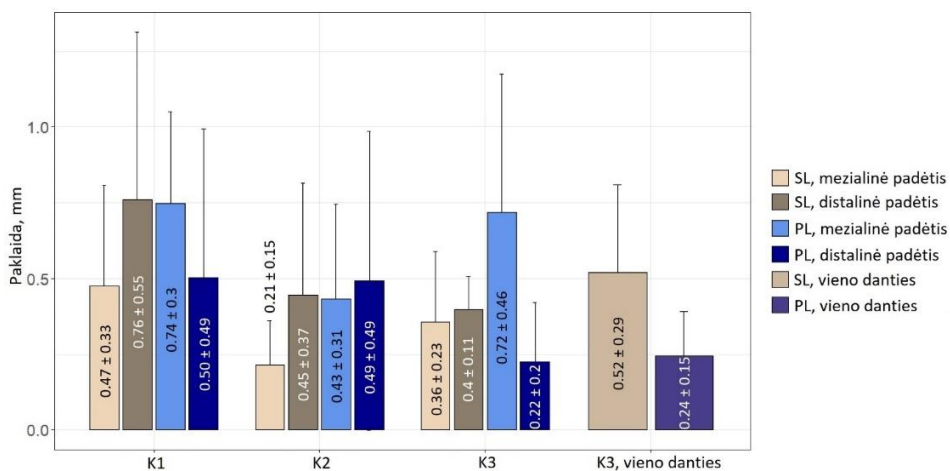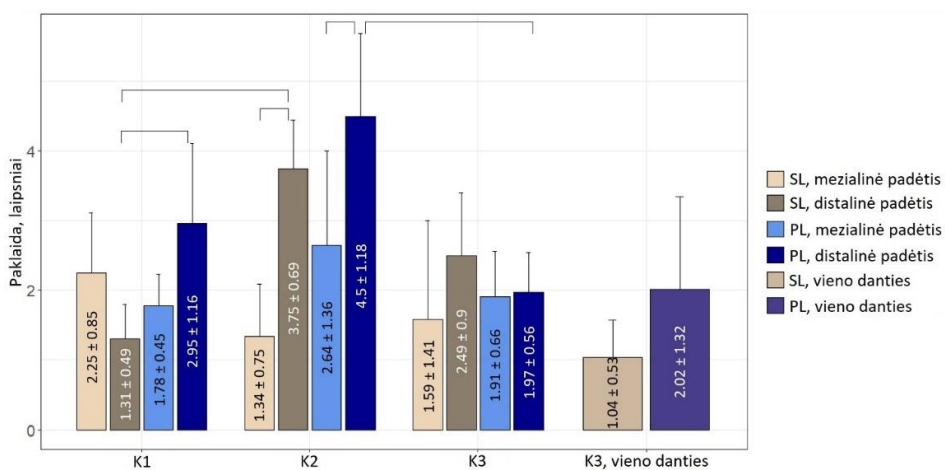
10 pav. Absoliučios gylio (a) paklaidos (vidurkiai ir standartiniai nuokrypiai) atsižvelgiant į bedančių defektų *Kennedy* klasę, implanto dizainą (SL ir PL grupės) ir implanto padėtį (mezialinė ir distalinė).

Horizontalių paklaidų daugiafaktorinė analizė identifikavo statistiškai reikšmingą skirtumą (p = 0,017) tarp implanto pozicijos grupių: mezialinės padėties grupėje paklaidos mažesnės, nei distalinės (11 pav.). Skirtumas tarp defekto *Kennedy* klasės grupių šioje analizėje taip pat buvo arti statistinio reikšmingumo (p = 0,066), o kartu ir jos sąveika su implanto dizaino faktoriumi (p = 0,07). Vieno danties defekto (*single*) implanto dizaino grupių vidurkių palyginimas t-testu neatskleidė reikšmingo skirtumo.
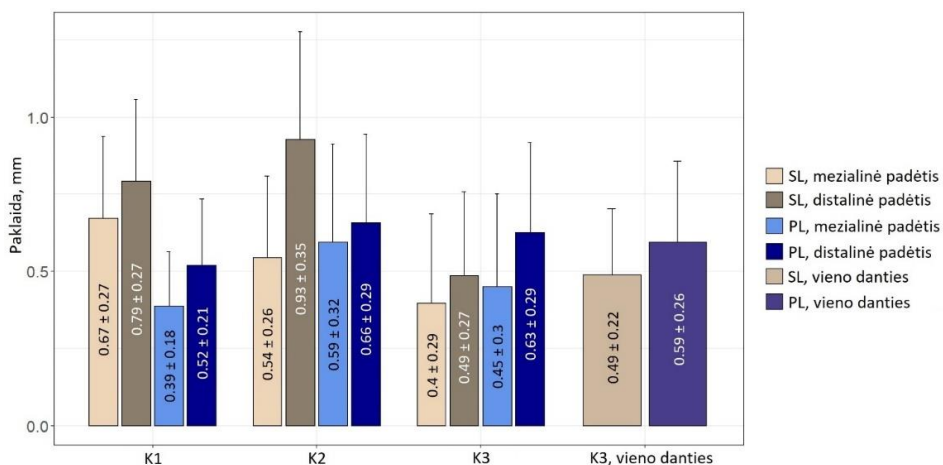
11 pav. Horizontalios paklaidos (vidurkiai ir standartiniai nuokrypiai) atsižvelgiant į bedančių defektų *Kennedy* klasę, implanto dizainą (SL ir PL grupės) ir implanto padėtį (mezialinė ir distalinė).

217

Kampo paklaidų daugiafaktorinė ANOVA identifikavo statistiškai reikšmingus skirtumus grupėse pagal kiekvieną faktorių individualiai (p < 0,05) bei sąveikose tarp defekto *Kennedy* klasės ir implanto pozicijos (p = 0,0008) ir visų trijų faktorių (p = 0,013, 12 pav.). K2 klasės defektų grupėje (3,1 ± 1,6 laipsniai) kampo paklaidos buvo statistiškai reikšmingai didesnės (post hoc porinių kontrastų testas koreguotas MVT metodu) nei K1 (2,1 ± 1,0 laipsniai, p = 0,001) ir K3 (2 ± 0,9 laipsniai, p = 0,0004) defektų grupėse. Vidutinės kampo paklaidos SL (2,1 ± 1,2 laipsniai) buvo statistiškai reikšmingai mažesnės (p = 0,0243) nei PL grupėje (2,6 ± 1,3 laipsniai). Mezialinės implanto padėties grupėje kampo paklaidos (1,9 ± 1,0 laipsniai) buvo statistiškai reikšmingai mažesnės (p = 0,0001) nei distalinės padėties grupėje (2,8 ± 1,3 laipsniai). Defekto *Kennedy* klasės ir implanto pozicijos sąveika identifikavo statistiškai reikšmingus skirtumus (p reikšmės <0,001) šiose grupėse: K1-K2 distalinėje padėtyje; K2-K3 distalinėje padėtyje, mezialinė-distalinė padėtis K2 klasės defekte (12 pav.). Vieno danties defekto (*single*) implanto dizaino grupių vidurkių palyginimas t-testu neatskleidė reikšmingo skirtumo.

12 pav. Kampo paklaidos (vidurkiai ir standartiniai nuokrypiai) atsižvelgiant į bedančių defektų *Kennedy* klasę, implanto dizainą (SL ir PL grupės) ir implanto padėtį (mezialinė ir distalinė). Daugiafaktorinės ANOVA sąveikos tarp visų faktorių statistiškai reikšmingi skirtumai tarp grupių pažymėti atsižvelgiant į post hoc porinių kontrastų testo rezultatus (p < 0,05; p-reikšmės koreguotos MVT* metodu).

*Monte Karlo metodu koreguotos p-reikšmės, remiantis daugiamačiu normaliuoju t-testo pasiskirstymu.

2.2. DINAMINĖS IR STATINĖS NAVIGACIJOS ĮTAKOS IMPLANTACIJOS TIKSLUMUI PALYGINIMAS

Viso buvo įsriegti 168 implantai, vienodu pasiskirstymu po 84 abiejų navigacijos metodų grupėse. Visų paklaidų aprašomoji statistika pagal navigacijos būdą yra pateikta 7 lentelėje. Šoninių dantų grupės defektų, kurie atstatomi tiltiniu protezu ant dviejų implantų ir pavienio defekto (K3, *single*) daugiafaktorinės ANOVA atliktos atskirai.

7 lentelė. Paklaidų aprašomoji statistika pagal navigacijos metodą (statinis ir dinaminis). SN – standartinis nuokrypis; *Min* – minimumas; *Max* – maksimumas; *IQR* – tarpkvartilinis plotis.

Paklaidos		Vidurkis	SN	Min	Max	Mediana	IQR
Įvesties taško	Statinis	0.52	0.28	0.09	1.7	0.45	0.27
	Dinaminis	0.77	0.32	0.20	1.5	0.76	0.48
Gylio (r)*	Statinis	-0.22	0.33	-1.38	0.40	-0.18	0.35
	Dinaminis	-0.27	0.48	-1.46	0.74	-0.25	0.67
Gylio (a)	Statinis	0.29	0.27	0	1.38	0.21	0.25
	Dinaminis	0.45	0.33	0.02	1.46	0.37	0.45
Horizontali	Statinis	0.37	0.21	0.03	0.98	0.34	0.23
	Dinaminis	0.56	0.28	0.1	1.37	0.51	0.41
Kampo	Statinis	2.9	1.3	0.5	6.3	2.8	1.6
	Dinaminis	2.3	1.3	0.4	6.2	2.0	1.7

* neigiama vertė indikuoja per giliai įsriegtą implantą, teigiama – nepakankamai giliai, lyginant su suplanuota padėtimi.

Viso fiksuotam tiltiniam protezui ant dviejų implantų buvo analizuotos 144 pozicionavimo paklaidos daugiafaktorine (keturi faktoriai) ANOVA, neįtraukiant K3 vieno danties defekto (*single*) grupės. Į šią analizę buvo įtraukti navigacijos (statinė, dinaminė), *Kennedy* klasės (K1, K2, K3), implanto dizaino (SL, PL) ir pozicijos (mezialinė, distalinė) faktoriai. Visais aspektais grupės buvo vienodos pagal implantų skaičių jose. Statistiškai reikšmingi daugiafaktorinės ANOVA skirtumai tarp grupių kiekvienai iš paklaidų rūšių pateikti 8 lentelėje. Svarbu pažymėti, kad kai kuriais atvejais stebėtas saikingas nuokrypis nuo normalumo, todėl interpretuojant rezultatus reikėtų į tai atsižvelgti. Vieno danties defekto (K3, *single*) daugiafaktorinė (trys faktoriai) ANOVA atlikta analogiškai tačiau nesant padėties faktoriaus (M, D).

Šioje analizėje navigacijos metodas visų paklaidų atvejais buvo identifikuotas kaip statistiškai reikšmingas faktorius (p ≤ 0,005; 8 lentelė). Statinio metodo grupėje paklaidos buvo mažesnės visais paklaidų atvejais (p ≤ 0,005), išskyrus kampo paklaidą, kuri buvo statistiškai reikšmingai mažesnė dinaminio metodo grupėje (p = 0,002; 7 lentelė ir 13 paveikslas).
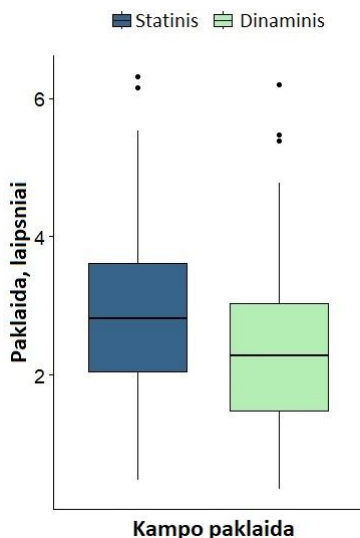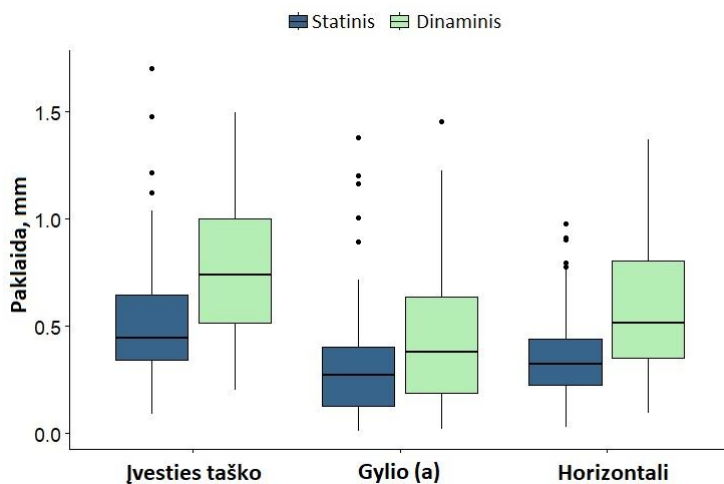
13 pav. Paklaidų pasiskirstymo stačiakampės diagramos pagal navigacijos metodą kiekvienam paklaidos tipui (išskyrus gylio (r)).

8 lentelė. Daugiafaktorinės ANOVA statistiškai reikšmingi rezultatai ir visų keturių veiksnių sąveikos rezultatas. *Guidance* – navigacijos metodas (dinaminis, statinis); *Kennedy* – bedančio defekto *Kennedy* klasė (K1, K2, K3); *Implant* – implanto dizainas (SL, PL), *Position* – implanto pozicija (mezialinė, distalinė).

Faktoriai ir sąveikos	Sum Sq	F value	Pr(>F)
Įvesties taško (3D)*			
Guidance	2.458	36.072	< 0.0001
Guidance : Kennedy	0.6995	5.133	0.007
Implant : Kennedy	0.692	5.078	0.008
Implant : Position	1.589	23.322	< 0.0001
Kennedy : Position	1.412	10.36	< 0.0001
Guidance : Implant : Kennedy : Position	0.335	2.457	0.09
Gylio (a)**			
Guidance	0.698	8.025	0.005
Implant : Position	0.923	10.613	0.001
Kennedy : Position	0.767	4.407	0.01
Guidance : Implant : Kennedy : Position	0.046	0.266	0.77
Horizontali*			
Guidance	1.537	34.774	< 0.0001
Guidance : Kennedy	0.734	8.307	0.0004
Implant : Kennedy	0.304	3.438	0.04
Guidance : Position	0.424	9.592	0.002
Implant : Position	0.396	8.950	0.003
Kennedy : Position	0.494	5.585	0.005
Implant : Kennedy : Position	0.376	4.254	0.02
Guidance : Implant : Kennedy : Position	0.318	3.60	0.03
Kampo			
Guidance	9.482	9.754	0.002
Position	17.283	17.778	< 0.0001
Guidance : Kennedy	22.137	11.386	< 0.0001
Guidance : Position	5.013	5.157	0.02
Kennedy : Position	20.112	10.344	< 0.0001
Guidance : Implant : Kennedy	11.008	5.662	0.004
Guidance : Kennedy : Position	11.616	5.975	0.003
Guidance : Implant : Kennedy : Position	5.165	2.657	0.07

* ANOVA modelių paklaidų Šapiro–Vilko normalumo testo vertės 0,03
** ANOVA modelio paklaidų Šapiro–Vilko normalumo testo vertės ≤0,001

Iš visų įvesties taško paklaidų reikšmingų sąveikų daugiafaktorinės ANOVA rezultatuose, vienintelė apimanti ir pagrindinį nagrinėjamą faktorių (navigacijos metodą) nustatyta su *Kennedy* defekto klase (p = 0,007; 8 lentelė). K1 (p < 0,0001) ir K2 (p = 0,0001) grupėse statinis metodas pasižymėjo mažesnėmis paklaidomis, tuo tarpu K3 grupėje šis skirtumas nebuvo statistiškai reikšmingas (p = 0,9). Pavienio danties defekto grupės atskira daugiafaktorinė ANOVA taip pat identifikavo statinio navigacijos metodo statistiškai reikšmingą įtaką (p = 0,009) mažesnėms paklaidoms, tačiau kiti faktoriai ar jų sąveikos nesiekė statistiškai reikšmingo lygmens (14 pav.).

Gylio (r) paklaidose stebima aiški dominuojanti duomenų neigiamų verčių tendencija (15 pav. ir 7 lentelė). Tai nurodo implantų sriegimo giliau nei suplanuota polinkį. Dėl teigiamų ir neigiamų verčių antagonistinės sąveikos gylio (r) paklaidų rezultatų skaitinė statistinė analizė nebuvo taikyta ryšium su komplikuotu klinikiniu ir statistiniu tokių rezultatų prasmės interpretavimu.

Absoliučių gylio (a) paklaidų (16 pav.) daugiafaktorinė ANOVA be jau minėto navigacijos faktoriaus (7 lentelė, 13 pav.), statistiškai reikšmingus skirtumus (8 lentelė) identifikavo sąveikose tarp implanto pozicijos (M, D) ir dizaino (SL, PL) bei pozicijos ir defekto *Kennedy* klasės (K1, K2, K3). Šiuo ir kitais paklaidų analizės panašiais atvejais, nuo sąveikų post hoc analizės susilaikyta, nes: pirmiausia, nei viena jų neįtraukė pagrindinio analizuojamo faktoriaus (navigacijos metodo); antra, buvo stebimas normalumo nuokrypis nuo ANOVA modelio paklaidų pasiskirstymo; trečia, vengiant bereikalingo rezultatų dalies perkrovimo dideliu kiekiu šalutinės papildomos informacijos.

Atliekant pavienio K3 grupės (*single*) gylio (a) paklaidų daugiafaktorinę ANOVA analizę dar kartą patvirtintas reikšmingas didesnis statinio navigacijos metodo tikslumas, lyginant su dinaminiu (p = 0,002). Taip pat statistinio reikšmingumo lygmuo pasiektas navigacijos ir implanto dizaino sąveikos: statinis metodas tikslesnis už dinaminį SL implantų dizaino grupėje (post hoc porinių kontrastų testas, MVT koreguota p = 0,002; 16 pav.).
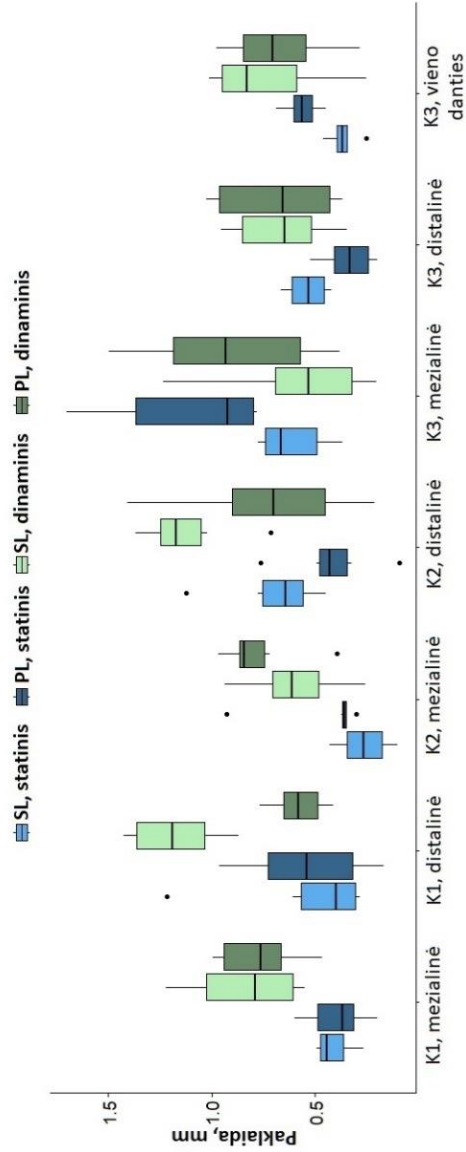
14 pav. Įvesties taško paklaidų pasiskirstymas, atsižvelgiant į navigacijos metodą, bedančių defektų *Kennedy* klasę, implanto dizainą ir implanto padėtį.
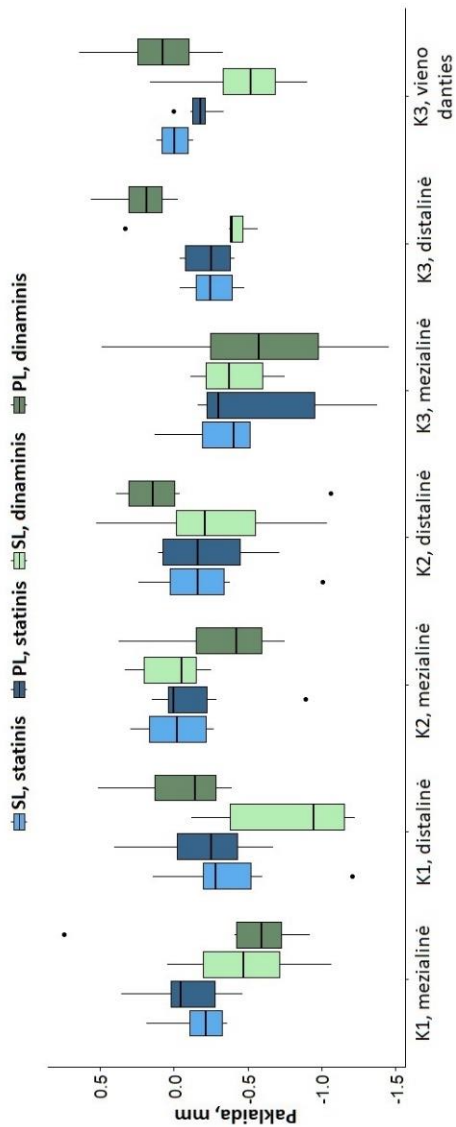
15 pav. Gylio (r) paklaidų pasiskirstymas, atsižvelgiant į navigacijos metodą, bedančių defektų *Kennedy* klasę, implanto dizainą ir implanto padėtį.
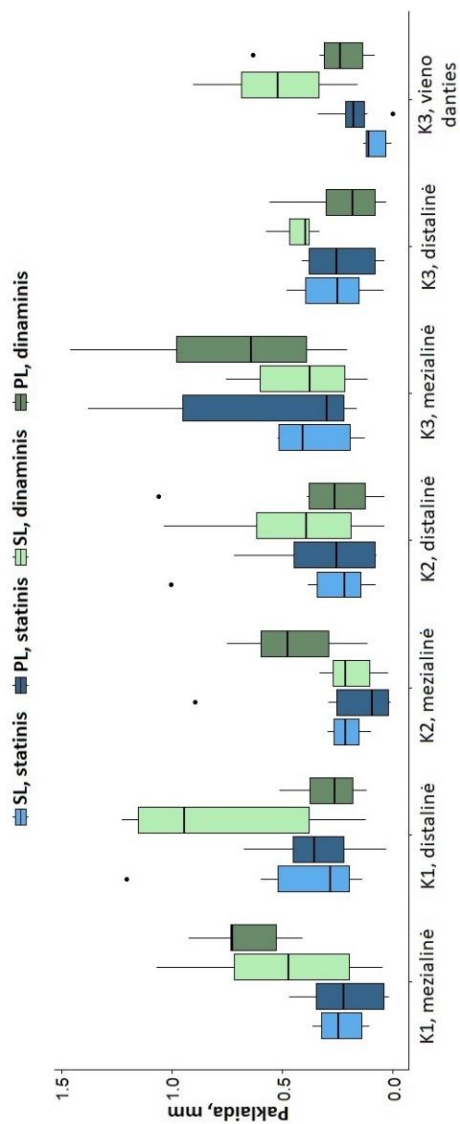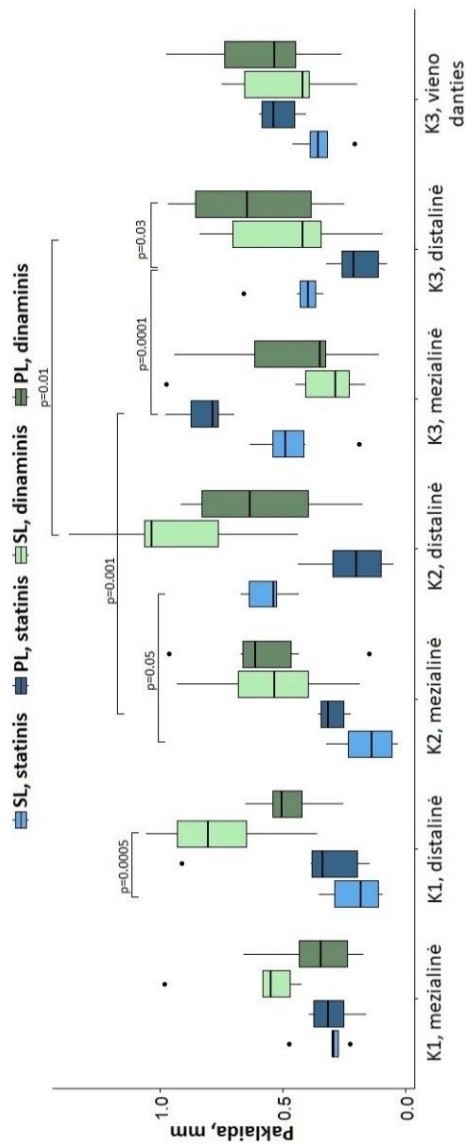
16 pav. Absoliučių gylio (a) paklaidų pasiskirstymas, atsižvelgiant į navigacijos metodą, bedančių defektų *Kennedy* klasę, implanto dizainą ir implanto padėtį. Daugiafaktorinės ANOVA statistiškai reikšmingi skirtumai tarp grupių pažymėti atsižvelgiant į post hoc porinių kontrastų testo rezultatus (p-reikšmės koreguotos MVT metodu).

Horizontalių paklaidų daugiafaktorinė ANOVA be anksčiau minėto navigacijos metodo (7 lentelė, 13 pav.), taip pat identifikavo kitas reikšmingas sąveikas (8 lentelė). Post hoc analizė nurodė statinį metodą kaip tikslesnį K1 (MVT koreguota p = 0,0005) ir K2 grupėse (MVT koreguota p < 0,0001). Dinaminio navigavimo atveju šiek tiek žemesnės paklaidos stebėtos K3 grupėje, lyginant su K2 (MVT koreguota p = 0.03). Distalinėje implanto padėtyje statinė navigacija pasižymėjo mažesnėmis paklaidomis nei dinaminė (MVT koreguota p < 0.0001), o taip pat dinaminės navigacijos atveju mezialinė padėtis buvo susijusi su mažesnėmis paklaidomis, lyginant su distaline (MVT koreguota p = 0,007). Statistiškai reikšmingi skirtumai tarp grupių pagal visų keturių faktorių sąveiką pažymėti 17 pav.

Daugiafaktorinė ANOVA vieno danties defekto (K3, *single*) grupei neatskleidė jokių reikšmingų skirtumų tarp jokių veiksnių ar sąveikų, susijusių su horizontalia paklaida.

Be navigacijos metodo (7 lentelė, 13 pav.), padėties faktorius taip pat pasižymėjo statistiniu reikšmingumu kampo nuokrypiui su mažesnėmis paklaidomis mezialinėje grupėje (p < 0,0001). Atsižvelgiant į tai, jog navigacijos metodas turėjo reikšmingas beveik visas įmanomas faktorių sąveikas (8 lentelė), siekiant rezultatų aprašymo aiškumo, paprastumo ir vengiant informacijos kolinearumo bei dubliavimo, statistiškai reikšmingi trijų faktorių sąveikos rezultatai pažymėti 18 pav.

Vieno danties defekto (K3, *single*) grupės daugiafaktorinė ANOVA analizė parodė, kad dinaminės navigacijos metodas buvo tikslesnis už statinį (p = 0,005; 18 pav.). Kiti faktoriai ir jų sąveikos statistiškai reikšmingais rezultatais nepasižymėjo.

17 pav. Horizontalių paklaidų pasiskirstymas, atsižvelgiant į navigacijos metodą, bedančių defektų *Kennedy* klasę, implanto dizainą ir implanto padėtį. Daugiafaktorinės ANOVA statistiškai reikšmingi skirtumai tarp grupių pažymėti atsižvelgiant į post hoc porinių kontrastų testo rezultatus (p-reikšmės koreguotos MVT metodu).
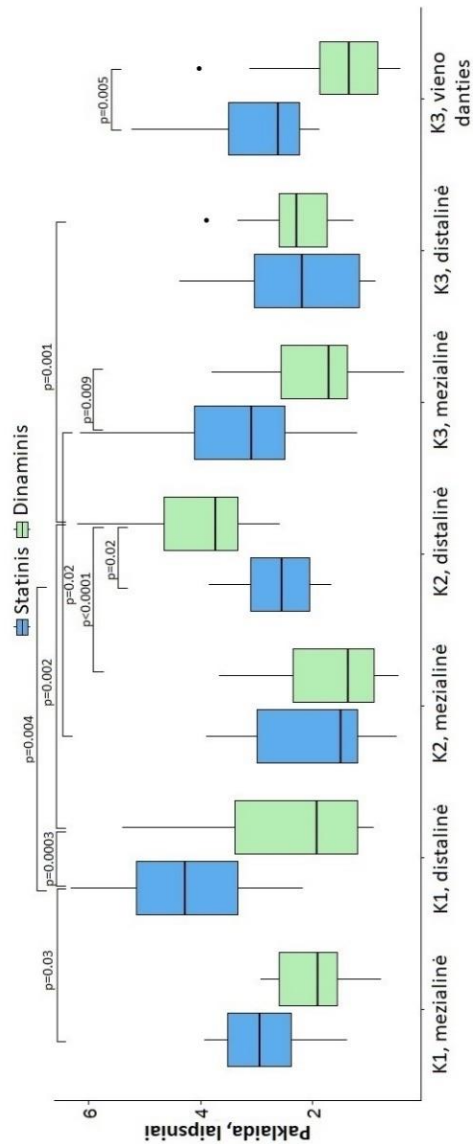
18 pav. Kampo paklaidų pasiskirstymas, atsižvelgiant į navigacijos metodą, bedančių defektų *Kennedy* klasę ir implanto padėtį. Daugiafaktorinės ANOVA statistiškai reikšmingi skirtumai tarp grupių pažymėti atsižvelgiant į post hoc porinių kontrastų testo rezultatus (p-reikšmės koreguotos MVT metodu).

2.3. DINAMINĖS NAVIGACIJOS TIKSLUMO VERTINIMAS TAIKANT DU REGISTRACIJOS METODUS

Šioje tyrimo dalyje vertinti viso 96 į modelius įsriegtų implantų rezultatai su vienodu skaitiniu pasiskirstymu abiejose registravimo grupėse. Lygintos dvi sekimo registracijos metodo grupės: registracija dantų paviršių pagalba (Kennedy1) ir atskaitos objektų pagalba (*Edentulous*). Taip pat vertinti ir kiti galimai susiję ir turintys įtakos faktoriai: implanto pozicija (mezialinė, distalinė), implanto dizainas (SL, PL) ir tik atskaitos objektų (*Edentulous*) grupėje galinių implantų palenkimas kampu.

Daugiafaktorinės ANOVA identifikavo, jog registravimas atskaitos objektų pagalba buvo tikslesnis visų paklaidų atžvilgiu nei registracija danų pagalba (19 pav.): įvesties taško (p = 0,0002), absoliuti gylio (a) (p = 0,01), horizontali (p = 0,02), ir kampo (p = 0,008). Nors ir įvesties taško daugiafaktorinės ANOVA modelis išpildė paklaidų normalumo prielaidą, reikia pažymėti, kad kitų paklaidų normalumo prielaida nebuvo įgyvendinta. Todėl interpretuojant rezultatus reikia tai įvertinti.

Absoliučių gylio (a) paklaidų daugiafaktorinė ANOVA pažymėjo reikšmingą implanto dizaino ir pozicijos sąveiką, (p = 0,01), tačiau neįtraukė pagrindinio faktoriaus (registracijos metodo), o taip pat post hoc analizė neidentifikavo reikšmingų skirtumų tarp porų (MVT koreguota p > 0.05).

Horizontalių paklaidų analizė, nurodė implanto poziciją kaip atskirą statistiškai reikšmingą faktorių (p = 0,03) su mažesnėmis paklaidomis mezialinėje pozicijoje (20 pav.).

Kampo paklaidų daugiafaktorinė ANOVA pasižymėjo reikšminga sąveika tarp implanto dizaino ir pozicijos faktorių (21 pav.). Remiantis pot-hoc analize, distalinėje implanto pozicijoje SL implanto dizainas pasižymėjo mažesnėmis paklaidomis nei PL (MVT koreguota p = 0.04). Tačiau dėl nedidelių duomenų nukrypimų nuo normalumo, pagrindinio veiksnio (sekimo registravimo) neįtraukimo ir ribotos sąveikos apimties, šio rezultato klinikinė reikšmė yra ribota tolesniam interpretavimui.

Registracijos per atskaitos taškus atveju (*Edentulous*), mezialiniai (lygiagretūs) ir distaliniai (30 laipsnių palenkti) implantai nepasižymi reikšmingais skirtumais. Kitų statistiškai reikšmingų skirtumų nestebėta.
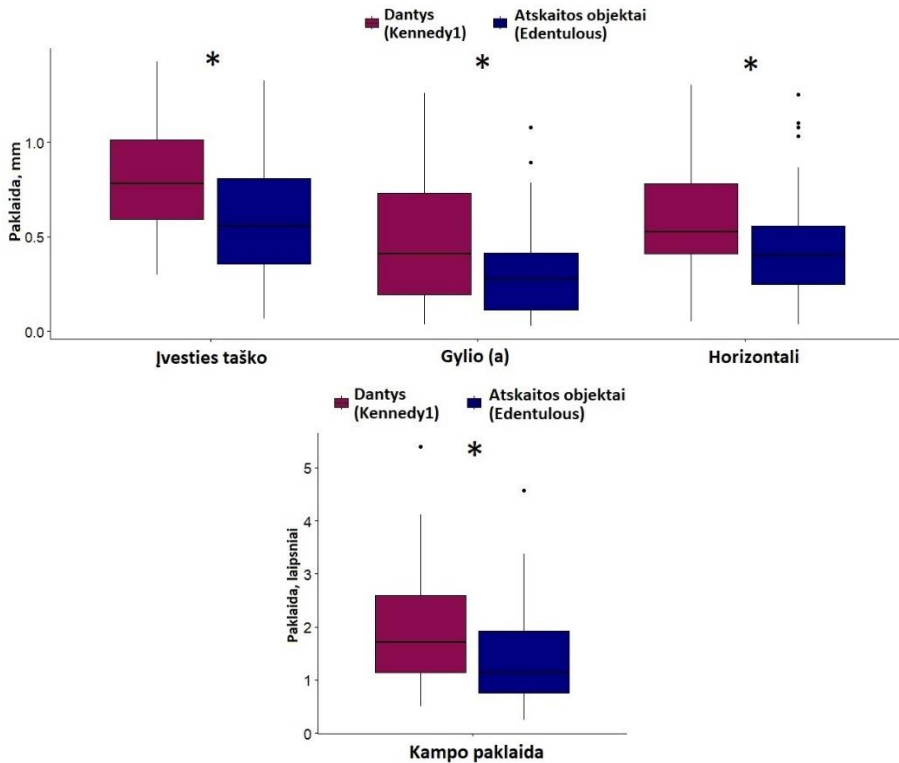
19 pav. Paklaidų pasiskirstymo stačiakampės diagramos pagal registracijos metodą kiekvienam paklaidos tipui (išskyrus gylio (r)). Kennedy1 – sekimo registracija dantų paviršių pagalba; *Edentulous* – atskaitos objektų.
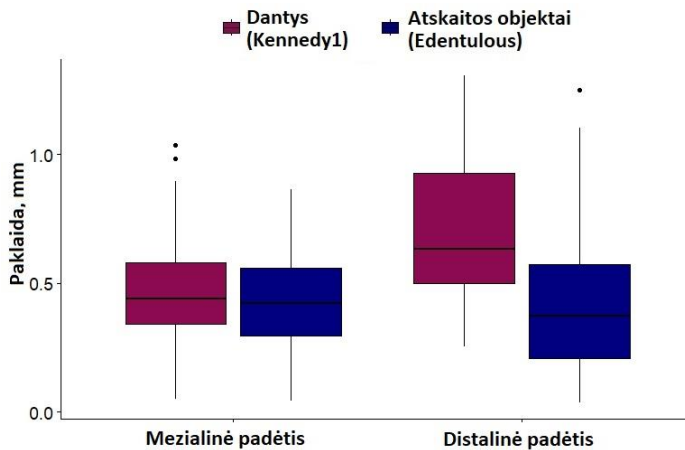
20 pav. Horizontalių paklaidų pasiskirstymo stačiakampės diagramos pagal registracijos metodą ir implanto poziciją. Kennedy1 – sekimo registracija dantų paviršių pagalba; *Edentulous* – atskaitos objektų.
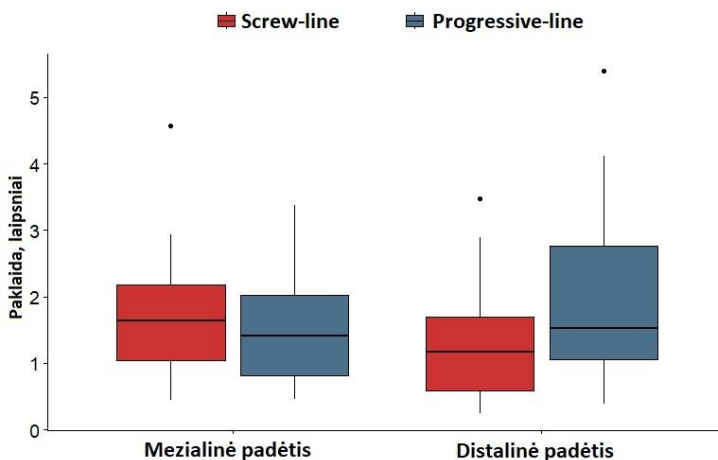
21 pav. Kampo paklaidų pasiskirstymo stačiakampės diagramos pagal implanto dizainą ir implanto poziciją. *Screw-line* (SL) – mažiau išreikšto kūgio implanto dizainas; *Progressive-line* (PL) – daugiau išreikšto.

## 2.4. POLIMERINIŲ MEDŽIAGŲ IR PAVIRŠIAUS PLOVIMO TYRIMAS

2.4.1. PAVIRŠIAUS ŠIURKŠTUMAS

Paviršių profilometrijos vertinimo rezultatai pateikti 9 lentelėje. *CCP* plovimo grupėje statistiškai reikšmingų skirtumų tarp skirtingų medžiagų grupių nestebėta. Pritaikius plovimą *RCP*, ZrO-HT grupės paviršiaus šiurkštumas buvo statistiškai reikšmingai žemesnis (Kruskalio-Voliso ir poromis Vilkoksono rangų sumų palyginimas, $p = 0{,}042$) už Ti, PMMA-Ker, PMMA-Bre, PEEK ir PEKK grupes. Reikšmingi medžiagų grupių paviršių šiurkštumo skirtumai, lyginant du plovimo protokolus, pažymėti 22 pav. Paviršių vaizdiniai pavyzdžiai konfokaliniu mikroskopu pateikti 23 pav.

Table 15. Paviršiaus šiurkštumo (Sa) vidutinės reikšmės kiekvienai medžiagos grupei kiekvieno plovimo protokolo atveju pateiktos mikrometrais (μm) kaip vidurkis ± standartinis nuokrypis.

CCP	Medžiagos grupė	RCP
0.157 ± 0.049	Ti	0.146 ± 0.033
0.136 ± 0.017	ZrO-HT	0.079 ± 0.017
0.235 ± 0.079	PMMA-Ker	0.125 ± 0.016
0.208 ± 0.049	PMMA-Bre	0.155 ± 0.052
0.234 ± 0.186	PMMA-3D	0.140 ± 0.097
0.278 ± 0.103	PEEK	0.174 ± 0.055
0.228 ± 0.084	PEKK	0.129 ± 0.042

Statistiškai reikšmingi (Kruskalio-Voliso ir poromis Vilkoksono testai, p-koreguota < 0,05) skirtumai, lyginant medžiagų grupių vidurkius kiekviename valymo protokole, pažymėti laužtiniu skliaustu atitinkamoje lentelės pusėje. CCP—įprastas plovimo protokolas; RCP— tyrimo.
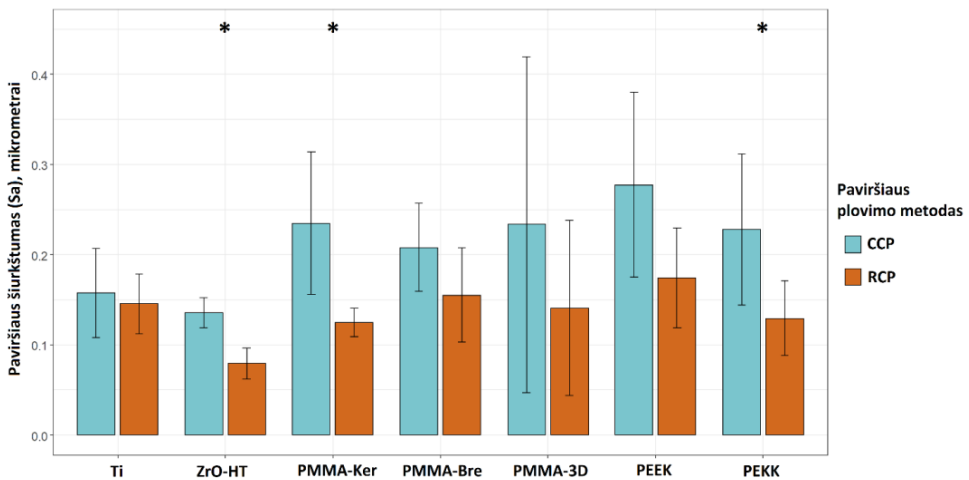
22 pav. Paviršiaus šiurkštumo vertės taikant du skirtingus plovimo protokolus. Rezultatai pateikti kaip vidurkiai ± standartiniai nuokrypiai. *— statistiškai reikšmingi skirtumai (Vilkoksono, p < 0,05) lyginant dvi plovimo grupes kiekvienai medžiagai. *CCP*— įprastas plovimo protokolas; *RCP*— tyrimo.
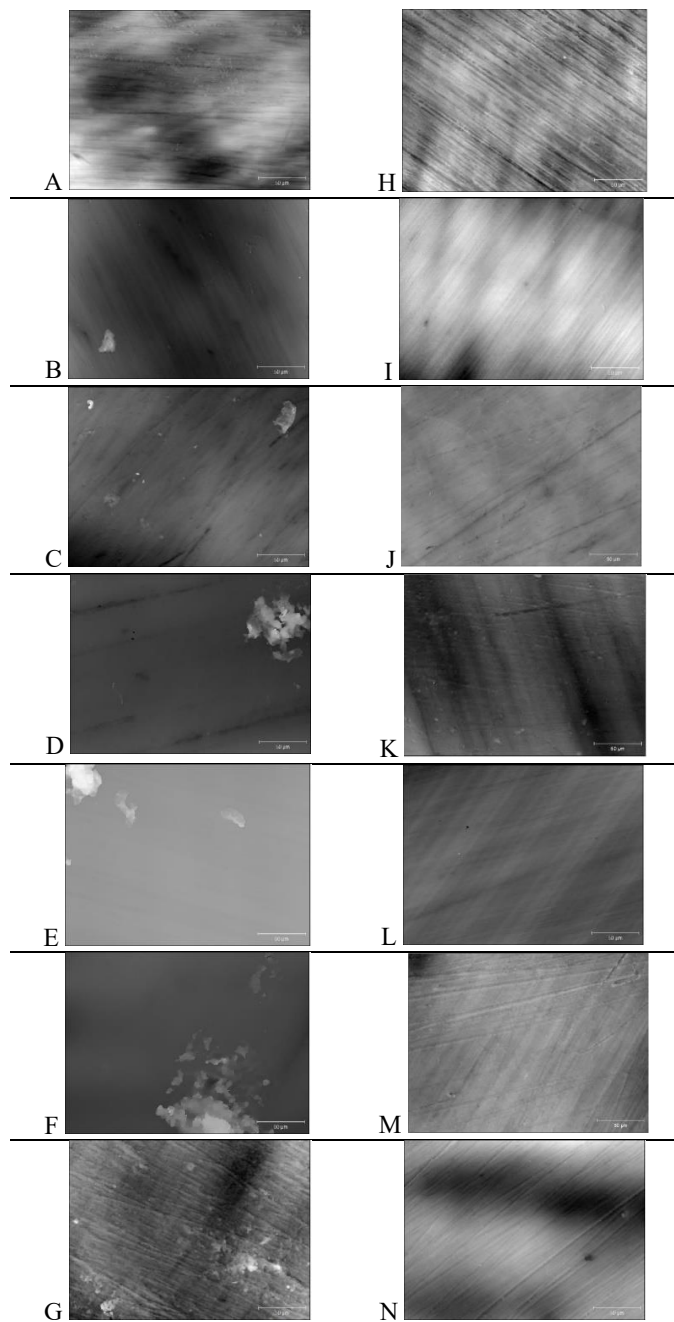
23 pav. Medžiagų paviršiai po plovimo *CCP* (**A**—Ti, **B**—ZrO-HT, **C**—PMMA-Ker, **D**—PMMA-Bre, **E**—PMMA-3D, **F**—PEEK, **G**—PEKK) ir *RCP* (**H, I, J, K, L, M, N** atitinkamai). Vaizdai gauti optiniu profilometru su konfokaliniu mikroskopu (×50). Balta juosta kiekvieno vaizdo apatiniame dešiniame kampe atitinka 50 μm.
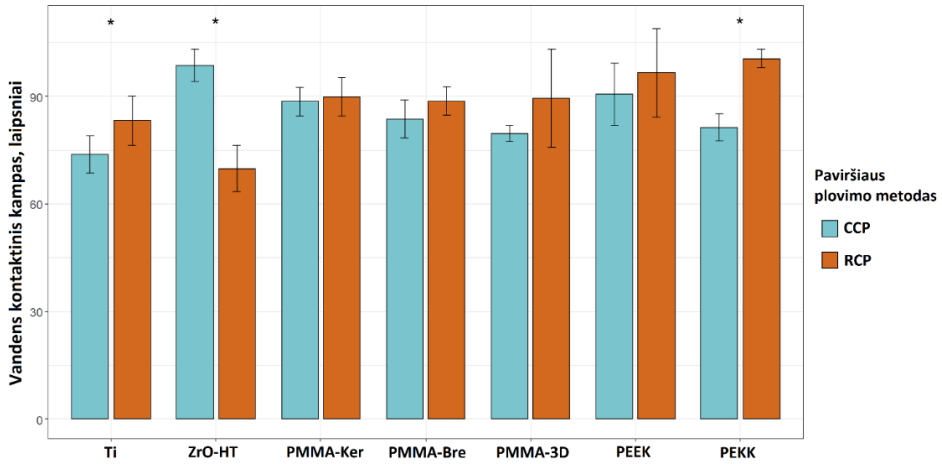
2.4.2. VANDENS KONTAKTINIS KAMPAS

Vandens kontaktinio kampo (*WCA*) matavimo rezultatai pavaizduoti 10 lentelėje. *CCP* atveju, ZrO-HT grupė pasižymėjo statistiškai reikšmingai didesniu (ANOVA su post hoc Tjuko kriterijumi) kontaktiniu kampu lyginant su Ti (p < 0,001), PMMA-Bre (p = 0,00163), PMMA-3D (p < 0,001) ir PEKK (p < 0,001) grupėmis. Negana to, Ti grupė pasižymėjo statistiškai reikšmingai mažesniais *WCA*, lyginant su PMMA-Ker (p = 0,00181) ir PEEK (p < 0,001) grupėmis. Galiausiai, PMMA-3D grupės kontaktinis kampas buvo statistiškai reikšmingai mažesnis nei PEEK grupės (p = 0,03175). *RCP* plovimo protokolo atveju, ZrO-HT grupė pasižymėjo statistiškai reikšmingai žemesniu *WCA* nei PMMA-Ker (p = 0,0107), PMMA-Bre (p = 0,0183), PMMA-3D (p = 0,0131), PEEK (p < 0,001) ir PEKK (p < 0,001) grupės. Taip pat ir Ti grupė pasižymėjo reikšmingai mažesniu *WCA* nei PEKK grupė (p = 0,036). Reikšmingi vandens kontaktinio kampo skirtumai kiekvienai medžiagai pagal paviršiaus plovimo metodus pavaizduoti 24 paveiksle. Vandens lašų pavyzdiniai vaizdai *WCA* ant skirtingų medžiagų paviršių matavimui yra pateikti 25 paveiksle.

10 lentelė. Vandens kontaktinis kampas (laipsniais; WCA) kiekvienai medžiagos grupei ir plovimo protokolui pateikta kaip vidurkis ± standartinis nuokrypis.

CCP	Medžiagos grupė	RCP
73.84 ± 5.18	Ti	83.24 ± 6.94
98.70 ± 4.49	ZrO-HT	69.90 ± 6.37
88.60 ± 4.03	PMMA-Ker	89.86 ± 5.32
83.76 ± 5.30	PMMA-Bre	88.74 ± 3.91
79.64 ± 2.15	PMMA-3D	89.46 ± 13.62
90.64 ± 8.73	PEEK	96.56 ± 12.41
81.34 ± 3.77	PEKK	100.6 ± 2.5

Statistiškai reikšmingi (ANOVA su post hoc Tjuko kriterijumi, p < 0,05) skirtumai lyginant medžiagų grupes kiekvieno plovimo protokolo atveju pažymėti laužtinių skliaustų principu atitinkamoje lentelės pusėje CCP—įprastas plovimo protokolas; RCP— tyrimo.

24 pav. Vandens kontaktinio kampo vertės taikant du skirtingus plovimo protokolus. Rezultatai pateikti laipsniais kaip vidurkiai ± standartiniai nuokrypiai. * – statistiškai reikšmingi skirtumai (t testas, p < 0,05) lyginant *CCP* ir *RCP* kiekvienai medžiagos grupei. *CCP* – įprastas plovimo protokolas; *RCP*— tyrimo
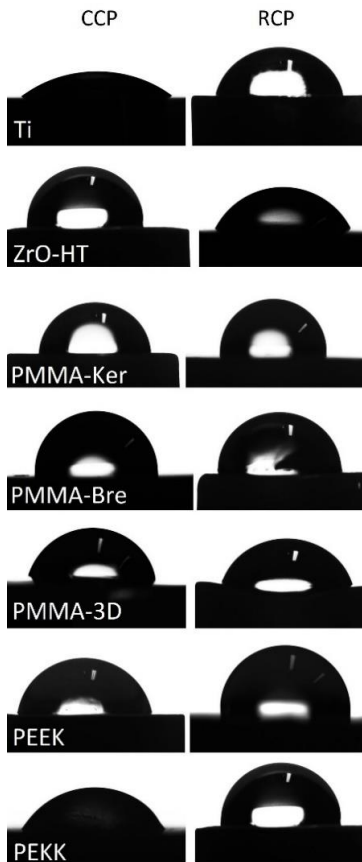
25 pav. Vandens lašo vaizdai ant medžiagų paviršių, kurie naudoti vandens kontaktinio kampo matavimui. *CCP*— įprastas plovimo protokolas; *RCP*— tyrimo.

2.4.3. ŽMOGAUS DANTENŲ FIBROBLASTŲ PROLIFERACIJA

Ląstelių gyvybingumo duomenys kiekvienam plovimo protokolui skirtinguose laiko taškuose yra pateikti 11 ir 12 lentelėse. ŽDF proliferacija pasižymėjo augančia tendencija laike abiem plovimo protokolo grupėms (26 pav.). Reikšmingi skirtumai lyginant abu laiko taškus (*t-test*, p < 0,05) stebėti taikant *CCP* su PMMA-3D, PEKK grupėmis. Taikant *RCP*, šie skirtumai stebėti Ti, PMMA-Ker grupėse. Ruošiant paviršius *CCP*, duomenys demonstruoja didesnę sklaidą ir variabilumą ŽDF proliferacijoje. Po 48 val. polimerinės medžiagos (išskyrus PMMA-Ker) plautos *RCP* rodė tendenciją didesnio gyvybingumo (reikšmingai PMMA-3D, PEKK grupėse, p < 0,05). Po 72 valandų, ši tendencija pasikeitė įprasto plovimo protokolo naudai, tačiau dėl didelės duomenų sklaidos skirtumas tarp abiejų plovimo protokolų šiame laiko taške nebuvo statistiškai reikšmingas.

11 lentelė. Žmogaus dantenų fibroblastų (ŽDF) proliferacija mėginių paviršiuje po įprasto plovimo protokolo (*CCP*), pateikta kaip ląstelių gyvybingumas – santykis su 24 val. kontrolinės grupės atskaita.

48 val.	Medžiagos grupė	72 val.
1.38 ± 0.15	Control	1.82 ± 0.14
1.22 ± 0.32	Ti	1.72 ± 0.48
1.11 ± 0.34	ZrO-HT	1.51 ± 0.18
1.14 ± 0.06	PMMA-Ker	1.44 ± 0.44
0.89 ± 0.19	PMMA-Bre	1.54 ± 0.80
0.79 ± 0.03	PMMA-3D	1.17 ± 0.24
0.88 ± 0.29	PEEK	1.17 ± 0.35
0.73 ± 0.12	PEKK	1.09 ± 0.12

Rezultatai pateikti kaip vidurkiai ± standartiniai nuokrypiai. Statistiškai reikšmingi (ANOVA su post hoc Tjuko kriterijumi, p < 0,05) skirtumai, lyginant medžiagos grupės vidurkius tuo pačiu laiko atskaitos momentu, yra pateikti laužtinių skliaustų pavidalu atitinkamoje lentelės pusėje.

12 lentelė. ŽDF proliferacija mėginių paviršiuje po tyrimo plovimo protokolo (*RCP*), pateikta kaip ląstelių gyvybingumas – santykis su 24 val. kontrolinės grupės atskaita.

48 val.	Medžiagos grupė	72 val.
1.20 ± 0.02	Control	1.41 ± 0.10
1.01 ± 0.04	Ti	1.13 ± 0.04
1.06 ± 0.09	ZrO-HT	1.32 ± 0.20
0.84 ± 0.05	PMMA-Ker	1.10 ± 0.11
0.98 ± 0.02	PMMA-Bre	0.88 ± 0.21
0.98 ± 0.08	PMMA-3D	0.99 ± 0.18
1.03 ± 0.02	PEEK	1.08 ± 0.08
0.96 ± 0.07	PEKK	1.08 ± 0.07

Rezultatai pateikti kaip vidurkiai ± standartiniai nuokrypiai. Statistiškai reikšmingi (ANOVA su post hoc Tjuko kriterijumi, $p < 0{,}05$) skirtumai, lyginant medžiagos grupės vidurkius tuo pačiu laiko atskaitos momentu, yra pateikti laužtinių skliaustų pavidalu atitinkamoje lentelės pusėje.
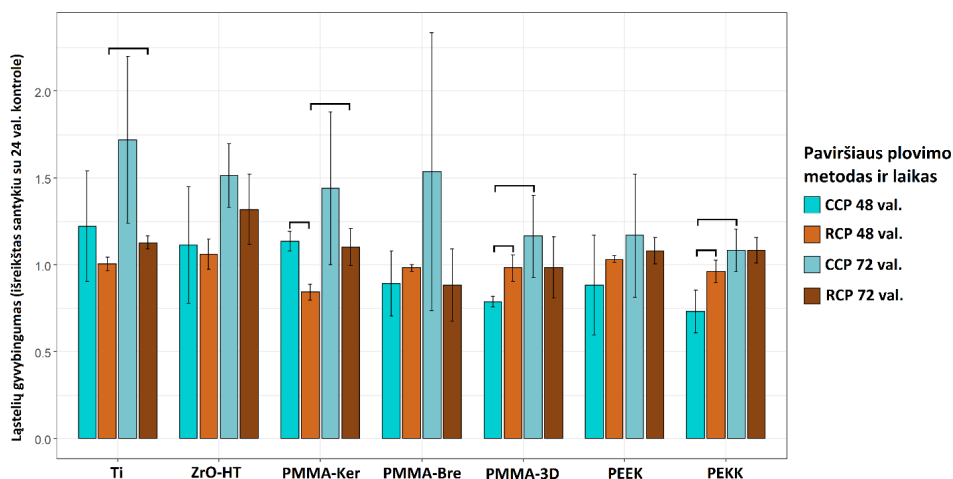

26 pav. ŽDF proliferacija mėginių paviršiuje po 48 ir 72 valandų taikant du plovimo protokolus. Rezultatai pateikti kaip ląstelių gyvybingumo (santykio su 24 val. kontrole) vidurkiai ± standartiniai nuokrypiai. Statistiškai reikšmingi skirtumai (t testas, $p < 0{,}05$) tarp plovimo protokolų ir laiko intervalų yra pažymėti. *CCP*— įprastas plovimo protokolas; *RCP*— tyrimo.

2.5. KERAMINIŲ MEDŽIAGŲ CIRKONIO PAGRINDU IR UV POVEIKIO TYRIMAS

2.5.1. PAVIRŠIAUS ŠIURKŠTUMAS

Vidutinis ZrO-HT paviršiaus šiurkštumas buvo $0,094 \pm 0,027$ μm, o ZrO-UTML – $0,11 \pm 0,036$ μm. Šapiro-Vilko normalumas ir dispersijos testų homogeniškumas (p > 0,05) leido įvertinti tiriamo parametro skirtumus naudojant t-testą. Testas nurodo, jog statistiškai reikšmingų skirtumų tarp medžiagų grupių nėra (p = 0,217). Grafiškai duomenys pavaizduoti 27 pav. Tolimesnėje duomenų analizėje ir rezultatų interpretavime abiejų medžiagų paviršių šiurkštumas laikomas lygus.
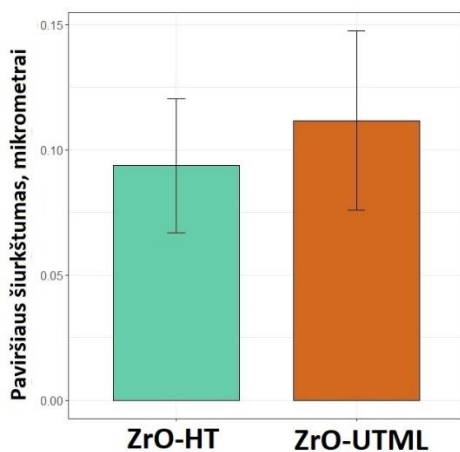
27 pav. Medžiagų paviršiaus šiurkštumas.

2.5.2. VANDENS KONTAKTINIS KAMPAS

Tirtų grupių vandens kontaktinio kampo matavimų vidurkiai ir standartiniai nuokrypiai pateikti 13 lentelėje.

Šapiro-Vilko normalumas ir dispersijos testų homogeniškumas (p > 0,05) leido taikyti ANOVA. Nors ir skaitine verte UV veiktos grupės pasižymėjo šiek tiek didesniu kontaktiniu kampu, tačiau vienfaktorinė ANOVA statistiškai reikšmingų skirtumų tarp grupių neidentifikavo (p = 0,292). Tai leidžia toliau interpretuoti grupes kaip vienodų hidrofiliškumo savybių.

13 lentelė. Vandens kontaktiniai kampai (laipsniais) pateikti kaip vidurkiai ± standartiniai nuokrypiai (SN) ir ANOVA rezultatas.

Tiriamoji grupė	Vidurkis	SN	F(Df)	p
ZrO-HT	69.9	6.4		
ZrO-HT-UV	73.7	13.9	3.50(16)	> 0.05
ZrO-UTML	79.5	12.8		
ZrO-UTML-UV	83.4	11.4		

2.5.3. ĮPRASTŲ IR UV SPINDULIUOYE AKTYVUOTŲ CIRKONIO KERAMINIŲ MEDŽIAGŲ CITOTOKSIŠKUMO VERTINIMAS

Citotoksiškumas buvo įvertintas kaip ŽDF gyvybingumo santykis su kontroline grupe po 12 valandų inkubacinio periodo (28 pav.). Vienfaktorinė ANOVA taikyta palyginti grupes tarpusavyje. Tos pačios medžiagos UV veiktos grupės pasižymėjo aukštesniu fibroblastų gyvybingumu, t.y. mažesniu citotoksiškumu.
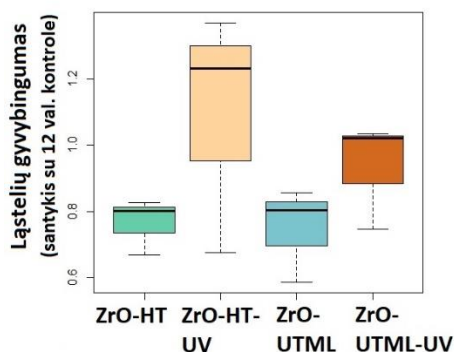
28 pav. Citotoksiškumo tyrimo rezultatai keturių tiriamų medžiagų paviršių, pateikiami kaip ŽDF ląstelių gyvybingumo santykis su 12 val. kontroline grupe.

2.5.4. ŽMOGAUS DANTENŲ FIBROBLASTŲ PROLIFERACIJA

ŽDF proliferacija tendencingai augo laike nepriklausomai nuo medžiagos ar UV poveikio paviršiui (14 lentelė ir 29 pav.). Aukščiausias santykis 24 ir 48 val. taškuose stebėtas ZrO-HT-UV grupėje, o tuo tarpu 72 val. – ZrO-UTML-UV grupėje. Žemiausias santykis visuose laiko taškuose stebimas ZrO-UTML grupėje.
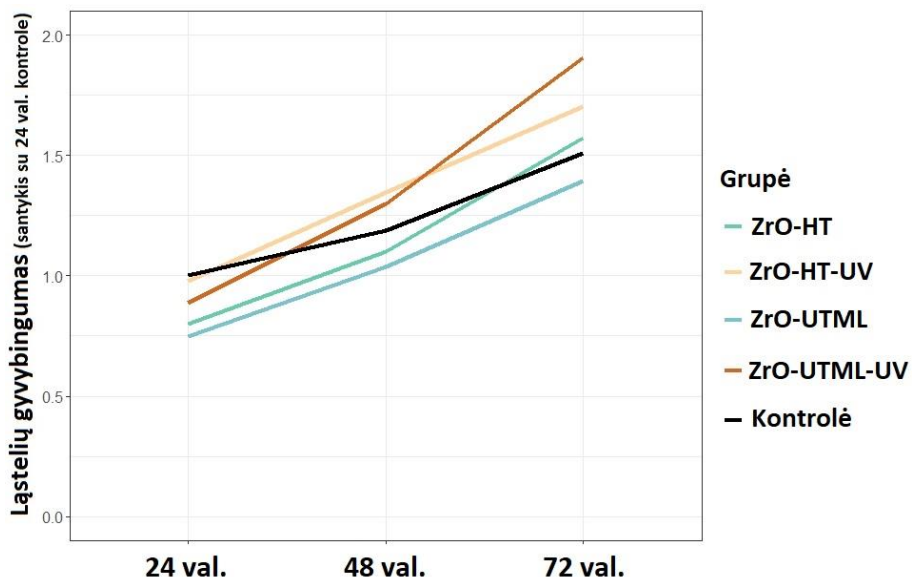
29 pav. ŽDF proliferacija tirtų medžiagų paviršiuose po 24, 48 ir 72 valandų inkubacijos.

Statistiškai reikšmingi skirtumai (14 lentelė) tarp grupių stebėti tik po 24 val. ($F(8) = 9{,}58$, $p = 0{,}005$). Post hoc Tjuko analizė atskleidė statistiškai reikšmingus skirtumus šiame laiko taške tarp ZrO-HT ir ZrO-HT-UV ($t = 3{,}875$, $p = 0{,}020$) bei tarp ZrO-UTML ir ZrO-HT-UV ($t = 4{,}976$, $p = 0{,}005$).

14 lentelė. ŽDF proliferacijos rezultatai, pateikti kaip gyvų ląstelių kiekio santykio su 24 val. kontrole verčių vidurkiai ir standartiniai nuokrypiai po 24, 48 ir 72 val. Statistiškai reikšmingi skirtumai porose pažymėti a ir b (post hoc Tjuko analizė).

Grupė	24 val.	48 val.	72 val.
ZrO-HT	0.80 ± 0.08 [a]	1.10 ± 0.17	1.58 ± 0.32
ZrO-HT-UV	0.98 ± 0.02 [ab]	1.35 ± 0.23	1.70 ± 0.39
ZrO-UTML	0.75 ± 0.06 [b]	1.04 ± 0.17	1.39 ± 0.42
ZrO-UTML-UV	0.89 ± 0.05	1.30 ± 0.32	1.91 ± 0.36
Control	1	1.19 ± 0.02	1.51 ± 0.32

2.6. KERAMINIŲ MEDŽIAGŲ PAVIRŠIAI IR JŲ ĮTAKA ŽDF IR Į EPITELIOCITUS PANAŠIOMS LĄSTELĖMS

2.6.1. PAVIRŠIAUS ŠIURKŠTUMAS

Tirtų medžiagų paviršiaus profilometrijos rezultatai pateikti 30 pav. Visos medžiagos, išskyrus ZrO-V (0,69 ± 0,15 µm), pasižymėjo vidutinėmis Sa vertėmis žemiau 0,25 µm. Kadangi grupių duomenų dispersijos nebuvo homogeniškos (Livyno kriterijus F = 3,33, p < 0,05), taikytas Velčo (*Welch*) vienfaktorinės ANOVA testas, siekiant įsitikinti, ar tarp tiriamų grupių yra skirtumų. Rezultatai atskleidė statistiškai reikšmingą paviršiaus šiurkštumo skirtumą tarp medžiagų grupių (F_{Welch} = 16,68, p < 0,001). *Games-Howell* post hoc porinė analizė identifikavo ZrO-V grupę besiskiriančią nuo visų kitų tirtų medžiagų grupių (p < 0,05).
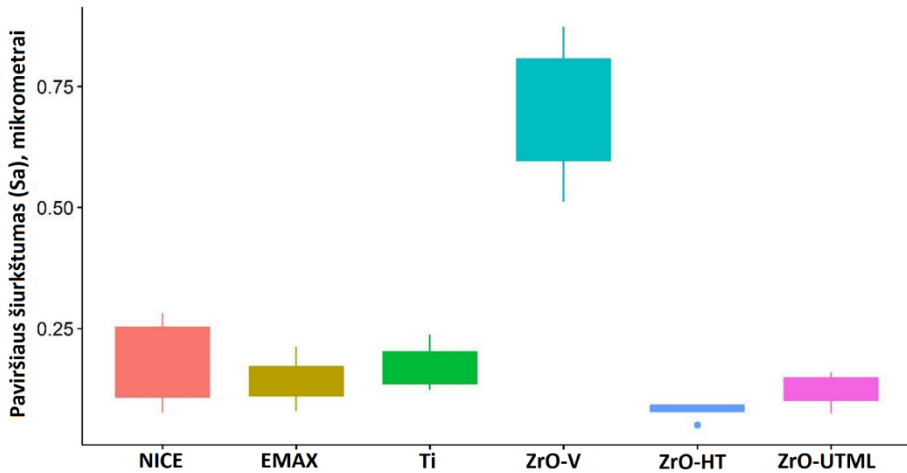
**30 pav.** Tirtų medžiagų paviršiaus šiurkštumas.

2.6.2. VANDENS KONTAKTINIS KAMPAS

Vandens kontaktinio kampo rezultatai pateikti 15 lentelėje. Normalumo ir homogeniškumo prielaidos duomenims buvo išpildytos (W = 0,93, p > 0,05; F_{Levene}= 2,07, p > 0,05), todėl analizei taikyta vienfaktorinė ANOVA.

15 lentelė. Tirtų medžiagų paviršių vandens kontaktinio kampo (*WCA*) rezultatai, iš-reikšti laipsniais, pateikti kiekvienai grupei kaip vidurkis ir standartinis nuokrypis (SN).

Medžiaga	Vidurkis	SN
EMAX	45.34	2.64
NICE	58.48	21.51
Ti	83.24	6.94
ZrO-V	51.56	2.16
ZrO HT	69.90	6.37
ZrO UTML	79.48	12.79

ANOVA rezultatas (31 pav.) nurodė statistiškai reikšmingus skirtumus tarp grupių (F = 9,70, p < 0,001). Tjuko post hoc analizė identifikavo statistiškai reikšmingus skirtumus tarp šių grupių: Ti – EMAX (p < 0,001), ZrO-HT – EMAX (p < 0,05), ZrO-UTML – EMAX (p < 0,001), Ti – NICE (p < 0,05), ZrO-V – Ti (p < 0,01) ir ZrO-UTML - ZrO-V (p < 0,01).
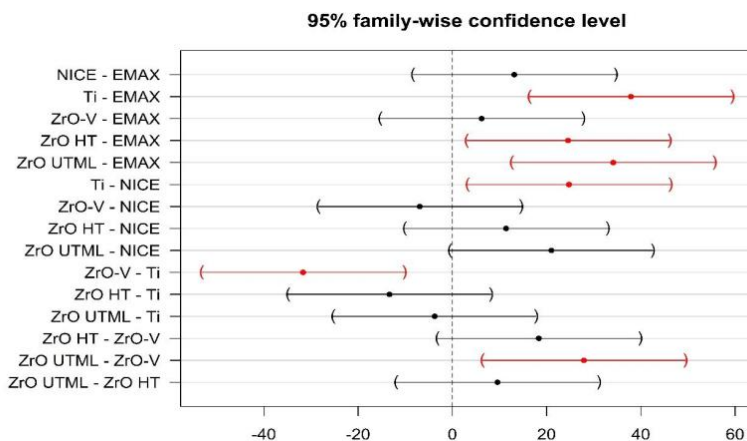
31 pav. Grafinis pavaizdavimas vidutinio vandens kontaktinio kampo skirtumo tarp skirtingų medžiagų grupių pavaizduoti raudonai.

2.6.3. CITOTOKSIŠKUMO VERTINIMAS

Abiejų tirtų ląstelių linijų citotoksiškumo aprašomoji statistika pateikta 16 lentelėje. Į epitelines panašių ląstelių minimumas ir maksimumas fiksuoti EMAX grupėje (min = 0,49; max = 1,21). ŽDF minimumas fiksuotas NICE grupėje (min = 0,56), o maksimumas Ti grupėje (max = 0,99).

16 lentelė. Į epitelines panašių ląstelių (EPL) ir ŽDF medžiagų paviršių citotoksiškumo tyrimo rezultatai, pateikti kaip ląstelių gyvybingumo (santykis su 12 val. kontrolės atskaita) vidurkiai ir standartiniai nuokrypiai (SN).

| Medžiaga | Ląstelės | | | |
| | EPL | | ŽDF | |
	Vidurkis	SN	Vidurkis	SN
kontrolė	1	-	1	-
EMAX	0,84	0,36	0,80	0,06
NICE	0,80	0,11	0,65	0,16
Ti	0,71	0,14	0,77	0,20
ZrO-HT	0,73	0,24	0,76	0,08
ZrO-UTML	0,75	0,16	0,75	0,14
ZrO-V	0,67	0,21	0,75	0,13

2.6.4. PROLIFERACIJA

Dviejų faktorių sąveikos analizė buvo taikyta siekiant įvertinti į epitelines panašių ląstelių ir ŽDF proliferaciją.
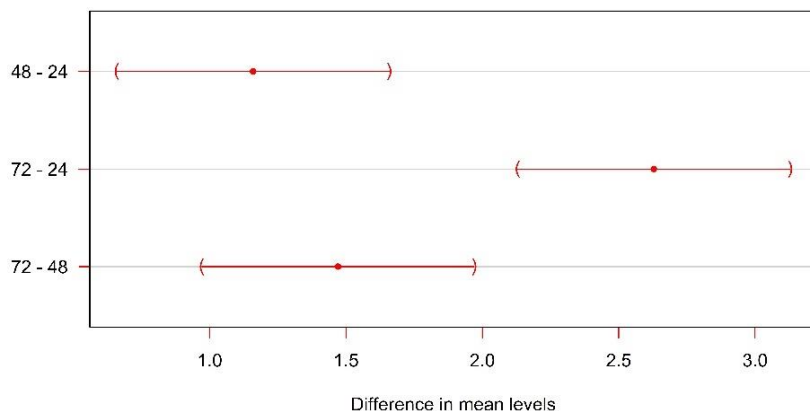
Į epitelines panašių ląstelių rezultatai pateikti 17 lentelėje ir 32 pav. Reikia pažymėti, kad ANOVA modelio paklaidos atskleidė nedidelį nukrypimą nuo normalumo, todėl pateikti rezultatai turėtų būti interpretuojami su saikinga atsarga. Stebimi statistiškai reikšmingi skirtumai tarp grupių medžiagos ir laiko kintamųjų, tačiau jų sąveika nereikšminga.

17 lentelė. Dvifaktorinės ANOVA rezultatai medžiagos ir laiko kintamųjų bei jų sąveikos įtakos į epitelines panašių ląstelių proliferacijai.

|	Df	Sum Sq	Mean Sq	F	P
Medžiaga	6	7.56	1.26	2.25	< 0.05
Laikas	2	72.91	36.54	94.01	< 0.001
Medžiaga : Laikas	12	8.05	0.67	1.73	> 0.05
Paklaidos	42	16.29	0.39		

Medžiagos kintamasis pasireiškė tik 72 val. taške lyginant ZrO-V ir kontrolinę grupes (p < 0,05). Kitais laiko atskaitos taškais statistiškai reikšmingų skirtumų tarp tiriamų medžiagų neidentifikuota.

32 pav. Vidurkių skirtumo tarp trijų laiko taškų į epitelines panašių ląstelių prolifera-cijos grafinis pavaizdavimas.

Tikėtas absoliutus ląstelių gyvybingumo didėjimas buvo stebimas skirtinguose laiko taškuose ir pavaizduotas 33 pav. Taip pat statistiškai reikšmingas skirtumas buvo stebimas visose lygintose laiko porose (48-24, 72-24 ir 72-48), kaip tai atsispindi ir 32 pav.
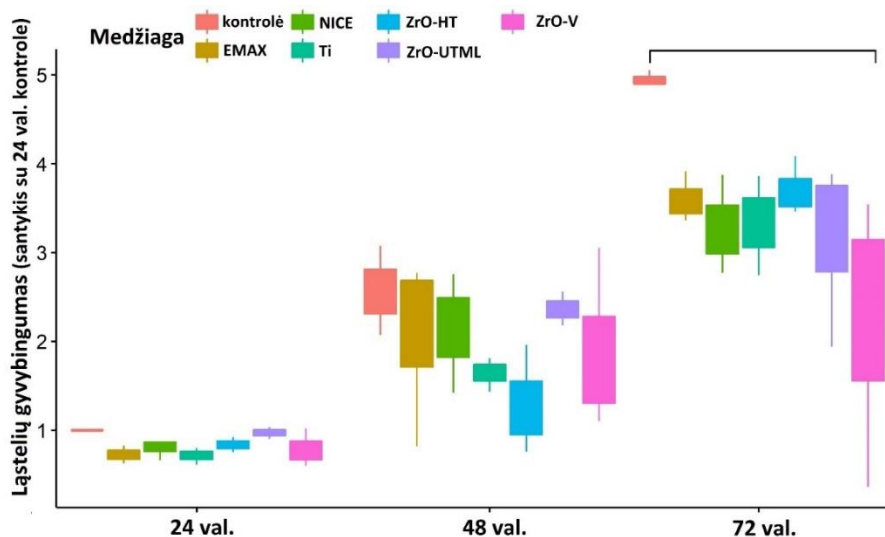
33 pav. Į epitelines panašių ląstelių proliferacija ant mėginių paviršiaus trijuose tir-tuose laiko taškuose išreikšta kaip gyvų ląstelių kiekio santykis su 24 val. kontrolės atskaita.

ŽDF proliferacijos rezultatai pavaizduoti 18 lentelėje ir 34 pav. Stebimi reikšmingi skirtumai medžiagos ir laiko grupėse, bet ne šių kintamųjų sąveikoje

18 lentelė. Dvifaktorinės ANOVA rezultatai medžiagos ir laiko kintamųjų bei jų sąveikos įtakos ŽDF proliferacijai.

	Df	Sum Sq	Mean Sq	F	P
Medžiaga	6	0.28	0.05	3.64	< 0.01
Laikas	2	1.72	0.86	67.23	< 0.001
Medžiaga : Laikas	12	0.1	0.01	0.68	> 0.05
Paklaidos	42	0.5	0.01		

Medžiagos kintamasis atskleidė reikšmingą skirtumą 24 val. tarp kontrolės ir ZrO-V (p < 0,05). Taip pat 48 val. taške skirtumas identifikuotas tarp kontrolės ir Ti bei ZrO-UTML (p < 0.05) ir 72 val. taške tarp kontrolės ir ZrO-V (p < 0,05), NICE bei Ti (p < 0,01). ŽDF proliferacija taip pat statistiškai reikšmingai skyrėsi 72 val. taške tarp Ti ir ZrO-HT grupių (p < 0,05).

95% family-wise confidence level
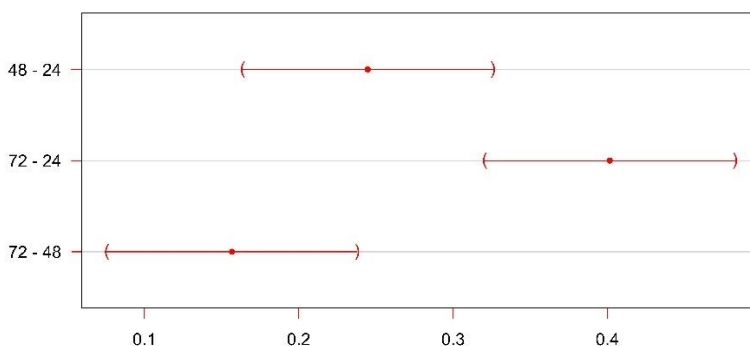
34 pav. Vidurkių skirtumo tarp trijų laiko taškų ŽDF proliferacijos grafinis pavaizdavimas

ŽDF taip pat demonstravo tikėtąjį augimą laike (35 pav.). Tai pagrįstas ir reikšmingais skirtumais visuose laiko taškuose (48-24, 72-24 ir 72-48), kaip vaizduojama ir 34 pav.
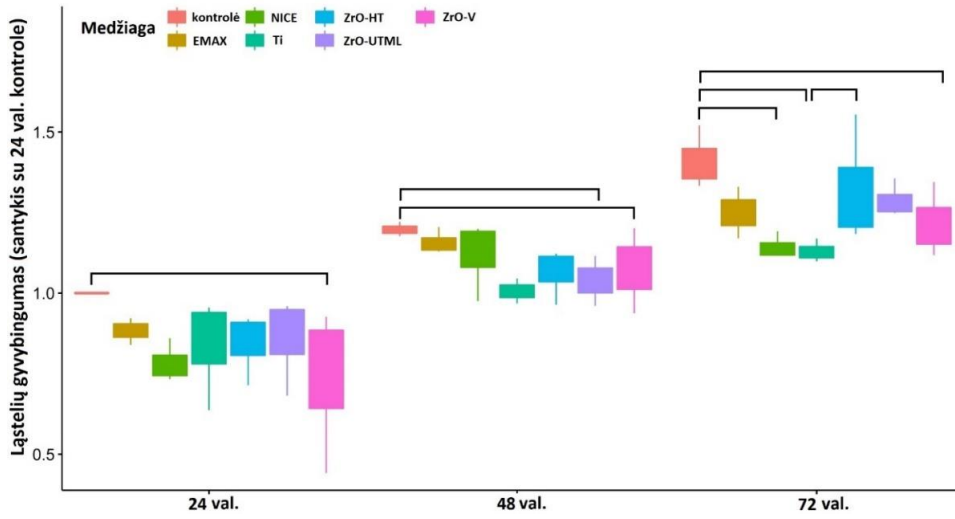
35 pav. ŽDF ląstelių proliferacija ant mėginių paviršiaus trijuose tirtuose laiko taš-
kuose, išreikšta kaip gyvų ląstelių kiekio santykis su 24 val. kontrolės atskaita.

3. REZULTATŲ APTARIMAS

Šis tyrimas įvertino dinaminės navigacijos tikslumą ir galimus įtakos turinčius veiksnius viršutinio žandikaulio modelių tyrime. Aptariant rezultatus, svarbu akcentuoti, jog dauguma studijų, su kuriomis lyginami šie rezultatai, taiko TKT pagrįstą tikslumo vertinimo metodiką. Kaip jau minėta darbo įvade, TKT pagrindu vertinamas tikslumas susijęs su kai kuriais esminiais metodologiniais trūkumais ir galimais netikslumais. Šis kontekstas yra ypač svarbus, nes atliktame tyrime vertintas tikslumas taikant IOS pagrįstą metodiką.

Atlikto tyrimo įvesties taško paklaidos yra tyrimuose publikuotame dinaminės navigacijos tikslumo intervale: 0,37–1,58 mm *in vitro* tyrimuose ir 0,67–1,37 mm klinikiniuose tyrimuose [36,39,43]. Skirtingose grupėse paklaidos varijavo santykinai plačiai, tačiau vis tiek tyrimuose aprašyto intervalo ribose: nuo 0,56 ± 0,33 (K3, SL, M) iki 1,2 ± 0,28 mm (K1, SL, D). Tyrimo duomenys rodo tendenciją (arti statistinio reikšmingumo lygmens), jog didėjant dantų skaičiui ir jų pasiskirstymo plotui, įvesties taško paklaida mažėja (didėjant *Kennedy* klasės numeriui). Tai gali būti susiję su tikslesniu vaizdų sujungimu bei registravimu, turint daugiau dantų paviršių ir jiems plačiau bei tolygiau išsidėsčius. Šiam pastebėjimui antrina ir kitoje tyrimo dalyje stebimas aukštas tikslumas naudojant registravimui atskaitos objektus vietoje dantų, kai atskaitos objektai yra plačiai pasiskirstę ir gerai apibrėžti, nors plotas jų ir mažesnis nei dantų. Tai taip gali būti pagrįsta ir anksčiau plačiai taikytu registravimo metodu naudojant specialius objektus (angl. *fiducial objects*), kurie buvo taikomi tiek atliekant TKT, tiek ir registruojant burnoje. Tokie tyrimai dažnai atžymi aukštą metodo tikslumą, pranokstantį šio tyrimo rezultatus: 0,38 ± 0,25 mm [481], 0,41 ± 0,12 mm [482]. Pagrindinis tokio registravimo metodo trūkumas yra ribotas universalumas, nes tokio objekto naudojimas reikalauja jį pasitelkti labai anksti, dar net nepradėjus skaitmeninio planavimo. Tačiau taip pat yra tyrimų, kurie praneša, jog nepakankamai kokybiški atskaitos objektai gali lemti gana dideles paklaidas tiek naujokams, tiek patyrusiems chirurgams – 1,39 ± 0,48 mm, ir 1,19 ± 0,45 mm atitinkamai [472]. Vertinant implanto dizaino įtaką, mažesnio kūgio implanto grupėje (SL) pastebėtos statistiškai reikšmingai mažesnės paklaidos mezialinėje implanto padėtyje nei distalinėje, tačiau didesnio kūgio (PL) dizaino grupėje ši tendencija neišryškėjo. Tai gali būti susiję ir su tuo, jog skirtinga grąžtų ir implanto dizaino kombinacija lemia kiek skirtingą

ložės ir implanto tikimą, bet taip pat reikia manyti, tikėtina, jog implanto plano perteikimas tikslesnis mezialinėje padėtyje (arčiau dantų atramos ir atskaitos) nei distalinėje. Dar viena galima didesnių paklaidų priežastis gali būti imituojama kieto kaulo situacija (D1) – didesnis pasipriešinimas grąžtui, modelis reikalauja ilgesnio darbo siekiant paruošti tinkamai ložę, nukrypus nuo centrinės ašies, sudėtingiau atstatyti kryptį, nei minkštame kaule. Panašūs labai kieto modelio situacijos tyrimai taip pat nustatė aukštas įvesties taško paklaidas $1,55 \pm 1,08$ mm – $1,74 \pm 0,64$ mm [484]. Norint išsamiau suprasti įvesties taško paklaidas, verta analizuoti jo komponenčių – horizontalios ir vertikalios paklaidos tendencijas.

Absoliučios gylio (a) paklaidos šio tyrimo duomenimis variavo įvairioms grupėms nuo $0,21 \pm 0,15$ mm iki $0,76 \pm 0,55$ mm. Šie rezultatai yra labai artimi apžvalgos tyrimų skelbiamų *in vitro* gylio paklaidų, kurios varijuoja nuo 0,26 mm iki 1,14 mm [36,39]. Gylio (a) paklaida statistiškai reikšminai mezialinėje padėtyje buvo mažesnė SL dizaino grupės, lyginant su didesnio kūgio (dar kliniškai vadinamo „agresyvesnio" implanto dizaino) grupes (PL). Tai gali būti susiję su įvairiais preparavimo ir implanto dizaino aspektais, pavyzdžiui, PL implanto 120 laipsnių rotacijos žingsnis lemia 0,3 mm gylio padidėjimą, tuo tarpu SL – 0,2 mm [485]. Nors SL dizaino atveju mezialinė implanto padėtis (ypač esant mažiau dantų – K1 ir K2 situacijose) taip pat kaip ir įvesties taškui turėjo žemesnes paklaidas nei distalinė padėtis, tačiau ši tendencija nebuvo būdinga PL dizaino grupėje, netgi priešingai – mezialinė padėtis pasižymėjo tendencija aukštesnėms gylio paklaidoms (pvz., K3 PL M grupėje $0,72 \pm 0,46$ mm). Panaši tendencija jau buvo pastebėta ir kai kuriuose kituose tyrimuose, Kang su bendraautoriais (2014), pilnai bedančių apatinio žandikaulio modelių studijoje pademonstravo didesnes gylio paklaidas iltinio danties zonoje ($1,14 \pm 1,25$ mm) lyginant su krūminių dantų sritimi ($0,76 \pm 0,84$ mm) [486]. Šio tyrimo apimtyje galima svarstyti ir tikėtiną įtaką skirtingo implanto skersmens bei ilgio – mezialinėje padėtyje buvo planuojamas ir sriegiamas siauresnis bei trumpesnis implantas, imituojant būdingą klinikinę situaciją. Taip pat absoliučias gylio paklaidas papildo ir realiosios gylio paklaidos (r), kurios atspindi, jog vyravo neigiamos vertės – per giliai susriegti implantai nuo $-0,01 \pm 0,28$ (K2, SL, M) iki $-0,76 \pm 0,55$ (K1, SL, D). Vienintelės išimtys pažymėtinos PL grupėse: distalinė K3 padėtis $0,21 \pm 0,21$ mm ir pavienis defektas $0,01 \pm 0,3$. Deja, tyrimų vertinančių realiąsias gylio paklaidų vertes nepavyko identifikuoti (arba nėra aiškiai aprašoma publikacijų metodinėje dalyje), tai paaiškinama sudėtingesne tokių duomenų

interpretacija. Vertinant paklaidas šioje perspektyvoje PL dizaino atveju, jos pasiskirsto tolygiau apie nulį, lyginant su SL dizaino grupe (vyrauja neigiamos vertės). Taip pat, PL grupėje mezialinėje padėtyje vyravo per gili implanto padėtis, su vidutiniškai 0,4-0,6 mm per gilia pozicija – tai suponuoja, jog trumpesnis ir siauresnis implantas mezialinėje padėtyje PL dizaino atveju turi polinkį per giliai padėčiai. Priešinga tendencija stebėta SL dizaino atveju, kai gilesnės implanto padėtys siejosi su distaline implanto padėtimi.

Atlikto tyrimo dinaminės navigacijos horizontalios implantų pozicionavimo paklaidos varijavo nuo 0,39 ± 0,18 iki 0,93 ± 0,35 mm įvairiose grupėse. Šie rezultatai atitinka, kitų tyrimų skelbiamus horizontalios paklaidos intervalus: 0,36–1,27 mm [36] ir 0,33–3,03 mm [39]. Šiame tyrime distalinė implanto padėtis statistiškai reikšmingai buvo susijusi su didesne horizontalia paklaida, o tai turėjo tiesiogiai įtakos ir įvesties taško paklaidų tendencijoms. Tai tikėtina siejasi su faktu, jog registravimui naudojant dantų paviršius, tos sritys, kurios yra arčiau priekinių dantų segmento, tiksliau perteikia implanto pozicijas dinaminės navigacijos metodu, nei distalinės padėtys, kurios yra atokiau ar visai neturi gretimų dantų, kurie pasitelkiami sekimo registravimui. Kang ir bendraautoriai (2014) pilnai bedančių modelių tyrime nustatė dideles horizontalias paklaidas iki 2–3 mm ir tendencijas didesnių paklaidų distaliniuose segmentuose [486]. Kitame šio tyrimo etape taikant atskaitos objektus sekimo registracijai pilnai bedančių modelių atveju gautos kur kas mažesnės horizontalios paklaidos (0,2–0,7 mm intervale), tai leidžia manyti, jog nuolat tobulėjančios dinaminės navigacijos technologijos ir registravimo metodai ženkliai sumažina šias paklaidas. Vienos mažiausių horizontalių paklaidų buvo Brief ir kt. (2005) tyrime (0,35–0,65 mm), tačiau šiame tyrime vertintas tik osteotomijos pilotiniu grąžtu tikslumas [487]. Pilnai gidinė implantacija, apimanti ne tik implanto ložės preparavimą visa grąžtų seka, bet ir implanto sriegimą, lemia kur kas daugiau proceso įvairumo ir su tuo susijusias klinikinei situacijai artimesnes didesnes paklaidas.

Kampo paklaida šiame tyrime dinaminės navigacijos metodui varijavo nuo 1,04 ± 0,53 iki 4,5 ± 1,18 laipsnių. Tai atitinka visų trijų apžvalgų, paskelbtų 2021 metais, kampo paklaidos rezultatus: 0,89°–4,45° [43]; 0,82°–5,49° [36]; 1,09°–12,37° [39]. K2 klasės bedantis defektas buvo susijęs su didesnėmis kampo paklaidomis, lyginant tiek su K1, tiek su K3 situacija. K2 atveju didesnės paklaidos buvo susijusios su distaline implanto padėtimi. Tai galėtų būti susiję su asimetriška (vienpusis) atviro distalinio defekto konfigūracija, kuriame nėra distalinio danties, kuris galėtų padidinti registracijos tikslumą.

Tai pagrindžia ir palyginimo su statiniu metodu duomenys: statinis metodas statistiškai reikšmingai sumažina K2 distalinio implanto kampo paklaidą, nors bendru atveju dinaminis metodas pasižymi statistiškai reikšmingu didesniu kampo tikslumu, lyginant su statiniu metodu. Dinaminės navigacijos metodo kampo tikslumui neigiamą įtaką turėjo distalinė implanto padėtis. Kai kuriuose ankstesniuose tyrimuose pranešama apie bedančių modelių atveju didesnes paklaidas mezialinėje implanto pozicijoje (iltinio srityje 12,37° ± 4,18°, lyginant su krūminio 8,97° ± 3,83°) [486]. Šie rezultatai tikėtina bus taip pat sąlygoti bedančio modelio situacijos ir mažiau išvystytos dinaminės navigacijos technologijos.

Skirtingų dinaminių navigacijos sistemų įvesties taško paklaidos yra labai panašios ir artimos bei vyrauja apie 1 mm ir statistiškai reikšmingai nesiskiria; tuo tarpu kampo nuokrypis vyrauja nuo 2,5° iki 6,5° (vidurkis skirtingų sistemų apie 3,5°), bet taip pat statistiškai reikšmingai nesiskiria [36,43]. 2021 m. duomenimis tyrimuose viso buvo vertintos 9 skirtingos dinaminės navigacijos sistemos, dažniausiai tyrimuose taikoma „*Navident*" sistema [36]. Atlikto tyrimo dinaminės navigacijos paklaidų rezultatai yra artimi, lyginant su šiais pateiktais panašių tyrimų duomenimis, apimančiais skirtingas navigacijos sistemas.

Nors modelių tyrimai akivaizdžiai neperteikia pilnos klinikinės situacijos ir dažnai pateikia mažesnes paklaidų vertes, tačiau sisteminių apžvalgų duomenimis lyginant su klinikiniais tyrimais statistiškai reikšmingų skirtumų dinaminės navigacijos tikslumo rezultatų nebuvo nustatyta (įvesties taško 0,91 mm ir 1,11mm bei kampo 2,78° ir 4,22° paklaidų vidurkiai atitinkamai) [43]. Šiai išvadai antrina ir kitos apžvalgos rezultatai, vertinantys *in vitro* ir klinikinį dinaminių sistemų tikslumą atitinkamai: 1,00 mm ir 1,03 mm bei 4,1° ir 3,7° [39]. Tačiau trečiojoje tų pačių 2021 metų apžvalgoje pateikiamos *in vitro* įvesties ir kampo paklaidos (0,46 mm ir 2,01°) buvo pažymėtos kaip reikšmingai mažesnės nei klinikinių tyrimų (1,03 mm ir 3,68°) [36]. Šio tyrimo dinaminės navigacijos tikslumo *in vitro* rezultatai atsiduria per vidurį tarp šių tyrimų rezultatų.

Dažnai modelių tyrimai, lyginantys statinio ir dinaminio metodo tikslumą, nurodo, jog statistiškai reikšmingų skirtumų tarp šių dviejų metodų nėra pastebėta [43]. Šiai išvadai antrina ir Wang bei bendraautorių (2021) klinikinių tyrimų sisteminė apžvalga [91]. Guzmán ir kiti (2019) modelių tyrime, nurodė įvesties taško paklaidas be reikšmingo skirtumo statiniam (0,78 ± 0,43 mm) ir dinaminiam (0,85 ± 0,48 mm) metodui, tačiau kampo paklaidas didesnes

dinaminiam (4,0° ± 1,4°) nei statiniam (3,0° ± 1,5°) metodui [483]. Dalis klinikinių tyrimų taip pat nurodo nesant reikšmingų skirtumų įvesties taško ir kampo paklaidoms naviguojant statiniu (0,97 ± 0,44 mm; 2,8° ± 1,7°) ir dinaminiu (1,05 ± 0,44 mm; 3,1° ± 1,4°) metodais [354]. Šio tyrimo rezultatai prieštarauja pateiktiems tyrimams. Statinio metodo įvesties taško paklaidos (0,52 ± 0,28 mm) statistiškai reikšmingai žemesnės nei dinaminio metodo (0,77 ± 0,32 mm), tuo tarpu kampo paklaidos statistiškai reikšmingai mažesnės dinaminio metodo (2,3° ± 1,3°) nei statinio (2,9° ± 1,3°). Žinoma klinikinė prasmė paklaidos skirtumo 0,25 mm ar 0,6° galbūt nėra didelės reikšmės. Nors dinaminio metodo paklaidos panašios, tačiau esminis skirtumas šio tyrimo nuo aukščiau pateiktų – kur kas didesnis statinio metodo tikslumas. Tai turėtų būti vertinama konservatyviai. Gerai žinoma, jog statinio navigavimo tikslumas klinikiniuose tyrimuose yra kur kas mažesnis nei modelių tyrimuose, meta-analizės duomenimis įvesties taško paklaida siekia 1,2 mm, o kampo – 3.5° [25,308]. Šio tyrimo rezultatai pilnai atitinka Stunkel ir kt. (2022) *in vitro* tyrimo rezultatus, kurie nurodo statistiškai reikšmingai didesnį statinio metodo tikslumą nuotolio paklaidoms (milimetrais), bet didesnį dinaminio metodo tikslumą kampo paklaidai (3° ir 4,6° atitinkamai) [537]. Kita vertus, dinaminio metodo kampo tikslumas jau ir ankstesnėse apžvalgose buvo pažymėtas kaip pranašesnis prieš statinį metodą (vidutinis skirtumas 0,86°) ir juolab implantavimą laisva ranka (4,33°) [36]. Taip pat reikėtų paminėti, jog nepaisant nedidelio esamų tokio dizaino tyrimų kiekio, kurie taiko IOS grįstą tikslumo vertinimo metodą, panašaus *in vitro* modelio tyrimo statinio metodo įvesties taško (0,67 ± 0,38 mm) ir kampo (2,7° ± 1,4°) paklaidų rezultatai atitinka šio tyrimo rezultatus [379].

Tyrimų vertinančių dinaminės navigacijos sekimo registravimo metodus yra mažai. Atvejų serijų publikacijoje pilnai bedančių žandikaulių dinaminės navigacijos registravimui taikant mini-implantus, pranešamas aukštas rezultatų tikslumas įvesties taško 0,66 ± 0,35 mm bei kampo 2,6° ± 1,3° [538]. Tai palyginti aukšto tikslumo rezultatai *in vivo* pilnai bedančių pacientų situacijoje, paremiantys fiksuotų gerai apibrėžtų rentgenokontrastiškų atskaitos objektų taikymą navigacijos registravimui. Atlikto tiriamojo darbo *in vitro* modelių rezultatai taip pat paremia ir yra suderinami su šiais klinikinio tyrimo duomenimis.

Minkštųjų audinių ląstelių tyrimo dalyje buvo vertintos neatidėliotino protezavimo polimerinės medžiagos, keraminės medžiagos ir jų paviršiaus aktyvavimas UV spinduliuote. Net jei klinikinis protokolas ne visada gydytoją

įgalina rinktis neatidėliotiną protezavimą, transmukozinio elemento medžiagos ir paviršiaus klausimai išlieka nemažiau svarbūs minkštųjų audinių atsakui ir sklandžiam pirminiam žaizdos gijimui. Laikinos atramos ir kiti dantenas formuojantys implantų komponentai yra svarbi gydymo proceso dalis, nes jie modeliuoja ir kondicionuoja minkštuosius audinius jautrios pradinės gijimo fazės metu [494]. Be to, kai kuriais neatidėliotinos implantacijos ar chirurginių minkštųjų audinių procedūrų atvejais (ypač estetinėje srityje), laikinos atramos gali tarnauti visą gijimo laikotarpį, kuris gali trukti nuo kelių savaičių iki kelių mėnesių [495–497]. Vis dažniau taikant vieno etapo chirurgiją ir greitą arba ankstyvą implantų apkrovimą, nuolatinės protezinės medžiagos naudojamos ankstyvoje gijimo fazėje [498–500]. Pagrindinis siekis šiais ankstyvaisiais gijimo etapais yra nukreipti minkštųjų audinių ląstelinę reakciją, siekiant formuoti sveiką audinių architektūrą ir barjerą aplink dantų implantų atramą, kuo artimesnį į esantį prie sveikų natūralių dantų. Keletas nuo medžiagos priklausančių veiksnių prisideda prie stabilaus minkštųjų barjero susidarymo aplink implantų atramas ir restauracijas, kurios liečiasi su burnos minkštaisiais audiniais: cheminės savybės, paviršiaus šiurkštumas ir hidrofiliškumas. Visi šie veiksniai yra nurodomi kaip reikšmingi tiek ŽDF, tiek ir epitelinių ar į jas panašių ląstelių, tiek ir bakteriniam atsakui [394,428,432,456,475,476,503,519–525].

Klinikinėje praktikoje polimerinės medžiagos yra naudojamos tiek kaip laikinos, tiek kaip ilgalaikės restauracinės medžiagos [492,493]. Šiame polimerinių medžiagų tyrime vertintos 5 skirtingos medžiagos ir 2 skirtingi jų paviršių plovimo protokolai. Plovimo protokolas turėjo statistiškai reikšmingos įtakos tirtam paviršiaus šiurkštumui, hidrofiliškumui (vandens kontaktinis kampas, *WCA*) ir ŽDF atsakui. Rezultatai, apimantys palankesnį paviršiaus plovimo protokolą, toliau lėmė jo pritaikymą keraminių medžiagų eksperimentuose.

Medžiagų paviršiaus profilį ir šiurkštumą lemia gydytojo arba laboratorijos atliktos poliravimo ir paviršiaus išbaigimo bei modifikavimo procedūros. Paviršiai pagal vidutinį šiurkštumą gali būti klasifikuojami kaip lygūs, minimaliai ir vidutiniškai šiurkštūs bei šiurkštūs [426]. Ankstesnių tyrimų duomenimis yra žinoma 0,2 µm vidutinio paviršiaus šiurkštumo slenkstinė riba [428,501–503]. Didelė dalis kasdien naudojamų standartinių titano atramų pasižymi būtent tokiu paviršiaus šiurkštumu Ra 0,15–0,24 µm [527,528]. Taip pat nurodoma, kad lygesni nei 0,1 µm titano paviršiai gali turėti neigiamos įtakos fibroblastų funkcijai [435]. Šiam pastebėjimui antrina ir kiti tyrimai,

nurodantys, kad labai lygūs (< 0,1 μm) paviršiai padidina jungties netekimą, zondavimo gylį ir BOP reikšmes [433,436]. Titano, cirkonio dioksido ir ličio disilikato medžiagų paviršiaus šiurkštumas 0,1–0,2 μm intervale demonstravo didesnį fibroblastų prisitvirtinimą nei lygesni ar šiurkštesni paviršiai [437]. Šiame tyrime taikyti tikslūs poliravimo ir plovimo protokolai iš esmės leidžia užtikrinti medžiagų šiurkštumą šiame intervale visais atvejais, išskyrus glazūruotą ZrO-V grupę. Nuplovus medžiagų paviršius įprastiniu būdu (*CCP*), į šį intervalą pakliuvo tik Ti ir ZrO, o pritaikius daugiapakopį plovimo protokolą (*RCP*) visos medžiagos įeina į šį intervalą išskyrus ZrO-HT (0,079 ± 0, 017 μm) ir ZrO-V (0,69 ± 0,15 μm). Didesnis paviršiaus šiurkštumas gali mažinti fibroblastų proliferaciją ir skatinti bakterijų adheziją, bioplėvelės susidarymą ir susijusius neigiamus padarinius [432,433]. Klinikinis tyrimas parodė, kad 0,8 μm paviršiaus šiurkštumas padidino bioplėvelės tūrį ir patogeniškumą 25 kartus [436]. Kita vertus, makrošiurkštūs >8 μm paviršiai, pagaminti lazeriu modifikuojant paviršių specifine tekstūra (*Laser-Lok®*), pasižymėjo pranašesnėmis dantenų morfologijos, proliferacijos, skaidulų orientacijos, taip pat bioplėvelės valdymo efektyvumo savybėmis [434,529,530]. Duomenų apie paviršiaus plovimo įtaką šiurkštumo parametrams yra nedaug. Heimer ir kt. (2016) nustatė, kad naudojant ultragarso vonelę 6,3 min. medžiagos paviršiaus šiurkštumo (Ra) vertės išlieka panašios (0,033 μm PEEK ir 0,066 μm PMMA) kaip ir su kitomis laboratorinėmis valymo sistemomis, veikiančiomis 15–20 minučių [414]. Šie duomenys neatitinka atlikto tyrimo rezultatų. Tikėtiniausia skirtumų priežastis tyrimo dizainas ir metodai: čia ultragarso vonelė *CCP* taikyta tik 3 minutes, bet taip pat skyrėsi ir medžiagų paviršių poliravimas, profilometrijos metodika (optinė, ne kontaktinė) bei paviršiaus šiurkštumo matas (dalyje tyrimų vertinamas ne ploto (Sa), o tik profilio (Ra) šiurkštumas). Nemaža dalis tyrimų, kurie teikia paviršiaus šiurkštumo duomenis neidentifikuoja taikyto paviršiaus plovimo protokolo [419,465,504]. Dažniausiai taikoma ultragarsinė vonelė 3–20 min su vandeniu ar alkoholiu (pvz., 70 % etanolis ar izopropanolis) su paskensiu plovimu vandeniu [411,413,415,416,466,505,507].

Polimerinių medžiagų vidutinės paviršiaus šiurkštumo vertės (Ra/ Sa) kituose tyrimuose varijuoja labai stipriai: PMMA 0,02–6,2 μm [413– 416,465], 3D spausdintas PMMA (SLA) 0,39–2,97 μm [465,504], PEEK 0,032–2,52 μm [411,413–415,419,465,466,505] ir PEKK 0,24–3,11 μm [506,507]. Tokie didžiuliai skirtumai labiausiai yra nulemti pasirinkto profilometrijos metodo, bet taip pat gali būti susiję su medžiagos savybėmis

(neorganinis užpildas), paviršiaus poliravimo/apdorojimo protokolu [411,413,415,416,419,465,466,504–507]. Literatūroje aptariami trys paviršiaus šiurkštumo lygiai: makro (Ra ⁓10 μm), mikro (Ra ⁓1 μm) ir nano (Ra ⁓0.2 μm) [432,526]. Skirtingos profilometrijos technologijos ir metodikos tą patį paviršių leidžia įvertinti skirtingu lygmeniu ir tai iš esmės gali lemti skirtingą paviršiaus šiurkštumo rezultatą. Vertinant tyrimų duomenis, reikia atsižvelgti į paviršiaus profilometrijos metodą (kontaktinis ar nekontaktinis) ir susijusius parametrus (adatos viršūnės spindulį, ribines vertes, FOV, matavimų skaičių vienam paviršiui ir kt.) [439–442]. Taip pat svarbu paminėti tai, jog kartais tyrimai vertina paviršiaus šiurkštumą kitame kontekste; pavyzdžiui PEKK paviršiai tikslingai šiurkštinti siekiant testuoti surišimo jėgą [506,507]. PMMA paviršiai po 3D spausdinimo nebuvo poliruoti, o šiurkštumas buvo susijęs su spausdinto objekto 3D orientacija [504,508]. Paviršiaus šiurkštumas svarbus ir tyrėjus dominantis kriterijus, tačiau pirmiau minėti rezultatai rodo, kad pasikliauti tik paviršiaus šiurkštumu kaip minkštųjų audinių barjero susidarymo ir *in vivo* ląstelių elgsenos prognoze gali būti nepakankamai patikima.

Žinoma, jog hidrofiliniai paviršiai yra palankūs eukariotinėms ląstelėms [443,444]. Jie palaiko ŽDF prisitvirtinimą, o tai gali lemti geresnį minkštųjų audinių sandarumą aplink implanto protezinį komponentą [438]. Tuo tarpu medžiagos hidrofobiškumas yra susijęs su tam tikrų bakterijų adhezija, bioplėvelės formavimusi ir lėtesniu gijimu [448,449]. Wassmann ir bendraautorių tyrime pademonstruota, jog hidrofobiniai paviršiai patrauklesni *Staphylococcus epidermidis*, kuris pasižymi citotoksišku poveikiu žmogaus fibroblastams ir trukdo sklandžiai osteointegracijai bei minkštųjų audinių gijimui [449–451]. Šio tyrimo išmatuoti polimerų *WCA* yra artimi arba šiek tiek aukštesni, lyginant su anksčiau atliktais tyrimais: PMMA 72–99º [415,416], 3D spausdintas PMMA (SLA) 71–79º [508], PEEK 10–114º [411,415,419,466], PEKK 64–83º [507]. Įprastas *CCP* plovimas lėmė hidrofobinius ZrO ir PEEK paviršius, tuo tarpu *RCP* lėmė hidrofobinius polimerinių medžiagų paviršius (PMMA, PEEK ir PEKK). Ši vandens kontaktinio kampo didėjimo tendencija po *RCP* buvo stebima visose polimerinėse medžiagose (statistiškai reikšminga PEKK), išskyrus ZrO (reikšmingai sumažėjo). Veikiausiai tai susiję su natūraliomis fizikocheminėmis medžiagos savybėmis, kurios išryškėja gerai nuplovus mėginių paviršių. Medžiagų paviršiaus hidrofiliškumo pokyčiai taikant skirtingus plovimo protokolus taip pat aprašyti anksčiau, pažymint, jog plovimas ultragarsinėje vonelėje PMMA ir PEEK medžiagoms lėmė

hidrofobiškiausius paviršius, lyginant su kitais metodais [414]. Keraminių medžiagų vandens kontaktiniai kampai buvo mažesni (nuo 45,3 ± 2,6° iki 79 ± 12,8°), susiję su hidrofiliškesniais nei polimerinių medžiagų paviršiais. Ypač mažais vandens kontaktiniais kampais išsiskyrė NICE, EMAX ir ZrO-V. Šie rezultatai atitinka mokslinėje literatūroje publikuotas Ti ir ZrO medžiagų *WCA* variacijas, atsižvelgiant į skirtingą paviršiaus poliravimą ir įvairų modifikavimą [524].

Nustatyta, jog būtent minkštųjų audinių zona esanti arčiausiai protezinio elemento medžiagos, pasižymi didžiausia fibroblastų santalka [516]. Įprastas plovimas (*CCP*) atliktame tyrime lėmė didesnę ŽDF proliferacijos variaciją ir mažiau nuspėjamą atsaką. Tai ypač pagrindžia eksperimento pakartojimo svarbą, siekiant įvertinti medžiagų savybes, tačiau esamos mokslinės publikacijos nedažnai pažymi, jog tyrime eksperimentas su ląstelėmis buvo atliktas kelis kartus. Gheisarifar ir kt. (2020) taikė PEEK paviršiaus modifikavimą plazma ir plovimą ultragarsine vonele, tokie paviršiai pasižymėjo dideliu šiurkštumu ir hidrofiliškumu (Sa 0,68–2,14 μm, *WCA* 10–12º) bei skatino ŽDF proliferaciją [411]. Šiame tyrime plovimas ultragarsinės vonelės pagrindu (*CCP*) lėmė PEEK paviršius (Sa 0,28 ± 0,1 μm, *WCA* 91 ± 9º), kurie buvo mažiau palankesni ŽDF gyvybingumui po 48 val. nei *RCP* būdu plauti (Sa 0.17 ± 0.06 μm, *WCA* 97 ± 12º), tačiau ši tendencija nebuvo stebima po 72 val. Panašūs rezultatai gauti, tačiau statistiškai reikšmingi su PMMA-3D ir PEKK (48 val.). Tuo tarpu PMMA-Ker po 48 val. demonstravo priešingus rezultatus, nurodančius *CCP* plovimą kaip palankesnį ŽDF. Polimerai metakrilatų pagrindu pasižymi skirtingomis ŽDF citotoksiškumo savybėmis priklausomai nuo jų sudėties ir gamybos būdo [416]. Šiame darbe tiriant PMMA medžiagas abu plovimo protokolai neturėjo įtakos ŽDF proliferacijai. Keraminių medžiagų tyrimo dalyje vertinant ŽDF proliferaciją skirtumų tarp medžiagų grupių nebuvo pastebėta, išskyrus 72 val. taške, ZrO-HT paviršiai buvo statistiškai reikšmingai palankesni nei Ti. Kiti skirtumai buvo pastebėti tik lyginant su kontroline grupe skirtinguose laiko taškuose reikšmingai atsiliko šios grupės: po 24 val. ZrO-V; po 48 val. Ti ir ZrO-UTML; po 72 val. NICE, Ti ir ZrO-V. Buvo pasiūlyta, kad hidrofilinių paviršių ir fibroblastų sąveiką geresnė, tačiau atrodo, kad šis parametras turi įtakos tik pradiniam prisirišimui, bet ne proliferacijai ar citoskeleto organizacijai [531]. Tai siejasi su šio tyrimo rezultatais, nes hidrofiliškesniais paviršiais pasižymėjusios NICE ir ZrO-V grupės nepasižymėjo reikšmingai palankiais ŽDF proliferacijos rezultatais.

Tirta į epitelines panašių ląstelių proliferacija priklausė nuo laiko, tačiau skirtumų tarp medžiagų grupių nebuvo stebima, o tai atitinka ankstesnius mokslinius tyrimus [394,456,522]. Tyrimas vertinęs imortalizuotus žmogaus dantenų epitelinius keratinocitus (*iHGEK*) nustatė, jog lygus Ti, šiurkštus ZrO ir vidutinio šiurkštumo PEEK paviršiai nesiskyrė ląstelių atsaku [419]. Šiame tyrime medžiagų paviršių šiurkštumas buvo kitoks, tačiau ŽDF atsakas taip pat reikšmingai nesiskyrė tarp šių medžiagų grupių, išskyrus 72 val. taške ZrO-HT paviršiuose fibroblastų santykinis gyvybingumas buvo didesnis nei Ti grupės. Šiame tyrime vertintos į epitelines panašios ląstelės ir keraminių medžiagų paviršiai, pademonstravo jog didesnio šiurkštumo ZrO-V grupė 72 val. taške lėmė reikšmingai mažesnę šių ląstelių proliferaciją, lyginant su neigiama kontrole. ZrO-V grupė neigiamą tendenciją ir šių ląstelių 12 val. citotoksiškumo tyrime turėjo (žemiausias gyvybingumas tarp medžiagų 0,67). Likusios medžiagos ir kiti proliferacijos laiko taškai reikšmingų skirtumų į epiteliocitus panašioms ląstelėms neturėjo. Tiek į epitelines panašios ląstelės, tiek fibroblastai neturi laike stabilaus selektyvaus atsako skirtingų nuolatinių protezų medžiagų klasėms [394,475,476,520]. Šio tyrimo ląstelių eksperimentų rezultatai patvirtina tokią tendenciją. Tačiau norint užtikrinti ilgalaikę gydymo sėkmę, svarbu pasiekti kuo greitesnę ląstelių adheziją ir sukurti stabilų jų ryšį su atramos bei protezinės struktūros paviršiais, taip užtikrinant gleivinės sandarumą [432,433].

Yra žinoma, jog cirkonio oksido pagrindu pagamintos medžiagos pasižymi geresnėmis biologinio suderinamumo savybėmis, lyginant su visomis kitomis šiuo metu klinikinėje praktikoje naudojamomis medžiagomis [468]. Tyrime buvo palygintos dvi skirtingos keraminės medžiagos pagamintos ZrO_2 pagrindu (ZrO-HT ir ZrO-UTML), bei jų paviršių aktyvavimo UV poveikis. Medžiagos nesiskyrė savo paviršiaus šiurkštumu, vandens kontaktiniu kampu, ŽDF citotoksiškumu bei proliferacija po 48 ir 72 val. (šiais atvejais priimta nulinė hipotezė). Tačiau 24 val. taške ŽDF pasižymėjo didesniu gyvybingumu ant UV veiktų ZrO-HT paviršių, lyginant su nepaveiktais ZrO-HT ir su ZrO-UTML paviršiais (priimta alternatyvi hipotezė).

Be kitų ZrO paviršių modifikavimo metodų, fotofunkcionalizavimas UV pasižymi geresniu gijimo potencialu, hidrofiliškumu bei biologiniu barjeru [469,513,514]. Tai galima atlikti pasitelkiant vieną iš apšvitos rūšių pagal naudojamą bangos ilgį: UV-A (100–400 nm), UV-B (290–320 nm) ir UV-C (100–290 nm; taikyta šiame tyrime) [515]. Poveikio ultravioletu protokolai gana stipriai skiriasi tarp skirtingų tyrimų, pavyzdžiui, nuo trumpo veikimo

vos 10 minučių, iki ilgo trunkančio daugiau kaip 24 valandas [469,513–515]. Ankstesni tyrimai pažymi skirtingą fotofunkcionalizavimo poveikį ZrO paviršių vandens kontaktiniam kampui [446,510]. Pagrindinis UV veikimo mechanizmas pasižymi tuo, jog ZrO paviršiuje sumažinamas anglies junginių (nusėdančių iš aplinkos ir oro) kiekis ir didėja deguonies kiekis, mažėja vandens kontaktinis kampas – didėja hidrofiliškumas [469]. Fotofunkcionalizavimo poveikis yra susijęs su apšvitos intensyvumu ir trukme, todėl rezultatai gali reikšmingai varijuoti, atsižvelgiant į eksperimento nustatymus. Att ir bendraautoriai (2009) nustatė, didžiausią neapdoroto paviršiaus (100,1°) ir žemiausią 48 val. UV veikto paviršiaus (20,8°) *WCA* rezultatą [511]. Kituose tyrimuose šis poveikis buvo mažesnis, tačiau dažnu atveju vandens kontaktinis kampas reikšmingai mažėjo 10°–50° [510,511,513]. Šiame tyrime taikytas ilgas 48 val. UV veikimo protokolas neturėjo statistiškai reikšmingos įtakos vandens kontaktiniam kampui galimai todėl, jog buvo naudotas labai detalus daugiažingsnis RCP plovimo protokolas, kuris galimai užtikrina paviršiaus priemaišų sumažėjimą.

Manoma, jog veikiant medžiagas UV didėja jų paviršių hidrofiliškumas, mažėjant angliavandenių kiekiui, didėja elektroteigiamumas bei baltymų ir kitų ekstraląstelinių medžiagų adsorbcija ir su tuo susijusi ląstelių adhezija [469,517]. Šio tyrimo rezultatai iš dalies atitinka tokius duomenis: grupių palyginimas 24 val. ir tolimesnės proliferacijos kreivių tendencijos nurodo palankų UV poveikį ŽDF. Šie rezultatai gali būti susiję su paviršiaus dekontaminacija ir aktyvavimu, nes kiti faktoriai buvo eliminuoti kaip galimos kovariantės [469]. Tai pastebima ir citotoksiškumo vertinimo rezultatų tendencijose su palankesniais UV veiktų paviršių rezultatais.

Vertinant tyrimo rezultatus būtina atsižvelgti į juos ribojančius veiksnius. Pirmiausia tiek skaitmeniniu būdu suplanuotos implantacijos navigacijos tikslumo tyrimo, tiek protezinių medžiagų biologinio suderinamumo tyrimo dalių rezultatus riboja tyrimo *in vitro* dizainas. Tyrimo metu sukuriamas gerai kontroliuojamas modelis, įgalinantis įvertinti konkrečius dominančius aspektus, tačiau tai neatspindi realios klinikinės situacijos, kurios metu visada dalyvauja kompleksinė įvairių veiksnių sąveika. Nors ir tyrimai nurodo, jog dinaminės navigacijos tikslumo rezultatai yra panašūs tiek *in vitro,* tiek klinikinių tyrimų [36,39,43], tačiau navigacijos tikslumo vertinimo atveju stacionari fantomo galva neimituoja pilnai visų chirurginį lauką ribojančių veiksnių, tokių kaip antagonistinio žandikaulio dantų lankas, minkštieji audiniai, ribotas išsižiojimas, paciento galvos, žandikaulio, liežuvio ir rijimo

judesiai, asistento užimama erdvė ir atliekami judesiai. Taip pat svarbu pabrėžti, jog tyrime naudotas vienas TKT įrenginys, vienas IOS, vienas 3D spausdintuvas bei vertinta viena statinės navigacijos (3Shape) ir dinaminės navigacijos (Navident) sistema, kai šiuo metu rinkoje yra daug alternatyvių produktų ir sistemų, kurių rezultatai gali skirtis dėl mažesnių ar didesnių technologinių ar metodologinių skirtumų. Svarbu paminėti, jog buvo simuliuota tik viršutinio žandikaulio klinikinė situacija ir su tuo susijęs galvos sekiklio (angl. *tracker*) taikymas, apatinio žandikaulio sekimas gali būti kiek nepatogesnis, nes reikalingas intraoralinis alternatyvaus sekiklio fiksavimas. Taip pat realioje klinikinėje situacijoje daug labiau tikėtinas sekiklio fiksacijos praradimas ir dėl to kylantis poreikis iš naujo jį tvirtinti, registruoti sekimą, o tai gali lemti skirtingas paklaidas. Tyrimo rezultatus taip pat riboja taikyta tik kieto kaulo situacija (D1), kuri klinikinėje praktikoje pasitaiko rečiau nei normalaus ar minkšto (D4) kaulo situacijos; minkščiausia kaulo situacija turi mažesnį pasipriešinimą implanto ložės paruošimo metu ir implanto sriegimo metu, o tai sukuria daugiau laisvės nukrypti nuo plano ir neretai reikalauja individualiai pritaikyti implanto ložės paruošimo strategiją [488]. Iš dalies tyrimo rezultatus riboja tai, jog buvo dirbta tik su vieno gamintojo implantų sistemomis (Camlog), techniniai grąžtų sekos, implanto ložės ir pačio implanto dizaino santykio skirtumai kitų gamintojų sistemose gali turėti įtakos skirtingiems rezultatams. Taip pat šiame tyrime buvo naudoti tik dviejų dydžių implantai, o klinikinėje praktikoje dažnai tenka rinktis įvairesnius. Papildomas tyrimo trūkumas yra tai, jog mezialinė ir distalinė implanto padėtis buvo surišta su skirtingo dydžio implantais ir nors tai ir kliniškai reprezentatyvu bei logiška, atsižvelgiant į anatominius veiksnius bei praktines gaires [489–491], tačiau skirtingo skersmens ir ilgio implantai reikalauja ne vienodo implanto ložės paruošimo, o tai gali lemti papildomus skirtumus, kurie sąveikaus su interpretuojama implanto mezialine ar distaline padėtimi. Galiausiai registravimo metodų palyginime naudotas bedantis modelis su atskaitos objektais, kurie nėra komerciškai prieinami ar standartizuoti, todėl pateikti griežtai apibendrintų išvadų negalima. Šie objektai buvo fiksuoti modelio pamate, kuris nėra kliniškai reali situacija. Dažniausia tokie objektai fiksuojami alveolinės ataugos plote ar gomuryje, o tai tikėtina gali riboti operacinio lauko laisvę ir patogumą, bei padidinti paklaidas. Atkreipiant dėmesį į visas tyrimą ribojančias aplinkybes ir rezultatų interpretaciją, galime siekti kuo tiksliau įgyvendinti planuotą implantų padėtį naudojant statines ar dinamines navigacijos metodus.

Ląstelių modelio tyrimo dalies *in vitro* dizainas taip pat ribotas, nes yra vertinamos išskirtinai po vieną ląstelių linijos palankiomis augimo sąlygomis. Taigi vietoje organotipinio trijų dimensijų modelio simuliuojama paprastesnė dviejų dimensijų paviršiaus situacija [513,518]. Klinikoje į chirurginę žaizdą nuolat patenka seilės, kurios padengia medžiagos paviršių ir keičia jo savybes, tuo pat metu formuojasi kraujo krešulys ir užsiveda su chirurgine invazija susijęs įvairaus laipsnio uždegiminis procesas. Paraleliai su minkštųjų audinių ląstelėmis (fibroblastais ir epeliocitais) varžosi burnoje reziduojantys mikroorganizmai, kurie kolonizuoja paviršius ir išskiria medžiagas neigiamai įtakojančias gijimo procesą. Negana to pačios epitelinės ląstelės varžosi su fibroblastais ir dažniausiai pirmauja žaizdos krašto uždengimo greityje dėl genetiškai lemtos spartesnės proliferacijos. Įvertinti tikrų epitelinių ląstelių nebuvo galimybės, nes jų adhezijai prie medžiagos paviršiaus reikalingas paviršiaus dengimas specialiais substratais, kas iškreiptų ir maskuotų pačios medžiagos poveikį ląstelėms. Naudota pirminė ląstelių kultūra nebuvo charakterizuota ir nebuvo identifikuoti reikalingi ląstelių paviršiaus žymenys. Taikytas į epitelines panašių ląstelių modelis nebūtinai tiksliai atspindi sveikų epeliocitų atsaką į tas pačias protezines medžiagas, todėl rezultatai turėtų būti vertinam konservatyviai. Nors siekiamybė yra sukurti minkštųjų audinių barjerą, atitinkantį esantį prie dantų, tačiau histologiniai tyrimai rodo, jog jungtyje su proteziniu komponentu ir implanto atrama vyrauja ilga epitelinė jungtis [58], o giliau esanti jungiamojo audinio tarpląstelinė medžiaga, fibroblastų adhezija ir vertikalios kolageno skaidulos beveik nepasitaiko [509]. Negana to, su išimtimi „*one-time one-abutment*" koncepcijai, dažnai gijimo metu protezinis komponentas gali būti nusuktas ir pakartotinai prisuktas, traumuojant ir keičiant minkštųjų audinių prisitvirtinimą. Šame tyrimas taip pat neatspindėta implanto-atramos jungties mikroplyšio įtaka [23]. Keli histologiniai tyrimai rodo, jog protezinės medžiagos skiriasi minkštųjų audinių ir bakterinių ląstelių rezultatais [532,533]. Stebimi kiekybiniai ir kokybiniai histologiniai skirtumai (ploto uždengimas, ląstelių morfologija, skaidulų orientacija) [532–535]. Galiausiai, nors atliktame tyrime ląstelių eksperimentai buvo kartoti tris kartus, rezultatų sklaida rodo didesnio pakartojimų skaičiaus poreikį, kurį riboja tyrimų materialieji ir žmogiškieji kaštai bei ištekliai, todėl neretai tyrimai šioje temoje publikuojami su vienu eksperimentu be pakartojimų. ANOVA yra laikoma pakankamai atspari mažiems nuokrypiams nuo normalumo [536], tačiau šio tyrimo statistinė analizė turi būti interpretuota su atitinkama atsarga. Nė vienas individualus

veiksnys negali pilnai paaiškinti ląstelių elgesio. Tačiau derinant kelis palankius aspektus, teisingai pasirinkus medžiagą, su paviršiaus apdorojimo protokolu, galima teigiamai paveikti ankstyvą barjero formavimąsi tarp protezinės komponentės ir burnos minkštųjų audinių.

Atliktas tyrimas turi apribojimų dėl jo *in vitro* dizaino ir kliniškai reikšmingų sąlygų nepilno išpildymo, tai gali turėti įtakos rezultatų interpretavimui ir apibendrinimui. Norint pateikti išsamesnes ir patikimesnes klinikines rekomendacijas, pašalinant aukščiau minėtus apribojimus, svarbu tęsti tyrimus šioje srityje. Gauti rezultatai yra vertinga šios srities orientacinė informacija ir prisideda prie pamatinio temos supratimo, o kartu siūlo potencialių būsimų klinikinių pritaikymo gairių. Šio tyrimo rezultatų svarba, atsispindi šiandienos realybėje, kai greita technologinė evoliucija įžengia į kasdienę praktiką labai sparčiai, kartais dar prieš spėjant patiesti tvirtą fundamentinių tyrimų pagrindą, kuris reikalingas argumentuojant platų ir mokslu pagrįstą jų įgyvendinimą klinikinėje praktikoje.

IŠVADOS

Atsižvelgiant į tyrimo apribojimus, daromos tokios išvados:

1. Intraoraliniu skenavimu pagrįstas vertinimas rodo aukštą dinaminės navigacijos implantacijos tikslumą, atsižvelgiant tiek į bedančio defekto klasę, tiek į implanto dizainą ir poziciją.

2. Statinis navigacijos metodas demonstravo didesnį tikslumą visais analizuotais aspektais, išskyrus kampo nuokrypį, lyginant su dinaminiu metodu.

3. Atskaitos objektų taikymas dinaminėje navigacijoje potencialiai didina implantacijos tikslumą.

4. Daugiapakopis polimerinių medžiagų plovimo protokolas reikšmingai keičia paviršiaus šiurkštumą, vandens kontaktinį kampą, ir turi palankią įtaką žmogaus dantenų fibroblastų proliferacijai ant 3D spausdintų polimetilmetakrilato ir polieterketonketono paviršių.

5. Cirkonio oksido keraminių medžiagų aktyvavimas UV spinduliuote turi teigiamos įtakos žmogaus dantenų fibroblastų gyvybingumui ir proliferacijai.

6. Lauko špatu užkepta ir glazūruota cirkonio keramika pasižymėjo reikšmingai didesniu šiurkštumu ir prastesne dantenų ląstelių proliferacija.

PRAKTINĖS REKOMENDACIJOS

1. Rekomenduojama teikti pirmenybę intraoraliniu skeneriu pagrįstiems implantacijos tikslumo vertinimo metodams, nes jie yra saugi ir tiksli alternatyva įprastiems rentgeno metodams.

2. Skaitmeniniu būdu suplanuota implantacija, atsižvelgiant į protezinius kriterijus, taikant pilnai nukreipiančią navigaciją yra rekomenduojamas tikslus gydymo metodas.

3. Gerai apibrėžtų ir paskirstytų atskaitos objektų taikymas dinaminės navigacijos metodui gali suteikti didesnį tikslumą, ypač esant mažam likusių dantų skaičiui ir pilnai bedantėse situacijose

4. Kruopštus daugiapakopis protezinių komponentų plovimo protokolas gali skatinti palankią minkštųjų audinių reakciją.

5. Protezinių medžiagų paviršių veikimas UV spinduliuote yra cirkonio oksido keramikos aktyvinimo būdas, palankiai veikiantis supančių minkštųjų audinių ląsteles.

6. Glazūruotos keramikos nerekomenduojama naudoti vietose, kur tikimasi minkštųjų audinių ląstelių prisitvirtinimo.

PUBLIKACIJŲ SĄRAŠAS

Straipsniai, publikuoti tarptautinės duomenų bazės Clarivate Analytics Web of Science (CA WoS) referuojamuose leidiniuose su citavimo indeksu:

1. Rutkunas V, <u>Borusevicius R</u>, Liaudanskaite D, Jasinskyte U, Drukteinis S, Bukelskiene V, Mijiritsky E. The Effect of Different Cleaning Protocols of Polymer-Based Prosthetic Materials on the Behavior of Human Gingival Fibroblasts. IJERPH 2020; 17: 7753. DOI: 10.3390/ijerph17217753.

2. Rutkunas V, <u>Borusevicius R</u>, Balciunas E, Jasinskyte U, Alksne M, Simoliunas E, Zlatev S, Ivanova V, Bukelskiene V, Mijiritsky E. The Effect of UV Treatment on Surface Contact Angle, Fibroblast Cytotoxicity, and Proliferation with Two Types of Zirconia-Based Ceramics. IJERPH 2022; 19: 11113. DOI: 10.3390/ijerph191711113.

Publikuotos mokslinių konferencijų pranešimų santaukos (CA WoS):

1. <u>Borusevicius R</u>, Bukelskiene V, Alksne M, Balciunas E, Simonaitis T, Jurgaityte R, Liaudanskaite D, Rutkunas V. Implant abutment material and surface modifications effect on human gingival fibroblast behavior. Clin Oral Impl Res 2019; 30: 332–332. DOI: 10.1111/clr.288_13509

2. <u>Borusevicius R</u>, Rutkunas V, Simonaitis T, Gendviliene I, Pletkus J. Accuracy of dynamic implant navigation in partially- and fully-edentulous models: a novel NO-invasive x-ray free method. Clin Oral Impl Res 2020; 31: 20–1. DOI: 10.1111/clr.16_13643

3. Liaudanskaite D, <u>Borusevicius R</u>, Rutkunas V, Bukelskiene V, Alksne M, Simoliunas E, Gendviliene I, Jurgaityte R. The impact of implant abutment preparation on proliferation of human gingival fibroblasts. Clin Oral Impl Res 2020; 31: 167–167. DOI: 10.1111/clr.109_13644

Kitos mokslinės publikacijos:

1. Rutkunas V, <u>Borusevicius R</u>. Skaitmeniniu būdu paruoštų dantų implantacijos gidų tikslumas ir gydymo rezultatai. Stomatologija : VšĮ "Odontologijos studija". ISSN 1392-8589. 2016, T. 19, nr. 1, p. 11-17.

Monografijos, vadovėliai:

1. Rutkunas V, <u>Borusevicius R</u>, Geciauskaitė A, Pletkus J. Digital Technologies in Clinical Restorative Dentistry. Practical Advanced Periodontal Surgery 2020; 213–32.

GYVENIMO APRAŠYMAS

Name	Rokas
Surname	Borusevičius
Gimimo data	1990 11 14
Gimimo vieta	Klaipėda, Lietuva
El. paštas	rokas.borusevicius@gmail.com
Mokslinės veiklos interneto svetainė	https://www.researchgate.net/profile/Rokas-Borusevicius-3
Išsilavinimas	
1997–2005	Vydūno vidurinė mokykla, Klaipėda, Lietuva *Pradinis išsilavinimas*
2005–2009	"Ąžuolyno" gimnazija, Klaipėda, Lietuva *Pagrindinis ir vidurinis išsilavimas* *Brandos atestas su pagyrimu*
2009–2014	Vilniaus universitetas, Medicinos fakultetas, Odontologijos institutas, Vilnius, Lietuva *Odontologijos magistras*
2014–2017	Vilniaus universitetas, Medicinos fakultetas, Odontologijos institutas, Vilnius, Lietuva *Periodontologijos rezidentūra*
Darbo patirtis	
2014–2017	Gydytojas odontologas, VšĮ Vilniaus universiteto ligoninės Žalgirio klinika
2017–2019	Periodontologas, VšĮ Vilniaus universiteto ligoninės Žalgirio klinika ir privati praktika
2019–dabar	Periodontologas, privati praktika
2019–dabar	DIGITORUM mokslinės grupės narys
Licencijos	
2014–dabar	gydytojo odontologo profesinė kvalifikacija OPL-04400
2017–dabar	gydytojo periodontologo profesinė kvalifikacija, OPL-05053

NOTES

NOTES

NOTES